



ÉCOLE
CENTRALE LYON

N° d'ordre NNT : 2023-ECDL0029

THESE de DOCTORAT DE L'ÉCOLE CENTRALE DE LYON
membre de l'Université de Lyon

Ecole Doctorale N° 34
(Matériaux)

Spécialité de doctorat : Matériaux

Soutenue publiquement le 10/07/2023 par :

Tadashi OSHIO

**Anti-wear properties and mechanisms
of dialkyl phosphonates
in ester base oils**

Devant le jury composé de :

GEANTET, Christophe
MINAMI, Ichiro
MORINA, Ardian

DR CNRS
Professeur
Professeur

Ircelyon
Lulea University of Technology
University of Leeds

Président
Rapporteur
Rapporteur

MINFRAY, Clotilde
DASSENNOY, Fabrice

Professeur
Professeur

Ecole Centrale de Lyon
Ecole Centrale de Lyon

Directrice de thèse
Co-directeur de thèse

Thèse préparée au Laboratoire de Tribologie et Dynamique des Systèmes

CONTENTS

| | |
|--------------------------------------------------------------|-----|
| <i>Contents</i> | i |
| <i>Abstract</i> | v |
| <i>Résumé</i> | vii |
| | |
| <i>General Introduction</i> | 1 |
| | |
| <i>Chapter 1 Literature Review</i> | 4 |
| 1.1 Lubricant base oils and additives | 5 |
| 1.1.1 Base oils | 5 |
| 1.1.1.1 Mineral Base Oils (Group I-III) | 6 |
| 1.1.1.2 Poly- α -olefins (Group IV) | 6 |
| 1.1.1.3 Ester base oils (Group V) | 7 |
| 1.1.1.4 Poly alkylene glycols, PAG (Group V) | 11 |
| 1.1.1.5 Biodegradability of base oils | 12 |
| 1.1.2 Lubricant additives | 13 |
| 1.1.2.1 Friction modifiers | 13 |
| 1.1.2.2 Viscosity index improvers and pour point depressants | 15 |
| 1.1.2.3 Extreme pressure additives | 15 |
| 1.1.2.4 Antioxidants | 16 |
| 1.1.2.5 Corrosion inhibitors | 17 |
| 1.1.2.6 Dispersants and detergents | 17 |
| 1.1.2.7 Anti-wear additives | 19 |
| 1.2 Literature review of AW additives | 20 |
| 1.2.1 Research on AW additives in mineral base oils | 20 |
| 1.2.1.1 Tricresyl phosphate (TCP) | 20 |
| 1.2.1.2 Zinc dialkyldithiophosphate (ZDDP) | 24 |
| 1.2.1.3 Dialkyl phosphites | 27 |
| 1.2.1.4 Triphenyl phosphorothionate (TPPT) | 29 |

| | | |
|---------|-------------------------------------------------------------------------------|----|
| 1.2.1.5 | Others | 30 |
| 1.2.1.6 | Overview of research on AW additives in mineral base oils | 31 |
| 1.2.2 | Research of phosphorus AW additives in ester base oils | 32 |
| 1.2.2.1 | AW performance of phosphorus additives in ester base oil | 32 |
| 1.2.2.2 | Relationship between response of AW additives and polarity of ester base oils | 34 |
| 1.2.2.3 | Design of AW additives for ester base oils | 34 |
| 1.2.2.4 | Others | 35 |
| 1.2.2.5 | Overview of research on AW additives in ester base oils | 35 |
| 1.3 | Objectives of this thesis | 36 |
| | Reference | 38 |

Chapter 2 Material and experimental methods 45

| | | |
|-------|-------------------------------------------------------------------------------------|----|
| 2.1 | Materials | 46 |
| 2.1.1 | Base oils | 46 |
| 2.1.2 | AW additives | 47 |
| 2.2 | Tribotest conditions | 48 |
| 2.2.1 | Four-ball test | 48 |
| 2.3 | Surface analysis techniques for tribofilm characterizations | 50 |
| 2.3.1 | X-ray Photoelectron Spectroscopy (XPS) | 50 |
| 2.3.2 | Time-of-Flight Secondary Ion Mass Spectrometry and Infrared Spectroscopy (ToF-SIMS) | 51 |
| 2.3.3 | Polarization Modulation-Infrared Reflection-Adsorption Spectroscopy (PM-IRRAS) | 52 |
| 2.3.4 | Transmission Electron Microscope (TEM) using Focused Ion Beam (FIB) | 53 |
| | Reference | 54 |

Chapter 3 Antiwear Properties of Dialkyl Phosphonates in

| | |
|----------------------------------------------------------------------------------------|----|
| <i>Ester Base Oil</i> | 55 |
| 3.1 Antiwear Properties of Dialkyl Phosphonates in TMO | 56 |
| 3.2 Antiwear Properties of Dialkyl phosphonoacetic acid in TMO and PAO | 58 |
| 3.2.1 Impact of normal load | 61 |
| 3.2.2 Impact of test duration | 62 |
| 3.2.3 Impact of temperature | 63 |
| 3.3 Discussion | 63 |
| 3.3.1 Possibilities of phosphonate as AW properties for ester base oils | 63 |
| 3.3.2 AW properties of DAPA and conventional phosphorus additives | 63 |
| 3.3.3 Effect of load on AW performance of DAPA in base oils | 64 |
| 3.3.4 Influence of test time and temperature on AW performance of DAPA in base oils | 65 |
| 3.4 Summary of this chapter | 66 |
| Reference | 67 |

Chapter 4 Investigations of DAPA tribofilm compositions

| | |
|---------------------------------------------------------|-----|
| | 68 |
| 4.1 DAPA tribofilm analyses using XPS | 69 |
| 4.1.1 DAPA tribofilm compositions | 69 |
| 4.1.2 Detailed analyses of high resolution spectra | 71 |
| 4.1.3 Depth profile of DAPA tribofilm | 85 |
| 4.2 DAPA tribofilm analyses using TOF-SIMS | 86 |
| 4.3 DAPA tribofilm observations by FIB-TEM | 90 |
| 4.4 DAPA tribofilm analyses using Infrared Spectroscopy | 92 |
| 4.5 Discussion | 96 |
| 4.6 Summary of this chapter | 99 |
| Reference | 100 |

Chapter 5 Design of Phosphonate AW additives for Ester

| | |
|--------------------------------------------------------------------|-----|
| <i>lubricants</i> | 102 |
| 5.1 Influence of ester base oil polarity on AW performance of DAPA | 103 |
| 5.2 Modification of chemical structures of DAPA | 105 |
| 5.2.1 Influence of alkyl chain on AW performance | 105 |
| 5.2.2 Influence of functional groups on AW performance | 108 |
| 5.2.3 Influence of methylene between P and COOH on AW performance | 109 |
| 5.3 Discussion | 113 |
| 5.3.1 Effect of ester base oil polarity on AW performance | 113 |
| 5.3.2 Effect of DAPA alkyl chain length on AW performance | 113 |
| 5.3.3 Effect of functional group of DAPA | 115 |
| 5.3.4 Effect of carbon-based group between P and COOH of DAPA | 115 |
| 5.4 Summary of this chapter | 117 |
| Reference | 118 |

Chapter 6 Conclusions and Outlook

| | |
|--------------------------------------------------------------|-----|
| 6.1 Conclusions | 119 |
| 6.2 Outlook | 120 |
| 6.2.1 Possibilities of dialkyl phosphonates as AW additives | 120 |
| 6.2.2 Tribofilm compositions | 121 |
| 6.2.3 AW additives design using artificial intelligence (AI) | 121 |

Annexes

| | |
|------------------------------------------------------------------------|-----|
| Annex 1 Tribochemical reaction of DAPA investigated in ECAT tribometer | 122 |
| Annex 2 Pyrolysis reaction of DAPA | 147 |
| Annex 3 Dissolving states of DAPA in base oils | 151 |
| Reference of Annexes | 161 |

General Introduction

Issues surrounding lubricants

In order to contribute to the achievement of the United Nations' Sustainable Development Goals (SDGs), the reduction of environmental impact and the prevention of environmental pollution are being considered in various industrial sectors. Lubricants are also expected to provide solutions to these challenges, and environmentally acceptable lubricants have been developed. For example, efforts in hydraulic fluids are shown in Figure 1. Hydraulic fluids are lubricants used in hydraulic systems such as hydraulic excavators, which are responsible for preventing wear in hydraulic equipment and for transferring the hydraulic energy generated in a hydraulic pump to the individual components such as a drive motor and cylinder.

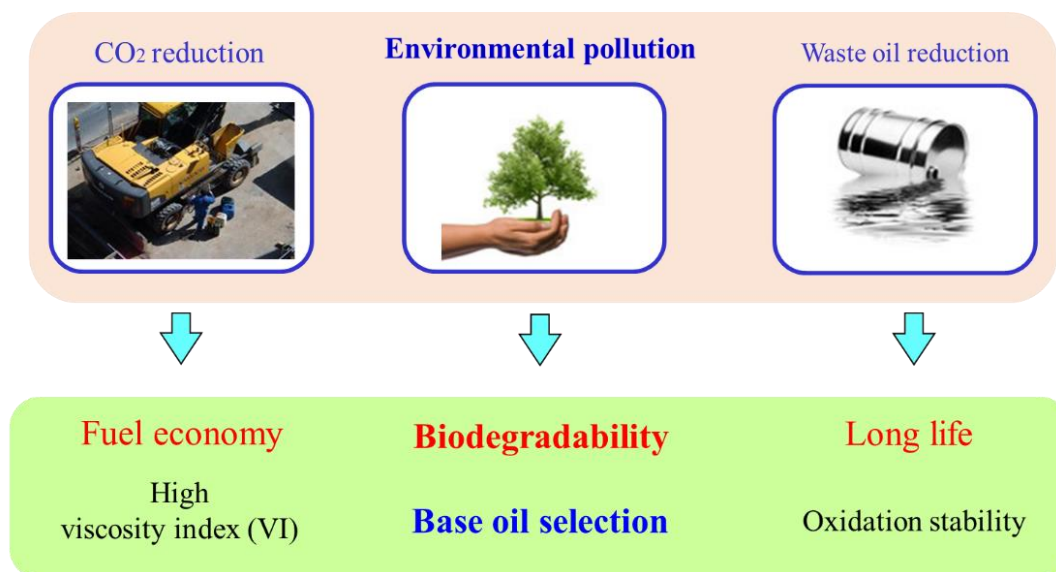


Figure 0-1. Efforts to reduce the environmental impact with hydraulic fluids

For CO₂ reduction, very high viscosity index fluids, which present small change of viscosity with temperature, are effective for improving fuel economy. Using such fluids allow to keep sufficiently low viscosity at low temperature and sufficiently high viscosity at high temperature in order to obtain the best compromise in terms of lubrication capability and fuel economy. For preventing environmental pollution, lubricant base oils with proper biodegradability are used for hydraulic fluids. For waste oil reduction, antioxidant technologies are important for improving oxidation stabilities of hydraulic fluids. From these considerations, the most extensive studies have been on biodegradable

lubricants, which lead to reduced environmental pollution.

Lubricants are a major concern affecting the environment such as soil and water pollution. Most lubricants consist of mineral base oils, which have poor biodegradability and sometimes cause harmful effects to animals and plants [1]. Worldwide usage of lubricants is more than 41 million tons per year and 40 % of these lubricants are released into the environment by leakage or accidents [2]. For example, the United States Environmental Protection Agency reported that the amount of lubricant leakage from commercial vessels to the ocean is more than 4.6 million liters each year [3]. Therefore, alternative materials of mineral base oils should be considered to prevent environmental pollution. The German government promoted the conversion of lubricants using mineral base oils to biodegradable lubricants in the 2000s. In the German market of hydraulic fluids used for construction machines, the biodegradable lubricants represent more than 15 % of the total market and their use are increasing [4-5]. In order to encourage the use of biodegradable lubricants and foster awareness of eco-friendly products, international and domestic labeling programs have been established mainly in Europe. Table 1 shows the features of each labeling program. These labels define methods to evaluate lubricant properties for whether they have enough qualities as environmentally accepted lubricants (EALs).

Table 0-1. International and national labeling programs for lubricants

| Name | European Eco-label | Nordic Swan | Blue Angel | Swedish Standard | Eco Mark |
|---------------------|-------------------------------------------------------------------------------------|-------------------------------------------------------------------------------------|-------------------------------------------------------------------------------------|---------------------------|---------------------------------------------------------------------------------------|
| Label image |  |  |  | No image |  |
| Country | International | International | Germany | Sweden | Japan |
| Establishment year | 2005 | 2004 | 1988 | 1986 | 1998 |
| Types of lubricants | Hydraulic fluid Grease Two-stroke oil etc. | Hydraulic fluid Grease Two-stroke oil Transmission/gear oil | Hydraulic fluid Grease | Hydraulic fluid Grease | Hydraulic fluid Grease Two-stroke oil others |

Biodegradable lubricants have been increasingly widespread, but technical problems have been also raised [4, 5]. In particular, the inferior lubricating performance compared to conventional mineral-based lubricants is a problem, which often leads to a serious damage on equipment. Thus, lubricant additives are needed for EALs with performance equal to that of conventional mineral oil-based lubricants. However, existing lubricant additives have been developed for mineral oils and are not always effective for EALs. Therefore, the developments of lubricant additives that are optimized for biodegradable lubricants are needed.

Reference

- [1] W. J. Bartz, Lubricants and the environment., *Tribology International*, **31**, 1998, 35-47
- [2] I. Madanhire and C. Mbohwa, Mitigating Environmental Impact of Petroleum Lubricants, Springer International Publishing Switzerland, 2016
- [3] United States Environmental Protection Agency report., Environmentally Acceptable Lubricants, 2001
- [4] H. Theissen, The German Market Introduction Program for Biobased Lubricants., *Tribology Online*, **5**, 2010, 225-229
- [5] H. Theissen, Effects of contamination of Biobased Hydraulic Fluids with Mineral Oil, *Journal of ASTM International*., **6**, 2009, 1-9

Chapter 1

Literature Review

| | | |
|---------|------------------------------------------------------------------------------------|----|
| 1.1 | Lubricant base oils and additives | 5 |
| 1.1.1 | Base oils..... | 5 |
| 1.1.1.1 | Mineral base oils (Group I -III) | 6 |
| 1.1.1.2 | Poly- α -olefins (Group IV) | 6 |
| 1.1.1.3 | Esters (Group V) | 7 |
| 1.1.1.4 | Poly alkylene glycols, PAG (Group V) | 11 |
| 1.1.1.5 | Biodegradability of base oils | 12 |
| 1.1.2 | Lubricant additives | 13 |
| 1.1.2.1 | Friction modifiers | 13 |
| 1.1.2.2 | Viscosity index improvers and pour point depressants..... | 15 |
| 1.1.2.3 | Extreme pressure additives | 15 |
| 1.1.2.4 | Antioxidants..... | 16 |
| 1.1.2.5 | Corrosion inhibitors | 17 |
| 1.1.2.6 | Dispersants and detergents..... | 17 |
| 1.1.2.7 | Anti-wear (AW) additives..... | 19 |
| 1.2 | Literature review of AW additives..... | 20 |
| 1.2.1 | Research on phosphorus AW additives in mineral base oils | 20 |
| 1.2.1.1 | Tricresyl phosphate (TCP) | 20 |
| 1.2.1.2 | Zinc dialkyl dithiophosphate (ZDDP)..... | 24 |
| 1.2.1.3 | Dialkyl phosphites | 27 |
| 1.2.1.4 | Triphenyl phosphorothionate (TPPT) | 29 |
| 1.2.1.5 | Others..... | 30 |
| 1.2.1.6 | Overview of research on AW additives in mineral base oils | 31 |
| 1.2.2 | Research on phosphorus AW additives in ester base oils | 32 |
| 1.2.2.1 | AW performance of phosphorus additives in ester base oils..... | 32 |
| 1.2.2.2 | Relationship between response of AW additives and polarity of ester base oils..... | 34 |
| 1.2.2.3 | Design of AW additives for ester base oils..... | 34 |
| 1.2.2.4 | Others..... | 35 |
| 1.2.2.5 | Overview of research on AW additives in ester base oils | 35 |
| 1.3 | Objectives of this thesis | 36 |
| | Reference | 38 |

Commercial lubricants use various types of base oils and additives. This chapter summarizes literature reviews of lubricant base oils and additives. First, the properties and functions of lubricant base oils and additives are described. Secondly, previous researches on anti-wear (AW) additives performance and action mechanisms relevant to this research are presented. Lastly, the objectives of this thesis are explained.

1.1 Lubricants base oils and additives

Lubricants are made of base oils and additives (Figure 1-1). The development of environmentally friendly lubricants implies first the selection of the base oil that will govern the fundamental properties of the lubricants. Therefore, it is essential to understand features of base oils for developing lubricants which meet both required performance for applications and environmental properties such as biodegradability.

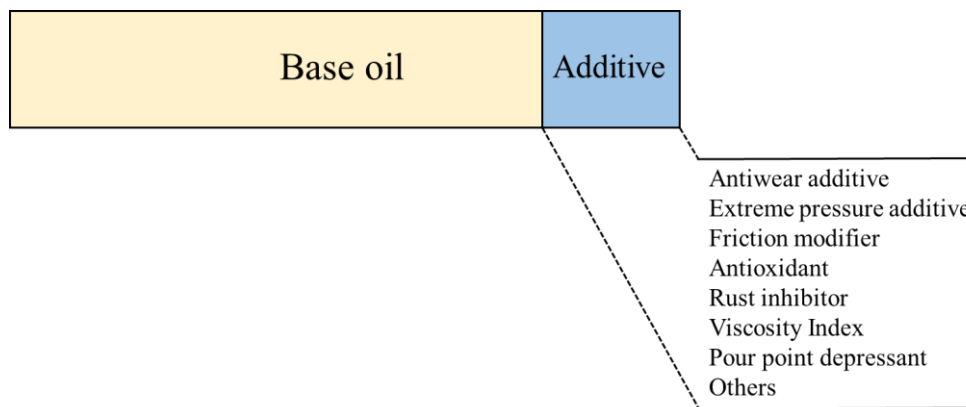


Figure 1-1. Composition of a lubricant

1.1.1 Base oils

As described in the previous section, base oils influence not only fundamental properties of lubricants but also environmental aspects. In this section, the different types of base oils and their properties are described according to the American Petroleum Institute (API) category.

Base oils are usually divided into two groups: mineral base oils and synthetic base oils. The former are produced from crude oils using the refinery process, and the latter are produced by chemical reactions of raw materials from biomass or fossil based chemicals. The API categorized the different types of base oils into 5 groups as shown in Table 1-1. Mineral base oils API categories are divided into three groups (Group I-III) and others synthetic base oils into two groups (Group IV and V).

Table 1-1. API categories of base oils

| Category | Sulphur, % | | Saturates, % | Viscosity Index |
|-----------|--------------------------------------|--------|--------------|-----------------|
| Group I | >0.03 | and/or | <90 | 80-120 |
| Group II | ≤ 0.03 | and | ≥ 90 | 80-120 |
| Group III | ≤ 0.03 | and | ≥ 90 | 120 |
| Group IV | Poly- α -olefin (PAO) | | | |
| Group V | Other than I -IV (mostly synthetics) | | | |

1.1.1.1 Mineral Base Oils (Group I-III)

Mineral base oils are the most commonly used for lubricants, because they are cheap and easily available compared to synthetic oils. The main chemical component of mineral base oils is hydrocarbon with roughly 30 carbon atoms [1]. Each molecule consists of three types of hydrocarbons: paraffin, naphthenic and aromatic described in Figure 1-2.

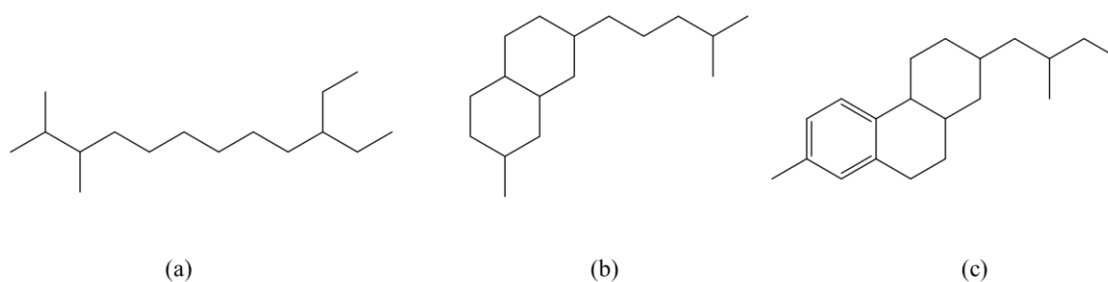


Figure 1-2. Types of mineral base oils: (a) paraffin, (b) naphthenic, and (c) aromatic

Other compounds are also found in mineral base oils, for example sulfur, nitrogen, and wax. These are impurities which affect the performance of mineral base oils such as thermal stability, pour point and viscosity-temperature characteristics, e.g. viscosity index. Therefore, API categorized mineral base oils according to the amount of the impurities as described in Table 1-2.

1.1.1.2 Poly- α -olefins (Group IV)

Poly- α -olefins (PAOs) started to be used as lubricant base oils in the early 1950s [2]. Nowadays, PAOs are the most widely used among synthetic base oils, and are manufactured by the oligomerization of α -olefins (e.g. 1-decene, 1-dodecene, the mixture of C8-C12 α -olefins), which are produced from ethylene (Figure 1-3) [3]. PAOs contain no impurities unlike mineral base oils. The properties of PAOs are superior to those of mineral base oils in terms of viscosity index, volatility, pour point and thermal stability.

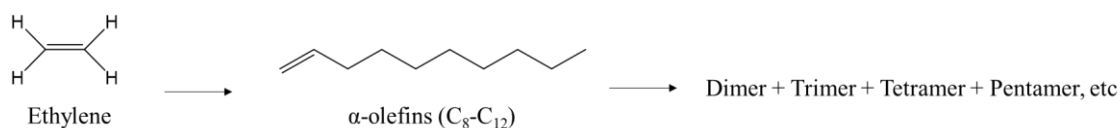


Figure 1-3. PAO's production scheme

Commercial PAOs are generally listed according to their kinematic viscosity at 100 °C. For example, PAO6 has a kinematic viscosity of 6 mm²/s at 100 °C. Commercial PAOs are ranged from PAO2 to PAO100.

1.1.1.3 Esters (Group V)

There are two types of ester base oils: natural esters such as vegetable oils and animal fats, and synthetic ester base oils produced from the esterification reaction between acids and alcohols described in Figure 1-4.

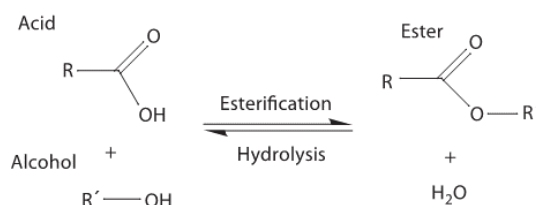


Figure 1-4. Chemical structure and formation of ester base oils [1]

The earliest use of natural ester base oils was confirmed in 1400 BC. They were the main lubricants until the production of mineral oils started in the early nineteenth century. Compared to mineral base oils, natural ester base oils are expensive, and their thermal and oxidation stabilities are insufficient for modern lubricants which are used under severe conditions. Figure 1-5 illustrates the decomposition mechanism of natural ester base oils. Beta-hydrogen in their structures can be removed easily, and the following decomposition reaction occurs [4]. Their thermal stability is, therefore, too low and applications as lubricants are limited.

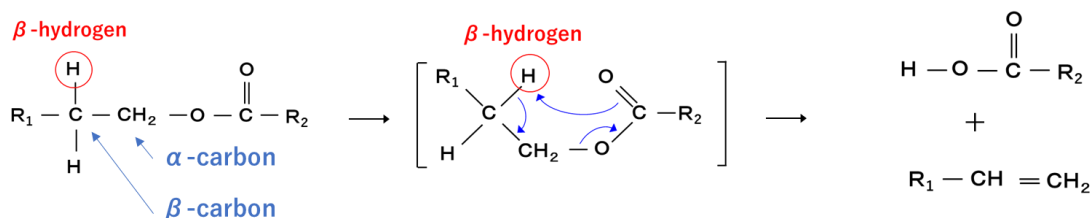


Figure 1-5. Decomposition mechanism of natural ester base oils (adapted from [4])

In order to improve the thermal stabilities, the development of synthetic ester base oils started in Germany in 1937. Through these studies, it was found that synthetic ester base oils from hindered alcohols showed superior oxidation stabilities to natural esters and mineral base oils [5]. Figure 1-6 presents the hindered alcohols and glycerol that is the raw material of natural esters. The hindered alcohols have no beta-hydrogen, although glycerol has five beta-hydrogens in the structures. Due to the absence of beta-hydrogen, synthetic ester base oils, produced from hindered alcohols, have higher thermal stabilities and are more suitable for lubricant base oils than natural esters.

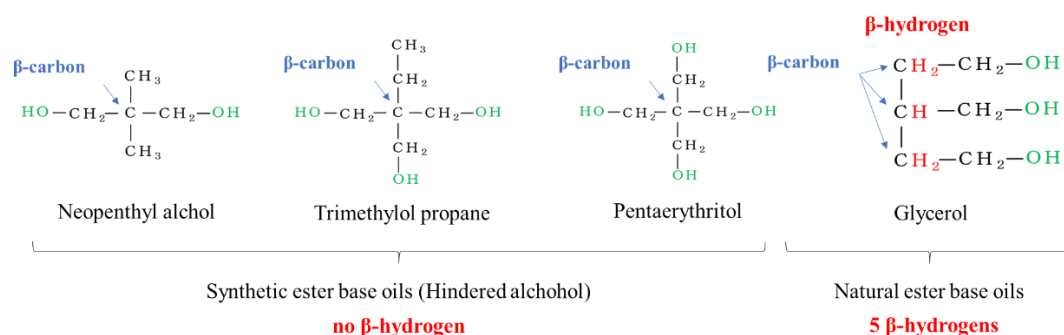


Figure 1-6. Alcohols for synthetic and natural ester base oils with absence or presence of beta-hydrogen respectively

In addition to the types of alcohol, the alkyl chain structure influences the physical/chemical properties significantly. The viscosity of ester base oils generally increases with alkyl chains length of raw materials (alcohol or acid). The ester base oils with straight alkyl chains show higher viscosity-index and biodegradability than those of branched alkyl chains. Regarding the fluidity at low temperature, the straight alkyl chains compounds show higher pour point than branched alkyl chains ones. The structures and properties of typical ester base oils are shown in Figure 1-7 and Table 1-2, respectively. The relationship between their chemical structures and their physical/chemical properties has been well documented [1].

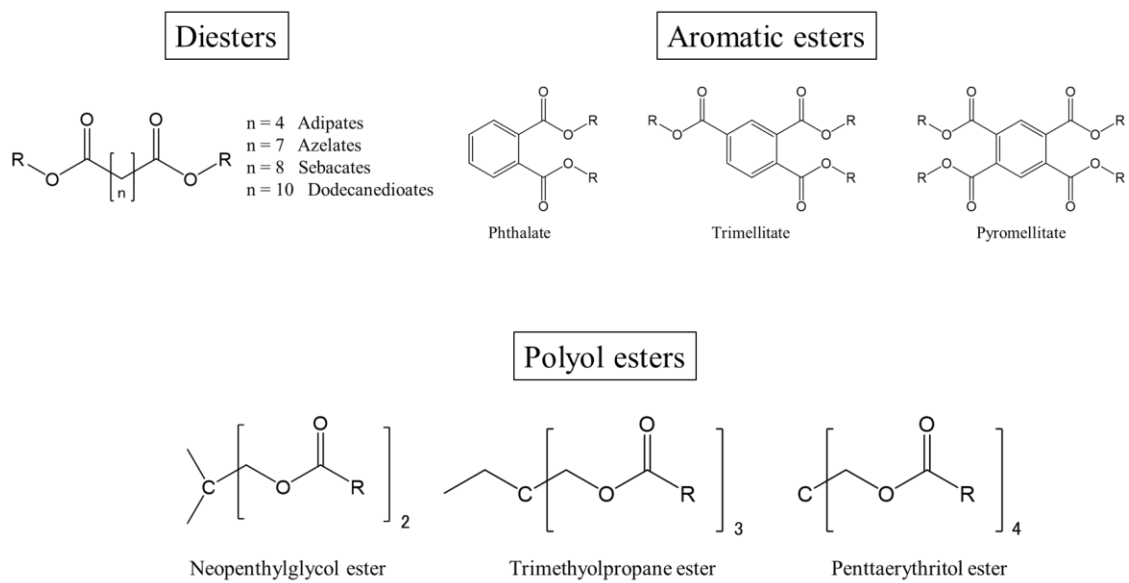


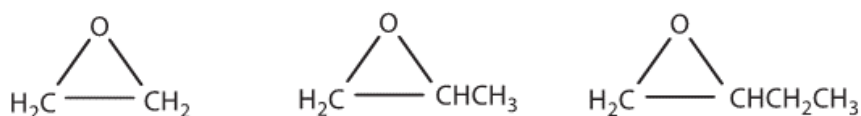
Figure 1-7. Chemical structure of synthetic esters

Table 1-2. Typical properties of ester base oils (adapted from [1])

| Category | Alcohol | Acid | Viscosity at 40°C (mm ² /2) | Viscosity at 100°C (mm ² /2) | Viscosity index | Pour point (°C) | Biodegradability CEC-L-33-A-93 (%) |
|--------------------|-------------------|---------------------------|-------------------------------------------|--------------------------------------------|-----------------|--------------------|------------------------------------------|
| Monoesters | Methyl | Oleic | 4.5 | 1.8 | - | -12 | - |
| | Iso-propyl | Oleic | 5.3 | 2.0 | 221 | -21 | - |
| | Iso-buthyl | Oleic | 6.0 | 2.2 | 219 | -50 | - |
| | 2-ethyl hexyl | Oleic | 8.0 | 2.8 | 238 | -35 | - |
| | Iso-octhyl | Oleic | 9.1 | 2.9 | 192 | -29 | - |
| | Decyl | Oleic | 10.2 | 3.4 | 246 | -3 | - |
| Diesters | 2-ethyl hexyl | Adipate | 8.0 | 2.4 | 124 | -68 | 97 |
| | | Azelate | 10.7 | 3.0 | 137 | 64 | 99 |
| | | Sebacate | 11.8 | 3.1 | 126 | -60 | 96 |
| | | Dodecanediolate | 14.3 | 3.8 | 168 | -57 | - |
| | Iso-decyl | Adipate | 15.2 | 3.6 | 121 | -62 | 84 |
| | | Azelate | 18.1 | 4.3 | 151 | -65 | 86 |
| | | Sebacate | 20.2 | 4.8 | 169 | -60 | 100 |
| | | Dodecanediolate | 23.4 | 5.2 | 162 | -41 | 93 |
| | Iso-tridecyl | Adipate | 27.0 | 5.4 | 139 | -51 | 92 |
| | | Azelate | 33.8 | 6.4 | 143 | -55 | 85 |
| | | Sebacate | 36.7 | 6.7 | 141 | -52 | 80 |
| | | Dodecanediolate | 40.7 | 7.6 | 156 | -50 | 76 |
| Aromatic esters | Iso-heptyl | Phthalate | 19.0 | 2.8 | - | -51 | 92 |
| | Iso-octhyl | | 28.8 | 4.5 | 39 | -42 | 69 |
| | 2-Ethyl hexyl | | 26.4 | 4.2 | 21 | -43 | 64 |
| | Iso-nonyl | | 38.5 | 5.3 | 50 | -44 | 53 |
| | Iso-decyl | | 45.5 | 5.8 | 49 | -47 | 69 |
| | Iso-tridecyl | | 80.5 | 8.2 | 56 | -43 | 46 |
| | nC7/nC9 | Trimetric anhydride | 48.8 | 7.3 | 108 | -45 | 69 |
| | nC8/nC10 | | 51.9 | 8.1 | 126 | -45 | 61 |
| | nC9/nC11 | | 72.5 | 9.8 | 116 | -45 | 3 |
| | 2-Ethyl hexyl | | 90.2 | 9.7 | 82 | -36 | 14 |
| | Isodecyl | | 144.2 | 13.0 | 79 | -30 | 0 |
| | Isotridecyl | | 305.2 | 20.4 | 76 | -9 | 9 |
| | 2-Ethyl hexyl | Pyrometlilic anhydride | 172.0 | 16.3 | 98 | -27 | 3 |
| Polyolesters | Neopentylglycol | nC7 | 5.6 | 1.9 | - | -64 | 100 |
| | | nC9 | 8.6 | 2.6 | 145 | -55 | 97 |
| | | nC8/nC10 | 8.4 | 2.5 | 129 | -33 | 100 |
| | | Oleic | 30.0 | 7.0 | 207 | -24 | 100 |
| | | 2 Ethyl hexanoic | 7.0 | 2.0 | 76 | -54 | - |
| | Trmethylolpropane | nC7 | 13.9 | 3.4 | 120 | -60 | 100 |
| | | nC9 | 21.0 | 4.6 | 139 | -51 | 100 |
| | | nC8/nC10 | 20.4 | 4.5 | 137 | -43 | 96 |
| | | Oleic | 46.8 | 9.4 | 190 | -39 | 100 |
| | | 2 Ethyl hexanoic | 24.8 | 4.4 | 75 | -50 | - |
| | Penthaerythritol | nC7 | 22.2 | 4.9 | 151 | -40 | 100 |
| | | nC9 | 32.2 | 6.1 | 140 | -7 | 100 |
| | | nC8/nC10 | 30.0 | 5.9 | 145 | -4 | 100 |
| | | Oleic | 64.0 | 10.0 | 141 | -21 | 98 |
| | | 2 Ethyl hexanoic | 44.8 | 6.4 | 88 | 8 | - |

1.1.1.4 Poly alkylene glycols, PAG (Group V)

Poly alkylene glycols (PAGs) have a high viscosity index (180 to 400), excellent fire resistance and biodegradability. In addition to these properties, PAGs burn off with leaving no deposit unlike other base oils. Therefore, PAGs are used for many applications such as fire-resistant water glycol hydraulic fluids, two-cycle engine oils and environmentally friendly lubricants. The initial use of PAGs for lubricants began in the 1950s. PAGs are manufactured by the polymerization reaction of alkylene oxides (polyaddition) shown in Figure 1-8. The selection of oxides determines the water/oil solubility: PAGs produced from ethylene oxide or propylene oxide are water soluble, while PAGs produced from butylene oxide are oil soluble.



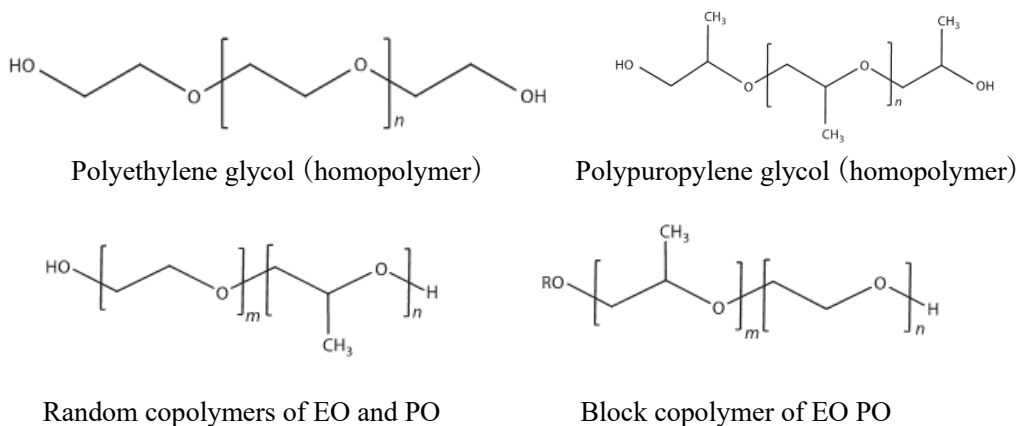
Ethylene oxide (EO)

Propylene oxide (PO)

Butylene oxide (BO)

Figure 1-8. Different types of alkylene oxide used for the synthesis of PAGs [6]

Figure 1-9 illustrates three types of PAGs: homopolymers, random copolymers and block copolymers. Homopolymer PAGs are produced from single oxides. Random copolymer PAGs contain more than two types of alkylene oxides, and each alkylene oxide is randomly distributed in the structures. Block polymer PAGs contain two or more homopolymers fashions.



Polyethylene glycol (homopolymer)

Polypuropylyene glycol (homopolymer)

Random copolymers of EO and PO

Block copolymer of EO PO

Figure 1-9. Types of PAGs: homopolymers, random copolymers and block copolymers [1]

1.1.1.5 Biodegradability of base oils

Figure 1-10 summarizes the biodegradability of each base oil introduced in the above sections. Mineral base oils have poor biodegradability. The poly- α -olefins biodegradability depends on several parameters including their viscosity: lower viscosity PAOs (PAO2 and PAO4) have excellent biodegradability, whereas higher viscosity PAOs (PAO6-PAO100) have poor biodegradability. Natural ester base oils have high biodegradability, however the synthetic ester base oils biodegradability depends on their alkyl chain structures. The synthetic ester base oils with straight alkyl structures have high biodegradability while that of the branch alkyl structures is much lower. EO type of PAG have high biodegradability.

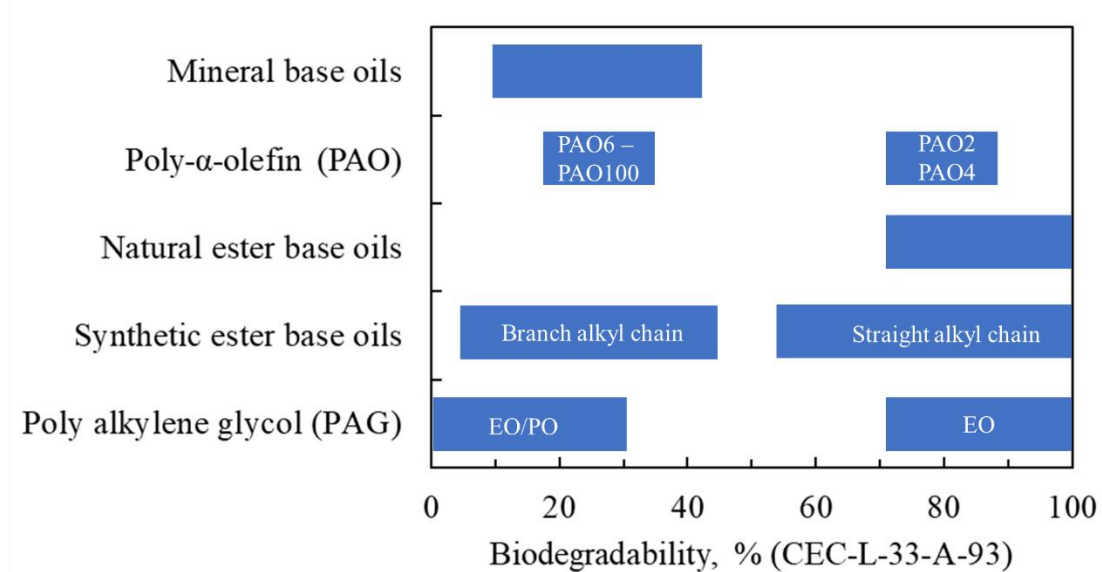


Figure 1-10. Biodegradability of lubricant base oils (summarized from [1, 7-9])

Among the different base oils of the Figure 1-10, the low viscosity PAOs, the synthetic ester base oils with straight alkyl chains, the natural ester base oils and the PAG (EO type) have excellent biodegradability. However, the viscosity of PAO2 and PAO4 is quite low and the natural ester base oils have low thermal stability. PAG (EO type) is water soluble, therefore, the seal compatibility of PAG is completely different from mineral base oils, and this should be taken into account in the design of machine system with poly alkylene glycol. From these reasons, synthetic ester base oils are the most accepted for biodegradable lubricants.

In addition to biodegradability, synthetic ester base oils have superior physical/chemical properties (viscosity index, pour point and oxidation stabilities) compared to mineral base oils [1, 10]. Therefore, recently, demands for synthetic ester base oils have been increasing for many applications [11].

1.1.2 Lubricant additives

Although properties of base oils govern the performance of lubricants, they are usually insufficient for practical applications such as modern engines, gears and machinery. Most lubricants contain additives used to improve the general performance of the lubricant. Lubricant additives are organic or metal-containing organic compounds which can dissolve in base oils. Many lubricants additives have been developed since the 1910s. The history of lubricant additives is described in Figure 1-11. The numbers written in red between brackets indicates sections in which each additive is described.

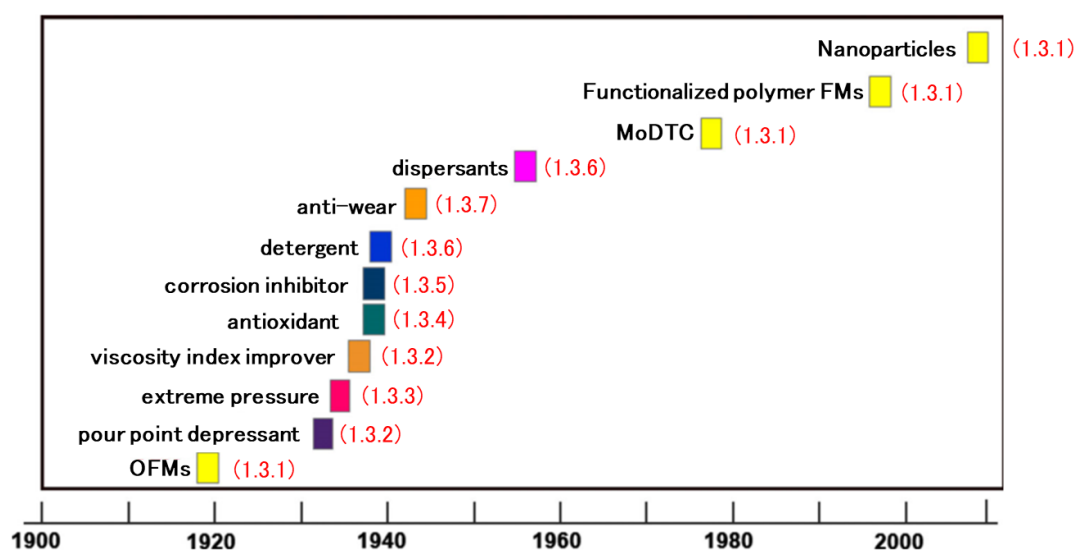


Figure 1-11. The chronology of development of lubricant additives (adapted from [12])

1.1.2.1 Friction modifiers

Friction modifiers (FMs) have been used for automatic transmission fluids, slideway lubricants, multipurpose tractor fluids and slip gear oils in order to obtain a smooth shift from a static to dynamic mode or to reduce noise and friction heat [6]. FMs are generally categorized into 4 groups: organic friction modifiers (OFMs), soluble organo-molybdenum, functionalized polymers, and dispersed nanoparticles [12]. Figure 1-12 shows an example of FM for each family.

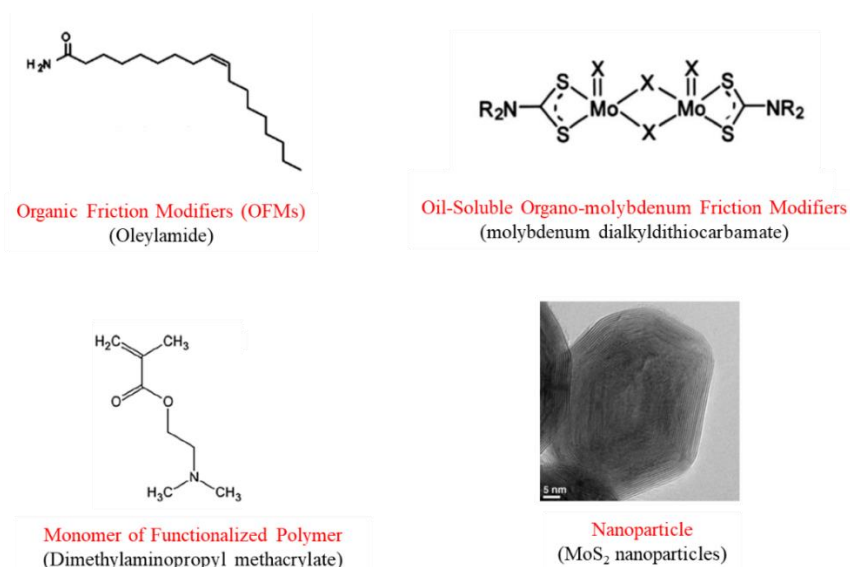


Figure 1-12. Representative examples of FMs additives (adapted from [12, 32])

Fatty acids were first used as OFMs in the 1910s [13], however, they sometimes caused corrosion of bearing metals such as copper, lead and tin [14, 15]. Therefore, amines, amides and esters, which were less reactive against metal corrosion, started to be used instead of fatty acids [16-18].

Molybdenum disulphide (MoS₂) is well known to reduce friction and prevent scuffing of metals, but it is usually difficult to maintain MoS₂ well dispersed in base oils. In order to overcome this problem, oil-soluble organo-molybdenum additives were developed in the 1950s [19, 20] and widely identified as FMs in the 1970s. Grossiord *et al.* analyzed the tribofilm generated from molybdenum dialkyldithiocarbamate (MoDTC). The authors observed the formation of MoS₂ sheets from MoDTC as shown in Figure 1-13 [21].

It is well recognized that polymer additives such as polymethacrylates (PMAs, details are described in 1.3.2) are used to improve the viscosity index of lubricants. In addition to this function, Okrent *et al.* found that these polymers reduce friction and wear in boundary conditions [22, 23]. In recent studies, functionalized polymer additives, which can adsorb on metal surfaces, have been designed as FMs and their tribological behaviors have been studied and reported [24].

In recent years, nanoparticles have received a lot of attention as lubricant additives. Many different

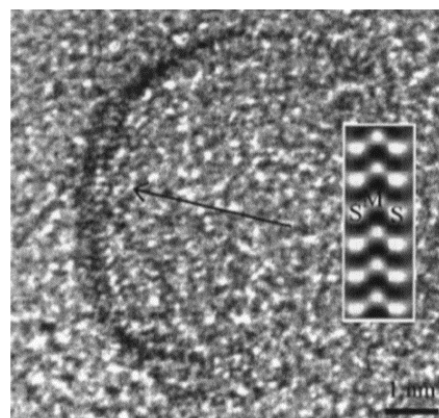


Figure 1-13. HRTEM image of MoS₂ sheets in wear debris from MoDTC tribofilm [21]

types of nanoparticles such as metal oxides, boron oxide and inorganic fullerene-like metal disulfides, have been found to be effective for reducing friction [25, 26]. Fullerenes and their analogue carbon structures have gained great interest as FMs. Gupta *et al.* found that a fullerene dispersion shows similar effectiveness as FMs to graphite and MoS₂. The authors also reported that the effect of fullerenes could be attributed to the formation of a transfer film in a sliding area or to fullerenes acting as “tiny ball bearings” [27]. Inorganic fullerenes (IF), which have fullerene-like morphology of inorganic compounds, have been also focused on. IF-MoS₂ and IF-WS₂ have been reported to show friction- and wear-reducing effects [28, 29]. The behaviors of IF nanoparticles have been observed using Scanning Electron Microscopy (SEM) and *in situ* Transmission Electron Microscopy (TEM). These studies reported a rolling of IF particles at low pressures and a sliding of IF particles, with or without exfoliation, at high pressures on sliding surfaces [30, 31].

1.1.2.2 Viscosity index improvers and pour point depressants

Viscosity Index Improvers (VIIs) are added to reduce the change of lubricant viscosity at low and high temperatures. Polymers such as polymethacrylate (PMA), polyisobutylene (PIB) and olefin copolymer (OCP) are largely used as VIIs to improve the viscosity index of the lubricants. At low temperatures, the molecular chain of VIIs shrink and no significant viscosity change occurs. At high temperature, the chain expands leading to an increase of the lubricant viscosity.

Pour Point Depressants (PPDs) are important for lubricants to keep a fluid state at low temperatures. Wax is generated by the crystal networks of paraffins in base oils at low temperatures. The formation of wax increases the viscosity of the lubricant that changes to a solid state. PPDs prevent the wax formation. PPDs have a similar alkyl chain length to base oils and interfere with the crystallization of paraffin fractions. In general, PMA is used as PPDs.

1.1.2.3 Extreme pressure additives

Extreme pressure (EP) additives are used to prevent scuffing or seizure of parts exposed to high contact pressure. The organic sulphur compounds shown in Figure 1-14 are typical EP additives, which are often used for gear oils and metal working fluids [33]. They form metal sulphide on metal surfaces to prevent metal-metal adhesion. EP performance of the organic sulphur compounds becomes more important with the increasing number of sulphur atoms in the chemical structures. Additionally, ZDDP or other phosphorus compounds which contain sulphur atoms are also efficient as EP additives [34].

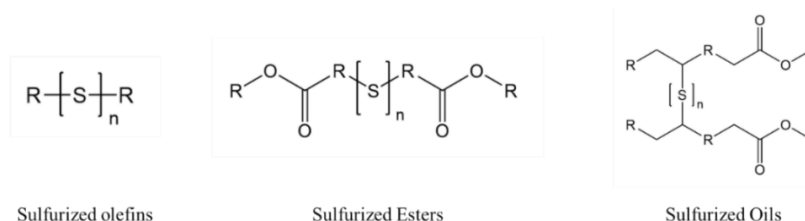
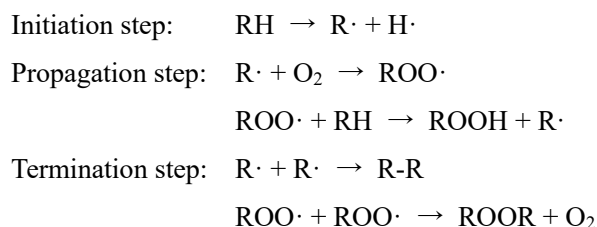


Figure 1-14. Chemical structures of organic sulphur compounds for EP additives

1.1.2.4 Antioxidants

Oxidation is a chemical reaction that occurs in lubricants base oil upon exposure to air. Antioxidants are used in the formulation of lubricants to reduce the rate of oxidation. Oxidation of lubricants can be presented as following elementary steps:



Based on this mechanism, antioxidants are categorized as primary or secondary as explained in the following. The primary antioxidants react with radical species generated from the initiation step and prevent them reaching the propagation step. The secondary antioxidants react with peroxides generated from both the propagation and termination step. As peroxides generate radicals ($\text{ROOH} \rightarrow \text{RO}\cdot + \text{OH}\cdot$ or $\text{ROOR} \rightarrow 2\text{RO}\cdot$) and promote further oxidations, the secondary antioxidants decompose and deactivate them to prevent further oxidations. Hindered phenols and secondary aromatic amines are used as the primary antioxidants and organo-sulphur compounds such as ZDDP are used as the secondary antioxidants [35, 36]. Typical antioxidants are illustrated in Figure 1-15.

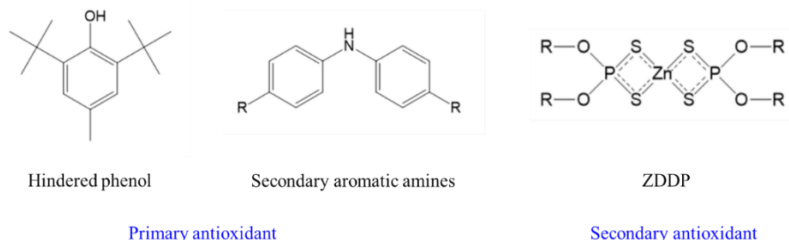


Figure 1-15. Chemical structures of typical antioxidants

The selection of antioxidants depends on the base oils, the application and the temperature of use. It is well known that the combined use of antioxidants is more effective than single use.

1.1.2.5 Corrosion inhibitors

Metal corrosion has been a crucial problem for manufacturers and the economic loss is estimated in billion dollars per year [6]. The mechanism of rust formation was reported by Whiteny in 1903. He stated that oxygen and carbonic acid were essential for rust formation and that basic compounds are effective in preventing corrosion [37]. Baker *et al.* first reported the mechanism of corrosion inhibition by additives in which they stated that inhibitors formed a monolayer as a protective barrier to prevent contact with water or other environments [38]. Thereafter, it was found that the alkyl chain of adsorbed inhibitors are closely packed on the surface as shown in Figure 1-16, and the matched chain lengths between inhibitors and base oils is important to form tight surface packing, which helps inhibitors to adsorb more firmly on the surface [39].

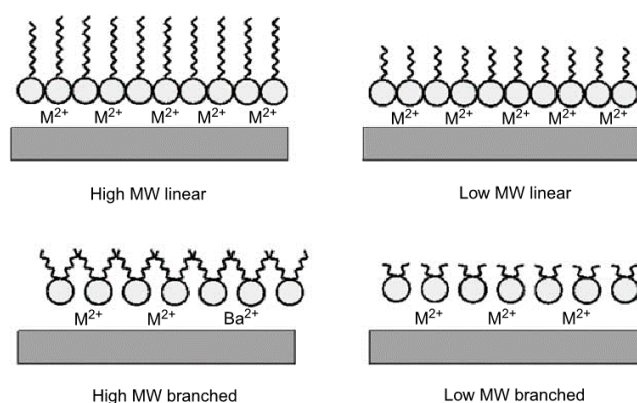


Figure 1-16. Monolayers formed by corrosion inhibitors on the surfaces [11]

Petrolatum, wax, oxidized wax, fatty acid soaps and rosin started to be used as rust preventatives in the 1920s. Then, it was found that sulfonates were useful as rust preventatives. Among them, barium and over-based barium sulfonates have been widely utilized since the second world war. Following these applications, other chemicals such as carboxylates, alkyl amines and phosphates were discovered as rust preventatives, and imidazolines, bezotriazoles, and thiadiazole have been used as the inhibitors of copper or lead corrosion.

1.1.2.6 Dispersants and detergents

Detergents are used to keep clean surfaces of metal parts and neutralize acids generated from fuel combustion and lubricants oxidation. They are mainly applied to engine oils and metal working lubricants [41]. Detergents have micellar structures including basic nano particles (e.g. $CaCO_3$, $MgCO_3$ and $BaCO_3$). They are categorized into three types according to the soap structures: sulfonate, phenate and carboxylate. Detergents often contain metal carbonate and hydroxide as the excess base. The amount of the excess base influences the performance such the cleaning metal surfaces and

neutralizing acids ability, corrosion control. Their general formulae are presented in Figure 1-17.

| | |
|--------------------------------------------------------------------------------------|-------------------|
| $(\text{RSO}_3)_a\text{M} \cdot x\text{M}_b\text{CO}_3 \cdot y\text{M}(\text{OH})_c$ | Basic sulfonate |
| $(\text{RPhO})_a\text{M} \cdot x\text{M}_b\text{CO}_3 \cdot y\text{M}(\text{OH})_c$ | Basic phenate |
| $(\text{RCOO})_a\text{M} \cdot x\text{M}_b\text{CO}_3 \cdot y\text{M}(\text{OH})_c$ | Basic carboxylate |

Figure 1-17. General formulas of detergents [11]

They are classified into three groups according to the basicity: neutral, low over-based and highly over-based detergents. Neutral detergents contain no carbonate: x and y are zero in Figure 1-17. Low over-based detergents have a small number of x and y , which show a base number (BN) of approximately 50 mgKOH/g. Highly over-based detergents have a large amount of carbonate: x is large and y is small. The structure of highly over-based detergents is shown in Figure 1-18.

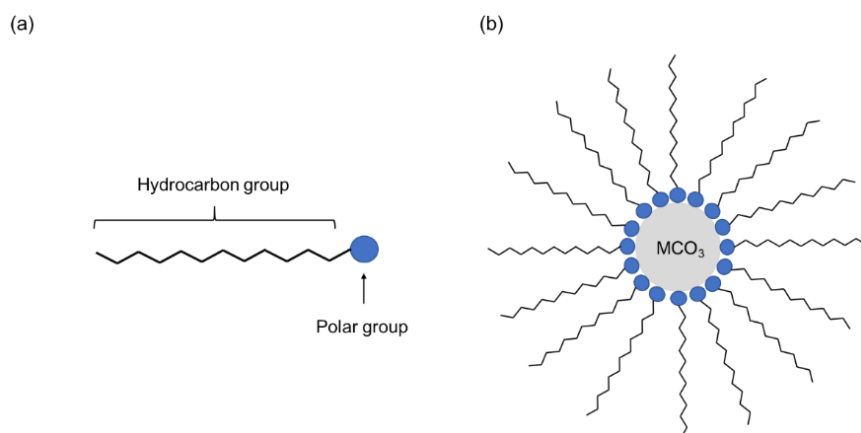


Figure 1-18. Structure of a polar acid (a) and an over-based detergent (b)

Dispersants also have the similar role to detergents, despite dispersants have less neutralizing ability than detergents. Their functions are more focused on suspending deposits such as diesel engine soot and wear particles in lubricants. Dispersants contain no metal compounds and typical examples are shown in Figure 1-19. In general, the combination of detergents and dispersants improve the neutralizing and suspending ability of lubricants.

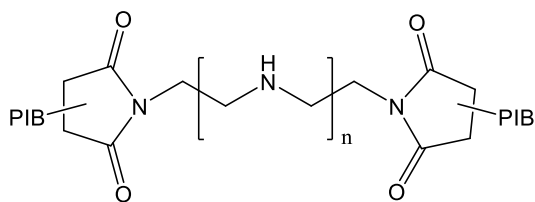


Figure 1-19. Chemical structure of a dispersant: bis-polyisobutenyl succinimide polyamine

1.1.2.7 Anti-wear additives

Anti-wear (AW) additives are used to protect surfaces of machine parts. In general, compounds including phosphorus atoms are used as AW additives, because they easily form under friction phosphorus based tribofilm that reduce wear [6]. Among phosphorus compounds, Tricresyl phosphate (TCP) and Zinc dialkyl dithiophosphate (ZDDP) have longer history than others. TCP has been used for aviation and industrial applications since its introduction in the 1940s [41, 42]. ZDDP has been used mainly for engine oils since 1960s [43-45]. ZDDP acts not only as AW additives but also as antioxidants and corrosion inhibitors, therefore, ZDDP has been the most preferred AW additive for engine oils.

The chemical structures of typical AW additives are illustrated in Figure 1-20. Alkyl phosphate and phosphite are also effective to reduce wear. Especially, dialkyl phosphate and dialkylphosphite are well known to show excellent AW performance [46]. The research concerning AW additives is outlined in next section (1.4).

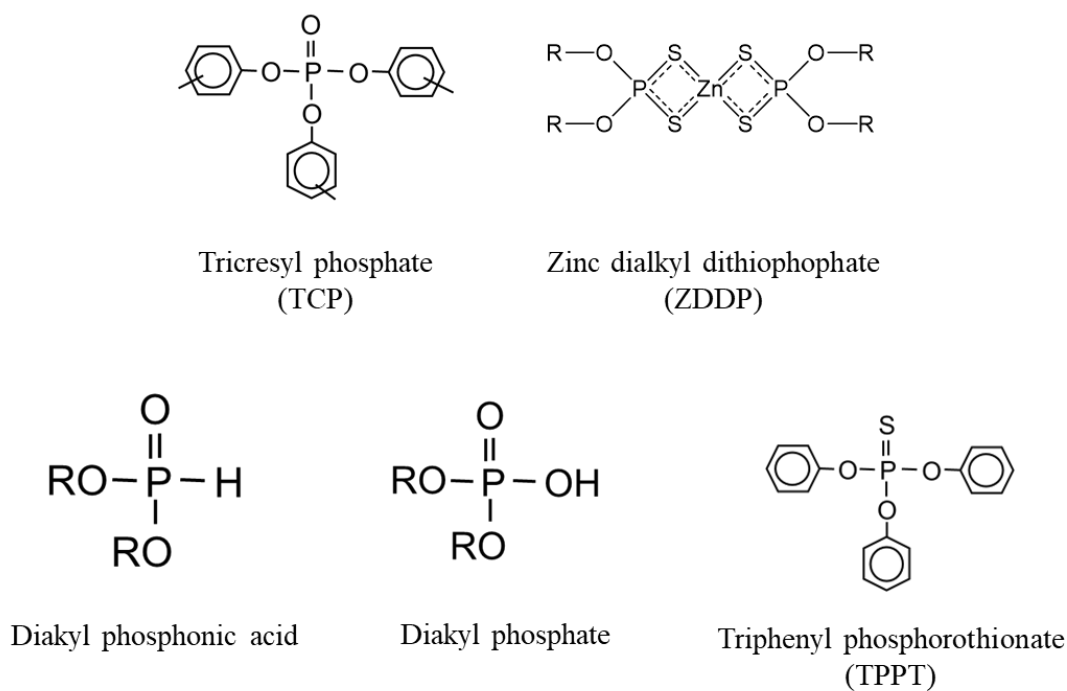


Figure 1-20. Chemical structures of typical AW additives for lubricants

1.2 Literature review of AW additives

Among lubricant additives, AW additives are of prime importance for lubricants, because mechanical damages by wear become serious problems to keep machines running or operating without interruptions. A lot of effort has been made to design AW additives that meet each requirement in machinery and their mechanisms have also been investigated by many researchers. Most commercial lubricants have been designed using mineral base oils because of their availability and low cost, therefore interests have been focused on the behavior of AW additives in these base oils (or PAOs as the model of mineral base oils). Recently, some researchers have investigated the behavior of AW additives in ester base oils and discussed the difference between blends in mineral or in ester base oils. In this section, firstly, the mechanisms of tribofilm formation of conventional AW additives in mineral base oils are presented. In a second step, those in ester base oils will be introduced.

1.2.1 Research on AW additives in mineral base oils

Most studies on AW additives have been carried out in mineral base oils. Among AW additives, TCP and ZDDP have been well studied, because they are used for commercial lubricants such as machine tools, aircrafts and automobiles. Other phosphorus AW additives, for example, dialkyl phosphite, dialkyl phosphate and triphenyl phosphorothionate, have also been used. Their antiwear performance and action mechanisms were investigated. For each additive, the AW protection is obtained thanks to the formation of a phosphate based tribofilm limiting adhesion between steel rubbing surfaces. The antiwear mechanism of typical AW additives (shown in Figure 1-20) in mineral base oils are described on the following sections from 1.4.1.1 to 1.4.1.5.

1.2.1.1 Tricresyl phosphate (TCP)

TCP was first designed in the 1850s, and started to be produced commercially during the second decade of the 19th century [6]. The research on TCP as AW additives started to be published in the 1940s [41, 47, 48]. For understanding the action mechanism of TCP, much research has been carried out. It is still under discussion [47].

Tribofilm composition of TCP

Early studies carried out with electron diffraction analysis identified that a mixture of ferric phosphate (FePO_4) and ferric phosphate dihydrate ($\text{FePO}_4 \cdot 2\text{H}_2\text{O}$) were detected on the worn surfaces lubricated with TCP [49].

Gauthier *et al.* reported that TCP could generate two types of tribofilms, a brown and a blue colored films, after a friction test performed with steel discs [50]. The brown colored film was formed at the initial stage of the friction test and the blue colored film was generated at a later stage when the wear

rate decreases. The brown and blue colored films were characterized using Auger Electron Spectroscopy (AES) and X-ray photoelectron spectroscopy (XPS). This research reveals that the brown colored film contains a mixture of ferrous oxide and ferrous phosphate, and that the blue colored film is composed of polymeric phosphate species such as $[-P(=O)(OR)-O-]_n$.

Sheasby *et al.* also found the formation of a colored tribofilm generated from TCP during wear tests using a lubricant containing TCP [51]. This study indicates that the blue colored film appears when the superior wear protection is observed in the wear test, whereas the darker film appears when the lubricant shows less wear protection. In this test, the TCP tribofilm contains iron, indicating the presence of iron phosphate.

The chemical structure of TCP film was characterized using Fourier transform infrared (FT-IR) spectroscopy by many researchers. For example, Johnson *et al.* analyzed the thermal films which were prepared on steel surfaces at 325 °C for 96 h with TCP, and reported that the peaks at 950 cm^{-1} and 1050 cm^{-1} assigned to the polyphosphate were observed, indicating the polymerization reaction of TCP on the steel surfaces [52]. Sasaki *et al.* studied the tribochemical reaction of TCP using *in-situ* Attenuated Total Reflection (ATR) infrared spectrometer. This experiment indicated that the various phosphate species such as PO^{2-} , PO^{3-} and PO^{4-} were formed under friction [53].

In order to clarify the chemical composition of TCP tribofilm, many efforts have been made by researchers and various phosphorus compounds, shown in Figure 1-21, were identified. However, the chemical composition seems to depend on friction conditions, therefore it is still difficult to determine the exact chemical structure of TCP tribofilm.

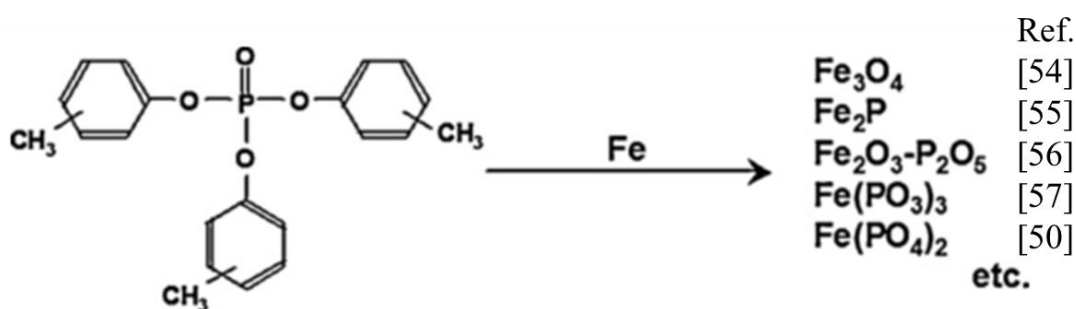


Figure 1-21. Possible chemical composition of TCP tribofilm on iron surfaces (adapted from [53])

TCP tribofilm formation mechanisms

The formation mechanism of TCP tribofilm has been studied since the 1960s. Although the mechanism is still under discussion, several hypotheses were proposed and detailed in the following:

(i) acid formation, (ii) thermal decomposition, (iii) hydrolysis and (iv) surface catalysis effect.

(i) Tribofilm formation induced by acid phosphate formation

Godfrey suggested that the iron phosphate film was generated by the reaction under friction between the iron surface and phosphoric acid: phosphoric acid can be considered as an impurity of TCP or formed by the decomposition of TCP [48]. Bieber *et al.* also confirmed the presence of phosphoric acid in commercial TCP and found that the AW performance of TCP was significantly related to the amount of acid phosphate as an impurity in TCP [58]. TCP acts as the source of phosphoric acid. It is at the origin of the formation of the iron phosphate film that helps preventing wear. Figure 1-22 represents the tribofilm formation mechanism induced by acid phosphate on iron surfaces.

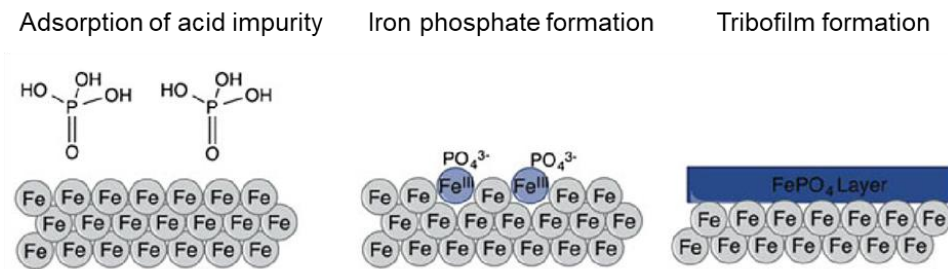


Figure 1-22. TCP tribofilm formation mechanism by acid phosphate

(ii) Tribofilm formation by thermal decomposition

Saba *et al.* suggested that the thermal decomposition of TCP could occurred due to the cleavage of the P-O bond or the C-O bond to form a tribofilm [59]. Sung and Gellman proposed thermal decomposition mechanism as shown in Figure 1-23. Firstly, TCP adsorbs onto metal surfaces. Secondly, TCP generates methylphenoxy intermediates via P-O bond scission, and then a considerable amount of phosphorus and oxygen accumulates on the surfaces, resulting in the formation of a tribofilm.

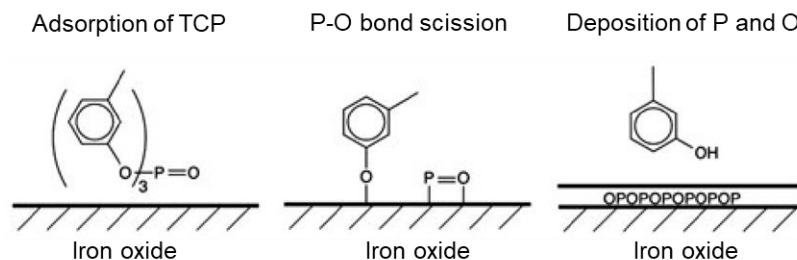


Figure 1-23. TCP tribofilm formation mechanism by thermal decomposition

(iii) Tribofilm formation by hydrolysis

Besides lubricant additives such as AW additives, water also exists in base oils because it can generally dissolve in base oils at the concentration of 10 - 2000 ppm, depending on the types of base oils and temperature. Many researchers reported the importance of water in activating TCP. Klaus and Bieber reported that hydrolyzed TCP, including mono-cresyl phosphate and di-cresyl phosphate, showed the same level or better AW performance than non-treated TCP [58]. The authors also reported that the higher concentrations of hydrolyzed species from TCP had better AW performance than TCP. Their results suggested the mechanism of tribofilm formation by TCP and H₂O shown in Figure 1-24.

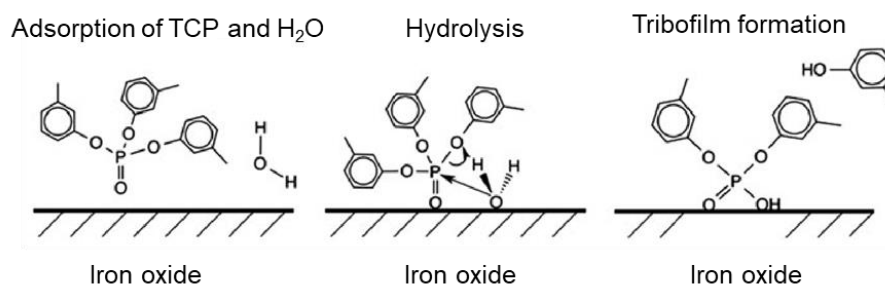


Figure 1-24. TCP tribofilm formation mechanism induced by hydrolysis

(iv) Tribofilm formation catalyzed by metal surfaces

Bertrand studied the effect of metal surfaces for the decomposition reaction of TCP [59]. This study demonstrated that TCP starts to decompose and generates cresol at 150 °C. Furthermore, TCP with NaOH aqueous solution, generates cresol at 110 °C, suggesting that NaOH promotes the decomposition of TCP. TCP heated at 110 °C with iron powder shows a similar result to the effect of NaOH, forming cresol at a lower temperature than TCP alone, whereas TCP heated at 110 °C with nitride powder generates no significant cresol. At the end, Bertrand concluded that iron surfaces act as base catalyst like NaOH to promote the decomposition reaction of TCP, and lowered the decomposition temperature of TCP.

Wheeler *et al.* investigated the decomposition mechanism of TCP on iron and gold surfaces using XPS [60]. The following results were obtained:

- 1) At room temperature, TCP adsorbs on iron surfaces chemically with the formation of PO-Fe and CO-Fe bonds, on the other hand, TCP adsorbs on gold surfaces physically without dissociation of chemical bond of TCP structure.
- 2) TCP desorbs from gold surfaces without decomposition reaction at 200 °C. The decomposition reaction of TCP is more dominant than desorption on iron surfaces at about 200 °C, forming iron phosphate or an organic phosphate after the elimination of at least one tolyl group of TCP.

From this study, the decomposition mechanism of TCP on iron surfaces was proposed as presented in Figure 1-25. TCP firstly adsorbs onto iron surfaces and forms the coordination with iron oxides. The

coordination bond decreases the electrophilicity of the phosphorus atom. Then, the nucleophilic attack of oxygen in iron oxides results in the elimination of a cresyl group.

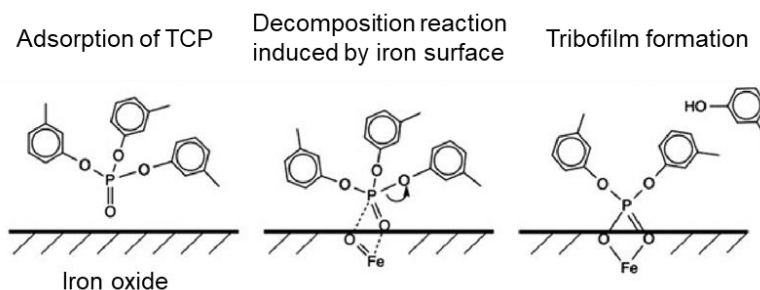


Figure 1-25. TCP tribofilm formation mechanism catalyzed by iron oxides

1.2.1.2 Zinc dialkyldithiophosphate (ZDDP)

Zinc dialkyldithiophosphate (ZDDP) was developed in the 1930s. ZDDP is another well-known and very efficient AW additive that has been used for almost a century. In addition ZDDP acts as an antioxidant and corrosion inhibitor, therefore, it has been used in many lubricants, especially in automotive engine oils. Many effort have been made to fully understand the action mechanism of ZDDP in steel-steel contacts since the 1950s. The characteristic and compositions of ZDDP tribofilms are well documented [43], however, the tribofilm formation mechanism is still under discussion.

Tribofilm composition of ZDDP

ZDDP tribofilm has been characterized using surface analysis techniques such as XPS, Raman spectroscopy, X-ray absorption fine structure analysis (EXAFS), X-ray absorption near-edge spectroscopy (XANES) and SIMS (Secondary ion mass spectrometry).

XPS is an effective tool in analyzing atomic compositions and chemical states of ZDDP tribofilm. From the oxygen O1s signal in XPS spectra, non-bridging oxygen (NBO: P-O⁻, P=O and P-O-H) and bridging oxygen (BO: P-O-P) can be identified [61, 62]. The calculation of BO/NBO ratios in tribofilm makes possible the identification of the structures of phosphate species shown in Figure 1-26.

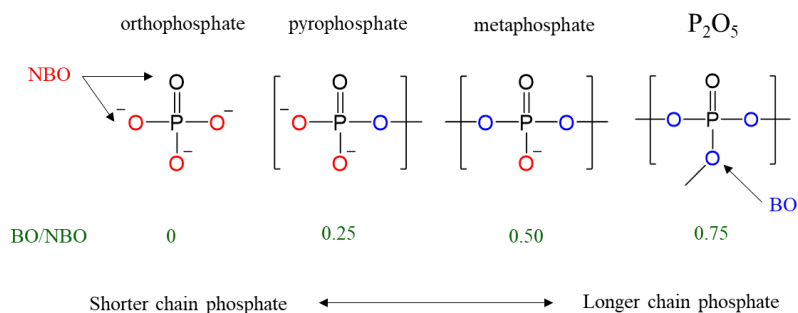


Figure 1-26. BO/NBO ratios of phosphate species in different types of phosphate glasses

Heuberger *et al.* calculated the BO/NBO ratio of ZDDP tribofilm at various contact pressures and found that ZDDP forms shorter chains at higher contact pressures [63]. The combinational analysis using XPS and XANES reported that ZDDP tribofilm contains longer chain polyphosphates (meta phosphate) in the outermost surface, and shorter chains (orthophosphate and pyrophosphate) near the metallic surfaces [64, 65]. Depth profiles of atomic compositions of ZDDP tribofilms can also be obtained by XPS using ion-beam sputtering. Depth profiles have revealed that ZDDP tribofilm has mixed structures including zinc and iron phosphate, and sulphides [66].

Raman spectroscopy is also a useful technique to analyze phosphate polymerization and structure changes, because it can distinguish NBO and BO. Gauvin *et al.* studied by Raman spectroscopy the effect of the contact pressure on the phosphate chains length using zinc phosphate glasses as a model of ZDDP tribofilm. The authors reported that short-chain zinc pyrophosphate and orthophosphate did not polymerize at high pressure [67, 68]. Mosey *et al.* showed that there is a change of metallic cation coordination in the phosphate glass under pressure that could explain the durability of ZDDP tribofilm under severe conditions [69, 70].

EXAFS and XANES confirmed that ZDDP tribofilms contain iron (III) and zinc (II) phosphate glass. Studies suggest that the iron atoms in the phosphate glass could arise from the reaction of ZDDP with Fe_2O_3 particles generated during friction through a “digestion like phenomenon” to form a mixed Fe/Zn phosphate glass, as shown in Figure 1-27 [71, 72].

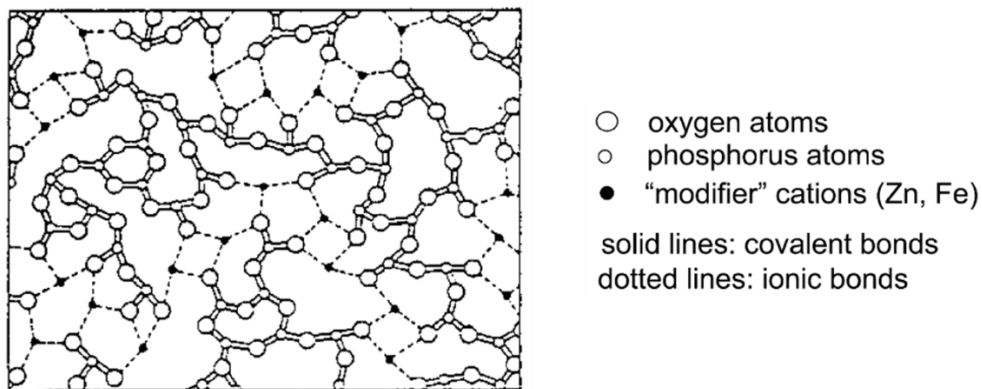


Figure 1-27. Arrangement of atoms in ZDDP tribofilm [72]

Bell *et al.* analyzed ZDDP tribofilm generated from a deuterated ZDDP using SIMS [73]. This study revealed that hydrocarbons on the tribofilm derives from the ZDDP, not from the base oil. Minfray *et al.* characterized ZDDP tribofilm by SIMS, and reported that ZDDP tribofilm was made of an iron and zinc phosphate matrix containing sulphide species, and that no iron oxide was detected at the interface of the tribofilm with the steel substrate [74]. This result supports the study using XANES [71, 72]. Crobu *et al.* succeeded in analyzing the chain length of zinc polyphosphate glasses using SIMS [75].

In addition to the chemical composition of ZDDP tribofilm, the physical properties were also investigated. Studies using SEM (Scanning Electron Microscopy) and AFM (Atomic Force Microscopy) revealed that ZDDP tribofilms have heterogeneous structures, which have a fragmentary structure with microscale pads and valleys. Nicholls *et al.* reported that pad regions of ZDDP tribofilms have longer-chain polyphosphates and that valleys regions have shorter-chain polyphosphates [76].

From the results using surface analysis techniques, Spikes proposed the structure of ZDDP tribofilms, as shown in Figure 1-28 [43].

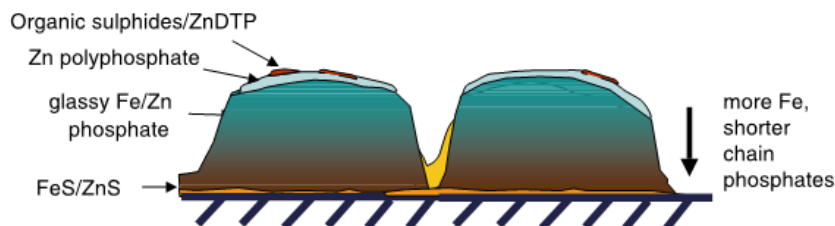


Figure 1-28. Schematic diagram of ZDDP tribofilm [43]

The scale of normal to the surface is about 100 times larger than that of horizontal. ZDDP tribofilms are 1/100th flatter than the model shown here.

ZDDP tribofilm formation mechanisms

Dickert *et al.* proposed the mechanism whose reaction starts with the removal of alkyl chains of ZDDP by a thermal decomposition process [77]. The author noted that the thermal stability of ZDDPs decreases with the increase of the number of β -hydrogen atoms, resulted in the lower stability of secondary ZDDPs than primary ones.

Spedding *et al.* suggested the mechanism induced by hydrolytic decomposition process of ZDDPs. In this process, ZDDPs react with water, and then the phosphoric acid species are formed. The species react with each other and generate zinc polyphosphates [78].

Willermet *et al.* proposed a thermo-oxidative decomposition process shown in Figure 1-29. ZDDPs generates various types of chemicals when ZDDPs work as antioxidants. The author suggested that these chemicals are precursors of ZDDP tribofilm [79].

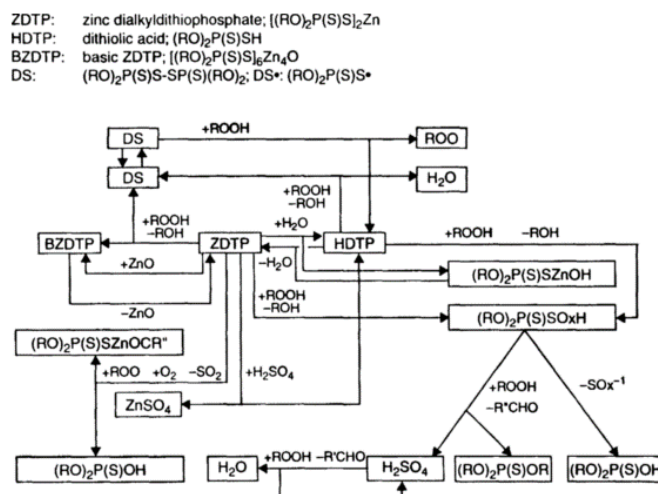


Figure 1-29. Thermo-oxidative decomposition process of ZDDPs [81]

Martin *et al.* introduced the HSAB (Hard and Soft Acid and Base) principle to explain the formation mechanism of ZDDP tribofilm [80, 81]. In this mechanism, firstly, thermally induced films, which contains long chain zinc phosphates, are generated on metal surfaces. Then, the film ‘digests’ wear debris of iron oxides, leading to the formation of short chain zinc and iron polyphosphates. The concept of iron oxide ‘digestion’ by zinc polyphosphate is based on the HSAB principle; the hard acid (Fe^{3+}) prefers to react with the hard base (phosphates) here.

The formation mechanism of ZDDP tribofilms has been discussed for over a half of century. Many hypotheses have been proposed from various points of view such as thermal, hydrolysis and thermo-oxidative decomposition process.

1.2.1.3 Dialkyl phosphites

Forbes *et al.* studied the tribological properties of dialkyl phosphites in mineral base oils using a four-ball machine, and discussed the effect of alkyl chain length of dialkyl phosphites on AW and EP performance [82]. They summarized the relationship between the tribological properties of dialkyl phosphites and the alkyl chain length, as shown in Figure 1-30. The results revealed that dialkyl phosphite with longer alkyl chains had better AW performance, whereas that of shorter alkyl chains showed superior EP performance. The authors suggested that this difference was strongly related to the hydrolysis reactivity of dialkyl phosphites. The dialkyl phosphites with short alkyl chains are decomposed easily and activate metal corrosion by phosphoric acid salts, thus preventing scuffing of metal surfaces. On the contrary, longer alkyl chains react on metal surfaces more slowly and generate a polymerized phosphorus based tribofilm, thus reducing wear.

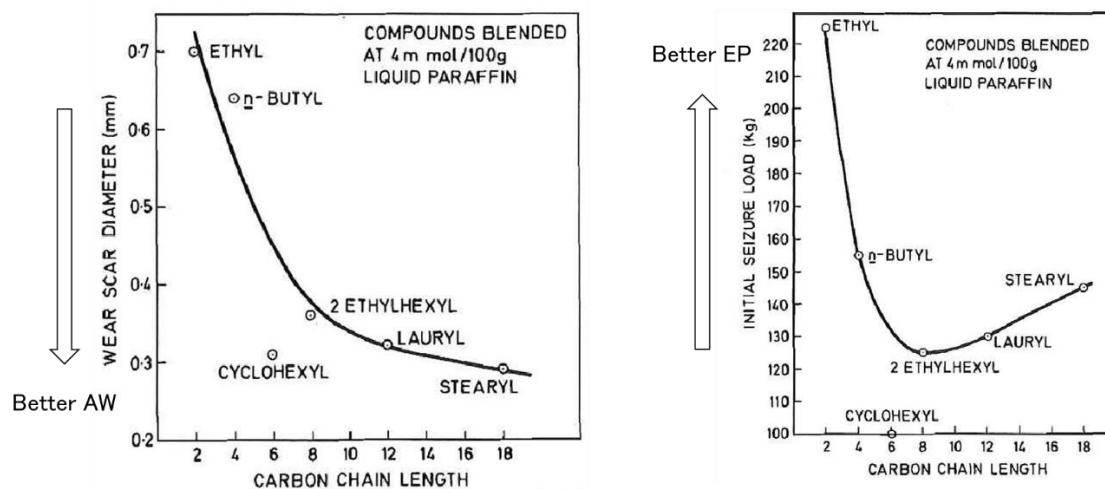


Figure 1-30. Effect of alkyl chain length of dialky phosphites on AW and EP performance [82]

Di-cyclohexyl phosphite deviated from the trend to di-n-alkyl phosphite, as shown in Figure 1-20. In addition, Minami *et al.* also found that di-cyclohexyl phosphite has better AW performance than di-n-hexyl phosphite. He proposed the following reaction mechanism (Figure 1-31) [83]. Regarding tribofilm formation, the key reaction for di-cyclohexyl phosphite was thermolysis, but that of di-n-alkyl phosphite was hydrolysis as proposed by Forbes *et al* [82]. The research by Forbes and Minami revealed that the superiority as AW or EP additives was due to alkyl chain structures of dialky phosphites.

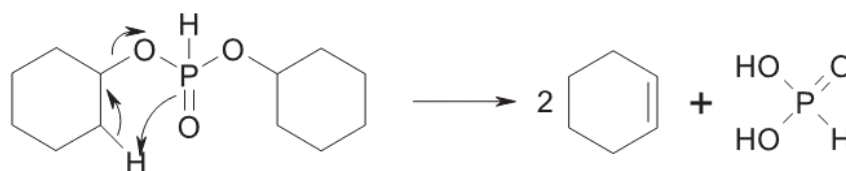


Figure 1-31. Decomposition mechanism of di-cyclohexyl phosphite [80]

1.2.1.5 Others

Zinc dialkyl phosphates (ZDPs), which does not contain sulfur, have attracted attention from environmental aspects, because the replacement of ZDDPs with ZDPs enable engine oils to reduce the amount of sulfur. Dorinson firstly reported the AW properties of ZDPs. In this study, ZDPs showed the equivalent AW performance of ZDDPs, but the author pointed out the poorer solubility of ZDPs in base oils than ZDDPs, which might affect practical uses [92]. The presence of sulfur in ZDDP can affect the activity of the automotive exhaust catalysts [93, 94], which is not the case with the sulfur-free ZP additive.

The tribological performance of dialkyl phosphonate and dialkyl phosphophosphate were investigated by Barber [95], but their AW properties were moderate and less effective than TCP. Forbes *et al.* concluded that the key step of AW mechanism was decomposition of AW additives to form acid phosphate, while phosphonates and phosphinates (Figure 1-33) are potential precursors of boundary film, they have not well applied in lubricant industry so far [96]. Therefore, the application of dialkyl phosphonate and dialkyl phosphophosphate to lubricants are rare, although they are often used for flame retardant materials [97].

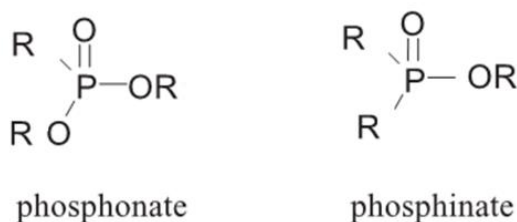


Figure 1-33. Chemical structures of phosphonate and phosphinate which have P-C bond

1.2.1.6 Overview of research on AW additives in mineral base oils

As mentioned above, various AW additives have been developed and their action mechanisms were studied by many researchers. From these investigations, a general mechanism of AW additive in mineral base oils can be summarized as shown in Figure 1-34. AW additives have polar structures that allows adsorption onto metal surfaces. Mineral base oils that consist of hydrocarbons have non-polar structures. Hence, AW additives can adsorb onto metal surfaces far more effectively than mineral base oils, and then form a tribofilm by a chemical reaction under friction (tribochemical reaction) to reduce wear.

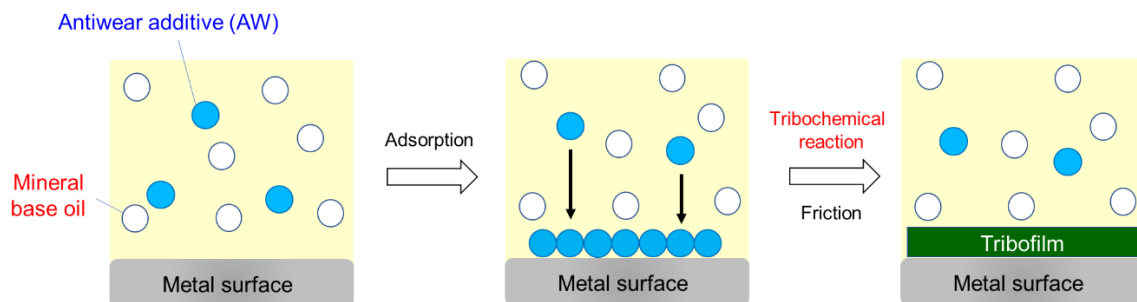


Figure 1-34. Action mechanism of AW additives in mineral base oils

In order to understand the action mechanisms of AW additives, tribofilm compositions have been analyzed using many surface analysis techniques. Various studies have shown that the tribofilms generated from phosphorus AW additives contain amorphous phosphates, which have different chain lengths, and iron/zinc polyphosphates. Phosphorus and sulphur containing AW additives such as ZDDP generate tribofilms composed of phosphates and metal sulphides. Thus, the chemical composition and morphology of tribofilms have been well investigated and understood.

However, tribofilm formation mechanisms are still under discussion. While many proposed mechanisms based on thermal decompositions, hydrolysis, thermooxidation decomposition, HSAB and catalytic effects by metal surfaces have been discussed, it is clear that AW additives are activated by oxygen or oxidized metal surfaces and that the way they are activated depends on conditions where lubricants are used.

Most research about action mechanisms of AW additives in mineral oils have been focused on how AW additives themselves react on metal surfaces and form tribofilms. The effect of mineral base oils is not usually considered, because they do not adsorb on metal surfaces, and do not form an effective tribofilm under boundary lubrication regime.

1.2.2 Research of phosphorus AW additives in ester base oils

As stated in the previous section, mineral base oils have non-polar structures, therefore, their adsorption capabilities and AW performance can be ignored. On the other hand, ester base oils, which have ester groups, have polar structures, and it is reported that they show better AW properties than mineral base oils, because they adsorb and form a monolayer film on metal surfaces that contributes to reduce the wear [98]. Therefore, their influence should be considered when mechanisms of AW additives are discussed. Figure 1-35 illustrates a possible action mechanism of AW additives in ester base oils. It is expected that competitive adsorption between AW additives and ester base oils may occur on metal surfaces. In addition, polar base oils may interact with AW additives, resulting in that base oils-AW additives interactions interfere with adsorption capabilities of AW additives.

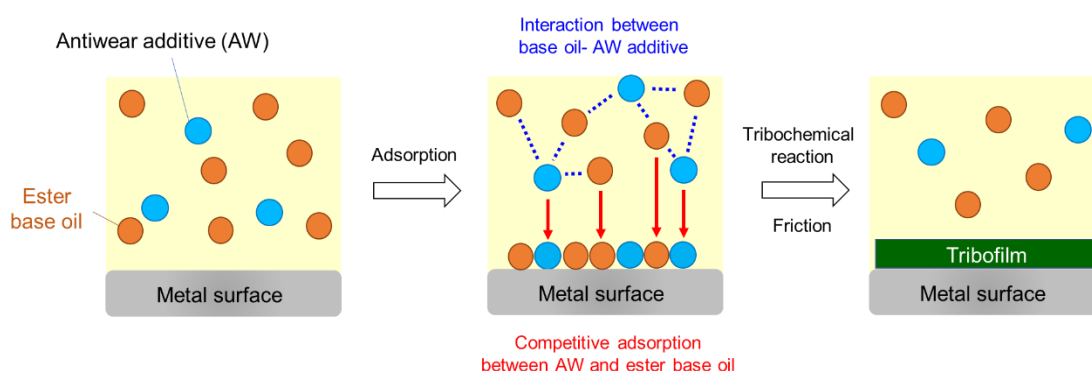


Figure 1-35. Action scheme of AW additives in ester base oils

The competitive adsorption and ester base oils-AW additives interactions probably affect the AW performance of the additive in ester base oils compared to what happens in mineral base oils. Few research on AW additives for ester base oils has been reported in the literature. Studies about AW additives for ester base oils are introduced in the following sections from 1.3.2.1 to 1.3.2.3.

1.2.2.1 AW performance of phosphorus additives in ester base oil

Hall investigated the AW performance of various phosphorus compounds such as dialkyl phosphite, dialkyl phosphite and dialkyl phosphonate, in a pentaerythritol ester base oil, which has the alkyl chain lengths from C₅ to C₉, on 440C stainless steel [99]. In this study, dialkyl phosphite and dialkyl phosphite showed better AW performance than neutral phosphorus compounds such as TCP and dialkyl phosphonate (Figure 1-36). The author concluded that the reactivity of the acid group in phosphorus compounds was primary factor in improving AW performance for ester lubricants.

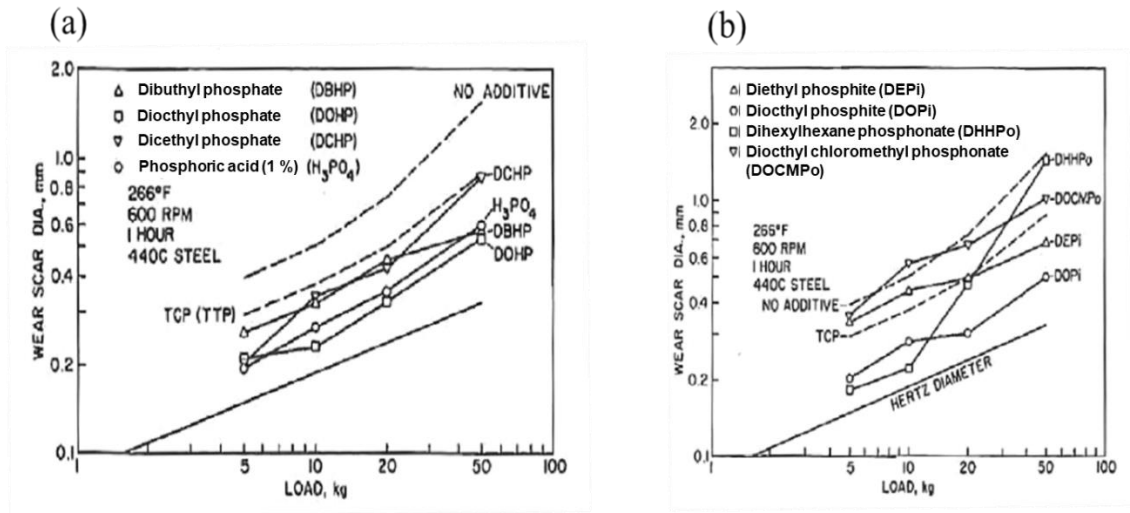


Figure 1-36. AW effect of phosphorus compounds in ester base oil [99]
 (a) dialkyl hydrogen phosphate, (b) dialkyl phosphite and dialkyl phosphonate

1.2.2.2 Relationship between response of AW additives and polarity of ester base oils

Van der Waals proposed the Non-Polarity Index (NPI) described in equation 2.1 to predict the polar characteristics of ester base oils from the chemical structures [100].

$$\text{Non - polarity index} = \frac{\text{total number of C atoms} \times \text{molecular weight}}{\text{number of carboxylic groups} \times 100} \quad (2.1)$$

Figure 1-37 shows the wear length of cams measured after an engine test carried out using lubricants with different non- polarity indexes. The results show that the cam wear length varies with the non-polarity index of lubricants: the cam wear length becomes lower with increasing the non-polarity index, indicating polar lubricants have poor AW performance in this engine test.

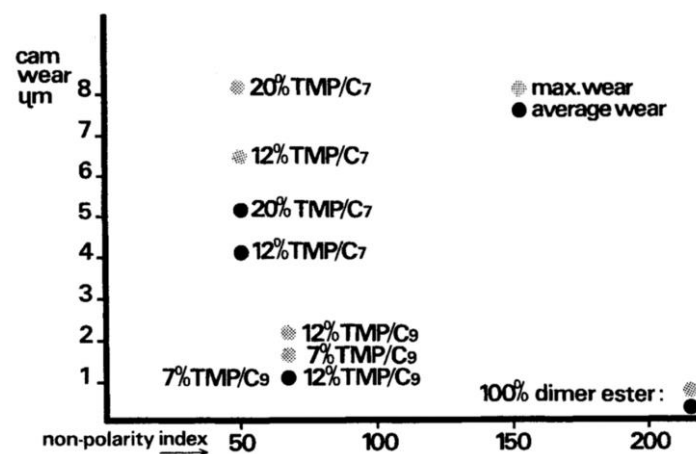


Figure 1-37. The relationship between cam wear and non-polarity index of ester base oils [100]

Minami *et al.* modified van der Waals' equation and proposed Polarity Index (PI) presented in 2.2 [101].

$$\text{Polarity index} = \frac{\text{number of carboxylic groups} \times 10,000}{\text{total number of C atoms} \times \text{molecular weight}} \quad (2.2)$$

This equation is more practical for understanding the polarity of base oils intuitively, because an index value increases with polarity of base oils, and non-polar base oils such as mineral oils and PAO could be treated as zero. They organized the effect of polarity of ester base oils against the AW performance of dibutyl phosphite using polarity represented in equation 2.2.

$$\text{Wear index} = \frac{\text{WSD of lubricant with AW additive} - \text{WSD of base oil}}{\text{WSD of base oil}} \quad (2.2)$$

Where: WSD is a wear scar diameter obtained in a four ball test

Figure 1-38 presents the relationship between wear index defined in equation 2.3 and the polarity index of tested ester base oils. It shows the clear correlation between polarity index of ester base oils and the effect of dibutyl phosphite, suggesting that the response of the additive become poorer when the polarity of ester base increases.

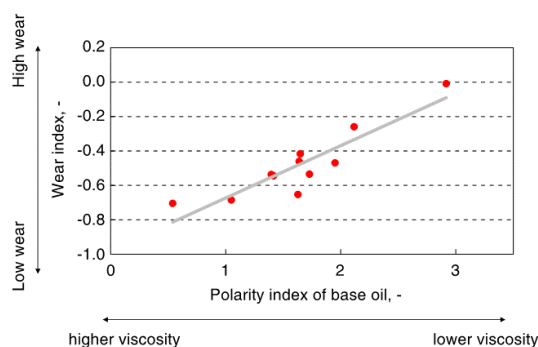


Figure 1-38. The relationship between polarity of ester base oils and AW effect of dibutyl phosphite on four-ball tests [101]

1.2.2.3 Design of AW additives for ester base oils

Minami *et al.* designed novel phosphorus additives, hydroxyalkyl phosphates/phosphonates, using a computer simulation: the semi-empirical molecular orbital method [102]. These new molecules, shown in Figure 1-39, exhibits excellent AW performance in ester base oils, where conventional additives are not effective. The author pointed out that the introduction of proper functional groups could increase the AW performance of phosphorus additives.

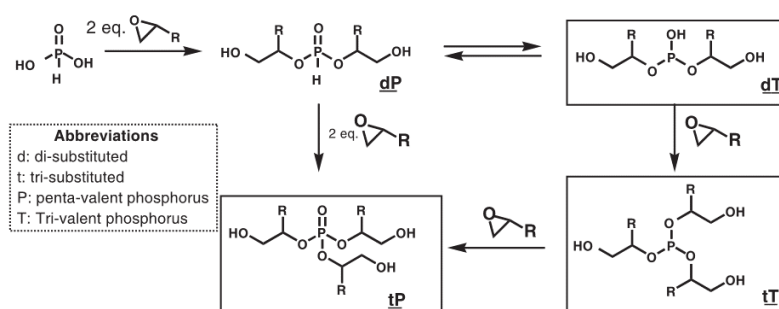


Figure 1-39. New phosphorus additives designed by computer simulation [102]

1.2.2.4 Others

The AW properties of conventional additives such as thiophosphates [103], trialkyl phosphates [104], dialkyldithiophosphate esters [105] and benzothiazole [106] were evaluated in ester base oils. The mechanisms of these AW additives in ester base oils were not yet discussed. Further investigations are needed to understand AW mechanisms in ester base oils and to design better AW additives than conventional ones.

1.2.2.5 Overview of research on AW additives in ester base oils

Hall reported that strong acid additives show superior AW performance compared to neutral ones in ester base oils. Minami *et al.* reported that functional groups of AW additives influence their performance to prevent wear. These studies imply that proper functional groups including acid structures promote adsorption of AW additives in ester base oils to overcome competitive adsorption process shown in Figure 1-34. However, it is well known that strong acids generate corrosive wear on worn surfaces [102], therefore the control of acidity is essential for AW additives used in ester lubricants.

In order to estimate how ester base oils affect the performance of AW additives, NPI and PI were proposed [100, 103]. These indexes showed that polar structures of ester base oils tend to prevent AW additives from reducing wear. Both functional groups of AW additives and polarity of ester base oils should be considered to design ester lubricants that present excellent AW performance.

Due to the lack of research carried out on AW additives for ester lubricants, further investigations are needed in order to improve our understanding of the AW mechanisms of additives in ester base oils.

1.3 Objectives of this thesis

As described in section 1.2.1.4, ester base oils have superior thermal stability, low temperature properties (pour point and VI) compared to mineral oils. That's why ester base oils have been widely applied to many lubricants such as engine oils, gear oils, compressor oils and refrigerating oils. In recent years, demands for environmentally acceptable lubricants (EALs) have been increasing for applications such as excavators, marine vessels and wind turbines [1]. EALs need to use higher biodegradable base oils. Thus, from the performance and environmental aspects, the interest in ester lubricants has grown steadily over the years.

However, an ester base oil alone has relatively poor lubricating performance, therefore, the addition of lubricant additives is required. Among lubricant additives, AW additives are of prime importance and phosphorous compounds are mainly used. In general, AW additives have been developed for non-polar base oils such as mineral base oils. Synthetic ester base oils have a polar structure, which often interferes with the action of AW additives. Competitive adsorption between ester base oils and AW additives occurs. Hall found that most of the phosphorus additives with strong acid structures, such as dialkyl phosphate and dialkyl phosphite, show excellent AW performance in ester base oils [99]. However, it is reported that strong acid sometimes causes corrosive wear because of their too strong acidity [100]. AW additives that do not have strong acid structures but have an appropriate functional group to aid adsorption onto metal surfaces are required for ester base oils.

In this PhD work, we focused on phosphonate structures as new AW additives for ester base oils. Although previous work revealed that phosphonates are not effective as AW additives [94, 95], we have considered that the stable structure can decrease the formation of phosphorus acid, which sometimes generates corrosion. In addition, the phosphonate structure makes possible the introduction of polar functional groups to the CH₂ moiety for improving the adsorption capability onto metal surfaces. The concept of new additives, which was designed for the present research, is summarized in Figure 1-40.

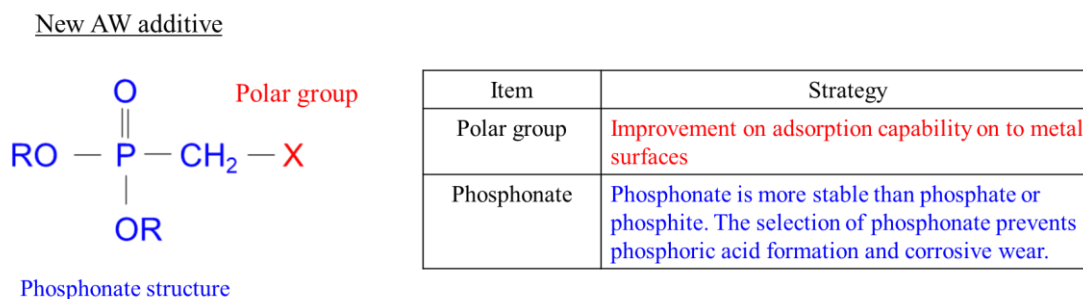


Figure 1-40. Concept of new AW additive for ester lubricants

This PhD thesis consists of general introduction and 6 chapters. The background is first presented in **General Introduction**, and the literature review and purpose of this research are described in this **Chapter 1**.

Chapter 2 shows the chemical structures of materials and the test conditions used in this study. Basic principles of surface analysis techniques used for this research are also introduced.

In **Chapter 3**, the AW performance of phosphonates, shown in Figure 1-41, are described. The possibility of using functionalized phosphonates as AW additives for ester base oils was investigated, and their AW properties were compared to conventional phosphorus AW additives. A special attention was paid on the phosphonate with carboxylic acid (DAPA, Dialkylphosphonoacetic acid). The detailed AW properties of DAPA were studied considering different test parameters such as load, test time and temperature.

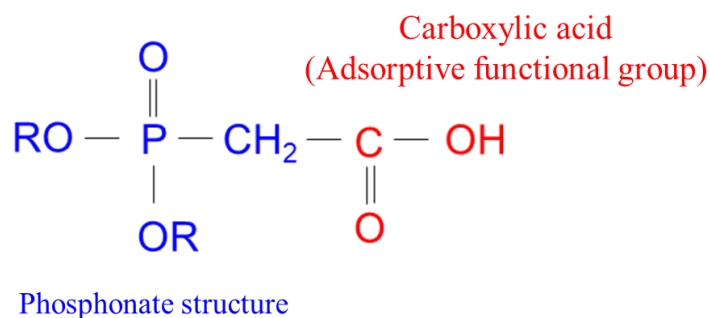


Figure 1-41. The selected phosphonate structure, dialkyl phosphonoacetic acid

In **Chapter 4**, DAPA tribofilms compositions were investigated. The chemical composition of DAPA tribofilms was analyzed using X-Ray Photoelectron Spectroscopy (XPS), Fourier Transform Infra-Red (FTIR) and Time-of-Flight Secondary Ion Mass Spectrometry (ToF-SIMS). Polarization Modulation-Infrared Reflection-Absorption Spectroscopy (PM-IRRAS) was also used to confirm the chemical structures of DAPA tribofilms. Cross sections of DAPA tribofilms were observed by Transmission Electron Microscopy (TEM) using a Focused Ion Beam (FIB) sample preparation technique.

In **Chapter 5**, the effects of ester base oil structures and the influence of phosphonate moieties on AW performance were investigated. From this study, the best candidates as AW additives for different polarities of ester base oils were discussed.

Chapter 6 summarizes all the results of this PhD work and propose outlooks.

Reference

- [1] L. R. Rudnick and R. L. Shubkin, SYNTHETIC LUBRICANTS AND HIGH-PERFORMANCE FUNCTIONAL FLUIDS, Second Edition, Marcel Dekker, Inc., 1999.
- [2] C. W. Montgomery, W. I. Gilbert and R. E. Kline., US Patent 2559984 to Gulf Oil Co.
- [3] G. R. Lappin and J. D. Sauer, Alpha Olefins Applications Handbook, Marcel Dekker, INC (1989)
- [4] S. Gryglewicz, W. Piechocki and G. Gryglewicz, Preparation of polyol esters based on vegetable and animal fats, *Bioresource Technology*, **87**, 2330, 35-39
- [5] E. Jantzen, The origins of synthetic lubricants: The work of Hermann Zorn in Germany part 2 esters and additives for synthetic lubricants., *Journal of Synthetic Lubrication*, **13**, 1996, 113–128.
- [6] L. R. Rudnick, Lubricant Additives Chemistry and Applications, Second Edition, CRC Press., 2009
- [7] T. Konishi, Fundamental properties of lubricants., *Nisseki technical review*, **40**, (1998) 91-97 (in Japanese)
- [8] E. Beran, Experience with evaluating biodegradability of lubricating base oils., *Tribology International*, **41**, 2008, 1212-1218
- [9] J.F. Carpenter, Biodegradability and Toxicity of Polyalphaolefin Base Stocks., *Journal of Synthetic Lubrication*, **12**, 1995, 13–20
- [10] P. Hamblin, Oxidative stabilisation of synthetic fluids and vegetable oils., *Journal of Synthetic Lubrication*, **16**, 1999, 157–181
- [11] D. Hörner, Recent trends in environmentally friendly lubricants., *Journal of Synthetic Lubrication*, **18**, 2002, 327–347
- [12] H. Spikes, Friction Modifier Additives., *Tribology Letters*, **60**, 2015, 1-5
- [13] H.M. Wells and J.E. Southcombe, The theory and practice of lubrication: the “Germ” process., *J. Soc. Chem. Ind*, **39**, 1920, 51–60
- [14] J. Kocsis, J.S. Vilardo, J.R. Brown, D. Barrer, R.J. Vickerman and P.E. Mosier, Tartaric acid derivatives in fuel compositions. US Patent 8,133,290, 13 March 2012
- [15] W.E. Heinz and K.F. Schiermeier, Corrosion inhibiting composition. US Patent No.2, 482, 517, 20 Sept 1949
- [16] T.L. Cantrell, J.G. Peters, H.G. Smith, Mineral oil compositions containing amidic acids or salts thereof. US Patent No.2,699, 427, 11 Jan 1955
- [17] G.W. Eckert, Adducts of aliphatic monocarboxylic acids and aliphatic amines in gasoline. US Patent No.3,055, 746, 25 Sept 1962
- [18] J.W. Schick, J.M. Kaminski, Lubricant composition for reduction of fuel consumption in

- internal combustion engines. US Patent No.4,304,678, 8 Dec 1981
- [19] G. Hugel, Fragen der Schmieröolforschung. Erdöl und Kohle **8**, 1955, 651–655
 - [20] G. Hugel, Bleu de molybène soluble dans les hydrocarbures. French Patent FR1099953A 1955
 - [21] C. Grossiord, K. Varlot, J.M. Martin, Th. Le Mogne, C. Esnouf, K. Inoue, MoS₂ Single sheet lubrication by molybdenum dithiocarbamate. *Tribology International*, **31**, 1998, 737–743
 - [22] E.H. Okrent, The effect of lubricant viscosity and composition on engine friction and bearing wear. *ASLE Transaction*, **4**, 1961, 97–108
 - [23] E.H. Okrent, The effect of lubricant viscosity and composition on engine friction and bearing wear. II. *ASLE Transaction*, **4**, 1961, 257–262
 - [24] M. Müller, K. Topolovec-Miklozic, A. Dardin, and H. Spikes, The design of boundary film forming PMA viscosity modifiers. *Tribology Transactions*, **49**, 2006, 225–232
 - [25] V.N. Bakunin, A. Suslov, G.N. Kuzmina, O.P. Parenago, Recent achievements in the synthesis and application of inorganic nanoparticles as lubricant components. *Lubrication Science*, **17**, 2005, 127–145
 - [26] J.M. Martin, N. Ohmae, Nanolubricants, vol.13. Wiley, New York (2008)
 - [27] B. K. Gupta, B. Bhushan, Fullerene particles as an additive to liquid lubricants and greases for low friction and wear. *Lubrication Engineering*, **50**, 1994, 524–528
 - [28] R. Tenne, Inorganic nanotubes and fullerene-like nanoparticles. *Nature Nanotechnology*, **1**, 2006, 103–111
 - [29] L. Joly-Pottuz, F. Dassenoy, M. Belin, B. Vacher, J.M. Martin, N. Fleischer, Ultra-low friction and wear properties of IF-WS₂ under boundary lubrication. *Tribology Letters*, **18**, 2005, 477–485
 - [30] O. Tevet, P. Von-Huth, P. R. Popovitz-Biro, R. Rosentsveig, H.D. Wagner, R. Tenne, Friction mechanism of individual multilayered nanoparticles. *Proceedings of the National Academy of Sciences*, **108**, 2011, 19901–19906
 - [31] I. Lahouij, F. Dassenoy, L. de Knoop, J.M. Martin, and B. Vacher, *In-situ* TEM observation of the behavior of an individual fullerene-like MoS₂ nanoparticle in a dynamic contact. *Tribology Letters*, **42**, 2011, 133–140
 - [32] I. Lahouij, F. Dassenoy, B. Vacher, and J.M. Martin, Real Time TEM Imaging of Compression and Shear of Single Fullerene-Like MoS₂ Nanoparticle. *Tribology Letters*, **45**, 2012, 131–141
 - [33] W. Davey and E. D. Edwards, The extreme-pressure lubricating properties of some sulphides and disulphides, in mineral oil, as assessed by the Four-Ball Machine., *Wear*, **1**, 1958, 291–304
 - [34] E. S. Forbes, The load-carrying action of organo-sulphur compounds - A review., *Wear*, **15**,

- 1970, 87-96
- [35] J. L. Paddy, P. S. Brook, and D. N. Waters, Oxidation of basic zinc dibutyl dithiophosphate by cumyl hydroperoxide at 25 °C; kinetic studies by h.p.l.c., *J. Chem. Soc. Perkin Trans. 2*, 1989, 1703-1706
 - [36] J. L. Paddy, N. C. J. Lee, D. N. Waters, and W. Trott, Zinc Dialkyldithiophosphate Oxidation by Cumene Hydroperoxide: Kinetic Studies by Raman and ³¹P NMR Spectroscopy, *Tribology Transactions*, **33**, 1990, 15-20
 - [37] W. R. Whitney, The corrosion of iron., *J. Chem. Soc* **25**, 1903, 394-406
 - [38] D. L. Lake, Approaching environmental acceptability in cooling water corrosion, *Corros. Prev. Control*, **35**, 1988, 113-115
 - [39] H. E. Reis, J. Gabor, Chain length compatibility in rust prevention, *Chem. Ind.*, 1967, 1561
 - [40] L. Cizaire, J. M. Martin, Th. Le. Mongne, and E. Gresser, Chemical Analysis of Overbased Calcium Sulphonate Detergents by Coupling XPS, ToF-SIMS, XANES and EFTEM, *Colloids and Surface A: Phiscochem. Eng. Aspects*, **228**, 2004, 151-158
 - [41] O. Beeck, J. W. Gives, and E. C. Williams, On the mechanism of boundary lubrication. II. Wear prevention by addition agents, *Proceedings Royal Society A, Mathematical Physical and Engineering Sciences*, **177**, 1940, 103-118
 - [42] B. Guan and B.A. Pochopien, and D. S. Wright, The chemistry, mechanism and function of tricresyl phosphate (TCP) as an anti-wear lubricant additive., *Lubrication Science*, **28**, 2016, 257–265.
 - [43] H. Spikes, The history and mechanisms of ZDDP, *Tribology Letters*, **17**, 2004, 469-489
 - [44] A. M Barners, K. D. Bartle, and V. R.A. Thibon, A Review of Zinc Dialkyldithiophosphates (ZDDPs): Characterization and Role in the Lubricating Oil, *Tribology International*, **34**, 2001, 389-395
 - [45] M. A. Nicholls, T. D. Peter, R. Norton, M. Kasrai, and G. M. Bancroft., Review of the lubrication of metallic surfaces by zinc dialkyl-dithiophosphates., *Tribology International*, **38**, 2005, 15-39
 - [46] R. I. Barber, The preparation of some phosphorus compound and their comparison as Load-Carrying Additive by the Four-Ball Machine., *ASLE transaction*, **19**, 1975, 19-328E.S
 - [47] British Patent 446, 547, The Atlantic Refining Co., 1936
 - [48] D. Godfrey, The Lubrication Mechanism of Tricresyl Phosphate on Steel., *ASLE Transactions*, **8**, 1965, 1-11.
 - [49] N. H. Furman, F. J. Welcher, W. W. Scott, Standard Methods of Chemical Analysis., van Nostrand, New York, 1962.
 - [50] A. Gauthier, H. Montes, J. M. Georges, Boundary Lubrication with Tricresyl phosphate (TCP). Importance of Corrosive Wear., *ASLE Transactions*, **25**, 1982, 445–455.

- [51] J. Sheasby, T. Caughlin, W. Mackwood, The effect of steel hardness on the performance of antiwear additives., *Wear*, **201**, 1996, 209–216.
- [52] D. Johnson, M. Bachus, J. Hils, Interaction between Lubricants Containing Phosphate Ester Additives and Stainless Steels., *Lubricants*, **1**, 2013, 48–60.
- [53] K. Sasaki, N. Inayoshi, K. Tashiro, Friction-induced dynamic chemical changes of tricresylphosphate as lubricant additive observed under boundary lubrication with 2D fast imaging FTIR-ATR spectrometer., *Wear*, **268**, 2010, 911–916.
- [54] Y. Yamamoto, F. Hirao, Proceedings of the Conference on JAST 23rd, 1979, 97.
- [55] F. T. Barcroft, A technique for investigating reactions between EP additives and Metal surfaces at high temperatures., *Wear*, **3**, 1960, 440–453.
- [56] I. L. Goldblatt, J. K. Appledorn, The antiwear behavior of TCP indifferent atmospheres and different base stocks., *ASLE Transactions*, **12**, 1970, 203–214.
- [57] A. Gauthier, H. Montes, J. M. Georges, ASLE/ASME Lubric. Confer. Preprint No.81-LC-6A-3, 1981.
- [58] H. E. Bieber, E. E. Klaus, E. J. Tewksbury, A study of tricresyl phosphate as an additive for boundary lubrication., *ASLE Transactions*, **11**, 1968, 155–161.
- [59] P. Bertrand, Reactions of tricresylphosphate with bearing materials. *Tribology Letters*, **3**, 1997, 367–377
- [60] D. Wheeler, O. Faut, The Adsorption and Thermal Decomposition of Tricresylphosphate (TCP) on Iron and Gold., *Applied Surface Science* **18**, 1984, 106–122.
- [61] E. C. Onyiriuka, Zinc phosphate glass surfaces studied by XPS. *Journal of Non-Crystalline Solids*, **163**, 1993, 268–273.
- [62] R. K. Brow, An XPS study of oxygen bonding in zinc phosphate and zinc borophosphate glasses., *Journal of Non-Crystalline Solids*, **194**, 1996, 267–273
- [63] R. Heuberger, A. Rossi and N.D. Spencer, Pressure Dependence of ZnDTP Tribochemical Film Formation: A Combinatorial Approach. *Tribology Letters*, **28**, 2007, 209–222
- [64] M. Eglin, A. Rossi, N. D. Spencer, X-ray photoelectron spectroscopy analysis of tribostressed samples in the presence of ZnDTP: a combinatorial approach. *Tribology Letters*, **15**, 2003, 199–209.
- [65] R. Heuberger, A. Rossi, N. D. Spencer, Pressure dependence of ZnDTP tribochemical film formation: a combinatorial approach. *Tribology Letters*, **28**, 2007, 209–222.
- [66] J. M. Martin, C. Grossiord, Th. L. Mogne, S. Bec, A. Tonck, The two-layer structure of Zndtp tribofilms: Part I: AES, XPS and XANES analyses., *Tribology International*, **34**, 2001, 523–530.
- [67] M. Gauvin, F. Dassenoy, C. Minfray and J.M. Martin, Zinc phosphate chain length study under high hydrostatic pressure by Raman spectroscopy. *Journal of Applied Physics*, **101**,

- 2007, 063505.
- [68] M. Gauvin, F. Dassenoy, M. Belin, C. Minfray, C. Guerret-Piécourt, S. Bec, J. M. Martin, G. Montagnac and B. Reynard, Boundary Lubrication by Pure Crystalline Zinc Orthophosphate Powder in Oil. *Tribology Letters*, **31**, 2008, 139–148.
 - [69] N.J. Mosey, M.H. Müser, and T.K. Woo, Molecular mechanisms for the functionality of lubricant additives. *Science*, **307**, 2005, 1612-1615.
 - [70] N.J. Mosey, T. Woo, M. Kasrai, P.R. Norton, G.M. Bancroft M.H. Müser, Interpretation of experiments on ZDDP anti-wear films through pressure-induced cross-linking. *Tribology Letters*, **24**, 2006, 105–114
 - [71] M. Belin, J. M. Martin, J. L. Mansot, Role of iron in the amorphization process in friction-induced phosphate glasses. *Tribology Transactions*, **32**, 1989, 410–413.
 - [72] J. M. Martin, M. Belin, J. L. Mansot, H. Dexper, P. Lagarde, Friction-induced amorphization with ZDDP—an EXAFS study. *ASLE Transactions*, **29**, 1986, 523–531.
 - [73] J. C. Bell and K. M. Delargy, The composition and structure of Model Zinc Dialkyldithiophosphate Anti-wear Films, *Proc. Int. Conf. on Tribology Eurotrib 93*, Budapest, Hungary,
 - [74] C. Minfray, J. M. Martin, M. I. De Barros, T. Le Mogne, R. Kersting and B. Hagenhoff, Chemistry of ZDDP Tribofilm by ToF-SIMS., *Tribology Letters*, **17**, 2004, 351–357.
 - [75] M. Crobu, A. Rossi, F. Mangolini, and N. D. Spencer, Chain-length-identification strategy in zinc polyphosphate glasses by means of XPS and ToF-SIMS., *Analytical and Bioanalytical Chemistry*, **403**, 2012, 1415–1432.
 - [76] M. A. Nichollas, G. M. Bancroft, M. Kasrai, T. Do, B.H. Frazer, and G. De Stasio, Nanometer Scale Chemomechanical Characterization of Antiwear Films., *Tribology Letters*, **17**, 2004, 205–216.
 - [77] J.J. Dickert Jr. and C.N. Rowe, The thermal Decomposition of Metal O,O-Dialkylphosphorodithioates. *J. Org. Chem*, **32**, 1967, 647-653
 - [78] H. Spedding and R.C. Watkins, The Antiwear Mechanism of zddp's Part I, *Tribology International*, **15**, 1982, 9-12
 - [79] P.A. Willermet, D.P. Dailey, R.O. Carter III, P.J. Schmitz, W. Zhu, Mechanism of formation of antiwear films from zinc dialkyldithiophosphates. *Tribology International*, **28**, 1995, 177-187
 - [80] J.M. Martin, C. Grossiord, T. Le Mogne, S. Bec, A. Tonck, The two-layer structure of Zndtp tribofilms: Part I: AES, XPS and XANES analyses, *Tribology International*, **34**, 2001, 523-530
 - [81] J.M. Martin, Antiwear mechanisms of zinc dithiophosphate: a chemical hardness approach, *Tribology Letters*, **6**, 1999, 1–8

- [82] E.S. Forbes and J. Battersby, The Effect of Chemical Structure on the Load-Carrying and Adsorption Properties of Dialkyl Phosphites, *ASLE Transactions*, **17**, 1974, 263-270
- [83] I. Minami, H.S. Hong, N.C. Mathur, Effect of alkenes on the antiwear mechanism of dialkyl hydrogen phosphites, *Lubrication Science*, **13**, 2001, 219-230
- [84] M.N. Najman, M. Kasrai and G.M. Bancroft, Chemistry of Antiwear Films from Ashless Thiophosphate Oil Additives, *Tribology Letters*, **17**, 2004, 217–229
- [85] M.N. Najman, M. Kasrai, G.M. Bancroft and A. Miller, Study of the Chemistry of Films Generated from Phosphate Ester Additives on 52100 Steel Using X-ray Absorption Spectroscopy, *Tribology Letters*, **13**, 2002, 209–218
- [86] F. Mangolini, A. Rossi, N.D. Spencer, Influence of metallic and oxidized iron/steel on the reactivity of triphenyl phosphorothionate in oil solution, *Tribology International*, **44**, 2011, 670-683
- [87] F. Mangolini, A. Rossi, N.D. Spencer, Reactivity of triphenyl phosphorothionate in lubricant oil solution, *Tribology Letters*, **6**, 1999, 191–194
- [88] F. Mangolini, A. Rossi, N.D. Spencer, Substituent Effect on the Reactivity of Alkylated Triphenyl Phosphorothionates in Oil Solution in the Presence of Iron Particles, *Tribology Letters*, **40**, 2010, 375–394
- [89] F. Mangolini, A. Rossi, N.D. Spencer, Chemical Reactivity of Triphenyl Phosphorothionate (TPPT) with Iron: An ATR/FT-IR and XPS Investigation. *J. Phys. Chem. C*, **115**, 2011, 1339-1354
- [90] F. Mangolini, A. Rossi, N.D. Spencer, Tribochemistry of Triphenyl Phosphorothionate (TPPT) by *In-Situ* Attenuated Total Reflection (ATR/FT-IR) Tribometry. *J. Phys. Chem. C*, **116**, 2012, 5614-5627
- [91] P. Njiwa, C. Minfray, T. Le Mogne, B. Vacher, J.M. Martin, S. Matsui, M. Mishima, Zinc dialkyl phosphate (ZP) as an anti-wear additive: comparison with ZDDP, *Tribology Letters*, **44**, 2011, 19–30
- [92] A. Dorison, The Antiwear Action of Zinc Di-n-Butyl Phosphate, *ASLE Transactions*, **22**, 1979, 190-192
- [93] K. Yagishita and J. Igarashi, Long Drain/Fuel Efficient Engine Oils Based on the ZDTP Substitute Additive Technology, *SAE Paper*, 2003-01-2003
- [94] K. Yagishita, E. Tominaga and T. Okawa, Development of Long-life Oil for Gas Engines, *SAE Paper*, 2006-32-0013
- [95] R.I. Barber, The preparation of some phosphorus compounds and their comparison as load carrying additives by the four-ball machine, *ASLE Transactions*, **19**, 1976, 319–328
- [96] E.S. Forbes, E.L. Neustadter, H.B. Silver, N.T. Upsdell, The effect of chemical structure on the load-carrying properties of amine phosphates, *Wear*, **18**, 1971, 269–278,

- [97] S. Wendels, T. Chavez, M. Bonnet, K.A. Salmeia and S. Gaan, Recent Developments in Organophosphorus Flame Retardants Containing P-C Bond and Their Applications, *Materials*, **10**, 2017, 784-815
- [98] L.R. Rudnick, Synthetics, Mineral Oils, and Bio-Based Lubricants, Chemistry and Technology, Third Edition, CRC Press, Boca Raton., 2020.
- [99] J.M. Hall, Antiwear additives in neopentyl ester oils. *ASLE Transactions*, **14**, 1971, 292–300
- [100] G. Van der Waal, The relationship between the chemical structure of ester base fluids and their influence on elastomer seals, and wear characteristics, *J. Synth. Lubr.* **1**, 1985, 280–301
- [101] I. Minami, K. Hirao, M. Memita, S. Mori, Investigation of anti-wear additives for low viscous synthetic esters, *Tribology International*, **40**, 2007, 626–631
- [102] I. Minami, S. Mori, Concept of molecular design towards additive technology for advanced lubricants, *Lubrication Science*, **19**, 2007, 127–149
- [103] L. Weimin, G. Qingye and H. Wanren, A study of the Tribological Behaviour and Action Mechanism of Thiophosphates in Rape Seed Oil, *J. Synth. Lubr.* **21**, 2004, 93–104
- [104] J. Li, Tribological Properties of Phosphate Ester as Additives in Rape Seed Oil, *J. Synth. Lubr.* **20**, 2003, 151–158
- [105] J. Li, Y. Zhang and T. Ren, A Study of the Tribological Behaviour of Dialkyldithiophosphate Esters as Additives in Rape Seed Oil, *J. Synth. Lubr.* **19**, 2002, 99–108
- [106] J. Li, T. Ren, Y. Zhang and D. Wang, Tribological Behaviour of Three Phosphate Esters Containing the Benzotriazole Group as Additives in Rapeseed Oil, *J. Synth. Lubr.* **18**, 2001, 225–231

Chapter 2

Material and experimental methods

| | | |
|-------|------------------------------------------------------------------------------------------|----|
| 2.1 | Materials | 46 |
| 2.1.1 | Base oils..... | 46 |
| 2.1.2 | AW additives | 47 |
| 2.2 | Tribotest conditions | 48 |
| 2.2.1 | Four-ball test..... | 48 |
| 2.3 | Surface analysis techniques for tribofilm characterizations | 50 |
| 2.3.1 | X-ray Photoelectron Spectroscopy (XPS)..... | 50 |
| 2.3.2 | Time-of-Flight Secondary Ion Mass Spectrometry and Infrared Spectroscopy (ToF-SIMS)..... | 51 |
| 2.3.3 | Fourier Transform Infra-Red (FTIR) | 52 |
| 2.3.4 | Polarization Modulation-Infrared Reflection-Adsorption Spectroscopy (PM-IRRAS)..... | 52 |
| 2.3.5 | Transmission Electron Microscope (TEM) using Focused Ion Beam (FIB)..... | 53 |
| | References..... | 54 |

This chapter describes the materials and the characterization techniques used in this work. First, the chemical structures and physical properties of base oils and additives are presented, followed by the preparation methods of each test oil. Secondly, tribological test conditions used in the present work are described. Next, fundamental principles and operating conditions of surface analysis techniques for tribofilm characterizations are explained.

2.1 Materials

2.1.1 Base oils

To investigate the AW performance of phosphorus additives in various base oils, ester and poly- α -olefin (PAO), were used. Trimethylolpropane trioleate (TMO) was selected as the representative of ester-base oil, because it is widely used in EALs [1, 2]. PAO8, which is the same viscosity grade (ISO VG46) as TMO, was used as the non polar-base oil for comparison. The chemical structures of TMO and PAO8 are presented in Figure 2-1.

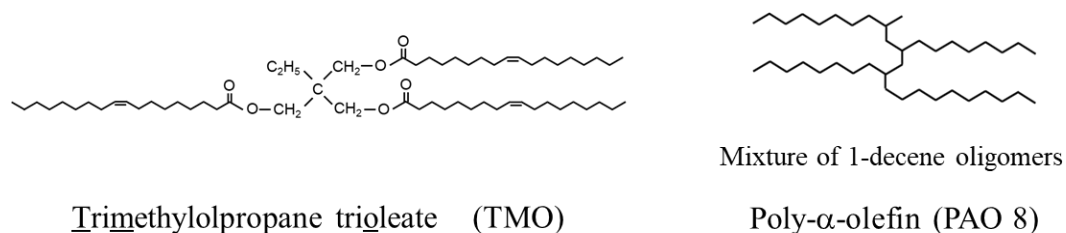


Figure 2-1. Chemical structures of base oils used in this study

Other ester base oils were also used. Their chemical structures are shown in Figure 2-2, together with their kinematic viscosity (ISO VG46). The kinematic viscosity and VI of ester base oils and PAO are summarized in Table 2-1.

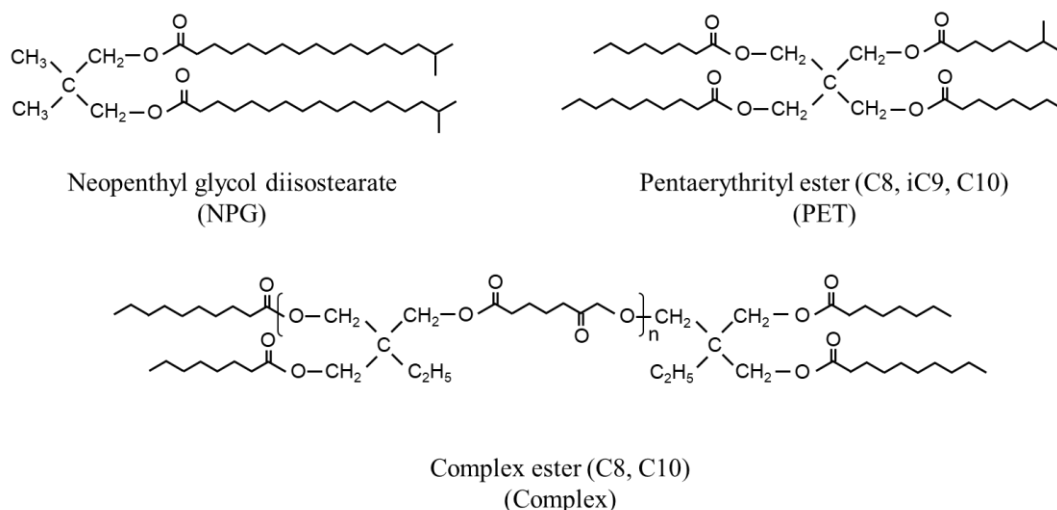


Figure 2-2. Chemical structures of ester base oils used in this study

Table 2-1. Kinematic viscosity and viscosity index of ester base oils and PAO

| | | TMO | NPG | PET | Complex | PAO |
|---------------------|----------------------|-------|-------|-------|---------|-------|
| Viscosity at 40 °C | [mm ² /s] | 49.50 | 46.71 | 45.67 | 46.00 | 45.89 |
| Viscosity at 100 °C | [mm ² /s] | 9.748 | 8.218 | 7.403 | 8.099 | 7.736 |
| Viscosity Index | | 187 | 151 | 126 | 150 | 137 |

2.1.2 AW additives

In this study, phosphonates with various functional groups were used as AW additives for lubricants. The phosphonates with different functional groups (X = COOH, OH, COOC₂H₅, and alkyl) shown in Figure 2-3 were used.

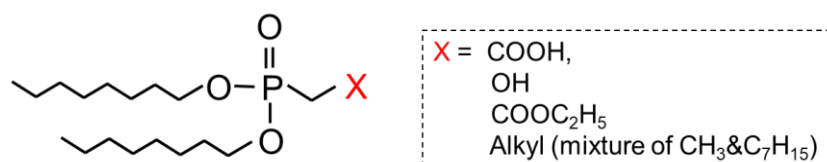


Figure 2-3. Phosphonates with various functional groups

Dialkyl phosphate (phosphate), dialkyl phosphite (phosphite), and tricresyl phosphate (TCP) were used for comparison as conventional phosphorus additives. These chemical structures are depicted in Figure 2-4.

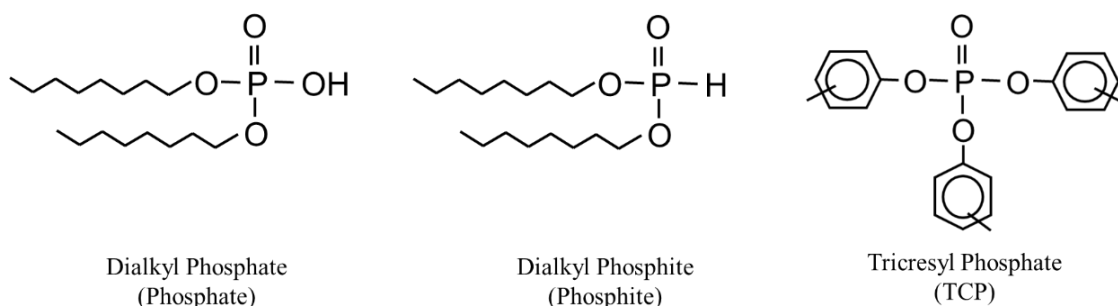


Figure 2-4. Conventional phosphorus AW additives used for comparison

The phosphonates, phosphate, and phosphite were supplied by Johoku Chemical Co., Ltd. The alkyl chain of these phosphorus compounds is nC₈H₁₇. TCP was purchased from Daihachi Kogyo Co. Gas chromatography-mass spectroscopy (GC-MS) and ³¹P nuclear magnetic resonance (³¹P NMR) spectroscopy showed that the purity of all phosphorus compounds used in this study was 95% or higher. The concentration of the AW additives (except for TCP) in the base oils was 3.1 mmol/kg, corresponding to a phosphorus content of 100 ppm. The concentration of TCP was ten times higher than that of the others, 31.0 mmol/kg, because of the low efficiency of triphenyl phosphate as an AW additive at low concentrations [3].

2.2 Tribotest conditions

2.2.1 Four-ball test

A four-ball testing machine was used to evaluate the AW performance of lubricants. This test was first reported in 1933 by Boerlage [4], and subsequently modified by Larson and Perry [5]. The experimental procedures of the four-ball tests are defined by specifications such as ASTM D 4172-94 for the wear preventative characteristics of lubrication fluid [6] and ASTM D2783-03 for the measurement of extreme-pressure properties of lubricating fluids [7]. Figure 2-5 illustrates the four-ball test machine used in this study. The machine consists of a rotating ball at the top and three fixed balls at the bottom. A normal load is applied using compressed air and controlled using a load cell.

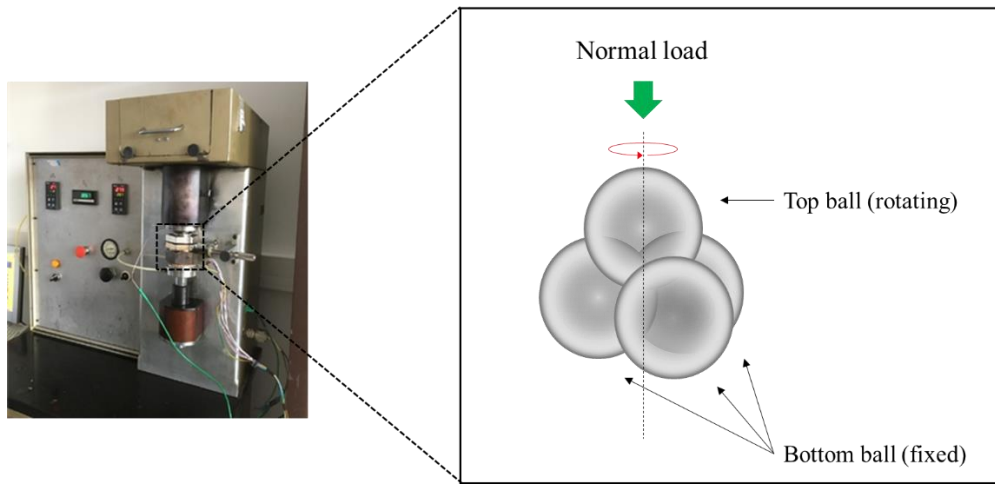


Figure 2-5. Picture and schematic image of four-ball test

In order to determine experimental conditions such as a sliding speed and contact pressure in a four-ball test, the geometry of contact points in Figure 2-6 was considered. The radius and the circumference of wear track are written as r and l , respectively. The equation 2.1 is expressed from the tetrahedron shown in Figure 2-6.

$$c^2 = \left(\frac{a\sqrt{3}}{2}\right)^2 - \left(\frac{a\sqrt{3}}{2} - 2r\right)^2 = a^2 - (2r)^2 \quad \text{Equation 2.1}$$

From equation 2.1, r is expressed as equation 2.2:

$$r = \frac{a\sqrt{3}}{6} \quad \text{Equation 2.2}$$

The diameter of the test balls used in this research (a) was 12.7 mm, therefore, r and l become 3.67 mm and 23.0 mm, respectively. The rotation speed of the four-ball test machine was 1200 rpm. The sliding speed used in this study was 460 mm/s.

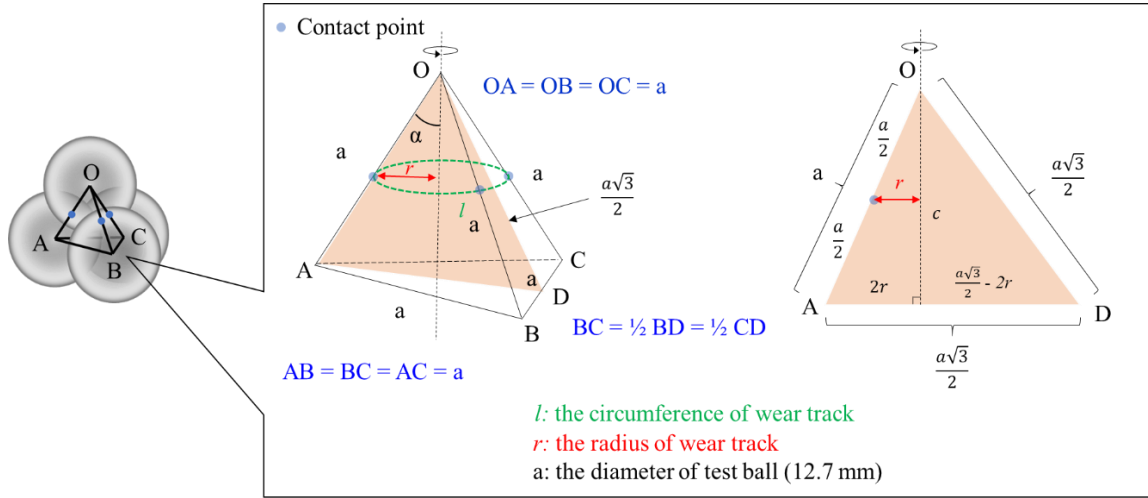


Figure 2-6. Geometry of contact points in four-ball test

Regarding the calculation of contact pressures, the normal force F_n at contact points was calculated from the applied load F_{app} and the angle α . The relationship between F_n and F_{app} is expressed in equation 2.3.

$$F_n = 3F_{app} \cos \alpha \quad \text{Equation 2.3}$$

The details of the test parameters used in this study are described in Table 2-2. In this test, the AW performance was evaluated by measuring the wear scar diameter of the balls after each test. Stainless steel balls of AISI 52100 grade 10 ($R_a = 0.028 \pm 0.001 \mu\text{m}$), were used.

Table 2-2. Test conditions of the four-ball test.

| | This research | ASTM D4172 |
|-----------------------------------|--------------------|------------|
| Hertz pressure (P_{max}), GPa | 2.2, 2.7, 3.1, 3.7 | 2.4 or 3.7 |
| Load, N | 98, 196, 294, 392 | 147 or 392 |
| Test time, s | 10-7200 | 3600 |
| Temperature, °C | 25, 75, 125 | 75 |
| Rotation, rpm | 1200 | 1200 |
| Sliding velocity, mm/s | 460 | 460 |
| Material of ball | AISI 52100 | AISI 52100 |
| Diameter of ball, mm | 12.7 | 12.7 |

2.3 Surface analysis techniques for tribofilm characterizations

2.3.1 X-ray Photoelectron Spectroscopy (XPS)

XPS can provide qualitative and semi-quantitative information on all elements except H and He. This technique is based on the photoelectric effect that was found by Hertz and Hallwachs in the 19th century. Following this discovery, Siegbahn *et al.* developed XPS using the photoelectronic effect [8, 9]. This effect is illustrated in Figure 2-7. An electron is ejected from a core level of an atom by X-ray photon, when this photon has a larger energy than the binding energy (E_B) of the electron. The basis of this process can be expressed by the Einstein equation as shown in equation 2.4.

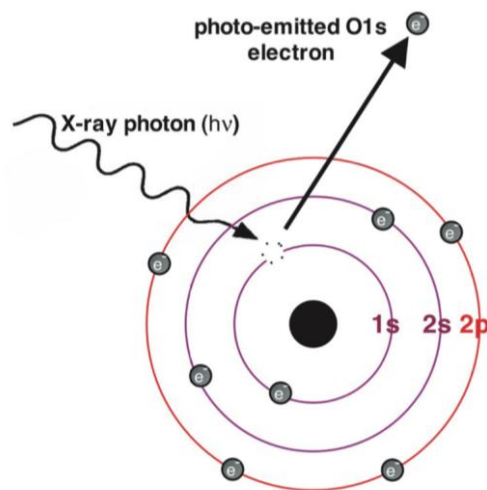


Figure 2-7. Photoemission in the photoelectric effect [10]

$$E_B = h\nu - KE - \phi$$

Equation 2.4

where E_B is the binding energy of an electron in an atom, $h\nu$ is the energy of the X-ray source, KE is the kinematic energy of an emitted electron that is measured in an XPS spectrometer, and ϕ is the spectrometer work function. The values of $h\nu$ and ϕ are determined from an X-ray source and a spectrometer, respectively. KE is obtained from XPS measurements, thus E_B can be calculated. E_B is important for identifying chemical compositions of unknown materials because the specific values vary according to a valence and bonding state of an element. Moreover, XPS is a surface-sensitive technique because photo-emitted electrons only include information of the surface depth of few nm. XPS is a very powerful surface analysis technique and is widely used for analyzing chemical compositions of tribofilms formed on worn surfaces.

In this study, a PHI VersaProbe II (Figure 2-8) was used to perform the X-ray photoelectron spectroscopy (XPS) analyses of the adsorbed films and tribofilms after the four-ball tests. XPS analyses were performed at pressures below 10^{-7} Pa. The X-ray source was Al K α ($h\nu = 1486.6$ eV), which was operated at 50 W, and the beam diameter of the X-



Figure 2-8. XPS apparatus used in this study

ray was 50 μm . First, the survey spectra were acquired at a pass energy of 187.85 eV to identify the elements present on the surfaces. High-resolution spectra were obtained at 23.50 eV to analyse the chemical state of each element more precisely. All binding energies were corrected at 285.0 eV of C1s spectra. Each high-resolution spectrum was analyzed using MultiPak software (ver9.0) to perform curve-fitting procedures. The concentrations of the detected elements were calculated from their peak areas and sensitivity factor using equation 2.5.

$$X_A = \frac{I_{Aq,m}/S_{Aqm}}{\sum_{i=A,B,C} I_{iq,m}/S_{iqm}} \quad \text{Equation 2.5}$$

Where $I_{Aq,m}$ is the peak area of a particular energy level (q) with the X-ray source (m) on element A and $S_{Aq,m}$ is the sensitivity factor of element A. In this study, the sensitivity factors of C1s, O1s, P2p and Fe2p3 were 0.314, 0.733, 0.525 and 1.964, respectively [10].

The depth profiles of the detected elements were obtained using an Ar^+ ion gun. Etching was performed on a $2 \times 2 \text{ mm}^2$ area for 60 min at 250 V.

2.3.2 Time-of-Flight Secondary Ion Mass Spectrometry and Infrared Spectroscopy (ToF-SIMS)

ToF-SIMS is an extreme surface characterisation technique used to analyse the composition of solid surfaces or thin films by sputtering the surface of the sample with a focused primary ion beam and collecting/analyzing the ejected secondary ions. The mass of ion clusters is analyzed with a time-of-flight mass spectrometer, which identifies the mass of ion clusters using the difference in flight time from a sample to the detector. This flight time is proportional to the square root of the weight. Information regarding elements or molecular species within 1 nm of the sample surface at a high detection sensitivity can be obtained using ToF-SIMS. Figure 2-9 illustrates the principle of ToF-SIMS and the apparatus used in this study.

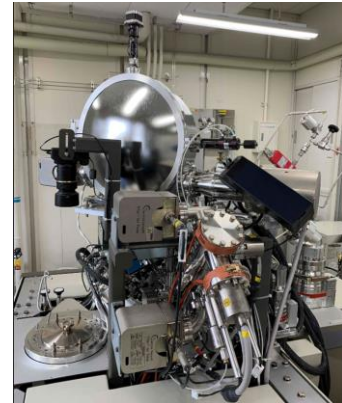
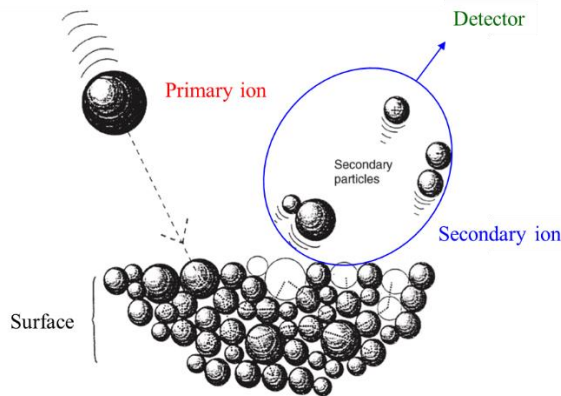


Figure 2-9. Principle and apparatus of ToF-SIMS used in this research (adapted from [11])

In this study, measurements were carried out using a TRIFT V nanoTOF spectrometer from ULVAC-PHI. A primary ion beam of Bi_3^{2+} with 30 keV acceleration voltage, a pulse width of 12 ns and a raster size of $100\ \mu\text{m} \times 100\ \mu\text{m}$ were used to record spectra in positive and negative modes. Both negative and positive ions spectra were collected from the scanned area and processed using Win CadenceN software (version 1.18.4.5). Both positive and negative ions spectra are acquired from the scanned area. In this experiment, chemical information comes from a depth of 0.1–1 nm below the surface. This is much more near-surface information than that obtained from XPS and infrared spectroscopy.

2.3.3 Fourier Transform Infra-Red (FTIR)

After the four-ball tests at 392 N with DAPA in PAO and DAPA in TMO, the surfaces were analysed using an infrared microscope (Bruker Vertex 70 with HYPERRION 3000 with LEICA S8AP0).

2.3.4 Polarization Modulation-Infrared Reflection-Adsorption Spectroscopy (PM-IRRAS)

Infra-Red Reflection Absorption Spectroscopy (IRRAS) is an established surface analytical technique for analyzing thin films on metal surfaces with high sensitivity. This technique uses a p-polarized light parallel to the plane of incidence as shown in Figure 2-10. The p-polarized light forms an electric field with stationary vibrations, which increase sensitivity. This method allows film thickness measurement at nano-order level.

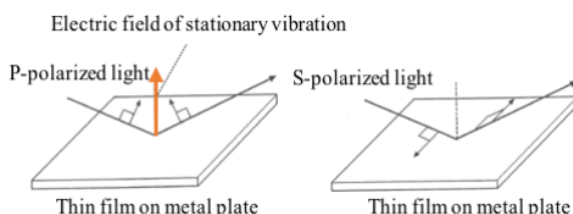


Figure 2-10. Diagram of IRRAS measurement method [12]

Absorption peaks of IRRAS are usually very small and can require a long accumulation time to obtain clear spectra. Moreover, a measurement of background spectra is mandatory to obtain characteristics spectra of samples. The data can be affected by the absorption of H_2O , CO_2 and metal oxides. Consequently, it is often difficult to obtain clear spectra of thin films on metal surfaces as more than 100 nm of thickness is essential for IRRAS system.

Furthermore, PM-IRRAS (IRRAS with a polarization modulator), is a method for finding the intensity difference in s- and p-polarized light ($\Delta I = I_p - I_s$) where s is vertical and p is parallel to the plane of incidence using a photo-elastic modulator (PEM). As s-polarized light does not generate an

electric field of stationary vibration, the absorption is much smaller than that of p-polarized light. In addition, in PM-IRRAS, the sum of s- and p- polarization signals ($\Sigma I = I_p + I_s$) is used as a reference and so there is no need to measure a reference substrate. Hence, the effect due to the absorption of atmospheric H₂O and CO₂ can be greatly decreased. As the measurement of a reference substrate is not required, the results are free from the effect of differences between substrates and the overall measurement time can be shortened. PM-IRRAS measurement allows higher sensitivity by detecting small ΔI signals using a direct lock-in detection by using adopting dual modulation spectroscopy of the FTIR interferometer and PEM. A great number of studies relating to tribology have been carried out with an IRRAS system to analyze the chemical structures of tribofilm [13, 14]. The apparatus is an IR-TF spectrometer Nicolet 850 combined with a photo-elastic modulator.

2.3.5 Transmission Electron Microscope (TEM) using Focused Ion Beam (FIB)

TEM observations were performed to analyze local structures of tribofilms formed on worn surfaces. The samples were prepared using Focused Ion Beam (FIB) technique. Thanks to this technique, thin layers (< 100 nm) of materials can be extracted from bulk samples. Worn surfaces and tribofilms can thus be easily observed by TEM. FIB was performed using an NB-5000 (Hitachi High-Tech) and a typical sample is shown in Figure 2-11. TEM observations were performed using an HD-2700 microscope (Hitachi High-Tech) with Energy Dispersive X-ray Spectroscopy (EDX, HORIBA X-Manx100^N TLE). An acceleration voltage of 200 kV was used for the TEM observations. The magnification range was from x 30,000 to x 500,000.

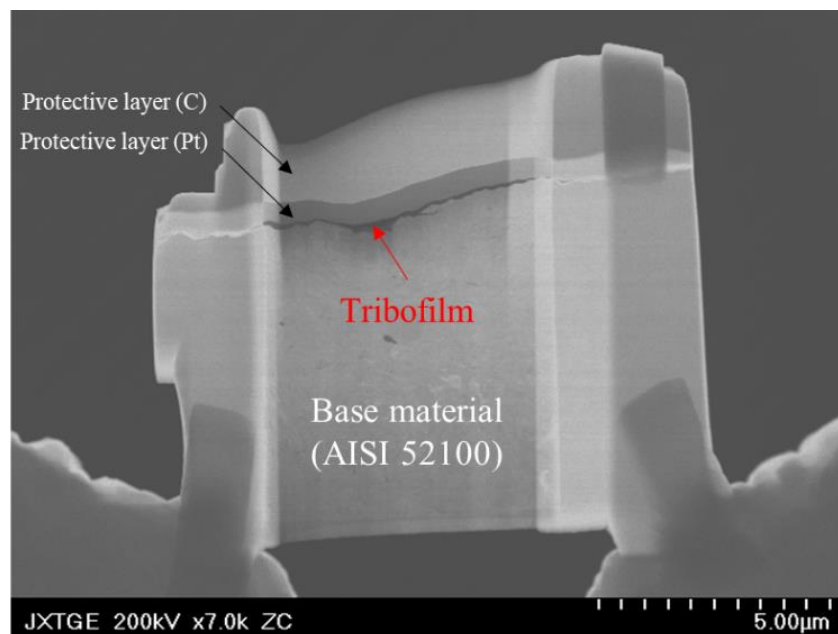


Figure 2-11. Sample for TEM observation prepared by FIB technique

References

- [1] Y. Wu, W. Li and X. Wang, Synthesis and properties of trimethylolpropane trioleate as lubricating base oil. *Lubrication Science*, **27**, 2015, 369-379.
- [2] A. Pettersson, High-performance base fluids for environmentally adapted lubricants. *Tribology International*, **40**, 2007, 638-654.
- [3] I. Minami and S. Mori, Antiwear Additives for Ester Oils, *J. Synthetic Lubrication*, **22**, 2005, 105-121.
- [4] G. D. Boerlage, Four-ball testing apparatus for extreme-pressure lubricants, *Engineering*, **136**, 1933, 46-47.
- [5] R. G. Larson and G. L. Perry, Investigation of friction and wear under quasi-hydrodynamic conditions, *Transactions ASME*, 1945, 45-80.
- [6] Standard Test Method for Wear Preventive Characteristics of Lubricating Fluid (Four-Ball Method), ASTM D 4172-94 (2016).
- [7] Standard Test Method for Measurement of Extreme-Pressure Properties of Lubricating Fluids (Four-Ball Method), ASTM D2783-03 (2014).
- [8] K. Siegbahn, C. Nordling, A. Fahlman, R. Nordberg, K. Hamrin, J. Hedman, G. Johansson, T. Bergmark, S-E. Karlsson, I. Lindgren and B. Lindberg, ESCA, Atomic, Molecular and Solid State Structure Studied by Means of Electron Spectroscopy, *Almquist and Wiksells Boktckeri AB*, Uppsala, 1967.
- [9] K. Siegbahn, C. Nordling, G. Johansson, J. Hedman, A. P.F. Hedén, K. Hamrin, U. Gelius, T. Bergmark, L.O. Werme, R. Manne, Y. Bear, ESCA, Applied to Free Molecules, North-Holland, Amsterdam-London, 1969.
- [10] C.D. Wagner, L.E. Davis, M.V. Zeller, J.A. Taylor, R.H. Raymond and L.H. Gale, Empirical atomic sensitivity factors for quantitative analysis by electron spectroscopy for chemical analysis, *Surface and Interface Science*, **3**, 1981, 211-225
- [11] J. C. Vickerman and I. S. Gilmore, Surface Analysis – The principle Techniques, 2nd Edition, John Wiley & Sons Ltd., 2009.
- [12] JASCO website (<https://jascoinc.com/applications/pm-irras/>)
- [13] S. Loehlé, C. Matta, C. Minfray, T. Le Mogne, R. Iovine, Y. Obara, A. Miyamoto and J.M. Martin, Mixed lubrication of steel by C18 fatty acids revisited. Part I: Toward the formation of carboxylate, *Tribology International*, **82**, 2015, 218-227
- [14] T. Massoud, R. P. De Matos, T. Le Mogne, M. Belin, M. Cobian, B. Thiebaut, S. Loehlé, F. Dahlem, C. Minfray, Effect of ZDDP on lubrication mechanisms of linear fatty amines under boundary lubrication conditions, *Tribology International*, **141**, 2020, 105954

Chapter 3

Antiwear Properties of Dialkyl Phosphonates in Ester Base Oil

| | | |
|-------|--------------------------------------------------------------------------|----|
| 3.1 | Antiwear Properties of Dialkyl Phosphonates in TMO | 56 |
| 3.2 | Antiwear Properties of Dialkyl phosphonoacetic acid in TMO and PAO | 58 |
| 3.2.1 | Impact of normal load..... | 58 |
| 3.2.2 | Impact of test duration | 61 |
| 3.2.3 | Impact of temperature | 62 |
| 3.3 | Discussion..... | 63 |
| 3.3.1 | Possibilities of phosphonate as AW properties for ester base oils..... | 63 |
| 3.3.2 | AW properties of DAPA and conventional phosphorus additives | 63 |
| 3.3.3 | Effect of load on AW performance of DAPA in base oils | 64 |
| 3.3.4 | Influence of test time on AW performance of DAPA in base oils | 65 |
| 3.4 | Summary of this chapter | 66 |
| | References..... | 67 |

In order to find effective AW additives for ester base oils, it was decided to focus on the tribological properties of dialkyl phosphonates with different functional groups in TMO (trimethylolpropane trioleate) and to compare their behavior to conventional phosphorus additives. Then, the phosphonates additives with the better AW performance were further investigated under different test conditions such as load, test time and temperature. Tests were carried out with a four balls tribometer, under conditions presented in chapter 2 table 2-2. Tests in PAO base oil are carried out for comparison.

3.1 Antiwear Properties of Dialkyl Phosphonates in TMO

Figure 3-1 shows the chemical structures of the phosphorus AW additives used in this investigation: the phosphonates with different functional groups (Figure 3-1(a)) and the conventional additives (Figure 3-1(b)). First of all, the AW performance of the phosphonates shown in Figure 3-1(a) was evaluated for ester base oil (trimethylolpropane trioleate, TMO). Figure 3-2 shows their AW performance. Each test was conducted at 294 N according to the guidelines specified in JCMAS P041 [1], which defines this load as relevant for the evaluation of hydraulic fluids. Phosphonate with polar functional groups such as COOH, OH, and COOC₂H₅ considerably reduce the wear compared to the pure ester base oil, while the phosphonate with an alkyl structure (R) does not improve the AW capability of the base oil. Among the phosphonates shown in Figure 3-1(a), the phosphonate with carboxylic acid (COOH), namely, DAPA, gives the smallest wear scar diameter. Based on these results, DAPA was then used for all further investigations.

Comparison was made between the AW properties of conventional phosphorus additives. The results of the four-ball tests obtained using DAPA and conventional phosphorus additives in TMO and PAO are summarized in Figure 3-3. In PAO, phosphate and phosphite reduced wear; however no significant AW effect was observed with DAPA and TCP. In TMO, DAPA produced the smallest wear scar diameter compared to those of the other tested additives. Finally, DAPA in TMO exhibited better AW properties than those of DAPA in PAO, and DAPA also exhibited better AW performance than that of conventional phosphorus additives in TMO.

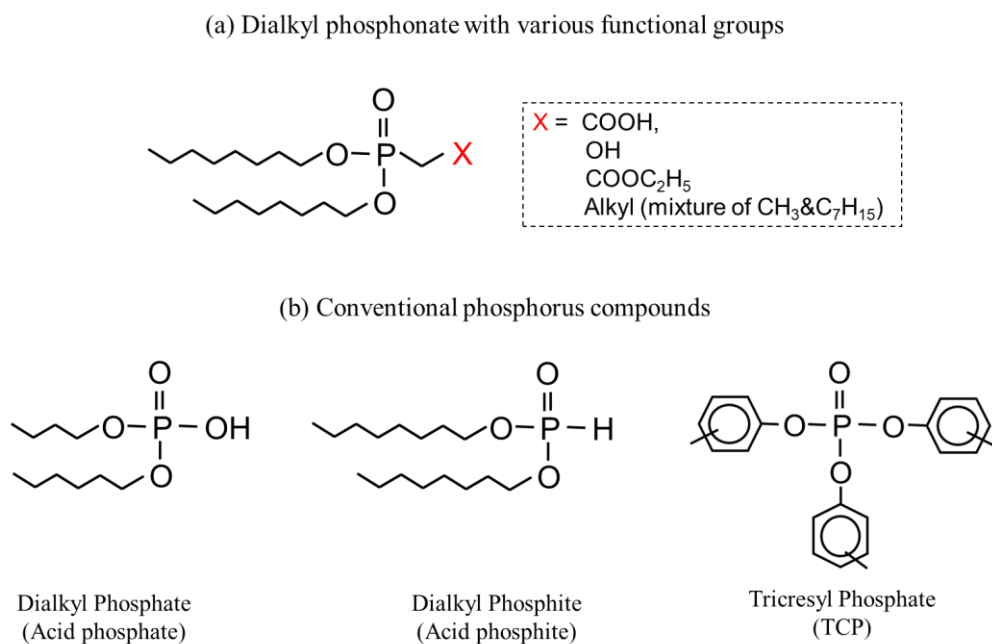


Figure 3-1. Chemical structures of phosphorus additives: (a) dialkyl phosphonates with various functional groups (X) and (b) conventional phosphorus compounds.

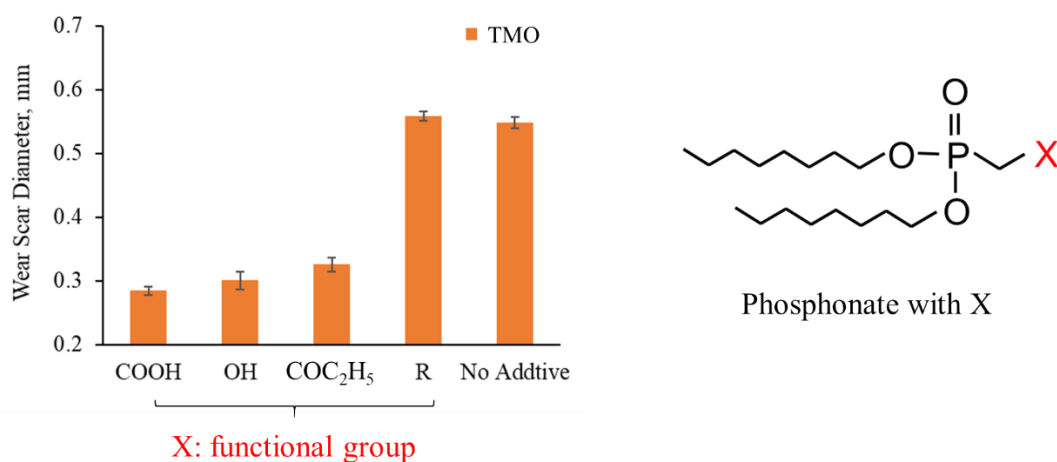


Figure 3-2. Effect of the phosphonate functional groups on the antiwear performance of the additives at 294 N for 30 min at 25 °C. The additive concentration in TMO was 3.1 mmol/kg, corresponding to a phosphorus content of 100 ppm. R is an alkyl chain of nC₈H₁₇.

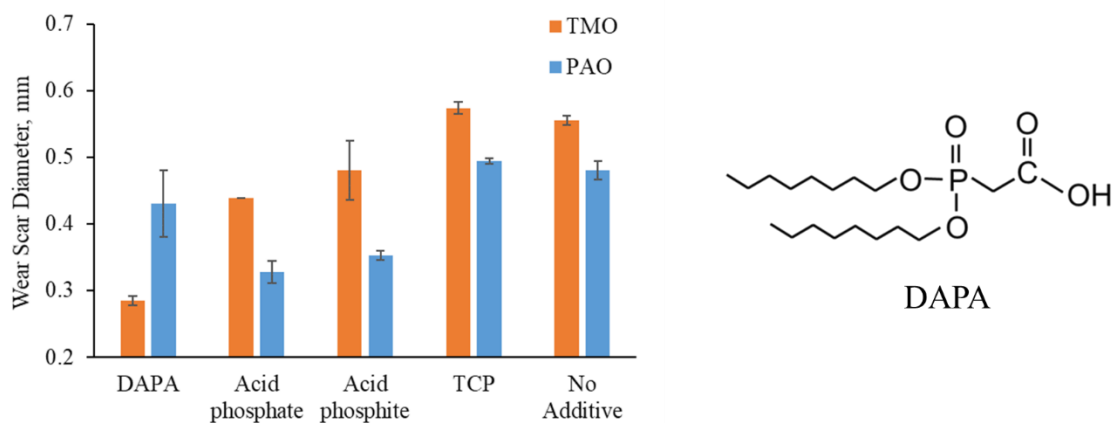


Figure 3-3. AW performances of DAPA and conventional phosphorus additives in TMO and PAO. Four-ball tests were conducted at 294 N for 30 min at 25 °C. The additive concentration in the base oils was 3.1 mmol/kg, corresponding to a phosphorus content of 100 ppm.

3.2 Antiwear Properties of Dialkyl phosphonoacetic acid in TMO and PAO

3.2.1 Impact of normal load

To further understand the origin of the AW properties of DAPA, further tests were performed using a four-ball machine with a range of normal loads (98–392 N). Figure 3-4(a) shows the evolution of wear scar diameters with the load for four tested oils (PAO, TMO, DAPA in PAO, and DAPA in TMO). PAO exhibited significant wear at all loads. Ester reduced the wear at 98 N in comparison to PAO but causes high wear at loads over 196 N. DAPA in TMO reduces the wear at higher loads compared to the pure ester base oil (TMO). DAPA in PAO showed significant improvements in the AW performance of the base oil up to 196 N, however, the AW performance was progressively lost for higher loads (294 and 392 N). In general, the AW effect of DAPA was better in TMO than in PAO at relatively high loads, although there was no significant difference below 196 N.

Figure 3-4(b) depicts the optical images of the worn surfaces of the test specimens after the tests were carried out at 98, 196, 294, and 392 N. DAPA in PAO formed a colored film on the top ball at 196 N, but no clear film was generated at 294 and 392 N and significant scratches were evident. In contrast, DAPA in TMO formed a blue-colour film on the surface of the top ball at 294 and 392 N, but no colour film and no scratches were observed at 98 and 196 N. The tribofilm formation observed at high loads with DAPA in TMO is attributed to be the source of the observed wear reduction. The absence of a tribofilm (determined optically) on the test specimens with DAPA in PAO appears to be related to the higher wear at high loads.

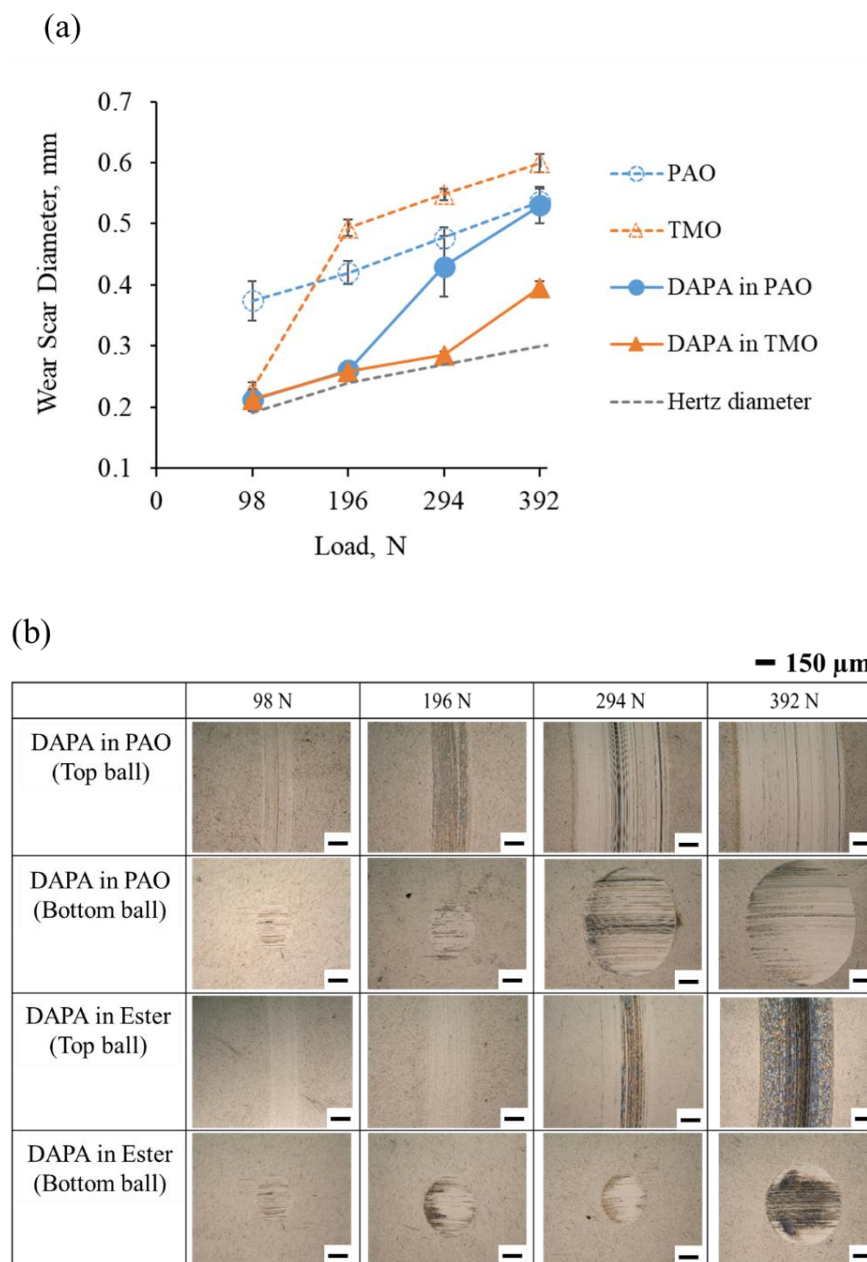


Figure 3-4. Impact of DAPA in TMO and PAO on antiwear properties. Four-ball tests were conducted with a load range between 98 and 394 N for 30 min at 25 °C. DAPA concentration in base oils was 3.1 mmol/kg, corresponding to a phosphorus content of 100 ppm.

The friction coefficients recorded during the four-ball tests are presented in Figure 3-5. At 98 N, DAPA in PAO exhibited a lower friction coefficient than PAO alone, whereas there was no significant difference in the friction coefficient between pure Ester (TMO) and DAPA in TMO. At 196 and 294 N, DAPA in TMO gave the lowest friction coefficient compared to the other lubricants. The friction coefficient of DAPA in PAO was relatively low and stable during the first 1400 and 800 s at 196 and 294 N, respectively, followed by a sharp increase. At 392 N, DAPA in PAO and DAPA in TMO showed a sudden increase of the friction coefficient in the initial stages. DAPA in TMO had a higher friction coefficient than DAPA in PAO, even though DAPA in TMO gave a smaller wear scar diameter than DAPA in PAO. The friction coefficient of the ester base oil increased with the test time, and that of PAO was unstable and had a wide range of values over 196 N.

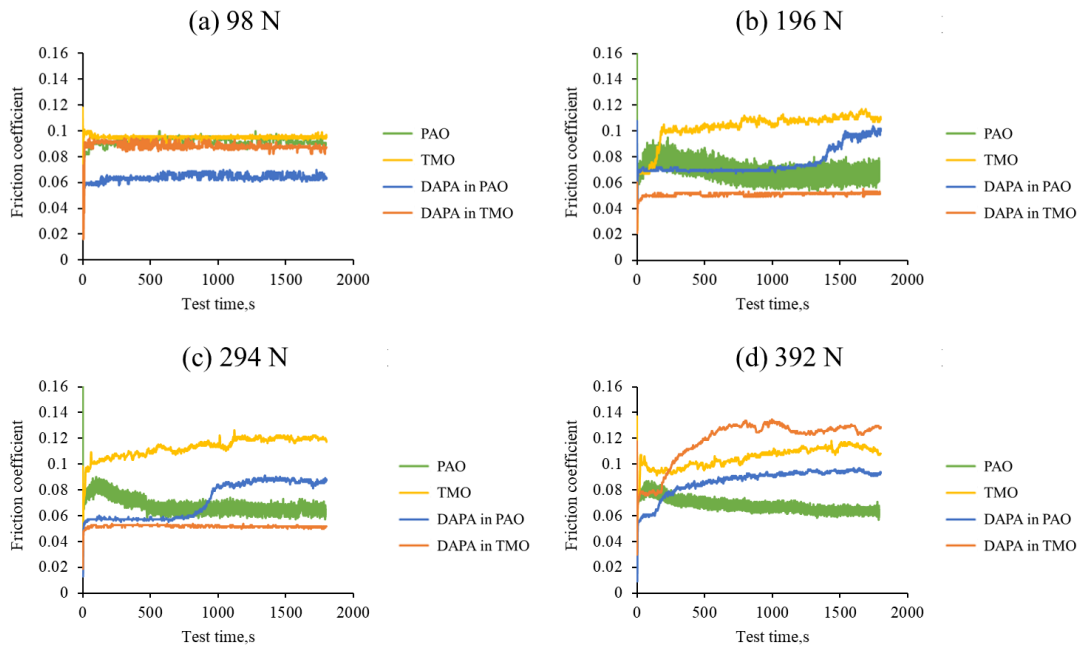


Figure 3-5. Friction curves of PAO, TMO, DAPA in PAO, and DAPA in TMO, recorded during four-ball testing conducted at (a) 98, (b) 196, (c) 294, and (d) 392 N.

3.2.2 Impact of test duration

Four-ball tests were performed at 392 N using the four lubricants for various test durations to investigate the kinetics of tribofilm formation. The results are presented in Figure 3-6. For DAPA in PAO, a colored film was formed after 10 seconds of testing. This film was no longer optically visible after a longer test period. In addition, the AW capability of DAPA in PAO progressively decreased after approximately 150 s of testing. For DAPA in TMO, no visible film was observed until 600 s, but a coloured film appeared after 1200 s. No significant increase in the wear scar diameter was observed, whereas a coloured film was present on the worn surfaces (1200-3600 s).

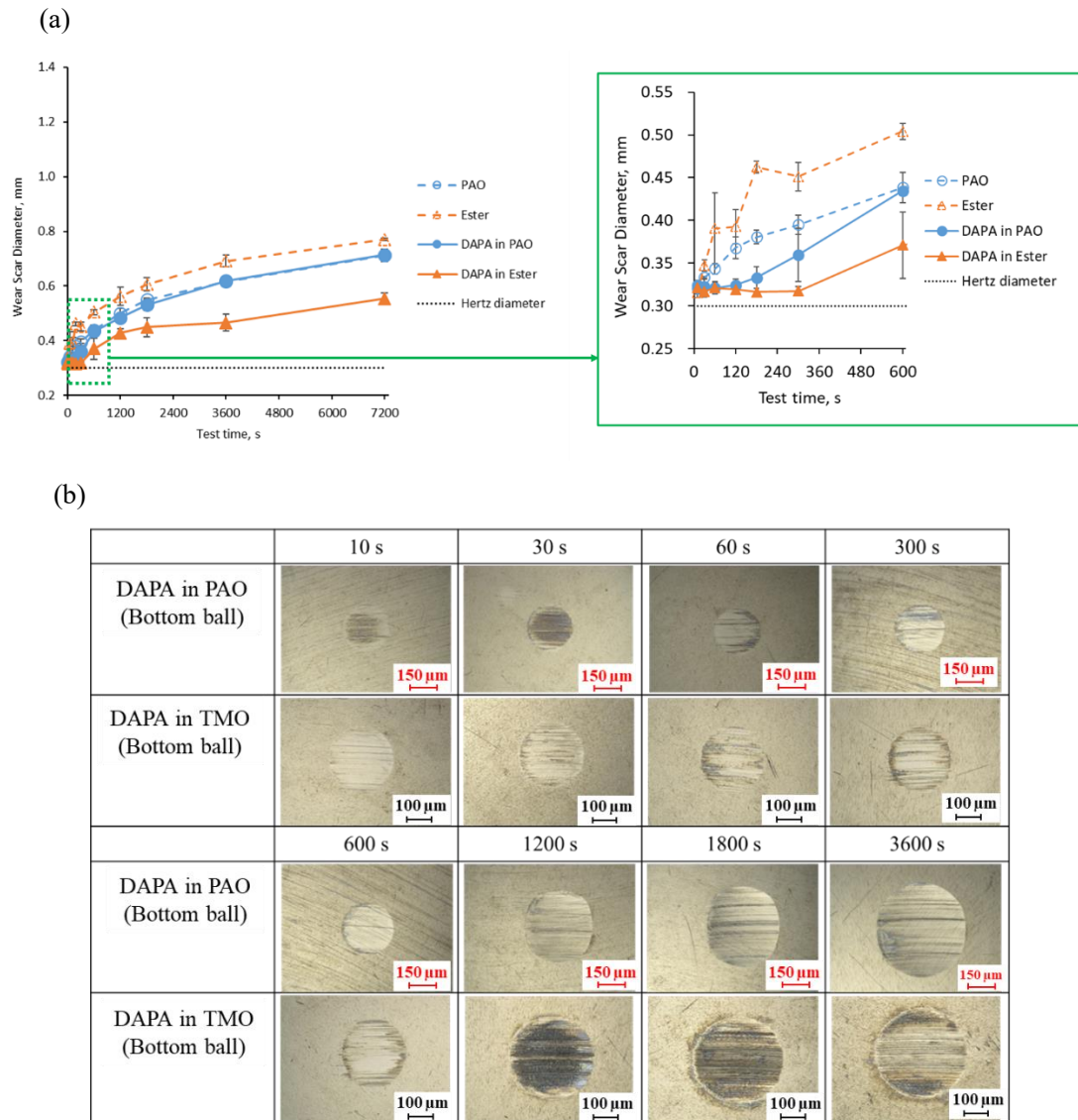


Figure 3-6. Impact of DAPA in PAO and TMO on antiwear capabilities. Four-ball tests were performed at 392 N and 25 °C for various test durations. e DAPA concentration in base oils was 3.1 mmol/kg, corresponding to a phosphorus content of 100 ppm.

3.2.3 Impact of temperature

To investigate the relationship between temperature and AW performance, four-ball tests were performed at various temperatures (25–125 °C) using the four lubricants at 392 N. The results are presented in Figure 3-7. With PAO, wear increased considerably with temperature. DAPA in PAO exhibited almost the same wear scar diameters at all temperatures. For TMO alone, no clear difference in the AW capabilities were found with changes in temperature; however, the wear scar diameters measured with DAPA in TMO became smaller at 125 °C in comparison to those at 25 °C.

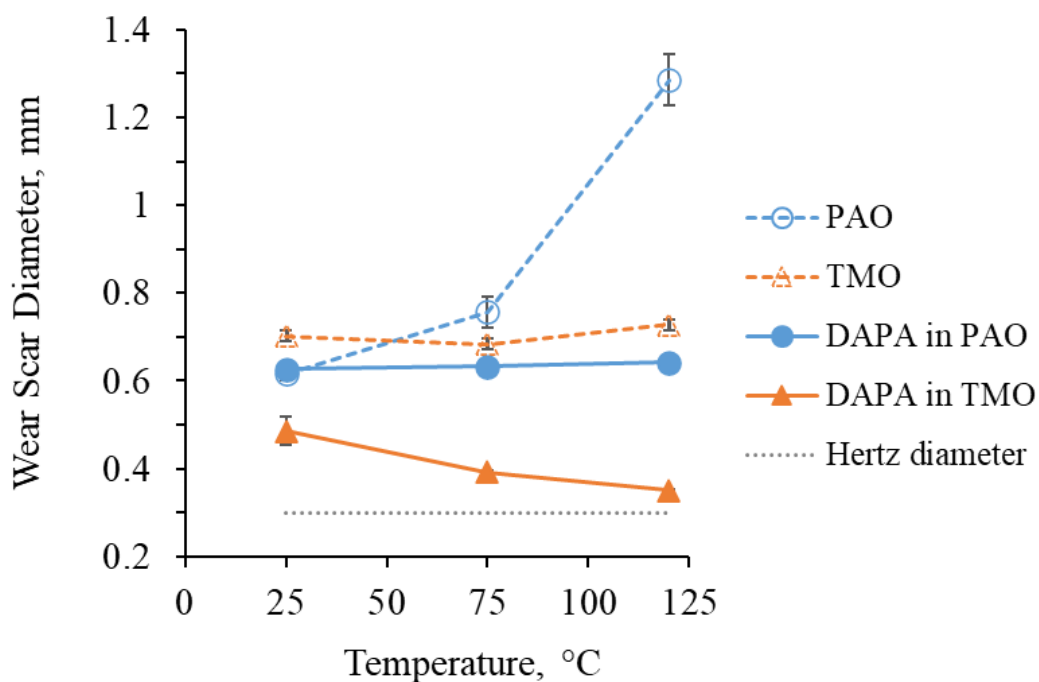


Figure 3-7. Impact of DAPA in TMO and PAO on antiwear performance of lubricants. Four-ball tests were performed at 392 N for 30 min at 25, 75, and 125 °C. DAPA concentration in base oils was 3.1 mmol/kg, corresponding to a phosphorus content of 100 ppm.

3.3 Discussion

3.3.1 Possibilities of phosphonate as AW properties for ester base oils

A previous study evaluated the AW performance of phosphonates in mineral based oils [2] (§ 1.4.1.5). It was concluded that phosphonates are unsuitable as AW additives because the P-C bond in phosphonates is highly stable, resulting in poor tribofilm formation capabilities. Consequently, the use of phosphonates as AW additives is rare.

In this study, phosphonates with polar functional groups, such as COOH, OH and COC₂H₅, exhibit excellent AW effects in TMO, suggesting that the polar functional groups improve the adsorption capabilities of the phosphonates onto metal surfaces under friction. Although phosphonates have been believed not being effective as AW additives in mineral base oil or PAO, this research reveals that the modification of polar functional groups to a phosphonate structure is an effective mean to design AW additive for ester base oils. For further exploring the potential of phosphonates as AW additives in ester base oils, additional investigations should be considered to elucidate the detailed AW properties and mechanisms of DAPA.

3.3.2 AW properties of DAPA and conventional phosphorus additives

Hall reported that phosphorus compounds with strong acidity (e.g. acid phosphate and acid phosphite) have better AW performance than neutral phosphorus ones (e.g. TCP and phosphonate) in neopentyl ester oils [3]. The author concluded that the AW effects of phosphorus additives are related to their acidic strengths. In Figure 3-3, the AW performance of DAPA was compared to the conventional phosphorus additives. In PAO, strong acid compounds (acid phosphate and acid phosphite) have better AW performance than the weak acid (DAPA) and neutral (TCP) additives, indicating that the AW performance of phosphorus additives in PAO are in good agreement with their acidities, as proposed by Hall [3]. On the contrary, in TMO, DAPA showed better AW performance than acid phosphate and acid phosphite. It seems that there is no clear correlation with the acidity in TMO.

Concerning dibutyl phosphite AW additive, the previous work (Figure 1-38) reported that the AW performance of dibutyl phosphite decrease with polarity of the base oils. Here with DAPA, it is not the case, as the AW capabilities are improved in polar base oil (TMO) compared to non polar base oil (PAO).

Esters are used as not only base oils but also lubricant additives and rust inhibitors. It is well known that combinations of lubricant additives often generate antagonistic or synergistic effects, and their tendencies are well documented [4]. The combinations of antirust inhibitors and extreme pressure additives cause competitive adsorption on metal surfaces, resulting in poorer performance than that with extreme pressure additives alone [5]. As shown in Figure 3-3, acid phosphate, acid phosphite and

TCP exhibited poorer AW performances in TMO than in PAO; however, DAPA exhibited the opposite tendency. This suggests that acid phosphate, acid phosphite, and TCP have the antagonistic effects with TMO for the AW performance, but that DAPA exhibits a unique AW performance in ester base oils, which is interesting for further investigation.

3.3.3 Effect of load on AW performance of DAPA in base oils

Regarding the AW properties of base oils, TMO exhibited excellent AW performance at 98 N, whereas PAO exhibited significant wear (Figure 3-4). Ester structures can function as lubricating additives [6-7], and previous studies have reported that ester base oils have better AW properties than those of mineral base oils [8]. Probably, TMO can reduce wear owing to its lubricating effect at low loads. At 98 N, the wear scar diameters and friction coefficient of DAPA in the TMO were similar to those of TMO alone (Figure 3-4(b) and Figure 3-5(a)). In addition, DAPA in TMO did not form a significant tribofilm (optically determined) on the surfaces after the four-ball test at 98 N. This suggests that, at 98 N, TMO may significantly adsorb onto metal surfaces in addition to DAPA (which needs to be confirmed); however, but that the tribological behaviour is controlled primarily by TMO. In other words, DAPA has no significant effect on ester-base oils under mild friction conditions.

Figure 3-8 shows the friction coefficient recorded during the last 5 min of the four-ball tests. The friction coefficient of DAPA in PAO increases with the test load, but that of DAPA in TMO is low at 196 and 294 N. Moreover, DAPA in TMO partially forms clear tribofilm on the surfaces. Accordingly, DAPA acts as AW additives to reduce wear in TMO at 196 N and 294 N. TMO is more efficient than DAPA at 98 N.

At 392 N, DAPA in TMO formed a clear blue-coloured tribofilm on the surfaces, but the friction coefficient is quite high in comparison with the other loads. It is well known that TCP and ZDDP also form blue-coloured tribofilms, and their friction coefficients are around 0.1-0.13 [9-11]. DAPA in PAO shows lower friction coefficient than DAPA in TMO, even though the former gives more significant wear than the latter. One explanation could be that the large wear scar obtained with DAPA in PAO decreases the contact pressure on the worn surfaces, resulting in the lower friction coefficient of DAPA in PAO compared to DAPA in TMO.

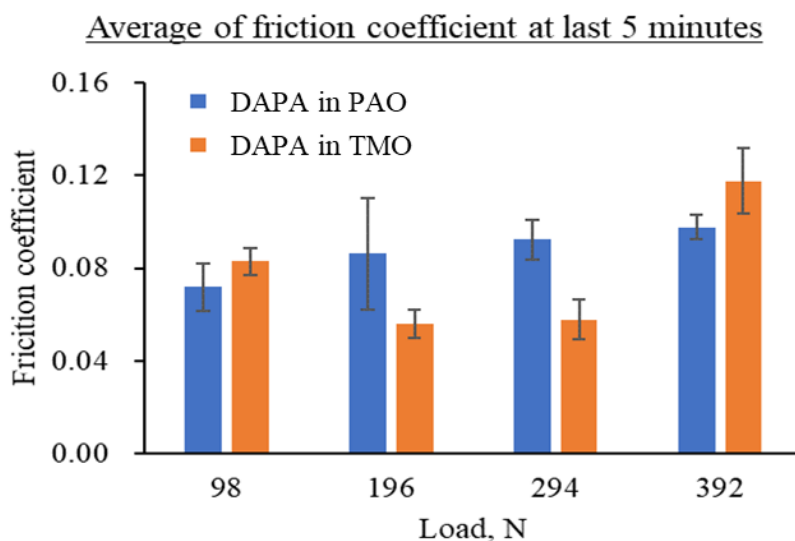


Figure 3-8. Average friction coefficient with DAPA in PAO and DAPA in TMO during the last five minutes of the four-ball tests.

3.3.4 Influence of test time on AW performance of DAPA in base oils

DAPA in PAO formed a clear tribofilm on the surfaces in the early stages of the four-ball tests, however, the tribofilm tended to disappear with the test duration. Consequently, the wear scar diameter became similar to that of PAO alone at 600 s (Figure 3-6). This suggests that DAPA in PAO may adsorb onto metal surfaces under static conditions (no friction) and form a tribofilm at the initial stage of the test, however, the ability of DAPA to generate a tribofilm in PAO under severe sliding conditions is low. For DAPA in TMO, no visible tribofilm was formed on the surfaces in the early stages; however, the sizes of the wear scars were equivalent to the Hertz contact diameters up to 600 s. Moreover, DAPA in TMO resulted in smaller wear scar diameters than those of TMO alone. Therefore, although no visible tribofilm was optically observed, DAPA in TMO may form a very thin and/or heterogeneous tribofilm, which is sufficient to reduce wear. The sizes of the wear scars began to increase after approximately 600 s. A blue tribofilm began to form at 1200 s, and the wear scar diameter stabilised. Therefore, DAPA in TMO appears to have excellent tribofilm formation capabilities, particularly under severe test conditions, compared to that of DAPA in PAO. We will further investigate this in the following chapters.

3.5 Summary of this chapter

The following conclusions can be drawn from this chapter:

1. Dialkyl phosphonates with polar functional groups are effective AW additives in ester base oil (TMO).
2. DAPA exhibits better AW performance than conventional phosphorus additives in TMO, although it was believed that phosphonates have poor performance as AW additives.
3. DAPA has better AW performance in TMO compared to PAO.
4. DAPA in PAO is able to form a thick blue-coloured tribofilm and is able to reduce wear at low loads (98 and 196 N). The AW capabilities of DAPA in PAO are lost at higher loads.
5. The TMO alone is able to reduce wear at 98 N. The combination of TMO and DAPA prevents wear and results in a low friction coefficient under mild conditions (196 and 294 N). At 392 N, DAPA in TMO is able to form a tribofilm that reduce wear.
6. For elucidating the AW mechanisms of DAPA, further investigations concerning the tribofilm composition of DAPA should be carried out.

References

- [1] JCMAS P041.2014: Hydraulic fluids for construction machinery. Tokyo, Japan: Japanese Construction Mechanization Association; 2014.
- [2] E.S. Forbes, E.L. Neustadter, H.B. Silver, N.T. Upsdell, The effect of chemical structure on the load-carrying properties of amine phosphates, *Wear*, **18**, 1971, 269–278.
- [3] J.M. Hall, Antiwear additives in neopentyl ester oils. *ASLE Transaction*, **14**, 1971, 292–300
- [4] H. A. Spikes, Additive-additive and additive-surface interactions in lubrication. *Lubrication Science*, **2**, 1989, 3–23.
- [5] H. A. Spikes, A. Cameron, Additive Interference in Dibenzyl Disulfide Extreme Pressure Lubrication., *ASLE Transactions*, **17**, 1974, 283-289
- [6] L. R. Rudnick, Lubricant Additives Chemistry and Applications, Second Edition, CRC Press., 2009
- [7] F. P. Bowden, F. P. Bowden, D. Tabor, The Friction and Lubrication of Solids, Oxford University Press., 2001
- [8] K. S. V. K. Reddy, N. Kabra, U. Kunchum, T. Vijayakumar, Experimental Investigation on Usage of Palm Oil as a Lubricant to Substitute Mineral Oil in CI Engines., *Chinese Journal of Engineering*, 2014, 1-5.
- [9] A. Gauthier, H. Montes, J. M. Georges, Boundary Lubrication with Tricresyl phosphate (TCP). Importance of Corrosive Wear., *ASLE Transactions*, **25**, 1982, 445–455.
- [10] J. Sheasby, T. Caughlin, W. Mackwood, The effect of steel hardness on the performance of antiwear additives., *Wear*, **201**, 1996, 209–216.
- [11] R. Heuberger, A. Rossi and N.D. Spencer, Pressure Dependence of ZnDTP Tribochemical Film Formation: A Combinatorial Approach. *Tribology Letters*, **28**, 2007, 209–222

Chapter 4

Investigations of DAPA tribofilm compositions

| | | |
|-------|------------------------------------------------------------|-----|
| 4.1 | DAPA tribofilm analyses using XPS | 69 |
| 4.1.1 | Measurement conditions and survey spectra | 69 |
| 4.1.2 | Detailed analyses of high resolution spectra..... | 71 |
| 4.1.3 | Depth profile of DAPA tribofilm | 85 |
| 4.2 | DAPA tribofilm analyses using ToF-SIMS | 86 |
| 4.3 | DAPA tribofilm observations using FIB-TEM..... | 90 |
| 4.4 | DAPA tribofilm analyses using Infrared Spectroscopies..... | 92 |
| 4.5 | Discussion | 96 |
| 4.5 | Summary of this chapter | 99 |
| | References..... | 100 |

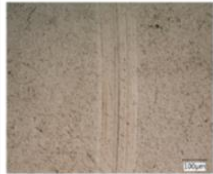
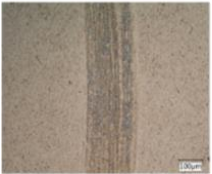
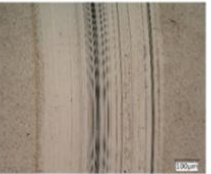
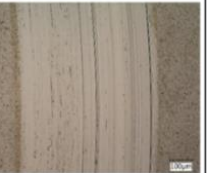


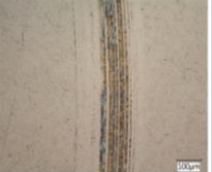
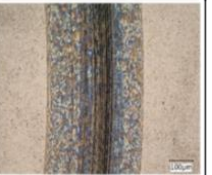
The previous chapter focused on the AW properties of DAPA. It was shown that DAPA in TMO has better AW performance than DAPA in PAO, especially at high loads. In this chapter, the compositions of the different DAPA tribofilms were investigated using various surface analysis techniques, such as X-ray Photoelectron Spectroscopy (XPS), Time-of-Flight Secondary Ion Mass Spectrometry (ToF-SIMS), Transmission Electron Microscopy with Focused Ion Beam (TEM-FIB), Fourier Transform Infra-Red (FTIR) and Polarization Modulation Infrared Reflection-Absorption Spectroscopy (PM-IRRAS). Based on these characterizations, the tribofilm formation mechanism is discussed together with the difference in tribological behavior of the DAPA additive whether it is dispersed in PAO or in ester base oil.

4.1 DAPA tribofilm analyses using XPS

4.1.1 Measurement conditions and survey spectra of DAPA tribofilm

The tribofilms obtained after the tribotests at various loads (98, 196, 294, and 392 N) presented in Chapter 3 (§3.2.1) were analysed using XPS. Each analysis was carried out below a pressure of 10^{-7} Pa using PHI VersaProbe II. The X-ray source was the Al K α ($h\nu = 1486.6$ eV) at 50 W, and the beam diameter of X-ray was 50 μm . First, the survey spectra were obtained at a pass energy of 187.85 eV, followed by the measurements of the high-resolution spectra of detected elements at 23.50 eV. The depth profiles of detected elements were also obtained using an Ar $^{+}$ ion gun. The etching was performed on a 2×2 mm 2 area for 60 minutes at 250 V. Table 4-1 shows the optical images of the surfaces analysed by XPS. The corresponding four-ball test results are shown in Chapter 3, Figure 3-4. The top balls were selected for the present investigations due to the homogeneous aspect of the tribofilms. Reference compounds (TMO and DAPA) were also characterised for comparison. The XPS spectra acquisition of the worn surfaces and TMO (reference compound) was carried out at 25 °C. To get the XPS spectra of DAPA, it was necessary to cool DAPA with liquid nitrogen because at ambient temperature, the DAPA evaporates in the XPS chamber (Ultra High Vacuum).

Table 4-1. Tribofilm generated from DAPA in PAO and DAPA in TMO after the four-ball tests

| | 98 N | 196 N | 294 N | 392 N |
|---------------------------|-------------------------------------------------------------------------------------|-------------------------------------------------------------------------------------|--------------------------------------------------------------------------------------|---------------------------------------------------------------------------------------|
| DAPA in PAO (Top ball) |  |  |  |  |
| DAPA in TMO (Top ball) |  |  |  |  |

The survey spectra recorded from the top balls are depicted in Figure 4-1. The peaks of carbon, oxygen and iron were detected in the survey spectra of all samples. The peaks of phosphorus (P_{2p}) are considered to derive from DAPA or its tribofilm. The samples with DAPA in PAO showed clear peaks of P_{2p} for all the tested loads, however, those of DAPA in TMO had no significant P_{2p} peak at 98 and 196 N. For reference compounds, peaks of the elements corresponding to the chemical structures of DAPA and TMO were detected.

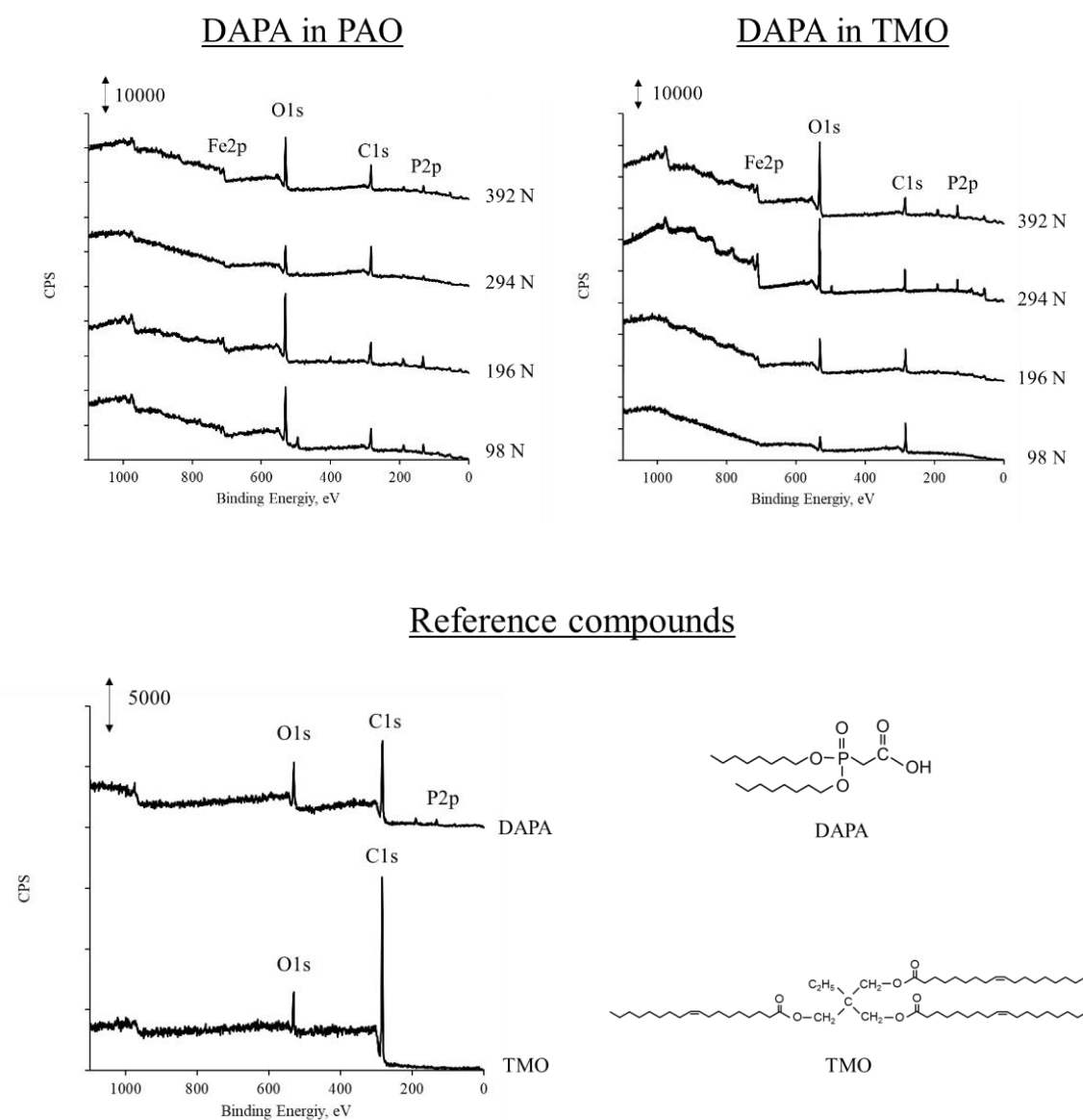


Figure 4-1. XPS survey spectra recorded from the worn surfaces of the top balls obtained after four-ball tests and the reference compounds (TMO and DAPA).

4.1.2 Detailed analyses of high resolution spectra

Atomic concentrations

Table 4-2 lists a summary of the atomic concentrations obtained from the high-resolution spectra. Quantifiable phosphorus signals were detected in all the samples. The worn surface obtained after the four-ball tests with DAPA in TMO at 98 N showed a high carbon concentration and low phosphorus concentration when compared with those of the others. For the reference compounds, the atomic concentrations of TMO and DAPA were in good agreement with their theoretical values.

Table 4-2. Atomic concentrations determined from XPS analyses of the worn surfaces after four-ball tests and reference compounds.

| Sample name | | [C] at % | [O] at% | [P] at% | [Fe] at% |
|---------------------|---------------------|----------|---------|---------|----------|
| DAPA in TMO | 98 N | 60.5 | 33.9 | 1.5 | 4.0 |
| | 196 N | 41.6 | 46.0 | 4.3 | 8.2 |
| | 294 N | 46.5 | 42.1 | 5.6 | 5.7 |
| | 392 N | 44.6 | 40.8 | 9.5 | 5.1 |
| DAPA in PAO | 98 N | 52.2 | 38.6 | 6.8 | 2.6 |
| | 196 N | 37.6 | 47.9 | 10.1 | 5.5 |
| | 294 N | 57.5 | 33.3 | 5.3 | 3.9 |
| | 392 N | 51.7 | 35.8 | 6.8 | 5.9 |
| Reference Compounds | TMO (experimental) | 90.1 | 9.9 | - | - |
| | TMO (theoretical) | 90.9 | 9.1 | - | - |
| | DAPA (experimental) | 76.4 | 20.1 | 3.5 | - |
| | DAPA (theoretical) | 75.0 | 20.8 | 4.2 | - |

Curve-fitting analyses

To study the chemical composition of the DAPA tribofilm, curve-fitting analyses were performed using high-resolution spectra obtained from the worn surfaces at 98, 196, 294, and 392 N and reference compounds. Table 4-3 presents the curve-fitting results, including the binding energies, full width at half maximum (FWHM), and atomic concentration of each chemical species.

Table 4-3. Curve fitting XPS parameters for C_{1s}, O_{1s}, and P_{2p} peaks of tribofilms obtained at 98, 196, 294, and 392 N using the four tested lubricants (PAO, ester, DAPA in PAO, and DAPA in TMO) and reference compounds.

| Sample | | Parameter | C1s | | | | O1s | | | | | P2p |
|---------------------|-------|--------------------|---------|-------|-------|---------|-------|----------------|----------------|------------------|--------------------|--------|
| | | | C-H/C-C | CO | COO | carbide | Oxide | NBO | C=O | BO | C-O | P2p3/2 |
| DAPA in PAO | 98 N | Binding energy, eV | 285.0 | 286.5 | 289.0 | - | 529.4 | 531.9 | - | 533.3 | - | 133.6 |
| | | FWHM, eV | 1.7 | 2.0 | 2.0 | - | 1.0 | 2.1 | - | 2.1 | - | 1.9 |
| | | atom% | 46.7 | 7.3 | 5.6 | - | 0.1 | 25.2 | - | 6.8 | - | 6.1 |
| | 196 N | Binding energy, eV | 285.0 | 286.6 | 288.8 | - | - | 531.7 | - | 533.3 | - | 133.3 |
| | | FWHM, eV | 1.7 | 1.3 | 2.1 | - | - | 2.1 | - | 1.9 | - | 1.9 |
| | | atom% | 26.2 | 4.6 | 7.8 | - | - | 38.4 | - | 8.6 | - | 9.8 |
| | 294 N | Binding energy, eV | 285.0 | 286.6 | 289.0 | - | 530.0 | 531.7 | - | 533.3 | - | 133.2 |
| | | FWHM, eV | 1.1 | 2.0 | 1.4 | - | 2.0 | 1.8 | - | 1.9 | - | 1.5 |
| | | atom% | 51.6 | 8.1 | 5.8 | - | 0.6 | 21.0 | - | 6.2 | - | 4.3 |
| | 392 N | Binding energy, eV | 285.0 | 286.6 | 288.9 | - | - | 531.5 | - | 533.3 | - | 133.1 |
| | | FWHM, eV | 1.3 | 1.7 | 1.5 | - | - | 1.8 | - | 1.6 | - | 1.4 |
| | | atom% | 35.4 | 6.6 | 5.7 | - | - | 34.3 | - | 6.8 | - | 7.0 |
| DAPA in Ester | 98 N | Binding energy, eV | 285.0 | 286.5 | 289.2 | - | 530.0 | 531.7 | 532.3 | - | 533.8 | 132.9 |
| | | FWHM, eV | 1.1 | 2.0 | 1.3 | - | 1.1 | 2.3 | 1.5 | - | 1.5 | 1.4 |
| | | atom% | 61.7 | 9.2 | 4.9 | - | 1.9 | 11.7 | 3.7 | - | 3.7 | 1.8 |
| | 196 N | Binding energy, eV | 285.0 | 286.6 | 289.1 | 283.8 | 530.0 | 531.7 | 532.3 | 533.2 | 533.8 | 133.5 |
| | | FWHM, eV | 1.5 | 2.1 | 1.6 | 1.1 | 1.1 | 2.1 | 1.2 | 0.6 | 1.2 | 1.5 |
| | | atom% | 33.6 | 6.7 | 4.9 | 10.2 | 1.8 | 27.4 | 3.0 | 0.4 | 3.0 | 4.1 |
| | 294 N | Binding energy, eV | 285.0 | 286.5 | 288.9 | 283.3 | 530.1 | 531.5 | 532.3 | 533.1 | 533.8 | 133.4 |
| | | FWHM, eV | 1.3 | 1.6 | 1.5 | 0.8 | 1.1 | 1.6 | 1.2 | 1.2 | 1.2 | 1.5 |
| | | atom% | 24.4 | 2.2 | 3.0 | 0.9 | 8.9 | 34.6 | 2.2 | 4.3 | 2.2 | 8.7 |
| | 392 N | Binding energy, eV | 285.0 | 286.6 | 289.1 | 283.7 | 530.0 | 531.7 | - | 533.3 | - | 133.7 |
| | | FWHM, eV | 1.6 | 1.7 | 1.9 | 1.6 | 2.2 | 1.7 | - | 1.6 | - | 1.8 |
| | | atom% | 19.1 | 1.8 | 2.3 | 5.8 | 1.5 | 38.4 | - | 9.0 | - | 11.5 |
| Reference compounds | TMO | Binding energy, eV | 285.0 | 286.3 | 289.3 | - | - | - | 532.3 (C=O) | - | 533.8 (C-O) | - |
| | | FWHM, eV | 1.1 | 1.5 | 0.8 | - | - | - | 1.2 | - | 1.2 | - |
| | | atom% | 77.5 | 9.3 | 3.2 | - | - | - | 5.0 | - | 5.0 | - |
| | DAPA | Binding energy, eV | 285.0 | 286.6 | 288.9 | - | - | 531.0 (P=O) | 532.0 (C=O) | 533.0 (C-O-P) | 533.9 (O=C-O-H) | 133.6 |
| | | FWHM, eV | 1.6 | 1.6 | 1.6 | - | - | 1.5 | 1.5 | 1.5 | 1.5 | 1.8 |
| | | atom% | 64.3 | 8.8 | 3.3 | - | - | 3.4 | 4.8 | 8.8 | 3.8 | 3.5 |

The detailed curve fitting results of the O_{1s} spectra on the worn surfaces obtained with DAPA in PAO and DAPA in TMO are shown in Figure 4-2.

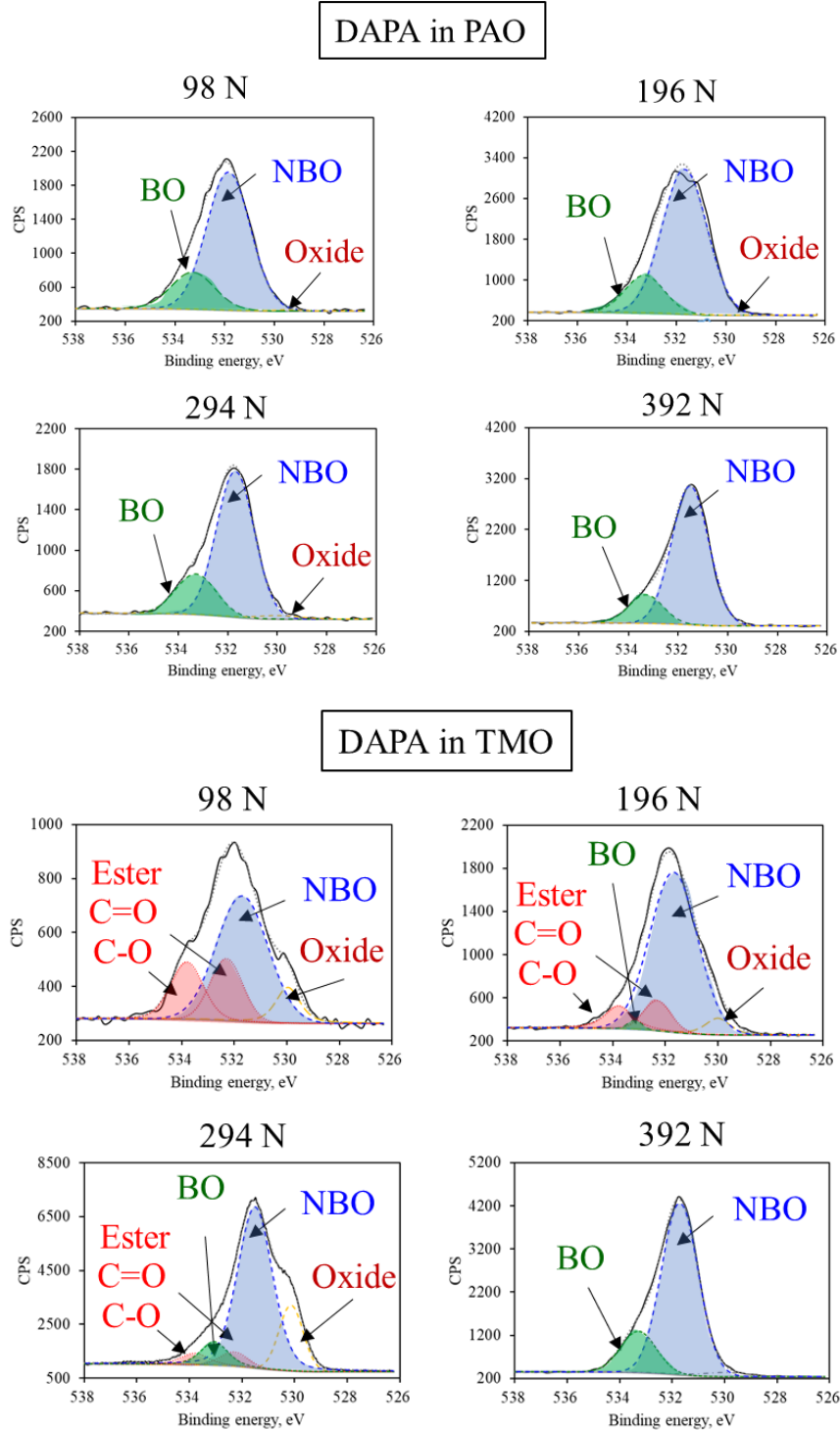


Figure 4-2. Curve fitting results of O_{1s} spectra on the worn surfaces of test specimens after four-ball testing at 98–392 N. NBO = non-bridging oxygen; BO = bridging oxygen.

O1s peak fitting

The tribofilm of DAPA in PAO shows three contributions in the O_{1s} peak. The first contribution at 529.7 ± 0.3 eV was assigned to metal oxide [1,2], the second peak at 531.7 ± 0.3 eV was assigned to non-bridging oxygen (NBO) in phosphate [3] however, this peak might also contain other oxidised compounds, such as FeOOH [4]). The third peak at 533.3 ± 0.0 eV was assigned to bridging oxygen (BO), between two phosphorus atoms in polyphosphates (P-O-P) [5], or between a carbon and a phosphorus atom in P-O-C bonds [7]. In addition to the three peaks found in the tribofilm obtained with DAPA in PAO, the tribofilm of DAPA in TMO had two additional contributions at 532.3 and 533.8 eV assigned to the C=O and C-O bonds in TMO, respectively. These contributions assigned to TMO (ester group) appeared to decrease with load, as the contribution at high binding energies decreased from 98 N to 392 N. To maintain an appropriate fit, the contribution of BO must be introduced, suggesting that DAPA forms a tribofilm on the surfaces more dominantly than does TMO at high loads.

For the neat DAPA, The O_{1s} peak had four contributions assigned to P=O at 513.0 eV, C=O at 532.0 eV [6], C-O-P at 533.0 eV [7] and COOH at 533.9 eV [6]. The binding energy of P=O was observed to be between 531.5 eV (assigned to TCP [7]) and 530.9 eV (assigned to triphenyl phosphine oxide with three P-C bonds [8]). Curve-fitting analyses of the DAPA tribofilm using the four detected oxygen species of the DAPA molecule were performed; however, the fitting procedures were not successful. It was so assumed that the chemical structure of DAPA changed significantly when the DAPA tribofilms were generated.

P2p_{3/2} peak fitting

The binding energy of P_{2p_{3/2}} in tribofilms obtained with DAPA in ester and DAPA in PAO were observed at 132.9 - 133.7 eV and 133.1 – 133.6 eV, respectively. Table 4-4 lists the binding energies of P_{2p_{3/2}} for orthophosphate, pyrophosphate, metaphosphate and P₂O₅ obtained from literature [9, 10]. Compared to these phosphorus compounds, the DAPA tribofilms obtained using DAPA in TMO and PAO had lower binding energies of P_{2p_{3/2}}. The binding energies of TCP, tributyl phosphate, DAPA and tributyl phosphonate as reported in literature, are compared in Table 4-5 [7, 8, 11]. The binding energies of P_{2p_{3/2}} tends to decrease based on the number of P-C bond in their chemical structures. Therefore, the lower binding energy of DAPA tribofilms in comparison with orthophosphate, pyrophosphate, metaphosphate and P₂O₅ implies that the chemical compositions of the DAPA tribofilm are not the same as those of the phosphate species. Furthermore, this suggests the presence of P-C bonds characteristic of phosphonate inside the DAPA tribofilms.

Table 4-4. $P_{2p_{3/2}}$ binding energies of phosphate species corrected with C_{1s} at 285 eV.

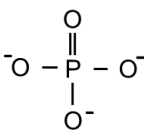
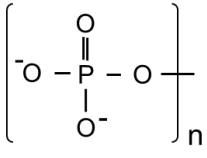
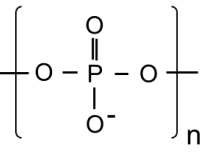
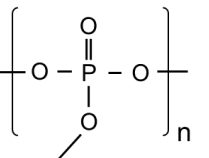
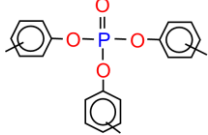
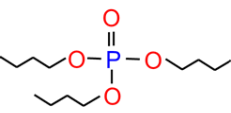
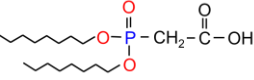
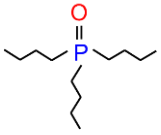
| | Orthophosphate | Pyrophosphate | Metaphosphate | P_2O_5 |
|--------------------|-----------------------------------------------------------------------------------|-----------------------------------------------------------------------------------|------------------------------------------------------------------------------------|-------------------------------------------------------------------------------------|
| Chemical structure |  |  |  |  |
| $P_{2p_{3/2}}$ | 134.1 eV | 134.4 eV | 134.8 eV | 135.4 - 135.8 eV |
| Ref. | [9] | [9] | [9] | [10] |

Table 4-5. $P_{2p_{3/2}}$ binding energies of phosphorus compounds corrected with C_{1s} at 285 eV.

| | Tricresyl phosphate (TCP) | Tributyl phosphate | DAPA | Tributyl phosphine oxide |
|--------------------|------------------------------------------------------------------------------------|------------------------------------------------------------------------------------|-------------------------------------------------------------------------------------|--------------------------------------------------------------------------------------|
| Chemical structure |  |  |  |  |
| $P_{2p_{3/2}}$ | 133.8 eV | 133.8 eV | 133.6 eV | 132.3 eV |
| P=O bind | 1 | 1 | 1 | 1 |
| P-O bond | 3 | 3 | 2 | 0 |
| P-C bond | 0 | 0 | 1 | 3 |
| Ref. | [7] | [11] | Table 4-3 | [8] |

Comparison of atomic concentrations inside and outside wear scars

To identify the species of DAPA adsorbed on steel surfaces, the chemical structure of DAPA before tribochemical reaction needs to be investigated. Thus, XPS analysis were also performed outside the wear tracks. The samples for XPS were selected from the top balls after four-ball tests performed at 98-392 N.

The atomic concentrations outside and inside the wear scars with DAPA in PAO and DAPA in TMO are summarised in Table 4-6. Compared with the atomic concentrations inside the wear scars, those obtained outside the wear scars had lower phosphorus concentrations. Regarding the phosphorus concentrations outside the wear scars, DAPA in TMO exhibited 1.0 at% or less at 98-294 N although it was higher for DAPA in PAO. Therefore, the lowest concentration of phosphorus found outside the

wear scar in the presence of TMO compared with that of PAO suggests a slightly better adsorption of DAPA on the steel surfaces in the presence of non-polar base oils.

Because the XPS spectra for the DAPA in TMO outside acquired at 392 N exhibited a higher phosphorus concentration, it was used to discuss the P_{2p} binding energies. For DAPA in PAO, the XPS spectrum obtained at 196 N, which had the highest phosphorus concentration, was also selected.

Table 4-6. Atomic concentrations determined from XPS analyses outside and inside the wear scars after the four-ball tests performed at 98-392 N.

(a) DAPA in PAO

| | | [C] at% | [O] at% | [P] at% | [Fe] at% |
|---------|-------|---------|---------|---------|----------|
| outside | 98 N | 66.6 | 29.7 | 2.9 | 0.8 |
| | 196 N | 47.7 | 46.0 | 5.3 | 1.0 |
| | 294 N | 66.2 | 28.6 | 1.7 | 3.6 |
| | 392 N | 54.0 | 38.7 | 2.6 | 4.7 |
| inside | 98 N | 52.2 | 38.6 | 6.8 | 2.6 |
| | 196 N | 37.6 | 47.9 | 10.1 | 5.5 |
| | 294 N | 57.5 | 33.3 | 5.3 | 3.9 |
| | 392 N | 51.7 | 35.8 | 6.8 | 5.9 |

(b) DAPA in TMO

| | | [C] at% | [O] at% | [P] at% | [Fe] at% |
|---------|-------|---------|---------|---------|----------|
| outside | 98 N | 75.9 | 21.5 | 0.8 | 1.8 |
| | 196 N | 55.5 | 37.6 | 1.0 | 5.9 |
| | 294 N | 58.4 | 34.6 | 0.9 | 6.0 |
| | 392 N | 62.4 | 30.7 | 3.8 | 3.2 |
| inside | 98 N | 60.5 | 33.9 | 1.5 | 4.0 |
| | 196 N | 41.6 | 46.0 | 4.3 | 8.2 |
| | 294 N | 46.5 | 42.1 | 5.6 | 5.7 |
| | 392 N | 44.6 | 40.8 | 9.5 | 5.1 |

Table 4-7 summarises the binding energies of $P_{2p3/2}$ observed on the outside and inside of the wear scars. Outside the wear scars, the binding energies of $P_{2p3/2}$ with DAPA in PAO at 196 N and that with DAPA in TMO at 392 N exhibited the same binding energies at 133.1 eV. Inside the wear scars, DAPA in PAO and DAPA in TMO had 0.2 eV and 0.6 eV higher energies than those on the outside, respectively.

Table 4-7. Binding energies of $P_{2p_{3/2}}$ observed after four-ball tests using DAPA in PAO and DAPA in TMO at 196 and 392 N.

| | outside | inside |
|---------------------|---------|--------|
| DAPA in PAO (196 N) | 133.1 | 133.3 |
| DAPA in TMO (392 N) | 133.1 | 133.7 |

The binding energies of $P_{2p_{3/2}}$ outside the wear scars provide information on the adsorption species of DAPA. There was no significant difference between DAPA in PAO and DAPA in TMO. However, the binding energy of $P_{2p_{3/2}}$ obtained from neat DAPA was 133.6 eV (Figure 3-2), which was 0.5 eV higher than those obtained outside the wear scars. These results suggest that DAPA forms similar adsorption species on steel, regardless of the types of base oil. However, DAPA adsorption species have different chemical states from neat DAPA.

Chemical composition considerations of DAPA tribofilms from high resolution spectra

Figure 4-3 shows the atomic concentration ratios of C_x/P and P/O_y , where C_x is the C_{1s} atomic concentration of the hydrocarbon detected at 285.0 eV and O_y is the sum of the O_{1s} atomic concentration of NBO at 531.7 ± 0.3 and BO at 533.0 ± 0.0 eV.

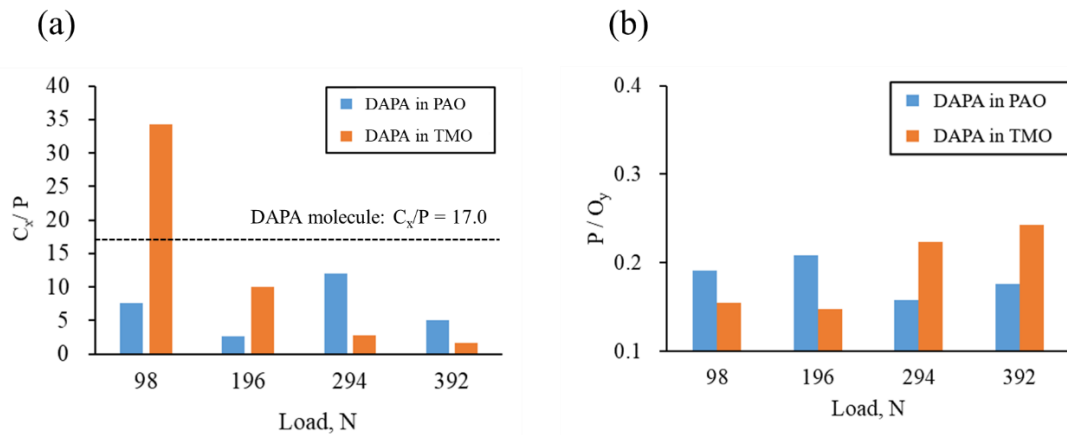


Figure 4-3. Ratio of atomic concentrations (C_x/P and P/O_y) on the worn surfaces of the test specimens calculated from XPS semi-quantification.

DAPA in TMO had a higher C_x/P ratio at 98 N than that of the DAPA molecule, with a value of 17.0, indicating that DAPA was not the only source of carbon on the worn surface. DAPA in TMO for loads higher than 196 N and DAPA in PAO for all tested loads had a lower C_x/P than that of the DAPA molecule. This suggests that the alkyl chains of DAPA were removed by friction. The C_x/P ratio of DAPA in TMO decreased as the test load increased. DAPA in PAO had the lowest C_x/P ratio at 196 N, where the clearest-coloured film was observed on the worn surfaces of the test specimens (see Table 4-1).

The P/O_y ratios of tribofilms have been previously investigated using XPS. For example, ZDDPs have been reported to form phosphate species with various chain lengths, such as orthophosphate, pyrophosphate and metaphosphate [9, 10]. The chain length of phosphates in a tribofilm can be estimated by calculating the P/O ratio from the XPS data. For ZDDP, it was reported that the formation of orthophosphate was observed at low loads; however, polyphosphates with a high degree of polymerisation were detected at high loads [10]. In the present study, the P/O_y ratios of the tribofilms of DAPA in TMO increased with the test load, suggesting that the degree of polymerisation of the phosphorus compounds increased with the load. In contrast, the P/O_y ratios of DAPA in PAO at 98 and 196 N were higher than those at 294 and 392 N. This results suggests that the P-O-P formation for tribofilm generation with DAPA in PAO occurs more efficiently under low loads.

Figure 4-4 depicts the P/O_y ratios of DAPA tribofilms, ZDDP tribofilms, four phosphates (orthophosphate, pyrophosphate, metaphosphate and P₂O₅) and three phosphonate model compounds with various degrees of polymerisation. The P/O_y ratios of the DAPA tribofilms for DAPA in TMO at 392 N and DAPA in PAO at 196 N are shown in Figure 4-3 (b). The P/O_y ratios of the ZDDP tribofilms were calculated from data reported in the literature [9,12], and those of the phosphates and phosphonates were calculated from their chemical structures. The P/O_y ratios of the ZDDP tribofilms are similar to those of metaphosphate and P₂O₅, indicating the formation of polyphosphates. In contrast, the P/O_y ratios of the DAPA tribofilms are lower than those of polyphosphates and closer to those of phosphonates. This finding suggests that the DAPA tribofilms still contain a phosphonate structure with P-C bond, and that the chemical composition of the DAPA tribofilms was different from that of the ZDDP tribofilms.

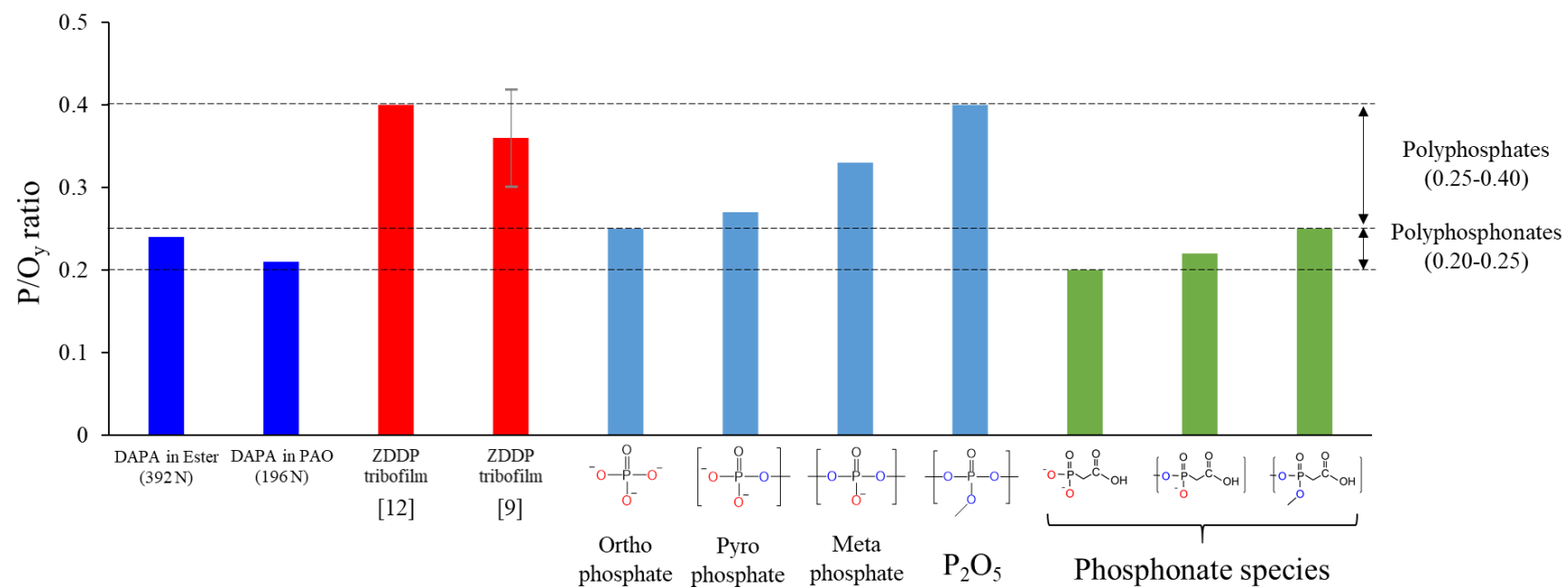


Figure 4-4. P/O_y ratio of DAPA tribofilms, ZDDP tribofilms, phosphate, and phosphonate species. O_y is the atomic concentration of oxygen, calculated as the sum of bridging oxygen and non-bridging oxygen for the DAPA and ZDDP tribofilms.

4.1.3 Depth profile of DAPA tribofilm

Figure 4-5 shows the XPS depth profiles that were conducted of the tribofilms obtained at 196 N (representative of low loads) and 392 N (representative of high loads) with DAPA in PAO and DAPA in TMO. At low loads (196 N), a thick tribofilm was observed for DAPA in PAO (blue area) and native iron oxide with a small amount of phosphorus and carbon adsorbed species was observed for DAPA in TMO (grey area). The opposite effect was observed at high loads (392 N), with iron oxide detected at low loads for DAPA in PAO (grey area) and a thick phosphorus-based tribofilm at high loads for DAPA in TMO (blue area). Carbon and iron were observed in both DAPA tribofilms, in addition to phosphorus atoms. The presence of carbon inside the tribofilms may confirm the presence of P-C bonds and carboxylic acid in the DAPA tribofilms.

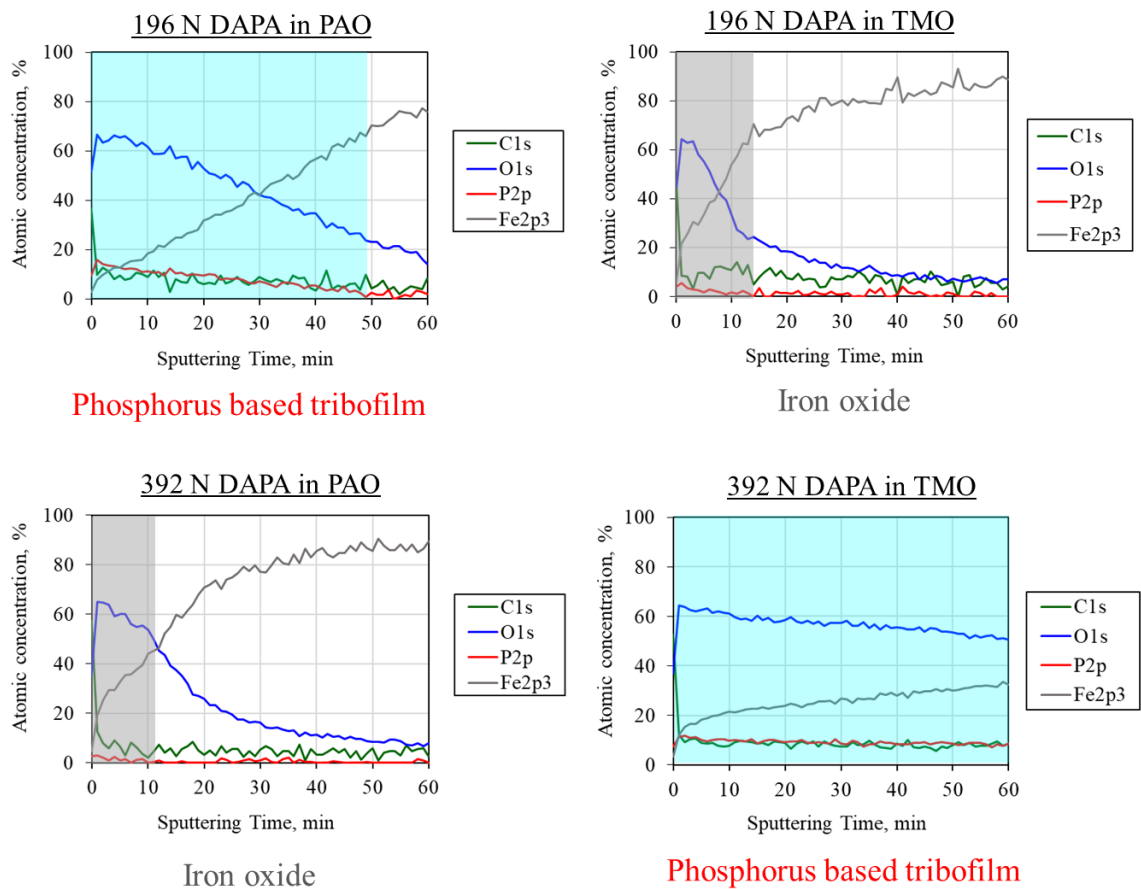


Figure 4-5. XPS depth profiles recorded on tribofilms obtained at test loads of 196 and 392 N with DAPA in PAO and DAPA in TMO.

4.2 DAPA tribofilm analyses using ToF-SIMS

Chemical species formed on steel surfaces after the four-ball tests were characterized using ToF-SIMS. Each measurement was performed using a TRIFT V nanoTOF spectrometer. A primary ion beam of Bi^{32+} with 30 keV acceleration voltage and a pulse width of 12 ns were used to record spectra in positive and negative modes. The spot size was $100 \times 100 \mu\text{m}^2$, which was smaller than the wear scar diameter found in the four-ball tests. The top balls after the four-ball tests at 392 N were selected for ToF-SIMS, because significant tribofilm differences were observed between DAPA in PAO and DAPA in TMO, as shown in Figure 4-6(a). The positive and negative ions spectra were analyzed by Win CadenceN software. Figure 4-6(b) reports the positive ion ToF-SIMS spectra obtained on the steel surfaces after the four-ball tests at 392 N with DAPA in PAO and DAPA in TMO. Although the peaks assigned to hydrocarbon (C_3H_7) were detected from both samples, the contaminants such as Na, K and silicon containing compounds were mainly detected, and no clear information regarding DAPA tribofilm was obtained in the positive ion ToF-SIMS spectra.

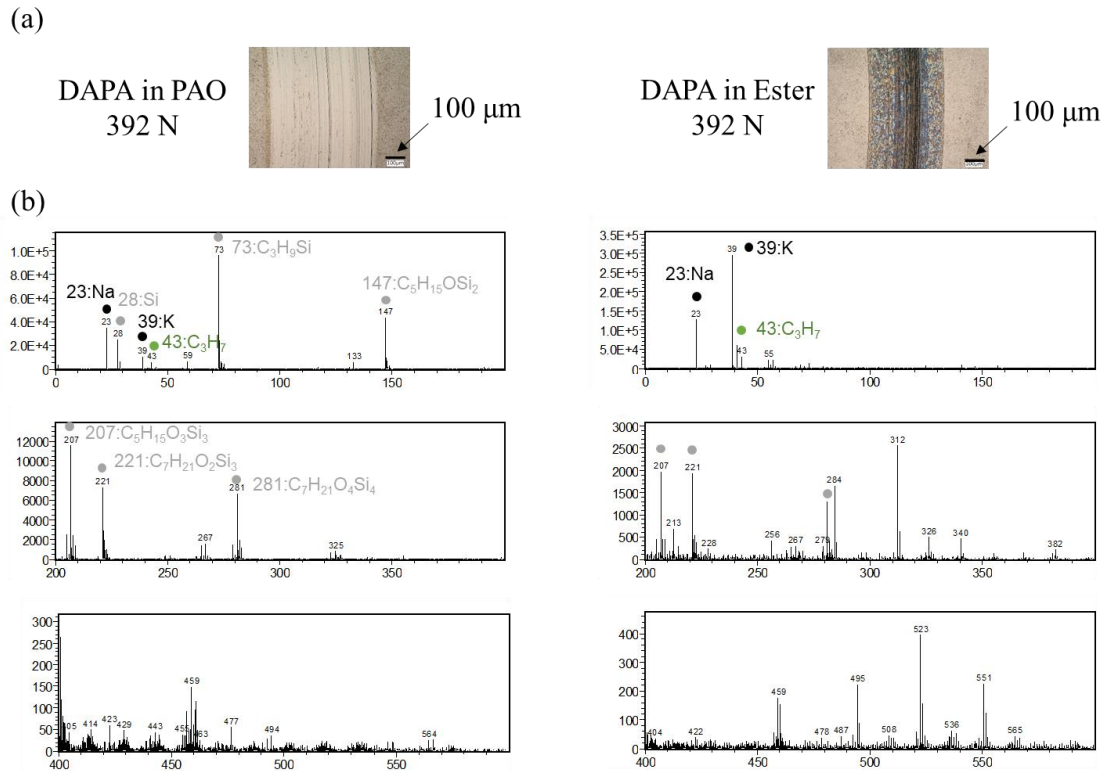


Figure 4-6. Positive ion spectra on worn surfaces after four-ball tests at 392 N with DAPA in PAO and DAPA in TMO

The negative ion spectra are presented in Figure 4-7. The peaks assigned to iron phosphate ($\text{Fe}_x\text{P}_y\text{O}_z$), PO_2 and PO_3 were observed from both samples. In the literature [13], zinc orthophosphate, zinc pyrophosphate and zinc metaphosphate were analyzed using ToF-SIMS. Their spectra contain not only the peaks assigned to PO_2 and PO_3 but also those of PO_4 ($m/z = 95.0$), as shown in Figure 4-8. However, no clear peak of PO_4 was detected in the present study. This suggests that the chemical structure of DAPA tribofilm is not the same as ZDDP tribofilm.

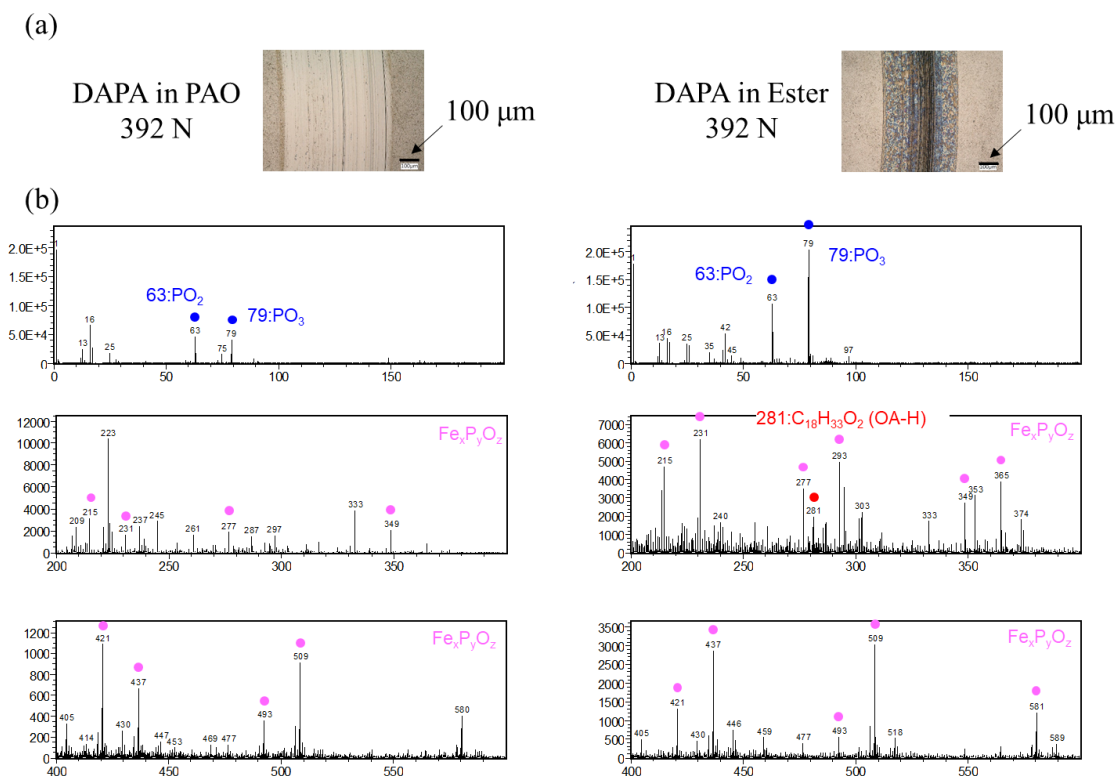


Figure 4-7. Negative ion spectra of worn surfaces after four-ball tests at 392 N with DAPA in PAO and DAPA in TMO

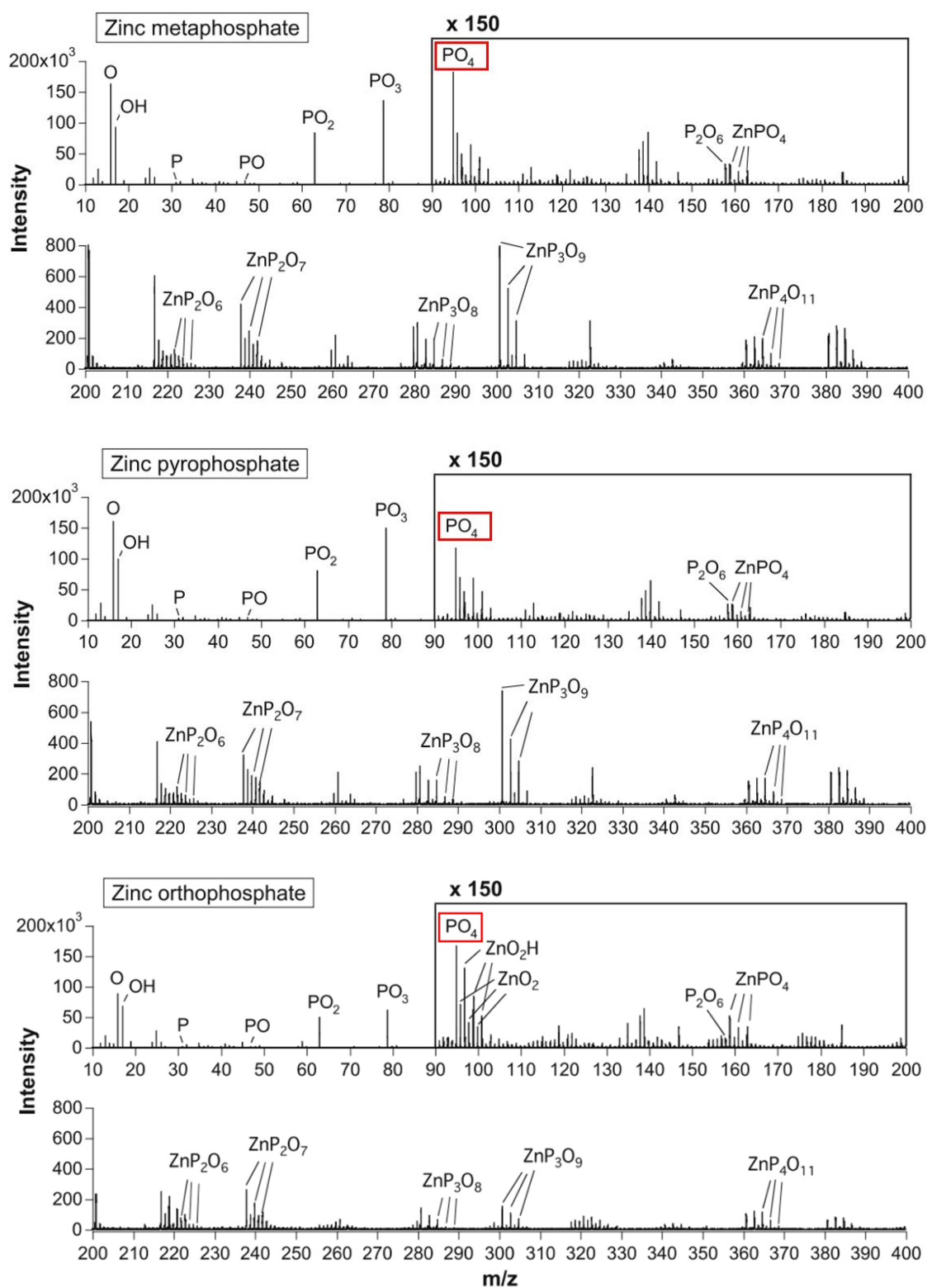


Figure 4-8. Negative ion spectra of zinc metaphosphate. Zinc pyrophosphate and zinc orthophosphate [13].

Figure 4-9 compares the negative ion spectra (m/z : 200-400) of worn surfaces after the four-ball tests at 98, 196 and 392 N with DAPA in TMO. The peak assigned to oleic acid ($C_{18}H_{33}O_2$) was found on the worn surfaces at 196 and 392 N. TMO is an ester base oil produced from oleic acid and trimethylolpropane. The presence of oleic acid indicates that TMO was decomposed under friction, following the formation of oleic by the cleavage of the ester bond. At 98 N, there is no significant peak of oleic acid. TMO shows excellent AW performance at 98 N, but no AW effect was observed at more than 196 N (Figure 3-4). Thus, the decomposition of ester group may reduce AW effect of TMO.

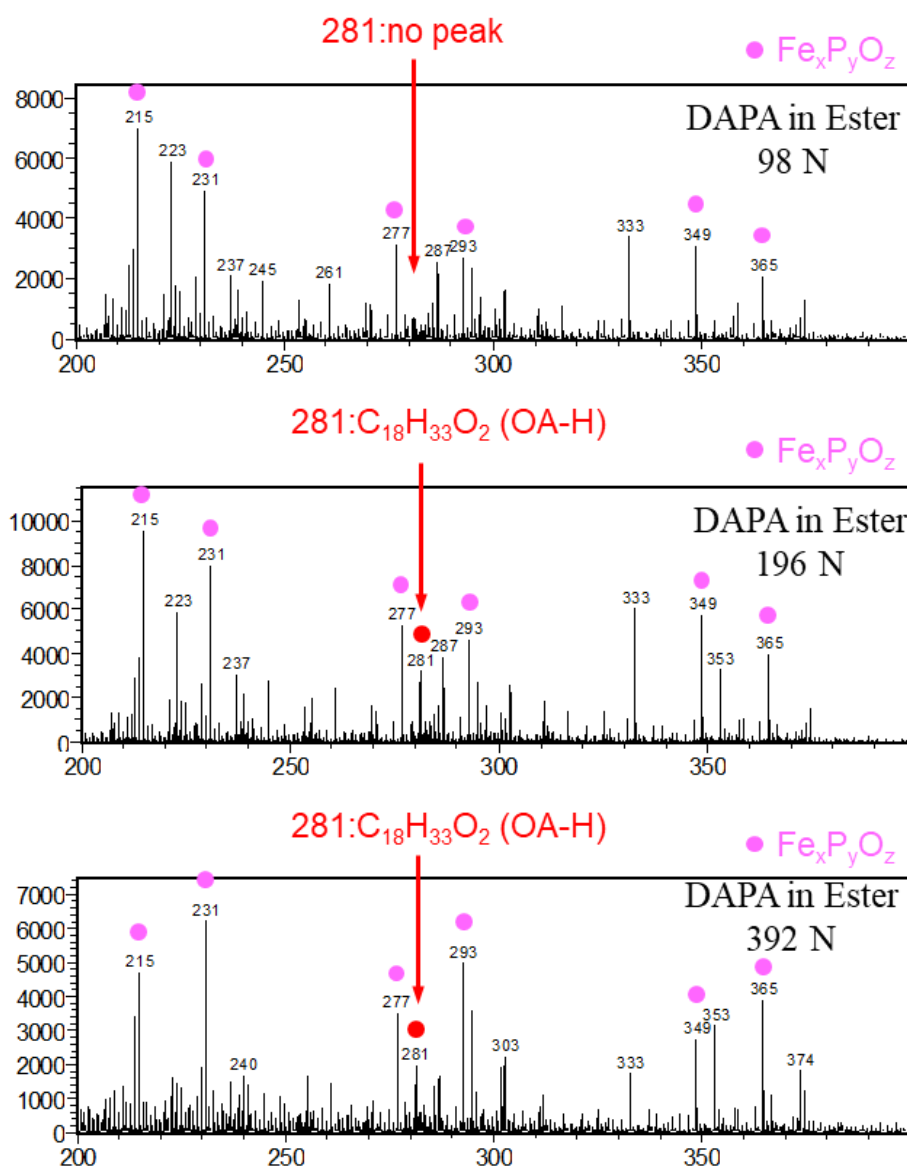


Figure 4-9. Negative ion spectra (m/z = 200-400) of worn surfaces after four-ball tests at 98 N, 196 N and 392 N with DAPA in TMO

4.3 DAPA tribofilm observations by FIB-TEM

The tribofilms generated in the four-ball tests at 392 N with DAPA in PAO and DAPA in TMO, shown in Figure 4-10, were characterised using TEM. The samples for TEM were prepared using the FIB technique described in section 2.3.4. The FIB cross sections were picked from three arbitrary areas on each tribofilm.

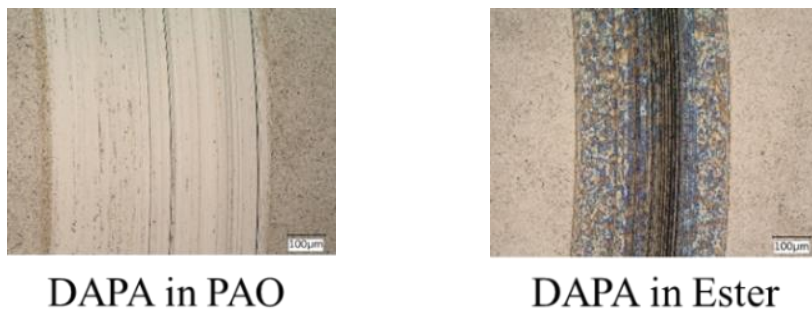


Figure 4-10. Samples for FIB-TEM observations. The surfaces after the four-ball tests at 392 N with DAPA in PAO and DAPA in TMO.

The cross sections of tribofilms formed by DAPA in PAO and DAPA in TMO are illustrated in Figure 4-11 and Figure 4-12, respectively.

DAPA in PAO formed a wispy tribofilm on steel surfaces. Its thickness was approximately 12.7 nm with a standard deviation of 6 nm (average and standard deviation calculated for six different locations on the FIB cross-section). In contrast, DAPA in TMO generated a homogeneous 170-nm-thick tribofilm with a standard deviation of 43 nm (average calculated for six different locations on the FIB cross-section). These results are consistent with the XPS depth profile data, showing that the tribofilm generated from DAPA in TMO at 392 N is thicker than that of DAPA in PAO. Notably, at 392 N, significant difference exists in the abilities to form the DAPA tribofilm between DAPA in TMO and DAPA in PAO.

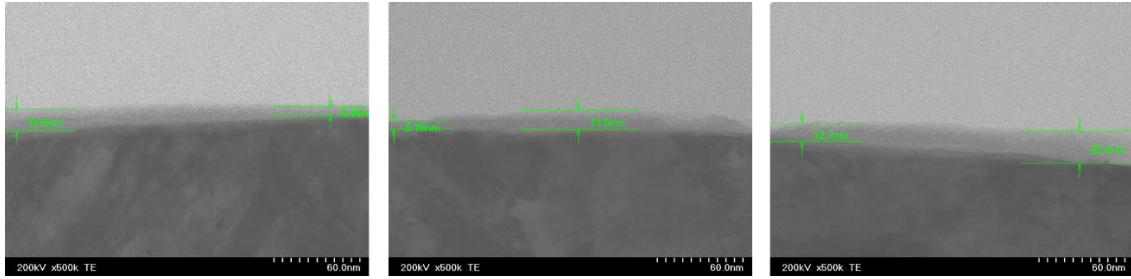


Figure 4-11. Cross section TEM images of tribofilm formed by DAPA in PAO at 392 N (four balls test).

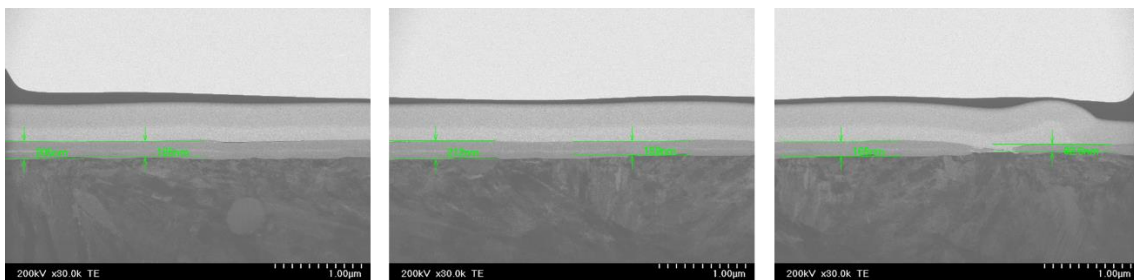


Figure 4-12. Cross section TEM images of tribofilm formed by DAPA in TMO at 392 N (four balls test).

4.4 DAPA tribofilm analyses using Infrared Spectroscopies

The surfaces after the four-ball tests at 392 N with DAPA in PAO and DAPA in Ester, which were used for XPS, ToF-SIMS and FIB-TEM, were analyzed using an infrared microscope, Bruker Vertex 70 with HYPERION 3000 with LEICA S8AP0. Figure 4-13 presents the FTIR spectra of the neat DAPA and the surfaces lubricated with DAPA in TMO at 392 N. For surfaces with DAPA in PAO, the results are not reported, because no clear peak was found (generally, a tribofilm thicker than 100 nm is required to obtain a relevant spectrum) [14].

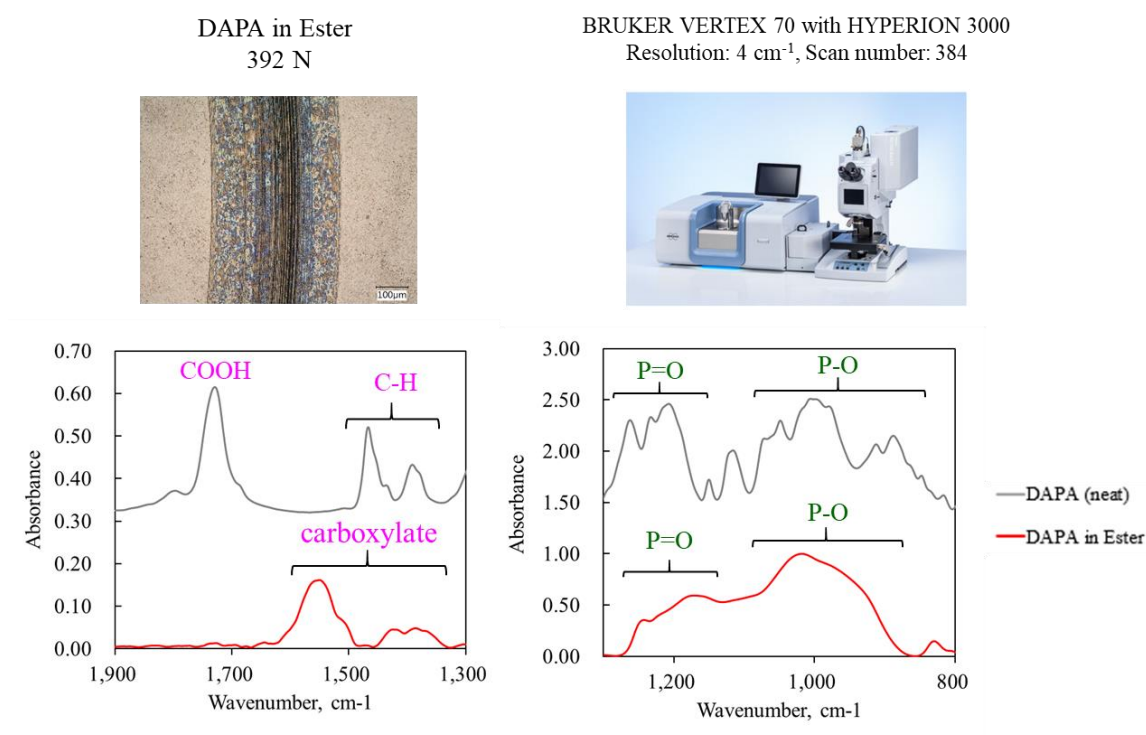


Figure 4-13. Infrared spectra on worn surfaces after four-ball test at 392 N with DAPA in TMO obtained using infrared microscope.

The IR spectrum of the neat DAPA showed peaks assigned to COOH, C-H, P=O and P-O, consistent with its chemical structure [15]. COOH and C-H peaks were not present in the spectrum recorded from the surfaces after the four-ball test with DAPA in TMO; however, a peak assigned to the carboxylate function (COO⁻) was present. For phosphorus species, regarding the resolution of our spectra and references in the literature, it was difficult to discuss the presence of P-O-P, P-O-C, and P-

C bonds in addition to P=O and P-O bonds, because many of these bands overlapped from 700 cm⁻¹ to 1300 cm⁻¹[16-17].

These IR results suggest that the DAPA alkyl chains were possibly removed during friction because of the disappearance of the C-H peak after friction. Moreover, the DAPA tribofilm contained iron carboxylate and phosphorus species.

A 100 nm thick sample/tribofilm is required to get infrared spectrum. That's why no information on the composition of the tribofilm formed from DAPA in PAO could be obtained. As a consequence, the comparison of tribofilm composition between DAPA in TMO and DAPA in PAO could not be carried out. Therefore, further analyses using PM-IRRAS, which can analyze thin film below 10 nm, were performed to characterize DAPA tribofilm from DAPA in PAO and DAPA in TMO. However, PM-IRRAS has limitation in sample sizes, which requires more than 10 × 10 mm² of analysis area. Thus, samples for PM-IRRAS were prepared by cylinder-on-flat tribotests instead of four-ball tests. The cylinder-flat tribotests were performed at 300 N ($P_{\max} = 0.9$ GPa), 75 °C and the speed of 0.06 m/s for 30 minutes. The contact pressure of the cylinder-on-flat tribotest tests is lower than that of four-ball tests ($P_{\max} = 2.2$ -3.7 GPa). As it is mandatory to use “large” friction surfaces to obtain PM-IRRAS spectra, a load condition of 300 N, the highest load feasible for the cylinder-on-flat tribometer used in this study, was selected. The size of wear scars was 10 × 10 mm². Both cylinders and discs were in AISI 52100. The apparatus of the cylinder-flat tribotests and the results are illustrated in Figure 4-14. DAPA in TMO showed lower friction coefficient than DAPA in PAO. The base oils alone (PAO and TMO) exhibited higher friction coefficient than the samples containing DAPA.

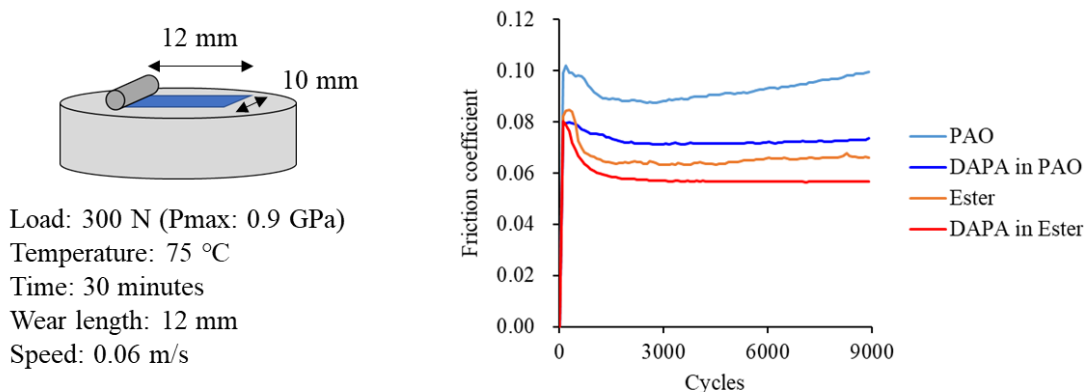


Figure 4-14. Cylinder on flat tribotest friction coefficients obtained with four lubricants (PAO, TMO, DAPA in PAO and DAPA in TMO).

The surfaces after the tribotests carried out with DAPA in PAO and DAPA in TMO are shown in Figure 4-15. DAPA in PAO formed a brown film on the surfaces. DAPA in TMO formed no colored film.

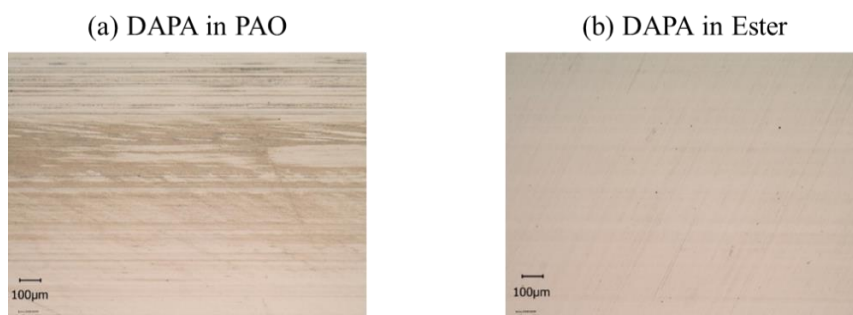


Figure 4-15. Worn steel surfaces after cylinder-flat tribotests with DAPA in PAO and DAPA in TMO.

The PM-IRRAS spectra obtained from neat DAPA and the worn surfaces with DAPA in PAO and DAPA in TMO are shown in Figure 4-16. Each peak was assigned according to the literature [16-19]. The spectrum of neat DAPA shows the peaks derived from carboxylic acid, hydrocarbon, P=O and C-O-P. Carboxylic acid and hydrocarbon are not found on the worn surfaces with DAPA in PAO and DAPA in TMO. The peaks assigned to carboxylate (bidendate) [9, 19, 20] are detected. For phosphorus species, like for FTIR, regarding the resolution of our spectra and references in the literature, it was difficult to discuss the presence of P-O-P, P-O-C, and P-C bonds in addition to P=O and P-O bonds, because many of these bands overlapped from 700 cm^{-1} to 1300 cm^{-1} [16-17].

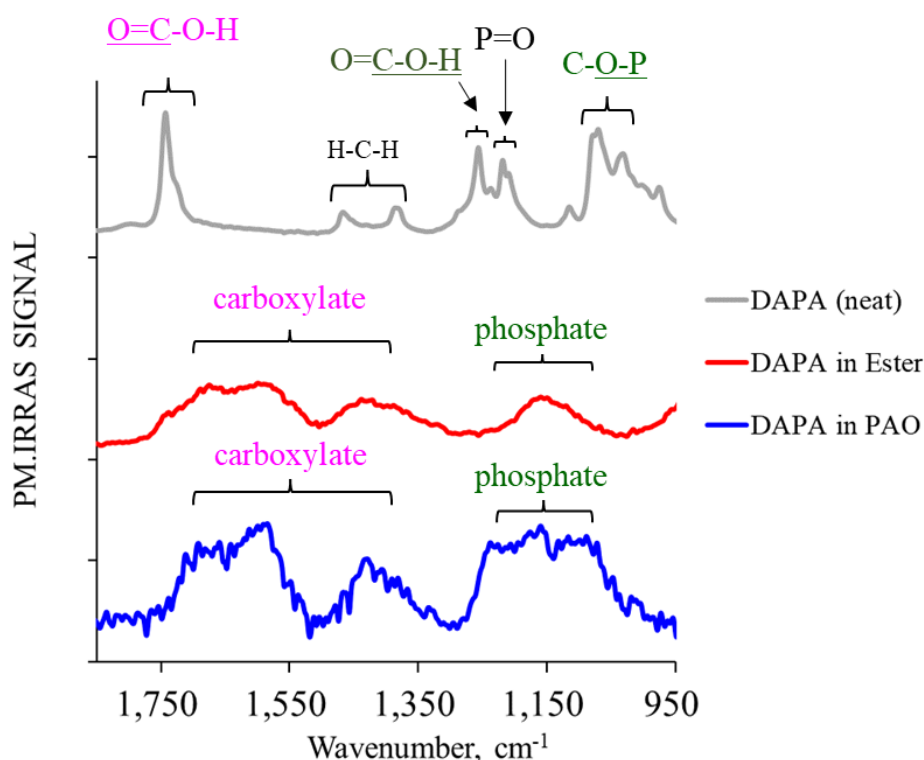


Figure 4-16. PM-IRRAS spectra obtained from worn surfaces with DAPA in PAO and DAPA in TMO after cylinder-flat tribotest. Neat DAPA was also analyzed as a reference.

No significant difference in terms of chemical composition was found by PM-IRRAS between the tribofilms obtained from DAPA in PAO and DAPA in TMO in Figure 4-16. However, the spectra of the DAPA tribofilms (in oils) were different from that of neat DAPA. No significant peaks derived from carboxylic acid and C-O-P were found but peaks assigned to carboxylates could be observed. The formation of carboxylates indicates that the carboxylic acid component in DAPA adsorbs onto metal surfaces. Then the carboxylic acid forms iron carboxylate on steel surfaces. Consequently to the alkyl chains removal during friction, the formation of P-O-P bonds may be suggested. These proposed chemical reactions of DAPA are summarized in Figure 4-17.

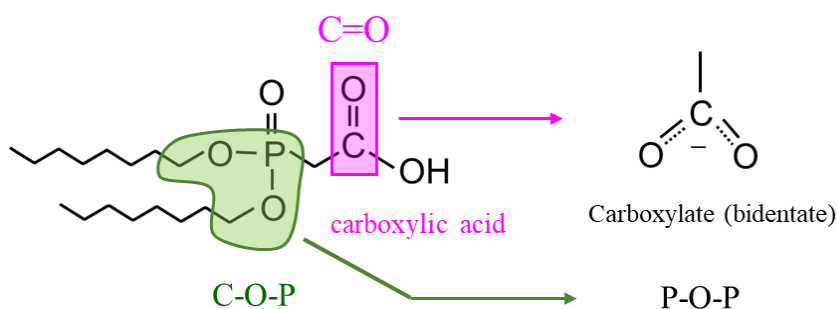


Figure 4-17. Structure changes of DAPA molecule after tribotest

4.5 Discussion

In general, the action mechanism of AW additives on metal surfaces under friction can be describe in several steps as shown in Figure 4-18 [21-23]. First, the additive is adsorbed on the surface, and a tribofilm is formed owing to tribochemical reactions under friction. In this study, the chemical compositions of both DAPA-adsorbed films and DAPA tribofilms formed from DAPA in PAO and DAPA in TMO were studied in detail to better understand the AW performance difference found in chapter 3.

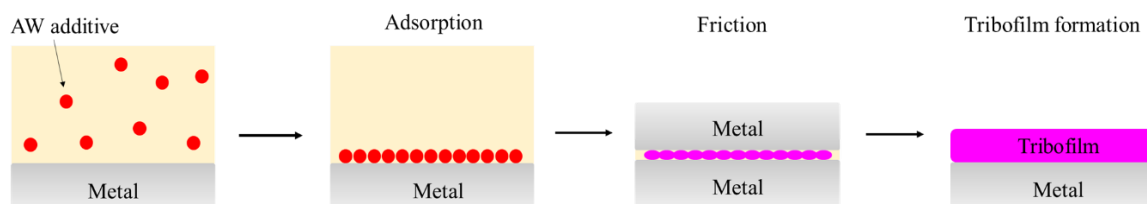


Figure 4-18. Action mechanisms of AW additives on metal surfaces for preventing wear

The DAPA adsorption species outside the wear scars exhibited the same $P_{2p3/2}$ binding energies for the two base oils even though the phosphorus content was lower in the case of DAPA in TMO in comparison to DAPA in PAO (Table 4-7). This proves a better ability of DAPA to adsorb onto steel surfaces in the presence of a non-polar base oil. In the presence of a polar-base oil (TMO), competition for adsorption may exist between the additive and base oil. Based on the XPS results, DAPA formed the same chemical structures of adsorption species on steel surfaces, regardless the type of the base oil.

XPS analyses indicated that the chemical structures of the DAPA tribofilms formed with PAO and TMO were significantly similar, but differed from the ZDDP tribofilm, which contained only phosphate species. The DAPA tribofilms appeared to have phosphonate structures, because the P-C bond of DAPA probably remained under friction as shown in Figure 4-4. The depth profiles of the DAPA tribofilms (Figure 4-5) indicated that the thickness of the DAPA tribofilms depends on the tribotest conditions and type of base oil. This was also confirmed by TEM results (Figures 4-11 and 4-12), which showed a thicker tribofilm obtained at 392 N with DAPA in TMO (≈ 170 nm) compared to DAPA in PAO (≈ 12 nm). The XPS depth profiles shown in Figure 4-5 also support the presence of iron and carbon inside the DAPA tribofilms. For the ZDDP tribofilm, it is well accepted that iron atoms coordinate with phosphates inside the ZDDP tribofilms [24, 25]; however, for DAPA tribofilms, iron atoms may also coordinate to the carboxylic group to form iron carboxylate, as the FTIR and PM-IRRAS results confirm this result as peaks assigned to carboxylate are observed for the DAPA tribofilms (Figure 4-17).

The XPS results also indicated that the C_x/P ratios of the DAPA tribofilms were much smaller than neat DAPA (Figure 4-3(a)). The elimination of alkyl chains of DAPA during friction was also suggested by the FTIR and PM-IRRAS results (Figures 4-13 and 4-16). Consequent to the disappearance of the alkyl chain, P-O-P bonds may form; this is supported by the presence of BO in the XPS spectra. In addition, the position of the $P2p$ peak confirmed the phosphonate character of phosphorus, suggesting that P-C bonding was still present in the tribofilm. The presence of P-C bonds in DAPA degradation products, and so possibly in DAPA tribofilms, is also supported by pyrolysis experiments reported in annex 2.

Additional tribological experiments carried out under vacuum in the environmental controlled analytical tribometer (ECAT) coupled with XPS analyses confirm the tribofilm composition obtained with DAPA molecule. The results are shown in annex 1. ToF-SIMS experiments also corroborate the composition of the DAPA tribofilm.

Based on the results obtained in this study, the tribofilm formation mechanism of DAPA can be proposed as illustrated in Figure 4-19. First, DAPA is adsorbed onto steel surfaces and forms carboxylate species (XPS and PM-IRRAS). Next, alkyl chains are removed under the action of friction, and the DAPA tribofilm appears to contain P-C and P-O bonds; possibly also P-O-P and P-O-C bonds, as well as carboxylate functions that may capture iron cations inside the tribofilm (XPS, FTIR and PM-IRRAS results).

At this point, irrespective of the nature of the base oil, it can be concluded that no significant difference in chemical compositions was found in adsorbed DAPA films as well as in DAPA tribofilms as summarized in Figure 4-19. Therefore, the difference in the tribological behaviour of DAPA in PAO and TMO (observed in chapter 3) cannot be solely explained by the formation mechanism of the DAPA tribofilm.

To go further, the dissolving states of DAPA in PAO and TMO were investigated using FT-IR (isotope labelling method), DFT calculations and ^{31}P NMR. The results are shown in annex 3. Those results showed that DAPA in PAO exists under dimer form, while DAPA interacts with TMO to form a 'complex' which seems to be easier to dissociate than the dimer form. This could suggest an easier and faster DAPA tribofilm formation in presence of TMO. However, this is not supported by the tribological results presented in Figure 3-6, as we observed a faster tribofilm formation with the PAO. For TMO, the competitive adsorption effect observed between the additive and TMO molecule could delay the DAPA tribofilm formation in comparison to PAO and explain the difference in the kinetics of the tribofilm formation. In fact, tribological results obtained at various temperatures (Chapter 3 § 3.3.4) suggest that temperature has a major effect on the DAPA in TMO system when compared with that of the DAPA in PAO system. For DAPA in PAO, all the DAPA molecules probably adsorb readily at all temperatures, because there is no competitor for adsorption; however, for DAPA in TMO, competition for adsorption between TMO and DAPA, which is sensitive to temperature, is found.

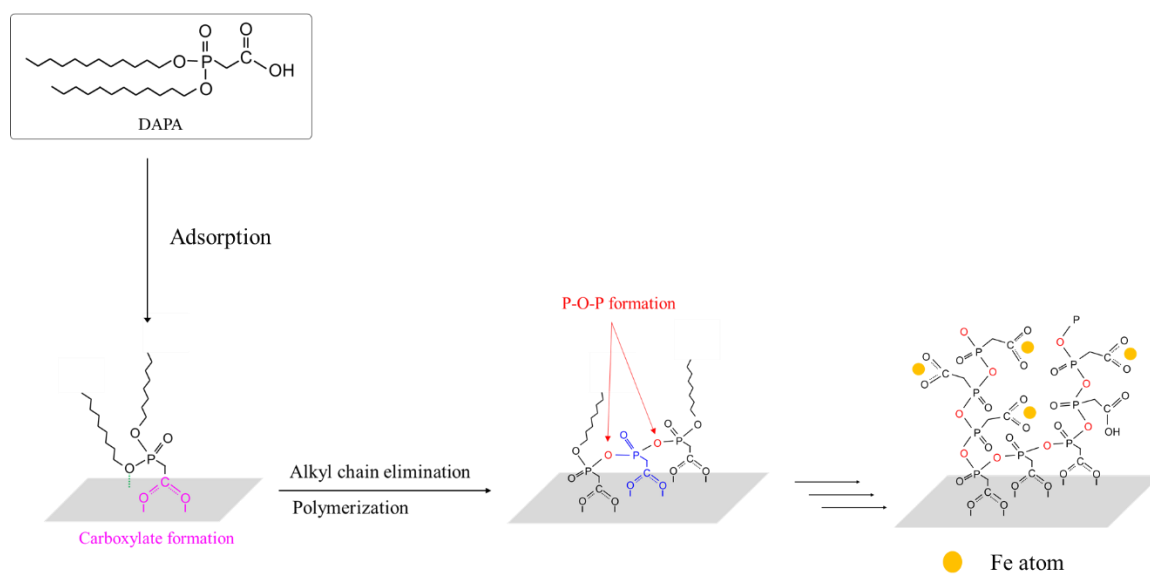


Figure 4-19. Proposed tribofilm formation mechanisms of DAPA

4.6 Summary of this chapter

The following conclusions can be drawn from this chapter:

1. The chemical composition of DAPA adsorbed films and DAPA tribofilms was investigated using various surface analysis techniques, and the formation mechanism of DAPA tribofilm was proposed.
2. The DAPA tribofilm contains poly phosphonate species, and that the P-C bond may maintain inside the tribofilm.
3. DAPA in PAO and DAPA in TMO form the same adsorption species and tribofilm on the steel surfaces.
4. The reasons for the difference in AW performance between DAPA in PAO and DAPA in TMO is related to a competition of adsorption between DAPA and TMO which delay DAPA tribofilm formation and provides long-lasting wear protection in presence of the polar-solvent.

References

- [1] C.R. Brundle, T.J. Chuang and K. Wandelt, Core and valence level photoemission studies of iron oxide surfaces and the oxidation of iron, *Surface Science*, **68**, 1977, 459–468.
- [2] M. Olla, G. Navarra, B. Elsener and A. Rossi, Nondestructive in-depth composition profile of oxy-hydroxide nano layers on iron surfaces from ARXPS measurement, *Surf. Interface. Anal.*, **38**, 2006, 964–974.
- [3] E.C. Onyiriuka, Zinc phosphate glass surfaces studied by XPS, *J. Non-Cryst. Solids.*, **163**, 1993, 268–273.
- [4] D. Wilson and M.A. Langell, XPS analysis of oleylamine/oleic acid capped Fe_3O_4 nanoparticles as a function of temperature, *Appl. Surf. Sci.*, **303**, 2014, 6–13.
- [5] R. Brückner, H.U. Chun, H. Goretzki and M. Sammet, XPS measurements and structural aspects of silicate and phosphate glasses, *J. Non-Cryst. Solids.*, **42**, 1980, 49–60.
- [6] F. Bournel, C. Laffon, Ph. Parent and Tourillon G. Adsorption of some substituted ethylene molecules on Pt(111) at 95 K Part 1: NEXAFS, XPS and UPS studies, *Surface Science*, **350**, 1996, 60–78.
- [7] D.R. Wheeler and O.D. Faut, The adsorption and thermal decomposition of tricresylphosphate (TCP) on iron and gold, *Applied Surface Science*, **18**, 1984, 106–122.
- [8] S. Hoste, D.F. Van De Vondel and G.P. Van Der Kelen. XPS Spectra of organometallic phenyl compounds of P, As, Sb and Bi. *J Electron Spectrosc Relat Phenom.*, **17**, 1979, 191–195.
- [9] M. Eglin, A. Rossi and N.D. Spencer, X-ray photoelectron spectroscopy analysis of tribostressed samples in the presence of ZnDTP: a combinatorial approach, *Tribology Letter*, **15**, 2003, 199–209.
- [10] R. Heuberger and A. Rossi, N.D. Spencer, Pressure dependence of ZnDTP tribochemical film formation: a combinatorial approach. *Tribology Letter*, **28**, 2007, 209–222.
- [11] A. Rossi, F. M. Piras, D. Kim, A. J. Gellman, N. D. Spencer, Surface reactivity of tributyl thiophosphate: effects of temperature and mechanical stress., *Tribology Letters*, **23**, 2006, 197–208.
- [12] P. Njiwa, C. Minfray, T.Le. Mogne, B. Vacher, J.M. Martin, S. Matsui and M. Mishima, Zinc dialkyl phosphate (ZP) as an anti-wear additive: comparison with ZDDP, *Tribology Letter*, **44**, 2011, 19–30.
- [13] M. Crobu, A. Rossi, F. Mangolini and N.D. Spencer, Chain-length-identification strategy in zinc polyphosphate glasses by means of XPS and ToF-SIMS, *Anal. Bioanal. Chem.*, **403**, 2012, 1415–1432.
- [14] T. Buffeteau, B. Desbat, J.M. Turllet, Surfaces and Ultra-thin Films: Experimental Procedure and Quantitative Analysis., *Applied Spectroscopy*, **45**, 1991, 380-389.

- [15] C. McFadden, C. Soto, N. D. Spencer, Adsorption and surface chemistry in tribology., *Tribology International*, **30**, 1997, 881-888
- [16] D.E.C. Corbridge, E.J. Lowe, The infra-red spectra of Inorganic phosphorus compounds. Part II. Some salts of phosphorus oxy-acids, *J. Chem. Soc. Part I*, **493** (1954) 4555–4564.
- [17] H. Doweidar, Y.M. Moustafa, K. El-Egili, I. Abbas, Infrared spectra of Fe₂O₃–PbO–P₂O₅ glasses, *Vib. Spectrosc.* **37** (2005) 91–96.
- [18] Lu and J.D. Miller, Carboxyl Stretching Vibrations of Spontaneously Adsorbed and LB-Transferred Calcium Carboxylates as Determined by FTIR Internal Reflection Spectroscopy., *Journal of Colloid and Interface Science*, **256**, 2002, 41-52.
- [19] K.D. Dobson and A.J. McQuillan, In situ infrared spectroscopic analysis of the adsorption of aliphatic carboxylic acids to TiO₂, ZrO₂, Al₂O₃, and Ta₂O₅ from aqueous solutions., *Spectrochimica Acta Part A*, **55**, 1999, 1395-1405.
- [20] E.G. Palacios, G. Juárez-López, A.J. Monhemius, Infrared spectroscopy of metal carboxylates: II. Analysis of Fe(III), Ni and Zn carboxylate solutions., *Hydrometallurgy*, **72**, 2004, 139-148.
- [21] C. McFadden, C. Soto, N. D. Spencer, Adsorption and surface chemistry in tribology., *Tribology International*, **30**, 1997, 881-888
- [22] J. M. Martin, Antiwear mechanisms of zinc dithiophosphate: a chemical hardness approach., *Tribology Letters*, **6**, 1999, 1-8
- [23] M. Ichiro, H. S. Hong, and N. C. Matur, Effect of Alkenes on the Antiwear Mechanism of Dialkyl Hydrogen Phosphite., *Lubrication Science*, **13**, 2001, 219-230
- [24] J.M. Martin, C. Grossiord, T. Le Mogne, S. Bec, A. Tonck, The two-layer structure of Zn₂TP tribofilms: Part I: AES, XPS and XANES analyses, *Tribology International*, **34**, 2001, 523-530
- [25] J.M. Martin, Antiwear mechanisms of zinc dithiophosphate: a chemical hardness approach, *Tribology Letters*, **6**, 1999, 1–8

Chapter 5

Design of Phosphonate AW additives for Ester lubricants

| | | |
|-------|-------------------------------------------------------------------|-----|
| 5.1 | DAPA tribofilm analyses using XPS | 103 |
| 5.2 | Modification of chemical structures of DAPA | 105 |
| 5.2.1 | Influence of alkyl chain on AW performance | 105 |
| 5.2.2 | Influence of functional groups on AW performance | 108 |
| 5.2.3 | Influence of methylene between P and COOH on AW performance | 109 |
| 5.3 | Discussion | 113 |
| 5.3.1 | Effect of ester base oil polarity on AW performance | 113 |
| 5.3.2 | Effect of DAPA alkyl chain length on AW performance..... | 113 |
| 5.3.3 | Effect of functional group of DAPA | 115 |
| 5.3.4 | Effect of carbon-based group between P and COOH of DAPA..... | 115 |
| 5.4 | Summary of this chapter | 117 |
| | Reference | 118 |

As mentioned in chapter 1, AW additives performance generally becomes poorer with the polarity of the ester base oils, therefore, the development of effective AW additives for high polarity ester base oils is essential to propose lubricants with excellent AW performance. In this chapter, first, the effectiveness of DAPA in the ester base oils with different polarities is studied. Secondly, the effects of the alkyl chain structures, polar functional groups, and methylene between P and COOH of dialkyl phosphonates on AW performance are investigated. Lastly, the effective chemical structures for dialkyl phosphonates as AW additives in high polar ester base oils are discussed.

5.1 Influence of ester base oil polarity on AW performance of DAPA

For the experiments presented in the previous chapters, TMO was selected as a representative of ester base oils because it has been widely used for commercial lubricants [1]. Previous research has shown that the polarities of base oils influence the performance of AW additives. Ester base oils, with high polarities, often hinder efficiency of classical AW additives designed to be effective in more neutral base oils [2,3]. Therefore, it is particularly important to find additives with AW properties preserved in high polarities ester base oils.

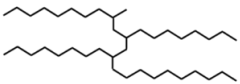
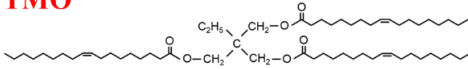
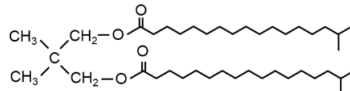
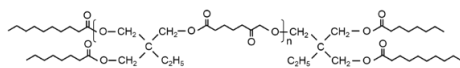
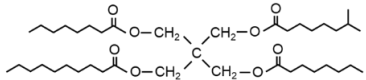
In the present study, the influence of base oil polarities on AW performance of DAPA was investigated. Four ester base oils with different polarities but with the same kinematic viscosity grade (ISO VG46) were used. Their chemical structures and polarity indexes are shown in Table 5-1. The polarity indexes are calculated using the below equation proposed by Minami *et al.* [3], which indicates that the higher the polarity index, the higher the polarity of the ester base oil.

$$\text{Polarity index} = \frac{\text{number of carboxylic groups} \times 10,000}{\text{total number of C atoms} \times \text{molecular weight}} \quad (6.1)$$

The AW performance of DAPA in the various ester base oils and PAO were evaluated using the four-ball test machine. Each test was carried out at 392 N, 1200 rpm and 25 °C for 1 h. Regarding the temperature conditions, DAPA in TMO gives smaller wear scar diameters at high temperatures, and the size of the wear scar diameters are equivalent to the Hertz diameter at 125 °C, as shown in Figure 3-7 (chapter 3). The tribotests in this present study were performed at 25 °C, in the most severe wear situation, to make clear the difference of the AW additive performance in each base oil. TCP was used as a reference AW additive. Some studies reported that TCP has no significant AW effect when the dosage is lower than 1.0 % [3,4], thus, TCP was added with a phosphorus concentration of 1000 ppm (dosage: 1.2 in mass% of TCP), which is 10 times larger than DAPA.

The four-ball test results with DAPA and TCP in the base oils (PAO and the four ester base oils) are summarized in Figure 5-1. DAPA improved the AW performance of all tested ester base oils, but no significant effect was found in PAO. The smallest AW effect of DAPA was found to be in the pentaerythritol (PET) ester base oil. This result is consistent with the previous findings in literature, reporting that efficiency of AW additives decreases with base oil polarity [2-3, 5-6]. Concerning the AW performance of TCP, it improved the AW performance of PAO, trimethyloltrioleate (TMO) and neopentylglycol (NPG) ester base oil, however, there was no effect in Complex and PET.

Table 5-1. Chemical structures, polarity indexes and kinematic viscosities of ester base oils.

| Chemical structures of ester base oils | Polarity index | Kinematic viscosity, mm ² /s | |
|----------------------------------------------------------------------------------------------------------------------------------|----------------|-----------------------------------------|--------|
| | | 40 °C | 100 °C |
| PAO  Mixture of 1-decene oligomers | 0 | 45.89 | 7.736 |
| TMO  | 0.5 | 49.50 | 9.748 |
| NPG  | 0.8 | 46.71 | 8.218 |
| Complex  | 1.2 | 46.00 | 8.009 |
| PET  | 1.6 | 45.67 | 7.403 |

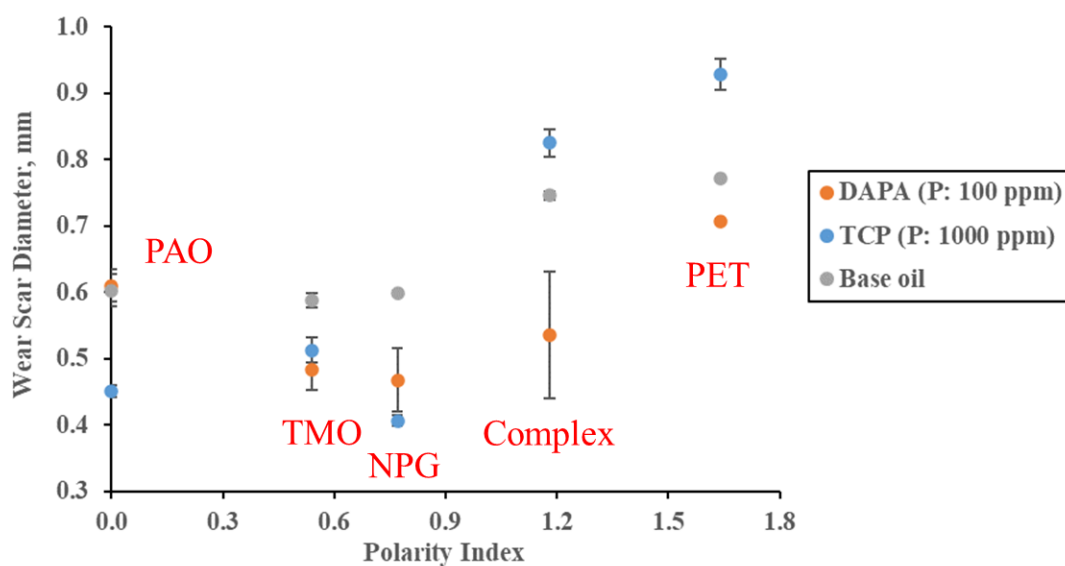


Figure 5-1. Influence of ester base oil polarities on AW performance of DAPA and TCP.

In this study, it has been found that DAPA is a more advantageous AW additive for the ester base oils than TCP, however, even more effective AW additives are desirable for high polarity ester base oils, such as PET. Consequently, the following research is focused on the modification of the DAPA molecule to improve the AW performance in high polarity ester base oil like PET.

5.2 Modification of chemical structures of DAPA

The DAPA molecule has three components, alkyl chains, methylene between P and COOH, and the functional groups, as illustrated in Figure 5-2. The influence of each component on AW effects in PET was investigated using the four-ball tests. The test conditions were the same than in the previous study in section 5.1.

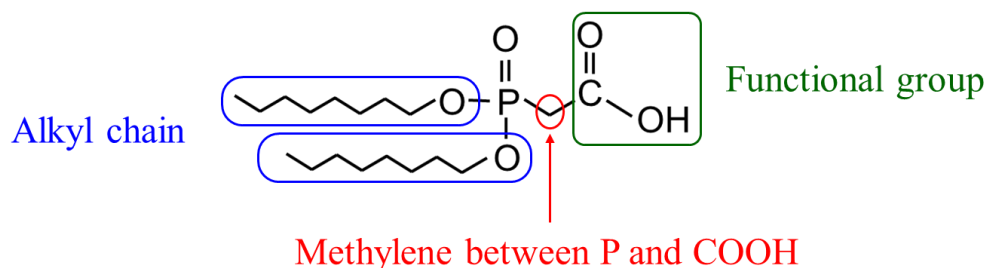


Figure 5-2. Modified chemical structure components of DAPA for this investigation

5.2.1 Influence of alkyl chain on AW performance

First, the effect of the alkyl chain moiety was investigated. The AW performance of DAPAs with different alkyl chain lengths (C_2 - C_{18}) and structures (n C_6 : n-hexyl, sec C_6 : 1,3-dimethylbutyl, n C_8 : n-octyl, 2EH: 2-ethylhexyl, n C_{18} : n-octadecyl, iso C_{18} : iso- octadecyl, and oleyl- C_{18} : cis-9-octadecen) were evaluated in PET with the four-ball tribometer. The four-ball tests were carried out at 392 N, 1200 rpm and 25 °C for 1 h, and the results of DAPAs with C_2 - C_{18} are summarized in Figure 5-3. The AW performance of DAPA improved with the alkyl chain length, and DAPA with n C_{18} showed the best AW performance among the tested DAPAs. These results could seem in agreement with the previous literature regarding the chain length effects of alcohol and carboxylic acid where it was shown that alkyl chains longer than C_{12} exhibit lower friction because of the formation of Self-Assembled-Monolayers [7-10]. We could imagine that if a SAM is formed between the alkyl chains DAPA, wear protection would be improved as well. However, we have no clear evidence of that and previous experiments in chapter 4 show that the alkyl chains of DAPA are removed during friction which discards SAM generation.

DAPAs with n C_4 and n C_6 have no AW effect, and the obtained wear scar diameters are larger than those obtained with the base oil alone. DAPA with C_2 does not follow this trend. The wear scar diameter obtained with C_2 is between n C_6 and n C_8 , and the repeatability is inconsistent compared to C_4 - C_{18} .

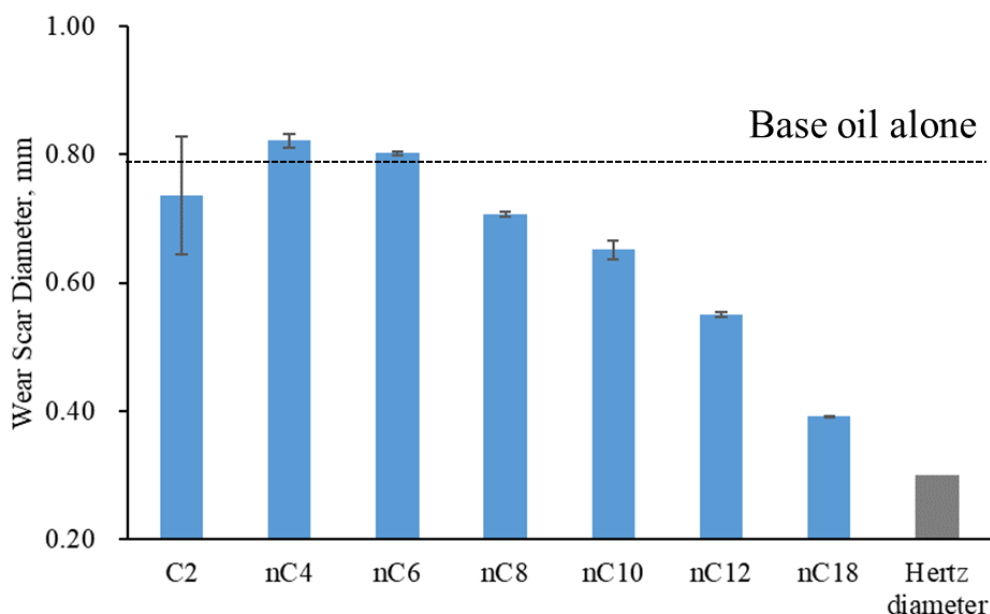
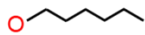
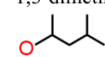
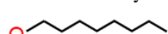
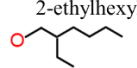
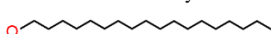
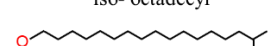
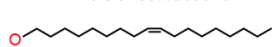


Figure 5-3. Effects of alkyl chain length on AW performance of DAPA in PET

Next, the effects of alkyl chain structures were studied using DAPAs with different chemical structures (C₆: nC₆ and sec C₆, C₈: nC₈ and 2EH, C₁₈: nC₁₈, isoC₁₈ and oleyl-C₁₈) illustrated in Table 5-2. Their four-ball test results of DAPAs with different chemical structures are shown in Figure 5-4. DAPA with secC₆ showed better AW performance than that of nC₆. It is well known that phosphorus AW additives, such as ZDDP and dialkyl phosphite, with secondary alcohol are more reactive than those of primary alcohol [11] because secondary alcohols are less thermally stable. This result suggests that the thermal stability of DAPA influences the AW performance to some extent. However, DAPA with nC₈, 2EH, nC₁₈, isoC₁₈, and oleyl-C₁₈ had better AW properties than those of secC₆. This indicates that the alkyl chain length influences AW performance of DAPA more significantly than the thermal stability of the alkyl chain structures. Among DAPAs with C₁₈, nC₁₈ decreased wear better than isoC₁₈ and oleyl-C₁₈. In fact, it seems that DAPAs with long and straight alkyl chains are suitable for AW additives in PET.

Table 5-2. Alkyl chain structures of DAPAs.

| R | | Chemical structures |
|-----------------|-----------------------|--------------------------------------------------------------------------------------------------------|
| C ₆ | nC ₆ | n-hexyl  |
| | secC ₆ | 1,3-dimethylbutyl  |
| C ₈ | nC ₈ | n-octyl  |
| | 2EH | 2-ethylhexyl  |
| C ₁₈ | nC ₁₈ | n-octadecyl  |
| | isoC ₁₈ | iso-octadecyl  |
| | Oleyl-C ₁₈ | cis-9-octadecene  |

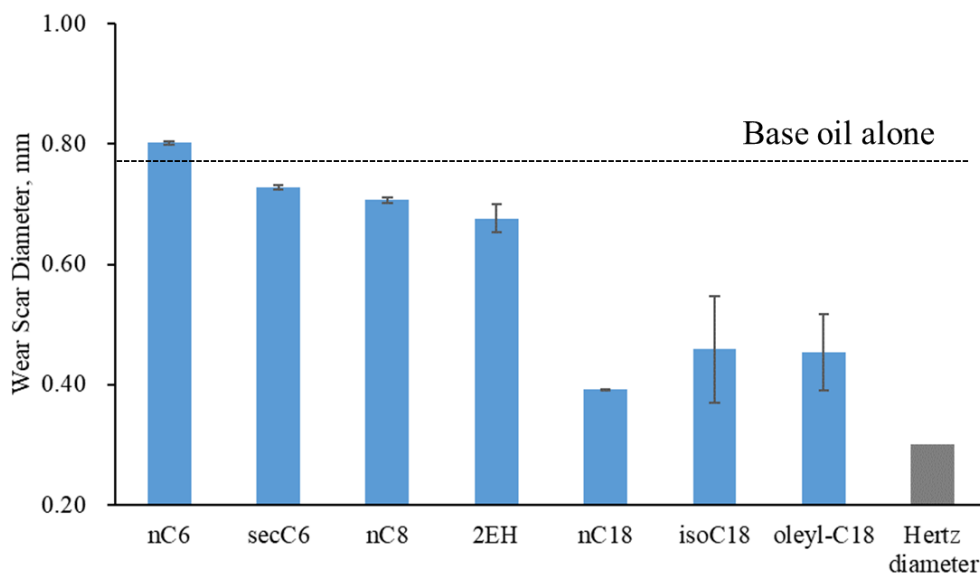


Figure 5-4. Effects of alkyl chain structure on AW performance of DAPA in PET.

5.2.2 Influence of functional groups on AW performance

Figure 5-5 compares the four-ball test results of dialkyl phosphonates with OH and CO-NH₂ to those of COOH in PET base oil. Dialkyl phosphonates with OH and CO-NH₂ showed smaller wear scar diameters than COOH. This result shows that OH and CO-NH₂ functional groups are effective as AW additives for ester base oils.

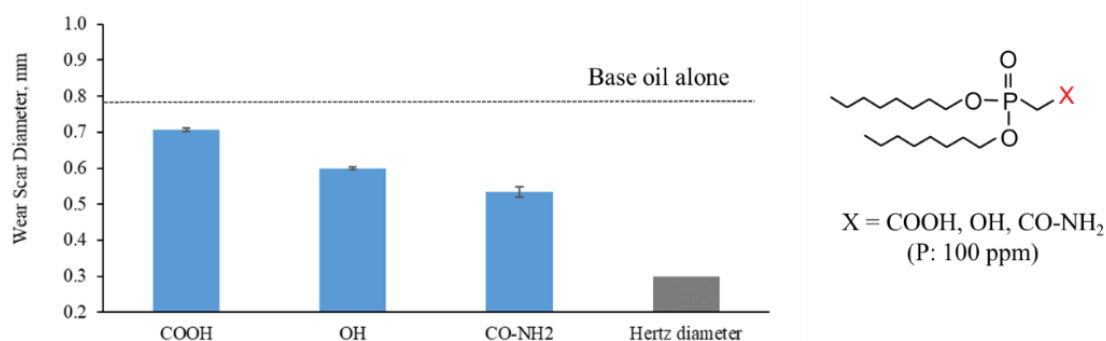


Figure 5-5. Effects of functional groups on AW performance of dialkylphosphonate in PET

Then, the AW effects of dialkyl phosphonates with COOH, OH and CO-NH₂ were studied in PAO, TMO, NPG, Complex and PET. The test results are summarized in Figure 5-6. All tested dialkyl phosphonates had no significant AW performance in PAO while AW effects were observed in the ester base oils. This result indicates that dialkyl phosphonates are effective in ester base oils and that they are not useful as AW additives in PAO. Phosphonate with CO-NH₂ exhibited the best AW performance in TMO and PET among the tested phosphonates, but phosphonates with COOH and OH have better AW performance in NPG. The compatibilities between types of ester base oils and functional groups of dialkyl phosphonates should be investigated and clarified more precisely as future work.

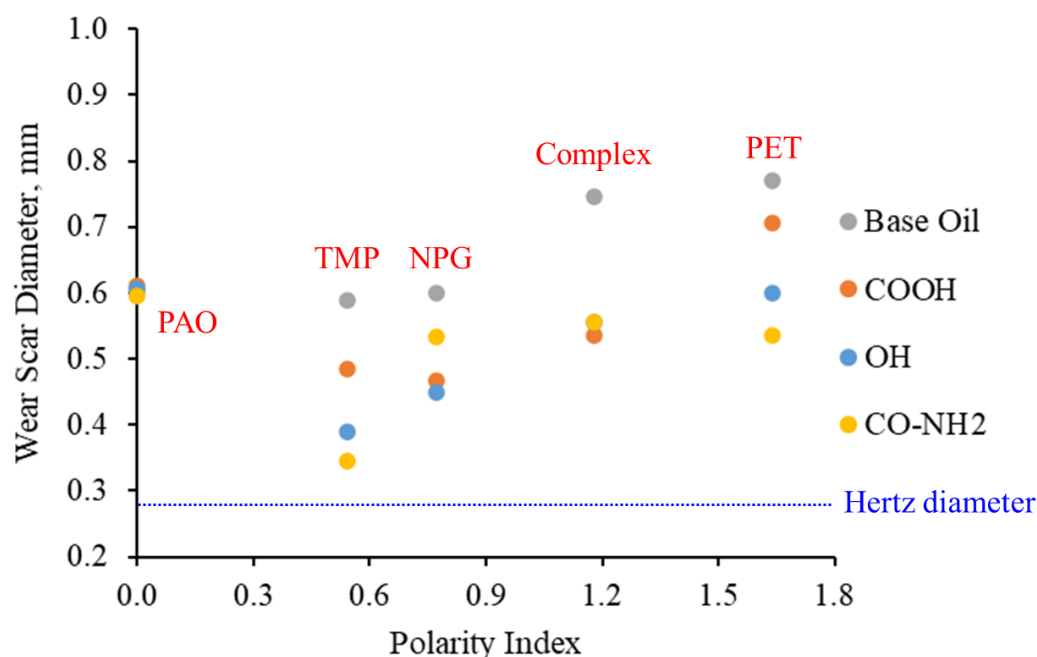


Figure 5-6. Effects of base oil polarities on AW performance of dialkylphosphonate with various functional groups.

5.2.3 Influence of carbon-based group between P and COOH on AW performance

This section focuses on the effect of methylene structure on AW performance of DAPA. Figure 5-7 illustrates two AW additives with different lengths of methylene structure used in this experiment: DAPA has CH_2 between P and COOH, and dialkyl phosphonopropionic acid (DAPP) has C_2H_4 between P and COOH.

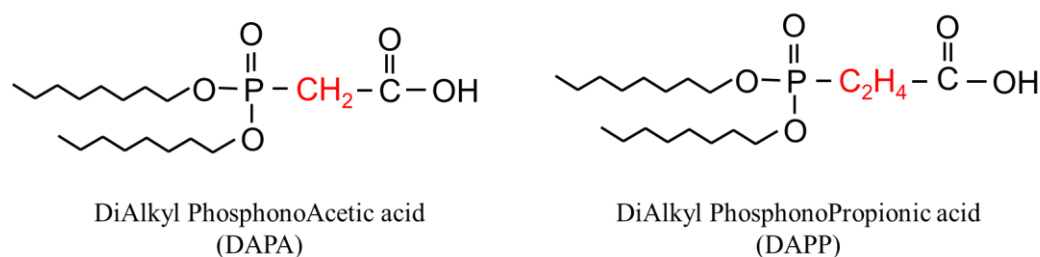


Figure 5-7. COOH dialkyl phosphonate with different carbon-based group between P and COOH.

The AW performance of DAPA and DAPP were evaluated by the four-ball tests. Figures 5-8 (a) and (b) show the test results in TMO and PET, respectively. In both ester base oils, DAPA has better AW performance than DAPP, suggesting that the methylene structure between P and COOH significantly negatively influences the AW properties of dialkyl phosphonates.

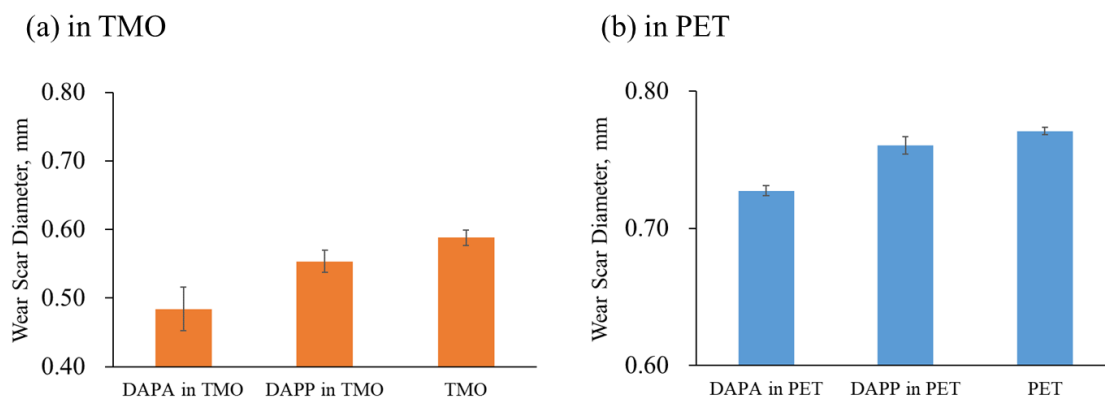


Figure 5-8. Effects of methylene structure between P and COOH on AW performance of dialkylphosphonate in ester base oils: (a) TMO and (b) PET.

Zinke *et al.* reported the relationship between thermal stability and AW performance of phosphorus compounds using thermogravimetric analysis. They concluded that AW additives should have enough thermal instability to decompose on sliding surfaces for tribofilm formation [12-13]. Therefore, thermal stabilities of DAPA and DAPP were measured using thermogravimetric analysis (SHIMADZU DTG-60) at a heating rate of 10 °C/min, operating from room temperature to 500 °C under an air atmosphere at a flow rate of 50 ml min⁻¹.

Figure 5-9 illustrates the TGA curves acquired from DAPA and DAPP. DAPA starts to decompose rapidly at around 200 °C and more than 95 % weight loss of DAPA decomposes before 300 °C. DAPP starts to decompose gradually at around 140 °C and the weight loss % of DAPP reached a plateau at around 300 °C. DAPA and DAPP have closed chemical structure as shown in Figure 5-7, but their TGA curves show quite different features.

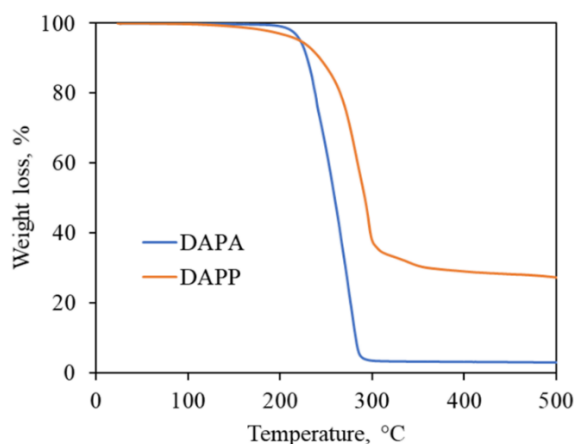


Figure 5-9. (a) TGA of DAPA and DAPP at a heating rate of 10 °C/min, operating from room temperature to 500 °C. (b) Temperatures at 5 %, 10 % and 50 % of weight loss

A headspace-GC-MS analysis was performed to investigate decomposition components generated from DAPA and DAPP. Figure 5-10 illustrates the experimental procedures of this analysis technique, which can identify volatile components in a vapor phase by GC-MS. In this experiment, the volatile components formed from DAPA and DAPP were collected at 250 °C, which is the temperature limit of the headspace-GC-MS used in this study, but both DAPA and DAPP can be decomposed thermally at this temperature condition.

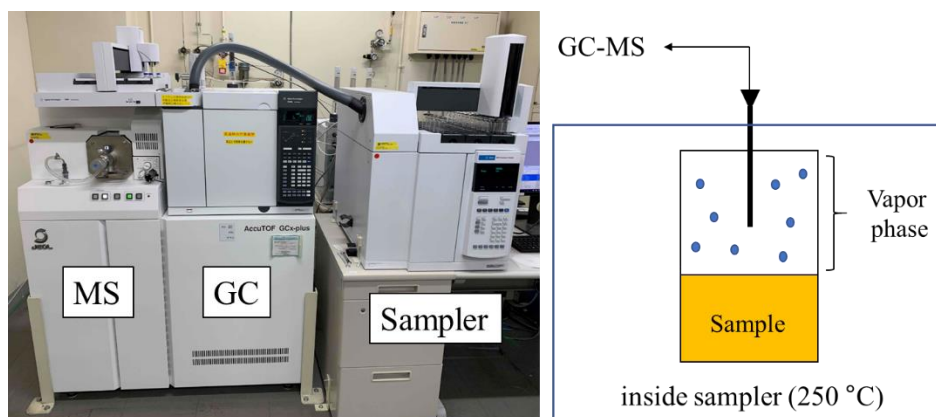


Figure 5-10. The experimental procedures of a headspace-GC-MS analysis

Figure 5-11 shows the GC-MS spectra of the vapor phase at 250 °C obtained from DAPA. The peaks derived from octanol and methylphosphonate were mainly detected and the small amount of octene was also identified. These results suggest that the P-O and CH₂-COOH bonds of DAPA are dissociated by thermal decomposition. The GC-MS spectra obtained from the volatile components of DAPP is illustrated in Figure 5-12. The peaks assigned to octanol and octene are detected, however no significant peak of phosphonate species was identified. This indicates that the P-O and C-O bonds of DAPP are dissociated by thermal decomposition, but the CH₂-COOH bond remains.

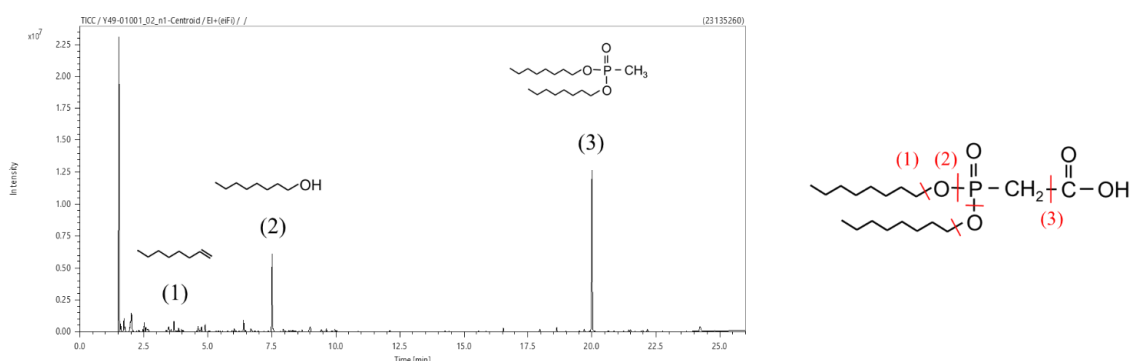


Figure 5-11. TG-MS spectra of volatile components generated from DAPA at 250 °C under an air atmosphere

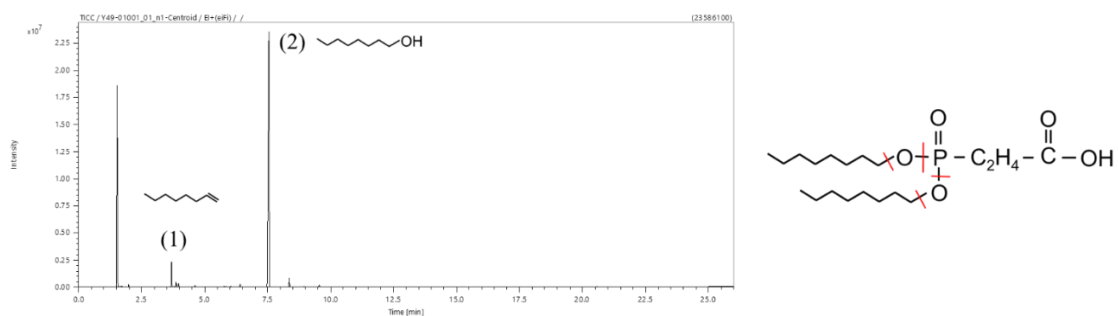


Figure 5-12. TG-MS spectra of volatile components generated from DAPP at 250 °C under an air atmosphere

5.3 Discussion

5.3.1 Effect of ester base oil polarity on AW performance

First, the effectiveness of DAPA in the ester base oils with different polarities was studied. This investigation reveals that the AW performance of DAPA becomes poorer with the polarity of the ester base oils, and that PET is the base oil for which DAPA gives the worst AW results. It has been reported that PET ester base oils have superior hydrolysis stabilities than other ester base oils, and that they are useful base oils for lubricants that require high durability such as aviation turbine oils, refrigeration oils and air compressor oils [14]. This means that the AW performance and durability of ester lubricants are likely to vary a lot regarding the type of ester base oils used. Therefore, the development of effective AW additives for high polarity ester base oils such as PET is essential to propose lubricants with both excellent AW performance and durability. In order to design effective AW additives for high polarity ester base oils, the influence of the chemical moieties of DAPA on AW performance was studied, focusing on alkyl chains, functional groups and the length of methylene between P and COOH.

5.3.2 Effect of DAPA alkyl chain length on AW performance

Regarding the effect of the alkyl chain length of lubricant additives, Jahanmir reported that oiliness additives with longer alkyl chains (around C₁₂) have lower friction coefficients than those of shorter alkyl chains. The author concluded that oiliness additives with long alkyl chains form ordered self-Assembled Monolayers, resulted in successfully friction reduction [7] on consequently wear reduction. Boyde also reported that ester base oils with linear alkyl chains had better AW performance than those of branch alkyl chains, and he proposed that linear alkyl chains can form more tightly packed tribofilm on metal surfaces than branch alkyl chains, consequently, resulting in better AW performance [14].

Forbes *et al.* found that dialkyl phosphites with longer alkyl chains have better AW performance than those of shorter ones. They suggested that dialkyl phosphites with short alkyl chains decompose rapidly by hydrolysis and react with metal surfaces, resulting in corrosive wear, whereas those with long alkyl chains are adequately stable and react slowly without metal corrosion, leading to the formation of effective tribofilm [15].

In the present study, the AW performance of DAPA is in good agreement with the above previous research. DAPAs with the longer alkyl chains show better AW performance than those with shorter ones. This is probably related to a better thermal stabilities of longer chain additives rather than the ability to form a Self-Assembled Monolayers as we have shown before that alkyl chain are removed during friction. Figure 5-14 illustrates the wear scars after the four-ball tests using DAPAs with different alkyl chains. These pictures show that the worn surfaces after the tests are successfully covered with tribofilm according to alkyl chain length.

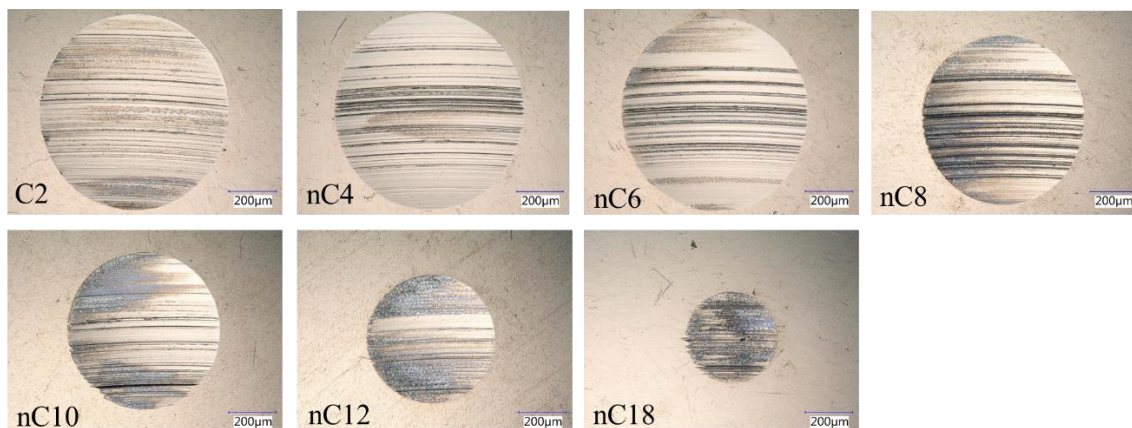


Figure 5-14. The tribofilm on the wear scars formed from DAPAs with different alkyl chain length. The four-ball tests were carried out at 392 N, 1200 rpm and 25 °C for 1 h.

The AW performance of DAPAs with the same alkyl lengths were compared in Figure 5-4, and the result showed that DAPA with nC₁₈ has superior AW performance than isoC₁₈ and oleiyl-C₁₈. This result is consistent with Boyde's research in that linear alkyl chains have better tribological properties than the branch alkyl chains. Figure 5-15 illustrates the wear scars after the tests using DAPA with nC₁₈, isoC₁₈ and oleiyl-C₁₈. DAPA with nC₁₈ gave slightly smaller wear scars and darker tribofilm on the surfaces than isoC₁₈ and oleiyl-C₁₈, indicating that DAPA with linear alkyl chain form tribofilm more effectively and have better AW performance than branch or bent alkyl chain structures.

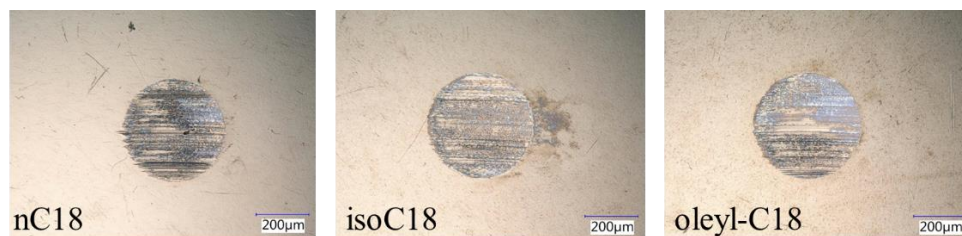


Figure 5-15. The tribofilm on the wear scars formed from DAPAs with nC₁₈, isoC₁₈ and oleiyl-C₁₈. The four-ball tests were carried out at 392 N, 1200 rpm and 25 °C for 1 h.

In order to discuss the influence of alkyl chain length of DAPA on the hydrogen bond between DAPA and ester base oils, the chemical shifts of DAPAs with nC₄, nC₈, nC₁₂ and oleiyl-C₁₈ in PET were measured by ³¹P NMR as summarized in Figure 5-16. In this result, no significant relationship is found between the alkyl chain length of DAPAs and their chemical shifts, indicating that the alkyl chain structures have no large influence on the hydrogen bond formations of DAPA with PET.

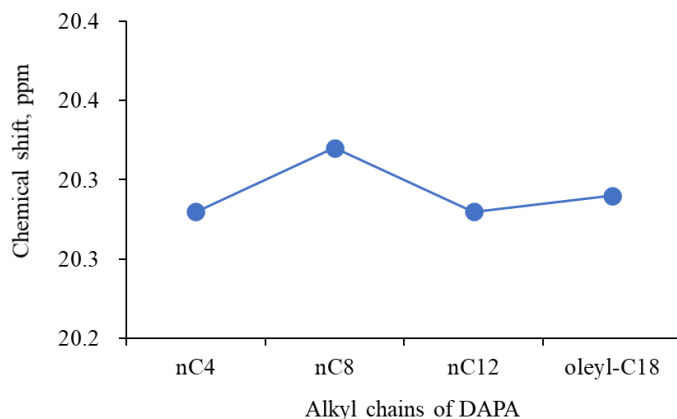


Figure 5-16. Chemical shifts of DAPAs with nC₄, nC₈, nC₁₂ and oleyl-C₁₈ in PET with 100 ppm of phosphorus concentrations measured by ³¹P NMR at 25 °C.

5.3.3 Effect of functional group of DAPA

It was shown that phosphonate with CO-NH₂ exhibited the best AW performance in TMO and PET among the tested phosphonates (COOH, OH and CO-NH₂). To understand why, further investigations should be carried out. For examples, a better understanding of the competition of adsorption on steel surfaces between polar-base oils and additives would provide interesting outputs as well as the study of interactions of functional group of additives with polar-base oils.

5.3.4 Effect of methylene between P and COOH of DAPA

The experiments using the headspace-GC-MS (Figure 5-11) detected octanol and dimethyl phosphonate as the main thermal decomposition products of DAPA. This indicates that the P-O and CH₂-COOH bonds were dissociated, and that the P-C bond was maintained, when DAPA is thermally decomposed. From this result, the proposed pyrolysis mechanism can be illustrated in Figure 5-17. In this mechanism, first, DAPA would form the six -membered ring, followed by the dissociation of the CH₂-COOH bond and the formation of the intermediate. Next, the alkyl chain moieties are removed from the intermediate, resulting in the formation of polymer compounds. It is likely that DAPA tribofilm has a composition very similar to that of this polymer, and that P-C bonds exist inside.

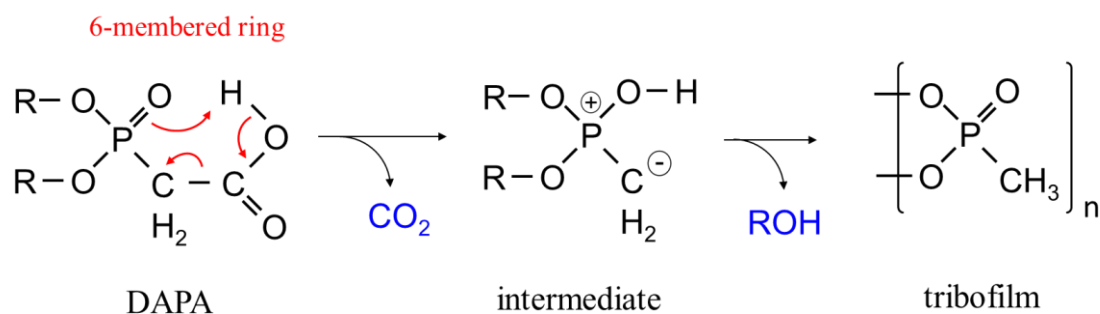


Figure 5-17. The proposed thermal decomposition mechanism of DAPA

In the case of DAPP, no phosphonate species was detected by the headspace-GC-MS, as shown in Figure 5-12. This suggests that DAPP cannot form the six-membered ring, and that elimination of alkyl chains mainly occurs, when DAPP is thermally decomposed.

Zinke *et al.* investigated the relationship between the thermal stabilities of various thiophosphate and the AW performance [12-13]. The author concluded that the primary factor in AW performance is a sufficient thermal instability to decompose the molecule and then for ensuring the tribofilm formation on sliding surfaces [13]. Minami *et al.* reported that di-cyclohexyl hydrogen phosphite (cHPi) had better AW properties than di-n-hexyl hydrogen phosphite (nHPi), and that cHPi decomposes by the formation of 6-member ring as shown in Figure 5-18, but nHPi does not form 6-member ring for pyrolysis. [16].



Figure 5-18. The pyrolysis mechanisms of di-cyclohexyl hydrogen phosphite (cHPi) [16].

The thermal stability difference seems to be the main reason why DAPA has better AW performance in ester base oils than DAPP. The length between P and COOH of DAPA looks important for AW performance, and methylene looks suitable for the formation of six-membered ring, thus promoting the degradation of DAPA, compared to ethylene of DAPP.

5.4 Summary of this chapter

The following conclusions of this chapter can be drawn:

1. DAPA is an effective AW additive in various ester base oils, however, its efficiency decreases with ester base oil polarities.
2. AW performance of DAPA increases with its alkyl chain length, and DAPAs with C₁₈ have excellent AW performance in the high polar ester base oils (PET).
3. Phosphonates with OH and CO-NH₂ show excellent AW performance in ester base oils with high polarities.
4. The length of the carbon-based group between P and COOH influences the AW performance of DAPA as it influences the formation of 6-membered ring transition states leading to different decomposition mechanisms of the molecule.

Reference

- [1] Y. Wu, W. Li, X. Wang, Synthesis and properties of trimethylolpropane trioleate as lubricating base oil., *Lubrication Science*, **27**, 2015, 369-379.
- [2] G. Van der Waal, The relationship between the chemical structure of ester base fluids and their influence on elastomer seals, and wear characteristics., *J. Synth. Lubr.* **1**, 1985, 280–301.
- [3] I. Minami, K. Hirao, M. Memita, S. Mori, Investigation of anti-wear additives for low viscous synthetic esters., *Tribology International*, **40**, 2007, 626–631.
- [4] I. L. Goldblatt, J. K. Appeldoorn, The Antiwear Behavior of TCP in Different Atmospheres and Different Base Stocks., *ASLE transactions*, **13**, 1970, 203-214.
- [5] I. Minami, S. Mori, Anti-wear additives for ester oils., *J. Synth. Lubr.* **22**, 2005, 105–121.
- [6] I. Minami, T. Hasegawa, M. Memita, K. Hirao, Investigation of antiwear additives for synthetic esters., *Lubrication Engineering*, **58**, 2002, 18-22.
- [7] S. Jahanmir, Chain length effects in boundary lubrication., *Wear*, **102**, 1985, 331-349.
- [8] O. Levine and W. A. Zisman, Friction and wettability of aliphatic polar compounds and effect of halogenation., *J. Phys. Chem.*, **61**, 1957, 1068-1077
- [9] O. Levine and W. A. Zisman, Physical properties of monolayers adsorbed at the solid-air interface. II. Mechanical durability of aliphatic polar compounds and effect of halogenation *J. Phys. Chem.*, **61**, 1957, 1188-1196
- [10] H. Okabe, M. Masuko, K. Sakurai, Dynamic behavior of surface-adsorbed molecules under boundary lubrication., *ASLE Trans*, **24**, 1981, 467-473
- [11] J. J. Dickert Jr, C. N. Rowe, Thermal decomposition of metal O,O-dialkylphosphorodithioates., *J. Org. Chem*, **32**, 1967, 647-653
- [12] H. Zinke, R. Schumacher, The thermal stability and antiwear performance of some thiophosphoric acid derivatives., *Wear*, **179**, 1994, 45–48.
- [13] R. Schumacher, H. Zinke, Tribofragmentation and antiwear behaviour of isogeometric phosphorus compounds., *Tribology International*, **30**, 1997, 199–208.
- [14] S. Boyde, Hydrolytic Stability of Synthetic Ester Lubricants., *Lubrication Science*, **16**, 2000, 297-312.
- [15] E. S. Forbes, J. Battersby, The effect of chemical structure on the load carrying and adsorption properties of dialkyl phosphites., *ASLE transactions*, **17**, 1974, 263-270.
- [16] I. Minami, H. S. Hong, N. C. Mathur, Effect of Alkanes on the Antiwear Mechanism of Dialkyl Hydrogen Phosphites., *Lubrication science*, **13**, 2001 219-230

Chapter 6

Conclusions and Outlook

In this final chapter, the conclusions drawn from this study are summarized. In addition, ideas for the further research of ester lubricant AW additive design are proposed.

6.1 Conclusions

In order to search for suitable AW additives for ester lubricants, the AW properties of various phosphorus additives in ester base oils were investigated using four-ball tests. From this study, it was found that DAPA has better AW performance than conventional phosphorus additives in TMO ester base oils. The tribological properties of DAPA are outlined here.

1. Phosphonates were believed to be unsuitable for AW additives because of their high stability. However, this study revealed that the introduction of appropriate polar functional groups to phosphonate structures can improve their AW performance, particularly, phosphonate with carboxylic acid, DAPA, has better AW properties in TMO than conventional AW additives, such as TCP, dialkyl phosphate and dialkyl phosphite.
2. DAPA shows better AW performance in TMO than PAO. This performance difference becomes significant especially at high loads, and DAPA in ester base oils forms thicker tribofilm than DAPA in PAO at higher loads (FIB-TEM and XPS depth profiles). It is likely that the types of base oils largely influence the AW performance and tribofilm formation capability of DAPA.
3. The chemical compositions of the DAPA-adsorbed films and DAPA tribofilms were investigated using various surface analysis techniques. It was found that DAPA in PAO and DAPA in TMO formed the same adsorption species and tribofilms on steel surfaces but in different proportions. DAPA tribofilms contains iron carboxylates and the phosphonate structures seems to be maintained.
4. The better AW performance of DAPA in the polar solvent is attributed to a competitive adsorption effect between the TMO and the DAPA additive. This phenomenon delayed the formation of the DAPA tribofilm, allowing its antiwear action to persist. The intrinsic AW capabilities of the TMO polar solvent, compared with those of PAO, also contributed to the better AW capabilities of DAPA in TMO, particularly at low loads.

In addition, for the improvement in AW performance of DAPA, influence of chemical moieties in a DAPA molecule on AW properties was investigated in more polar solvent than TMO, and the following results were obtained.

1. AW properties of DAPA in PET largely depend on the alkyl chain length. DAPA with longer alkyl chains has better AW performance than that of shorter chains, and DAPA with C₁₈ has the best AW properties among the tested DAPAs.
2. Dialkyl phosphonates with OH and CO-NH₂ show excellent AW properties in PET, although they have poor AW performance in PAO.
3. The carbon group between P and COOH in DAPA also effects AW performance in PET. Dialkyl phosphono propionic acid has higher thermal stability and poorer AW performance than dialkyl phosphono acetic acid (DAPA). This suggests that moderate thermal instability is essential to get AW capabilities in ester lubricants.

6.2 Outlook

In recent years, demands for ester lubricants have been increasing for many applications because of environmental aspects. Therefore, developments of ester lubricants become more important than ever before, especially, selections of AW additives should be key technologies. This present research found suitable AW additives and useful information for design of AW additives for ester lubricants. However, further studies are necessary for design of ester lubricants that have outstanding performance compared to conventional lubricants.

6.2.1 Possibilities of dialkyl phosphonates as AW additives

Phosphonate species were believed to be not effective as AW additives because of their high stabilities, however, the present study has succeeded in using them as AW additives in ester base oils, and it is relatively easy to install functional groups to dialkyl phosphonate structures. Thus, AW properties of extensive functional groups besides COOH, OH and CO-NH₂ should be evaluated in ester base oils.

Although dialkyl phosphonates are not effective in PAO, they show excellent AW performance in ester base oils. Their applications for other polar base oils such as poly alkylene glycols and vegetable oils are also possible. Further work needs to be carried out to find out the possibilities of dialkyl phosphonate as AW additives.

6.2.2 Tribofilm compositions

There are still open questions concerning the detailed compositions of DAPA tribofilm, which were not fully clarified in this research. The studies with XPS and ToF-SIMS suggested the presence of P-C bonds in DAPA tribofilm, but direct evidence related to P-C bonds could not be obtained in the current research. For example, EXAFS may be a useful analysis technique to confirm the presence of P-C bonds in DAPA tribofilm. Compared to research about tribofilm compositions formed from phosphate species (ex. ZDDP and TCP), less investigations of phosphonate species have been carried out. The difference of tribofilm compositions between phosphonates and phosphates needs to be clarified.

6.2.3 AW additive design using artificial intelligence (AI)

Much research has used various computer simulation techniques to understand tribochemical reactions of AW additives. Recently, computer simulations using artificial intelligence (AI) have been focused on, especially, material informatics (MI) have been widely used in material science for selection, development, and discovery of materials. MI should be one of the most powerful tools for selections of appropriate functional groups and estimations of hydrogen bond energies between AW additives and ester base oils without performing a considerable number of tribotests to design AW additives.

Finally, I believe that the future research described above would be helpful for design of AW additives that are used for environmentally friendly lubricants, which contribute to reductions of environmental pollution and realization of a sustainable society in near future.

Annex 1:

Tribochemical reaction of DAPA investigated in ECAT tribometer

For a fully understanding of the AW mechanisms, the detailed chemical reaction of DAPA under friction (tribochemical reaction) needs to be considered. Philippon *et al.* researched the tribochemical reaction mechanisms of phosphorus compounds using an *in-situ* XPS system equipped with a tribometer [1, 2]. Following their methods, in this section, the tribochemical reaction mechanisms of DAPA was investigated using the *in-situ* XPS system (ECAT) shown in Figure A1.1. In addition, those of TMO were also studied using the ECAT.

1. Experimental protocols for Environment Controlled Analytical Tribometer (ECAT)

Figure A1.1 illustrates the Environment Controlled Analytical Tribometer (ECAT) of the LTDS lab, which contains the following five main devices:

- XPS Ulvac-Phi Versaprove II : an X-Ray Photoelectron Spectroscopy (XPS) is a surface-sensitive quantitative spectroscopic technique based on the photoelectric effect used to identify the elements present at the surface of a material, as well as their chemical state. The details of XPS principles and measurement conditions are explained in section 2.2.1.
- UHV preparation chamber: additives and base oil can be evaporated in this chamber for adsorption on steel sample. Sputtering can be carried out as well.
- Environment controlled tribometer: it is equipped with a ball on disc type friction test machine. The ambient pressure and the temperature can be controlled. The three forces (F_x , F_y , F_z) and three torques (M_x , M_y , M_z) can be measured to calculate the friction coefficient during the friction tests [3-4].
- Load-lock chamber: it is used to introduce samples from ambient atmosphere to the ECAT.
- Radial distribution sample: it is used to get access to the different chambers and to store the samples under UHV.

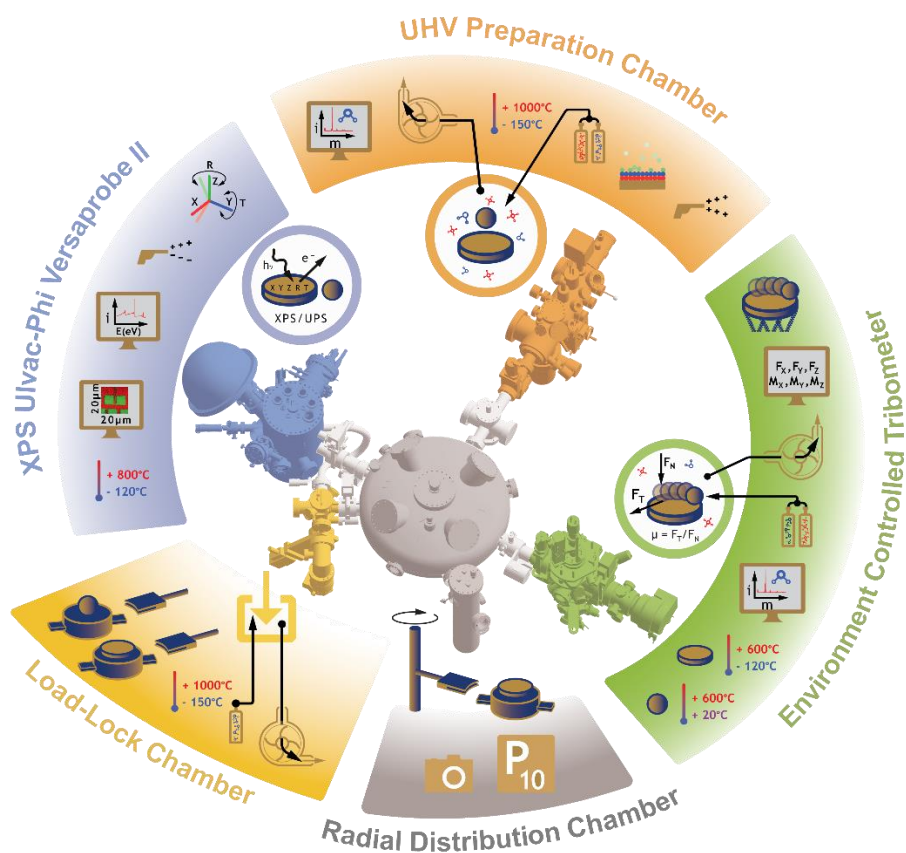


Figure A1.1. Configuration of Environment Controlled Analytical Tribometer (ECAT)

Due to their high boiling points, DAPA and ester base oils were difficult to evaporate in the UHV preparation chamber of the ECAT. Therefore, samples were prepared by a spin coating technique using a spin coater (POLOS Spin150) [5]. The sample preparation procedure is illustrated in Figure A1.2. First, the heptane solution of DAPA or TMO was dropped onto a flat specimen (AISI 52100, $R_a = 20$ nm), which was then rotated at 4000 min^{-1} for 1 minute to make a thin homogeneous layer of DAPA or TMO on a steel sample. After the thin layer was formed on the specimen, the sample was introduced to the ECAT system from the load-lock chamber.

In the ECAT, reciprocating friction tests were carried out at a load of 3 N, a pressure of 1.0×10^{-8} mbar and a sliding velocity of 4.3 mm/s. The ball used was in steel AISI52100.

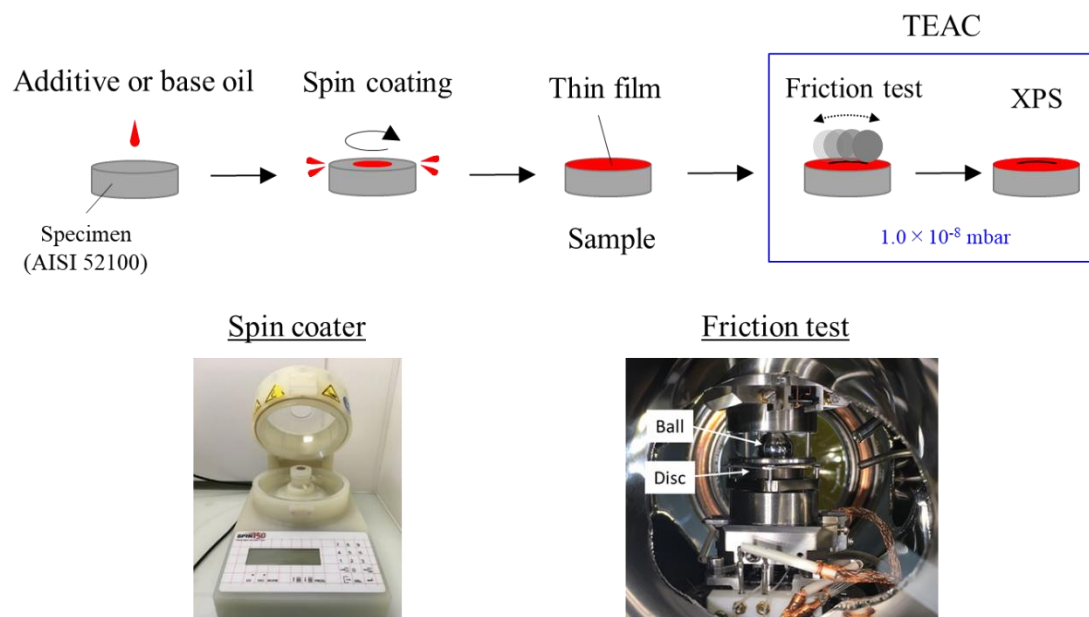








Figure A1.2. Procedure of sample preparation by spin coating and friction test using ECAT system

XPS is a powerful tool to get the chemical composition of the tribofilms and thus to understand the action mechanisms of lubricant additives. However, carbon and oxygen present in the air pollute or oxidize sample surfaces prepared for XPS analysis. The consequence is that the XPS spectra include information derived not only from samples but also from carbon and metal oxide. In XPS analysis, this effect can sometimes make difficult the understanding of a tribochemical reaction that occurs on the worn surfaces. In the ECAT system, shown in Figure A1.1, the samples after friction tests are directly transferred to the XPS chamber without being exposed to the air. This advantage enables us to perform *in-situ* analyses. Philippon *et al.* [1, 2] used ECAT system to investigate the tribochemical reactions of phosphite additives on steel surfaces. For that, the chemisorbed layer of a phosphite additive on steel plates needs to be prepared. A gaseous phosphite additive was introduced into the UHV preparation chamber, then the phosphite molecules were adsorbed onto iron surfaces. Trimethylphosphite was used as a model compound of phosphite additives because actual phosphorus additives have too heavy molecular weights to be evaporated and introduced into the UHV preparation chamber.

In the present study, the same procedure was first used to prepare the chemisorbed film of DAPA on steel surfaces. Diethylphosphonoacetic acid (C₂-DAPA), the smallest molecular weight and commercially available DAPA, was selected as a model molecule of DAPA. However, C₂-DAPA could not be evaporated at room temperature in the UHV preparation chamber. Thus, C₂-DAPA was heated for evaporation, but the thermal decomposition was found above 100 °C. Therefore, an alternative method was applied to prepare the DAPA film on steel surfaces.

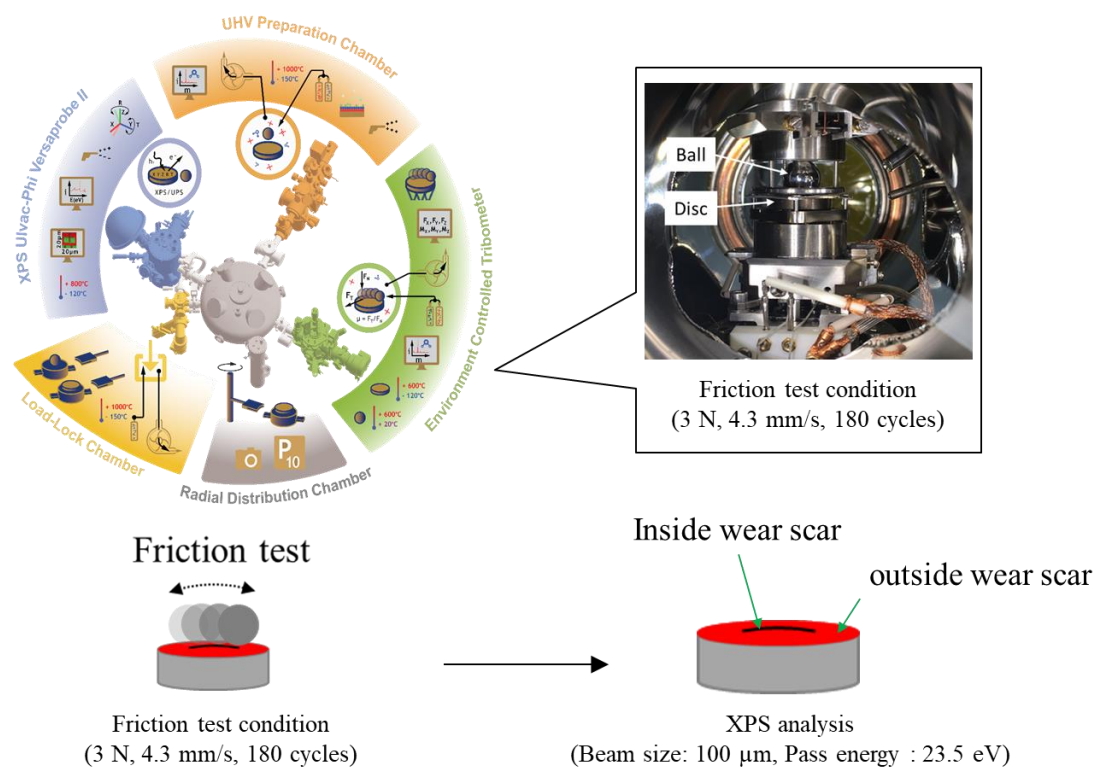
PAO, TMO, DAPA in PAO and DAPA in TMO, which were used in four-ball tests in the previous chapters, were coated onto steel discs by spin coating. First, all studied lubricants (PAO, TMO, DAPA in PAO and DAPA in TMO) were diluted in heptane at a concentration of 3.3 in mass%. Each solution (5-10 µl) was dropped onto the steel surfaces using micropipette, and then spin coating was carried out at 4000 min⁻¹ for 1 minute. After the evaporation of the solvent, only studied molecules remained on the steel surfaces. The appearance of the prepared samples and the weight of the coated samples are summarized in the first five columns of Table A1-1. The films obtained using this method were heterogenous. From these results, it appears that the sample preparation using liquid additives by spin coating was impractical, therefore a solid-state sample that can be dissolved in a solvent was used. In general, phosphorus additives with long alkyl chains are solid at room temperature. In the case of DAPA, the compound becomes solid at room temperature, when its alkyl chain length is more than C₁₀. Thus, DAPA with C₁₂ alkyl chains, dilauryl phosphonoacetic acid (C₁₂-DAPA), was selected for this study and was then dissolved in heptane. The film of C₁₂-DAPA formed homogeneously on the steel surfaces, as shown in the last column of Table A1-1.

Table A1-1. Disc samples for ECAT prepared by spin coating with all studied lubricants (PAO, TMO, DAPA in PAO and DAPA in TMO) and solid C₁₂-DAPA additive.

| Steel plate | PAO | TMO | DAPA in PAO | DAPA in TMO | C ₁₂ -DAPA |
|-----------------------------------------------------------------------------------|-----------------------------------------------------------------------------------|-----------------------------------------------------------------------------------|-----------------------------------------------------------------------------------|-------------------------------------------------------------------------------------|-------------------------------------------------------------------------------------|
|  |  |  |  |  |  |
| - | 0.4 mg | 0.3 mg | 0.4 mg | 0.4 mg | 0.5 mg |

5-10 μl of heptane solution (3.3 in mass%) was dropped to the steel surfaces using micropipette, then spin coating was carried out at 4000 min^{-1} for 1 minute.

From the pre-study of sample preparations, C₁₂-DAPA and TMO were selected as samples for the experiments using ECAT described in section 2.5 (chapter 2). A steel disc without lubricant was also used for comparison. The samples were inserted into the ECAT system, then the friction tests were carried out in the tribometer. The surfaces before and after the friction tests were analyzed by XPS in ECAT without exposing the samples to the air. The X-ray beam size in this system was 50 μm , which is smaller than the width of wear tracks obtained from each sample. These procedures are illustrated in Figure A1-3.



- 1) Samples were inserted from the load-lock chamber and transferred to the tribometer.
- 2) Ball-on-Disc tests were carried out in the tribometer below a pressure of 10^{-7} Pa.
- 3) Samples after the friction tests were transferred to XPS without exposing to the air. The inside and outside wear tracks were analyzed according to the peak fitting parameters described in section 2.2.3.

Figure A1-3. Experimental procedures using ECAT.

2. Results of ECAT

Tribotests in ECAT tribometer are carried out following the procedure described in §2.5. The results are presented in this section. The obtained XPS spectra were analyzed by curve fitting treatments to investigate chemical species present on the worn surfaces.

(1) Steel surface without lubricants

First, the steel disc with no additive was used to study the behavior of iron surfaces. Figure A1-4 (a) presents the friction coefficient of the steel surface without lubricant during a 180 cycles friction test performed at 3 N (P_{\max} : 0.68 MPa). The friction coefficient starts below 0.2, but increases quickly up to 1.0 just after the beginning of the test, then the value stabilizes at 0.8-1.0. This result is consistent with the results obtained by Martin *et al* [6]. Their study also showed that the friction coefficient of AISI 52100 discs with no lubricant starts at 0.1 and that it significantly jumps after a few cycles under UHV.

The Scanning X-ray Image (SXI) - image of the secondary electrons induced by the X-ray beams - after the friction test is shown in Figure A1-4 (b). In SXI, heavy elements have bright images compared to light elements. Figure A1-4 (b) shows that the wear scar is brighter than outside, indicating that heavier elements are present inside the wear track.

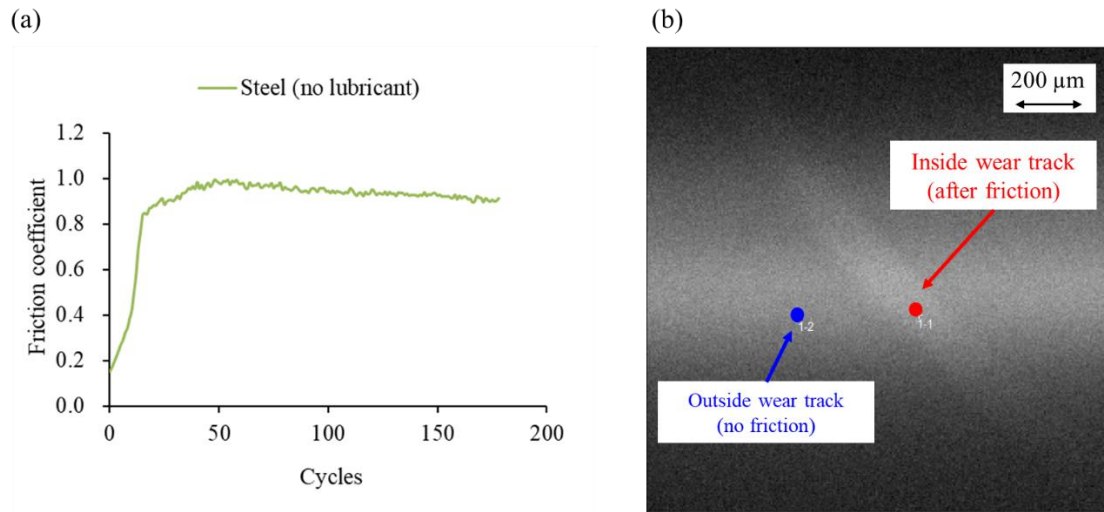


Figure A1-4. Friction coefficient as function of cycles for steel-steel contact test (normal load = 3 N, sliding speed 4.3 mm/s, chamber pressure = 10^{-8} mbar) and SXI image after the test.

Table A1-2 shows the atomic composition of the steel surface outside and inside the wear track. After the friction test (inside the wear track), the atomic concentration of carbon (C_{1s}) decreases while that of iron ($Fe_{2p3/2}$) increases. This is consistent with the contrast observed on the SXI image.

Table A1-2. Atomic concentration changes on the steel surfaces before and after the friction tests.

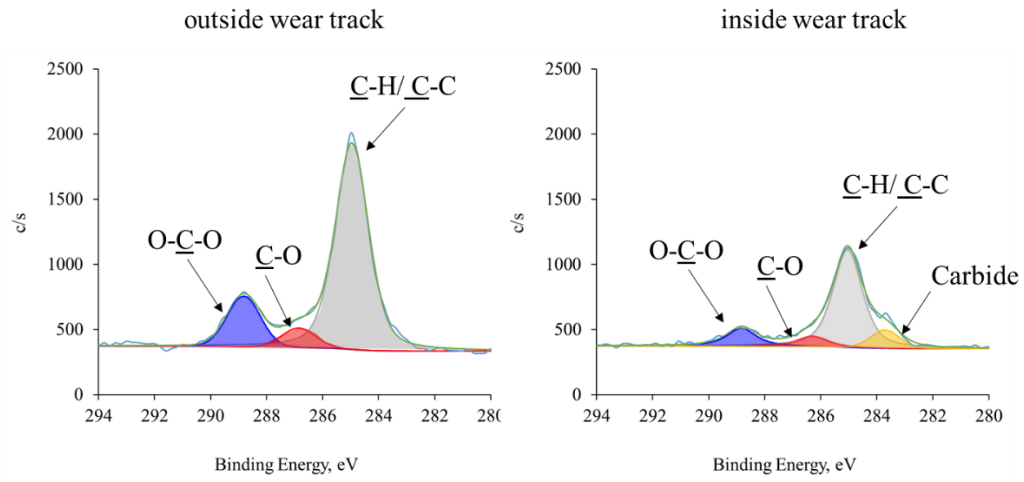
| Atomic concentration, % | Carbon (C _{1s}) | Oxygen (O _{1s}) | Iron (Fe _{2p3/2}) |
|------------------------------|---------------------------|---------------------------|-----------------------------|
| No friction (outside wear) | 57.2 | 38.2 | 4.6 |
| After friction (inside wear) | 35.0 | 39.7 | 25.3 |

The XPS spectra of each element on the steel surfaces (outside and inside the wear tracks) are shown in Figure A1-5. The intensity of whole C_{1s} spectrum decreases after friction. As mentioned above, it is well known that carbon contamination exists on sample surfaces and that XPS can detect it with high sensitivity [7]. Therefore, the intensity decrease of C_{1s} spectrum indicates that the adventitious carbon was removed by friction.

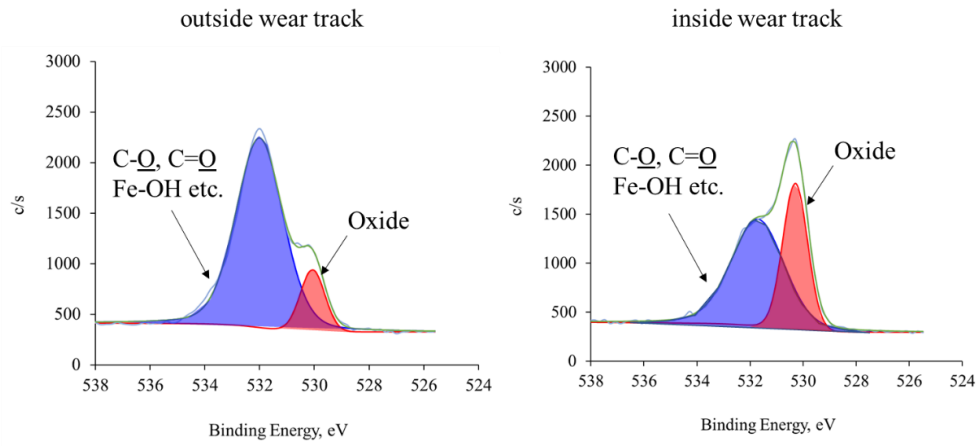
The peak around 530.0 eV on O_{1s} spectra, which is assigned to metal oxide [8, 9], increases after friction. The intensity of peaks at 709-712 eV and 707 eV on Fe_{2p3/2}, assigned to iron oxide and iron respectively [10], also increases after friction. These results indicate that iron and its oxide were revealed after carbon contamination removal (by friction) on the steel surface.

In [6] the authors suggested that the adventitious carbon on steel surfaces could explain the decrease of the friction immediately after the start of the test, and that the friction coefficient jump observed after the carbon removal could be due to contact generation between iron oxides. The change of the friction coefficient observed in our study (Figure A1-4) shows similar results.

(a) C1s



(b) O1s



(c) Fe2p3/2

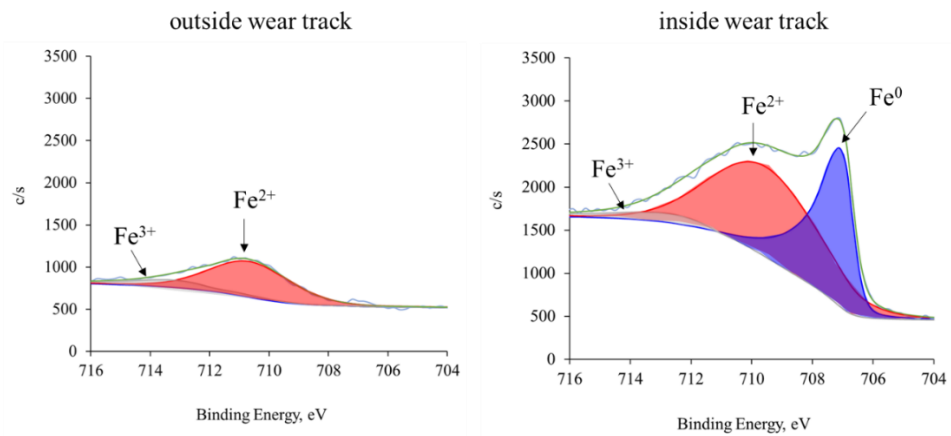


Figure A1-5. High resolution spectra on C1s, O1s and Fe2p3/2 before and after friction test.

(2) C₁₂-DAPA

Figure A1-6 (a) shows the friction coefficient of C₁₂-DAPA on the steel surfaces during the friction test for 180 cycles at 3 N. The friction coefficient become stable after 15 cycles, and no significant change is observed until the end of the test. The SXI after 180 cycles is presented in Figure A1-6 (b), and the wear track can be observed on the white areas. The XPS measurements were carried out on inside the wear track (red point) and outside (blue point).

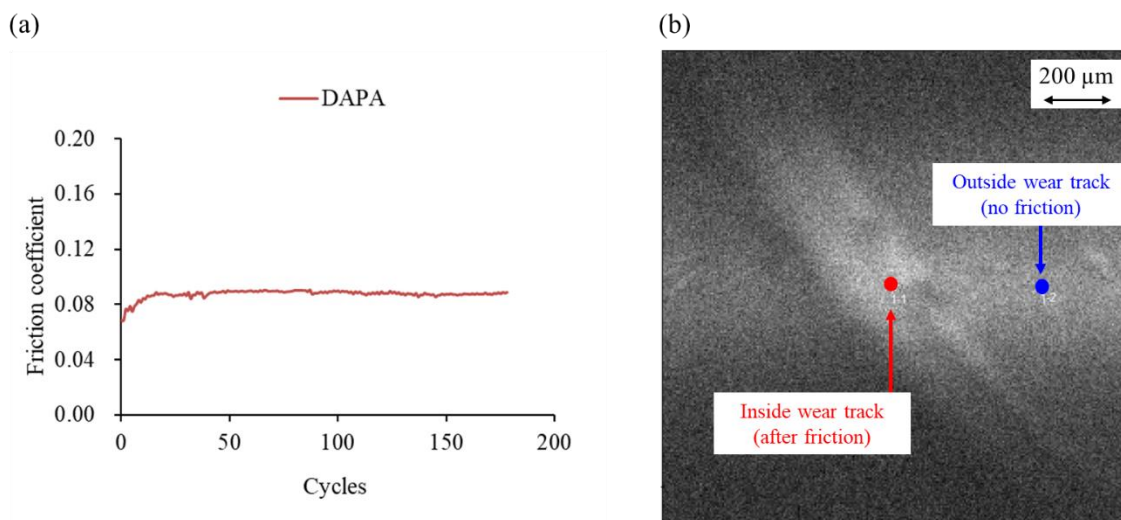


Figure A1-6. Friction coefficient as function of cycles for tribotest carried out with steel pin and with a steel flat coated with C₁₂-DAPA (normal load = 3 N, sliding speed 4.3 mm/s, chamber pressure = 10⁻⁸ mbar) and SXI after the test.

The atomic compositions outside and inside the wear track are summarized in Table A1-3. Those of C_{1s}, O_{1s} and P_{2p} outside the wear track were found to be in agreement with the theoretical values of C₁₂-DAPA which were calculated from its rational formula (C₂₆H₅₃O₅P). The atomic concentration of iron outside the wear track was less than 1 %, indicating that the sample surface was sufficiently covered with the C₁₂-DAPA molecules by spin coating. Inside the wear track (after friction), the atomic concentrations of O_{1s}, P_{2p} and Fe_{2p3/2} increase, while the C_{1s} atomic concentration decreases.

Table A1-3. Atomic compositions obtained outside and inside the wear track on steel plate with C₁₂-DAPA.

| Atomic concentration, % | C _{1s} | O _{1s} | P _{2p} | Fe _{2p3/2} |
|-------------------------------------------|-----------------|-----------------|-----------------|---------------------|
| outside wear track (no friction) | 82.4 | 14.5 | 2.9 | 0.2 |
| inside wear track (after friction) | 64.7 | 26.7 | 3.6 | 5.0 |
| C ₁₂ -DAPA (theoretical value) | 81.3 | 15.6 | 3.1 | - |

The curve fitting analyses were performed using the XPS spectra of each element (C_{1s} , O_{1s} , P_{2p} and $Fe_{2p_{3/2}}$) to identify chemical species existing on the surfaces. The C_{1s} spectra recorded outside and inside the wear track were fitted with four contributions. Each peak was determined thanks to literature references [11-13], and the four carbon species, hydrocarbon ($\underline{C}-C/\underline{C}-H$, $\underline{C}-COO$, $\underline{C}-O$ and $\underline{O}-C$), are found. These four carbon species are relevant with the carbon atoms of C_{12} -DAPA, as described in Figure A1-7.

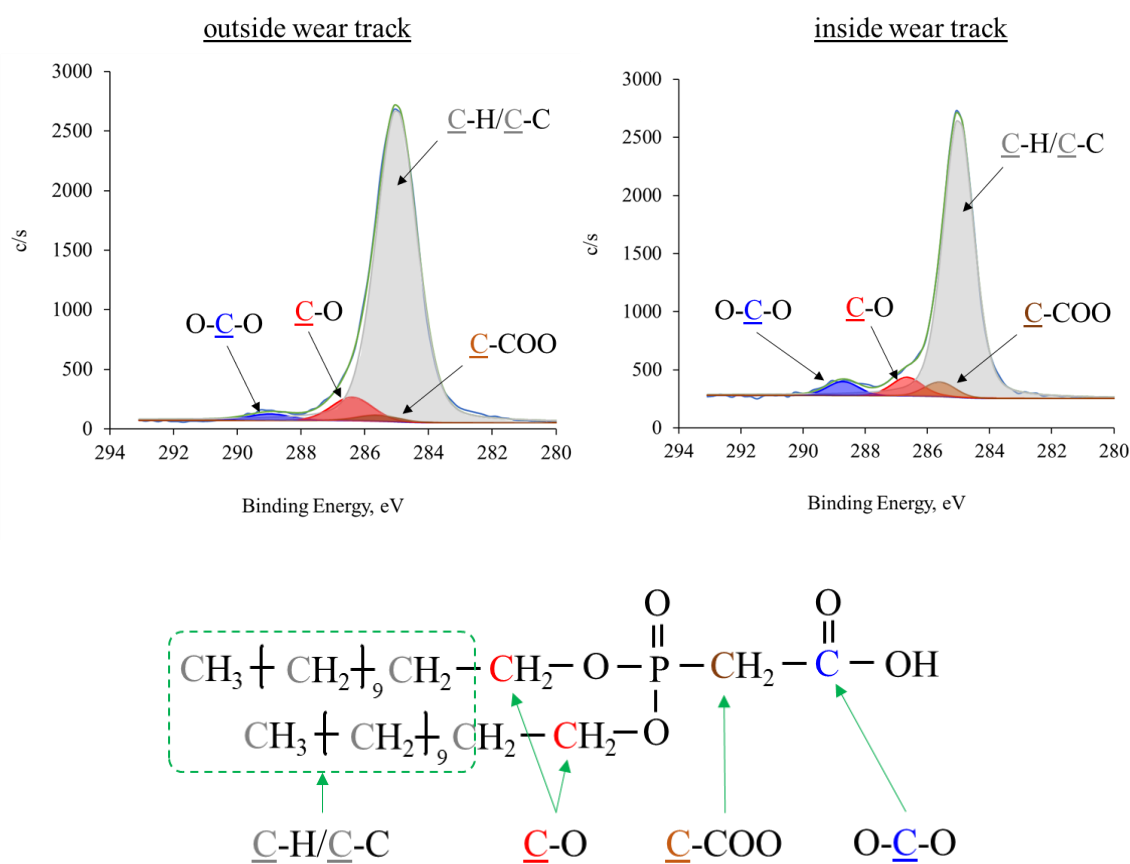


Figure A1-7. XPS Curve fitting results of C_{1s} obtained from outside and inside wear track after ECAT tribotest with C_{12} -DAPA.

Table A1-4. Binding energies of identified carbon species and their quantitative analysis obtained from XPS analyses of tribofilm after ECAT tribotest with C₁₂-DAPA. The total atomic concentrations (outside: 82.4 at% and inside: 64.7 at%) correspond to that of C_{1s} shown in Table A1-3.

| Name | | Outside wear track | | Inside wear track | |
|-----------------|--------------------------|--------------------|----------------|-------------------|----------------|
| | | Peak position, eV | Atomic conc, % | Peak position, eV | Atomic conc, % |
| C _{1s} | <u>C</u> -C/ <u>C</u> -H | 285.0 | 74.7 | 285.0 | 56.1 |
| | <u>C</u> -COO | 285.6 | 1.3 | 285.6 | 2.5 |
| | <u>C</u> -O | 286.4 | 5.1 | 286.7 | 3.6 |
| | <u>C</u> -OO | 289.0 | 1.3 | 288.7 | 2.5 |
| total | | - | 82.4 | - | 64.7 |

The ratio C-C/C-H at% / C-OO at % is lower inside (22.4) compared to the outside (57.5) of the wear track. The amount of hydrocarbon (C-C/C-H) compared to C-OO is so significantly lower inside the wear track compared to the outside. This result suggests that the alkyl chains of C₁₂-DAPA were removed under friction.

The peak positions of C-OO and C-O inside the wear track have also different values compared to outside. Alexander *et al.* reported that the binding energies of C-OO in carboxylic acids were shifted by 0.4-0.6 eV when carboxylic acids change to carboxylate forms (COOX, X = metal) [12-14]. Therefore, the peak shift of C-OO observed in this experiment suggests the formation of iron carboxylates (COO-Fe) on the worn surfaces. The binding energy of C-O inside wear track shows 0.3 eV higher value than outside. This result indicates that the carbon atom of C-O becomes electron poorer after the friction test.

Figure A1-8 and Table A1-5 show the curve fitting results on O_{1s} spectra recorded outside and inside the wear track. The O_{1s} spectrum recorded outside the wear track contains five contributions, which can be assigned to C-O, P-O, C=O, P=O and the oxygen of metal oxide, respectively [9, 13]. The atomic concentration ratio of C-O, P-O, C=O, and P=O is 1:2:1:1, which is equivalent to that of the C₁₂-DAPA molecule (Table A1-4). On the contrary, the spectrum recorded inside the wear track shows three peaks at 529.7 eV, 531.4 eV and 533.0 eV. The peak at 529.7 eV can be identified as the oxygen of metal oxide [8-10]. The peak at 531.4 eV is in agreement with the Non Bridging Oxygen (NBO) value in phosphorus compounds [16], C=O and Fe-O-H. The peak at 533.0 eV is consistent with Bridging Oxygen (BO) in phosphorus compounds [17] and C-O. These are two possibilities to explain this result. One is that C₁₂-DAPA forms phosphorus compounds including NBO and BO on the worn surfaces, and that iron oxides of the steel plate are exposed to the surface by friction (patchy tribofilm). Another is that a very thin layer of DAPA tribofilm is formed on the native iron oxide, consequently XPS detects both a phosphorus tribofilm and steel surfaces below.

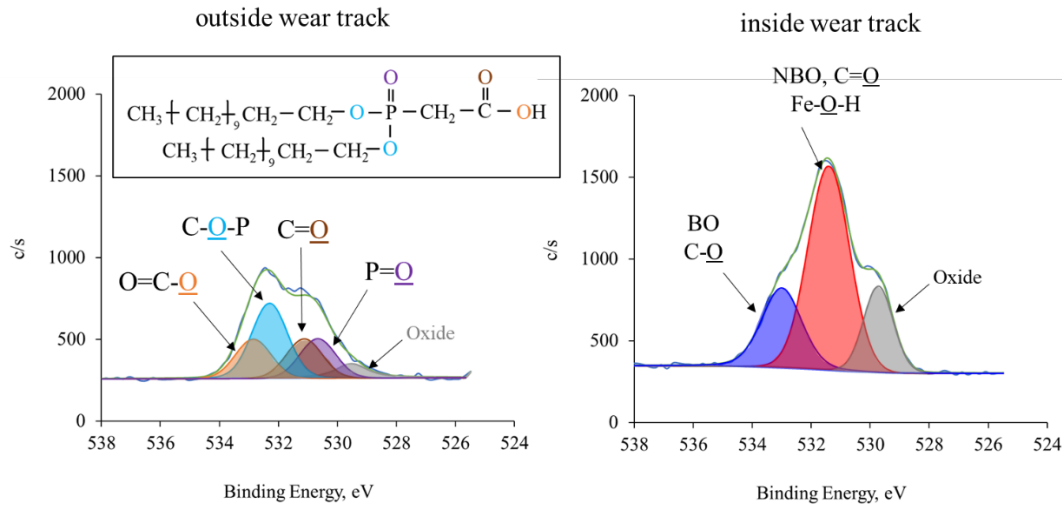


Figure A1-8. Curve fitting results of O1s obtained outside and inside the wear track from XPS analyses of tribofilm after ECAT tribotest with C₁₂-DAPA.

Table A1-5. Binding energies of identified oxygen species and their quantitative analysis results from XPS analyses of tribofilm after ECAT tribotest with C₁₂-DAPA. The total atomic concentrations (outside: 14.5 at% and inside: 26.7 at%) correspond to that of O1s shown in Table A1-3.

| Name | | Outside wear track | | Inside wear track | |
|-------|-------|--------------------|----------------|-------------------|----------------|
| | | Peak position, eV | Atomic conc, % | Peak position, eV | Atomic conc, % |
| O1s | Oxide | 529.5 | 1.2 | 529.7 | 4.9 |
| | P=O | 530.7 | 2.7 | 531.4 | 15.5 |
| | C=O | 531.1 | 2.7 | | |
| | P-Q | 532.3 | 5.3 | 533.0 | 6.3 |
| | C-Q | 532.9 | 2.7 | | |
| total | | - | 14.5 | - | 26.7 |

The curve fitting results of P_{2p} spectra are shown in Figure A1-9 and Table A1-6. The binding energy of P_{2p3/2} inside the wear track was observed at 133.1 eV, which is 0.3 eV higher value than outside. In addition, the atomic concentration on P_{2p3/2} slightly increases after the friction.

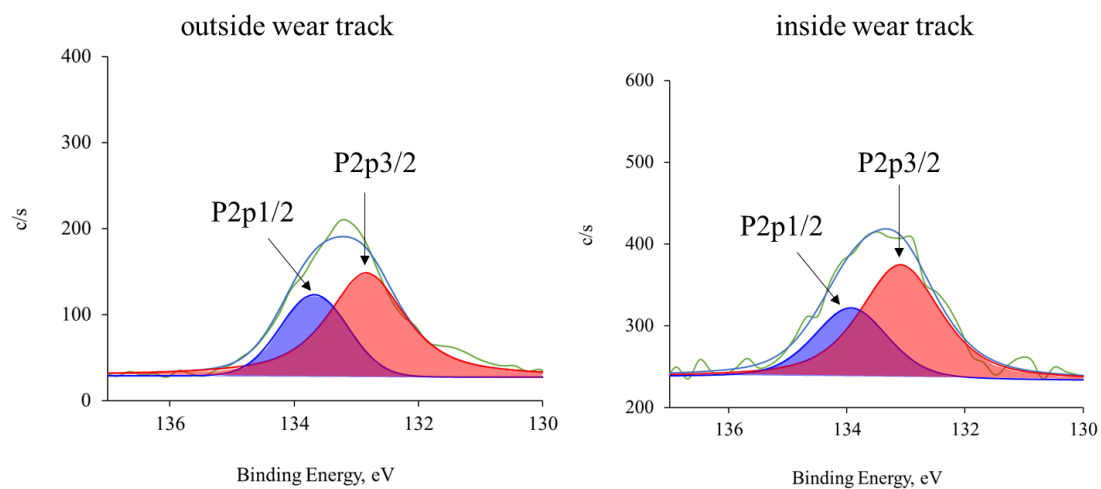


Figure A1-9. Curve fitting results of P2p obtained outside and inside the wear track from XPS analyses of tribofilm after ECAT tribotest with C₁₂-DAPA.

Table A1-6. Binding energies of identified phosphorus species and their quantitative analysis results from XPS analyses of tribofilm after ECAT tribotest with C₁₂-DAPA. The total atomic concentrations (outside: 2.9 at% and inside: 3.6 at%) correspond to that of P_{2p} shown in Table A1-3.

| Name | | Outside wear track | | Inside wear track | |
|------|--------|--------------------|----------------|-------------------|----------------|
| | | Peak position, eV | Atomic conc, % | Peak position, eV | Atomic conc, % |
| P2p | P2p3/2 | 132.8 | 2.9 | 133.1 | 3.6 |

Figure A1-10 and Table A1-7 illustrate the curve fitting data of the $\text{Fe}_{2p_{3/2}}$ spectra. No significant peak of $\text{Fe}_{2p_{3/2}}$ was observed outside the wear track, however, the peaks assigned to Fe (II) and Fe (III) were detected inside the wear track [18]. The O_{1s} spectrum in Figure A1-10 shows that metal oxides signal increases after the friction test (inside wear track), therefore the peaks of Fe (II) and Fe (III) can be assigned to iron oxides.

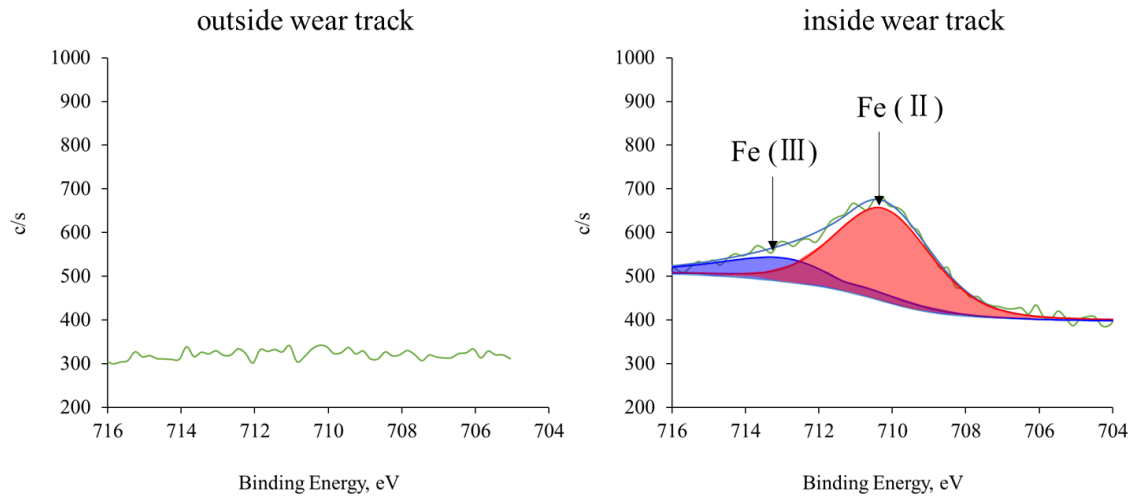


Figure A1-10. Curve fitting results of $\text{Fe}_{2p_{3/2}}$ obtained outside and inside the wear tracks from XPS analyses of tribofilm after ECAT tribotest with C_{12} -DAPA.

Table A1-7. Binding energies of identified iron species and their quantitative analysis results from XPS analyses of tribofilm after ECAT tribotest with C_{12} -DAPA. The total atomic concentrations (outside: 0.1 at% and inside: 5.0 at%) correspond to that of $\text{Fe}_{2p_{3/2}}$ shown in Table A1-3.

| Name | | Outside wear track | | Inside wear track | |
|------------------------|---------|--------------------|----------------|-------------------|----------------|
| | | Peak position, eV | Atomic conc, % | Peak position, eV | Atomic conc, % |
| $\text{Fe}_{2p_{3/2}}$ | Fe(0) | - | - | - | 0.0 |
| | Fe(II) | 710.5 | < 0.1 | 710.2 | 3.8 |
| | Fe(III) | 711.4 | < 0.1 | 711.1 | 1.2 |
| total | | - | 0.1 | - | 5.0 |

3. Discussion tribochemical reaction of DAPA

ECAT enabled us to perform *in-situ* XPS and to obtain clues for understanding the tribochemical reaction of DAPA by comparing the XPS spectra before and after friction. Figure A1-7 and Table A1-4 showed the carbon species change of DAPA. The ratio between $\underline{\text{C}}\text{-OO}$ and hydrocarbon ($\underline{\text{C}}\text{-C}/\underline{\text{C}}\text{-H}$) inside the wear track has a higher value than outside, suggesting that the contribution of alkyl chain moieties decreases after friction. This indicates that the alkyl chains of DAPA were removed by friction. Moreover, the binding energies of $\underline{\text{C}}\text{-OO}$ and $\underline{\text{C}}\text{-O}$ were changed after the friction tests. That of $\underline{\text{C}}\text{-OO}$ shifted to a lower energy, indicating the carboxylate formation on the worn surfaces [12-14]. In addition, that of $\underline{\text{C}}\text{-O}$ inside the wear track shifted to a slightly higher energy than outside. This suggests that the carbon atom of C-O become electron poorer after the friction, and that the interaction between the C-O and steel surfaces may occurred.

Table A1-8 compares the binding energies of $\text{P}_{2\text{p}3/2}$ obtained in this experiment and those of phosphorus compounds found in the literature (each value was corrected at 285.0 eV) [19-21]. The value of $\text{C}_{12}\text{-DAPA}$ outside the wear tracks was observed at 132.8 eV, and this is between the phosphates (TCP and TBP) at 133.8 eV and tri butyl phosphonate species at 132.3 eV. This indicates that the binding energy of $\text{P}_{2\text{p}3/2}$ is influenced by the number of oxygens surrounding a phosphorus atom. The binding energy inside the wear track with $\text{C}_{12}\text{-DAPA}$ is 133.1 eV, which is between the phosphates and tri butyl phosphonate. It is highly probably that $\text{C}_{12}\text{-DAPA}$ tribofilms after friction contains P-C bond, and this result is in good agreement with the surface analysis data obtained by ToF-SIMS and XPS described in chapter 4.

Table A1-8. Binding energies of phosphorus compounds corrected at 285.0 eV (C-C/C-H).

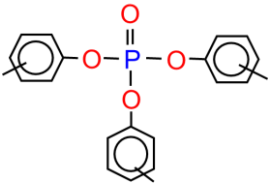
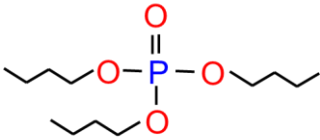
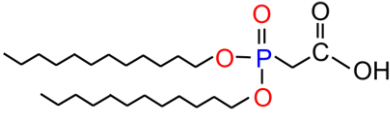
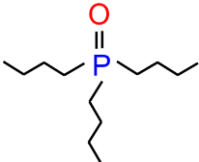
| Phosphorus compound | Binding energy, eV | Ref |
|----------------------------------------------------------------------------------------------------------------------------------------|--------------------|-----------|
|  <p>Tri cresyl phosphate (TCP)</p> | 133.8 | [29] |
|  <p>Tri Butyl Phosphate (TBP)</p> | 133.8 | [30] |
|  <p>C12-DAPA outside wear track (no friction)</p> | 132.8 | Table 5-7 |
| <p>C12-DAPA tribofilm inside wear track (after friction)</p> | 133.1 | Table 5-7 |
|  <p>Tri Butyl Phosphine oxide</p> | 132.3 | [31] |

Table A1-9 summarizes the $P_{2p3/2}$ binding energies of pyrophosphate, metaphosphate and polyphosphate, showing that the peak position shifts to higher energy according to the increase of polymerization. The binding energy of $P_{2p3/2}$ shifts to lower end from 132.8 eV to 133.1 eV after friction. The O1s spectra shown in Figure A1-7 also shows the formation of Bridging Oxygen (BO). These results suggest that the polymerization of the DAPA molecule occurs on the worn surfaces.

Table A1-9. $P_{2p3/2}$ binding energies of various phosphorus compounds.

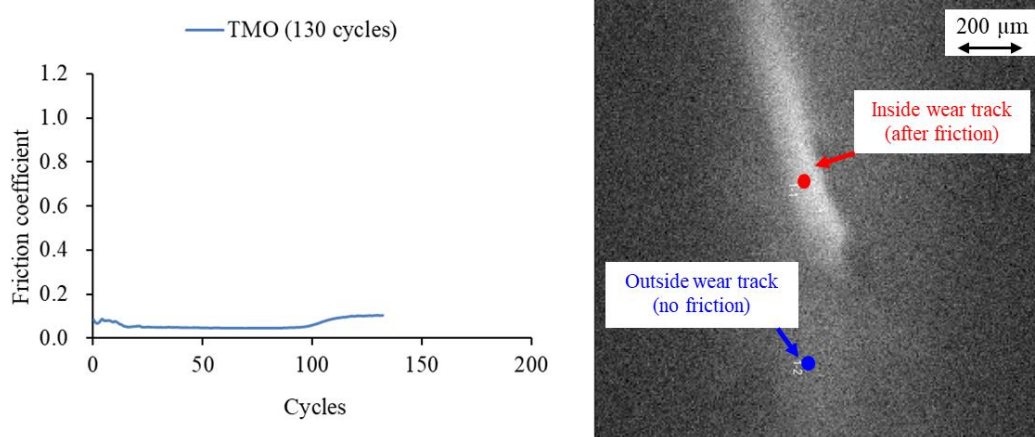
| Species | Orthophosphate | Pyrophosphate | Metaphosphate | P_2O_5 |
|--------------------|---------------------------------------------------------------------------------------------------------------|--------------------------------------------------------------------------------------------------------------------------------|-------------------------------------------------------------------------------------------------------------------------------|-----------------------------------------------------------------------------------------------------------------------------|
| Chemical structure | $\begin{array}{c} \text{O} \\ \parallel \\ ^-\text{O} - \text{P} - \text{O}^- \\ \\ \text{O}^- \end{array}$ | $\left[\begin{array}{c} \text{O} \\ \parallel \\ ^-\text{O} - \text{P} - \text{O} - \\ \\ \text{O}^- \end{array} \right]_n$ | $\left[\begin{array}{c} \text{O} \\ \parallel \\ -\text{O} - \text{P} - \text{O} - \\ \\ \text{O}^- \end{array} \right]_n$ | $\left[\begin{array}{c} \text{O} \\ \parallel \\ -\text{O} - \text{P} - \text{O} - \\ \\ \text{O} \end{array} \right]_n$ |
| $P_{2p3/2}$ | 134.1 eV | 134.4 eV | 134.8 eV | 135.4 - 135.8 eV |
| Ref. | [32] | [32] | [32] | [33] |

From the above detailed analysis and as was proposed in chapter 4, the tribochemical reaction of C_{12} -DAPA can be drawn as in Figure 4-20. First, DAPA adsorbs onto metal surfaces, then carboxylates are formed on the surfaces. Secondly, the alkyl chains of C_{12} -DAPA are removed. Next, polymerization of C_{12} -DAPA occurs and forms a P-O-P bond.

(3) TMO

Figure A1-11 shows the friction test results using TMO on the steel disc, carried out at 3 N during 130 and 180 cycles. The friction coefficient remains less than 0.1 up to 130 cycles, then the value increases to over 1.0. The XPS analyses were performed inside and outside the wear tracks as in the previous experiments.

(a) 130 cycles



(b) 180 cycles

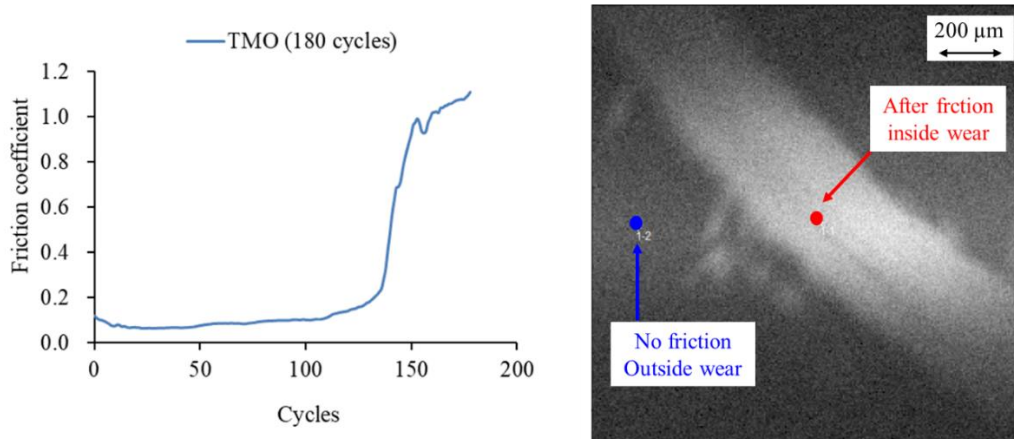


Figure A1-11. Friction coefficient as function of cycles for tribotest carried out with steel pin and with a steel flat coated with TMO (normal load = 3 N, sliding speed 4.3 mm/s, chamber pressure = 10^{-8} mbar) and SXI after the test:

(a) after 130 cycles and (b) after 180 cycles.

Table A1-10 shows the atomic compositions measured inside (red points) and outside (blue points) the wear tracks after 130 and 180 cycles. The values obtained outside the wear track were in good agreement with those of the TMO molecule, calculated from its chemical formula ($C_{60}H_{110}O_6$). This

suggests that the sample surfaces were homogeneously covered with the TMO molecules by spin coating. Regarding the atomic concentrations of O_{1s} and $Fe_{2p3/2}$, the values inside the wear track after 180 cycles were higher than those of 130 cycles, but those of C_{1s} decrease with test cycles.

Table A1-10. Atomic concentrations inside and outside the wear track with TMO on steel discs

| Atomic concentration, % | C_{1s} | O_{1s} | $Fe_{2p3/2}$ |
|-------------------------------------|----------|----------|--------------|
| TMO (theoretical value) | 90.1 | 9.1 | - |
| outside wear track after 130 cycles | 90.4 | 9.5 | 0.1 |
| outside wear track after 180 cycles | 90.3 | 9.7 | 0.0 |
| inside wear track after 130 cycles | 73.7 | 21.8 | 4.5 |
| inside wear track after 180 cycles | 68.8 | 21.3 | 9.9 |

In order to investigate the detailed chemical species, the curve fitting analyses were performed using the spectra on C_{1s} , O_{1s} and $Fe_{2p3/2}$. The results are presented in Table A1-11 and in Figures A1-12 to A1-14. Outside the wear tracks, after 130 cycles and 180 cycles, three carbon species, such as $O-C-O$, $C-O$ and hydrocarbon, were detected. These carbon species are consistent with the carbon species contained in TMO. Inside the wear tracks, in addition to these carbon species, a peak at around 283.5 eV was found. It can be assigned to carbide [22, 23]. The binding energy of $O-C-O$ inside the wear track after 130 cycles was observed at 289.2 eV, and this value was closed to the value measured outside (289.3 eV). However, after 180 cycles, a peak at 288.4 eV was found instead, indicating the formation of carboxylate on the worn surfaces [12-14]. This result suggests that the ester structure of TMO was maintained up to 130 cycles, but the ester structure was decomposed after 180 cycles when the friction conditions were severe (friction coefficient: over 1.0).

Figure A1-13 exhibits the curve fitting results of O_{1s} spectra outside and inside the wear tracks after 130 and 180 cycles. The O_{1s} spectra recorded outside the wear track were fitted with two peaks at 532.3 eV and 533.5 eV, and they were in good agreement with the binding energies of esters reported in the literature [24]. Inside the wear tracks, the spectra include four contributions: two peaks at 532.3 eV and 533.5 eV were assigned to the ester group ($C=O$ and $C-O$, respectively), the peak around 531.7 eV was attributed to metal hydroxide ($M-O-H$) and that of 530.0 eV to metal oxide ($M-O-M$) [9-11]. The contributions of $C-O$ and $C=O$ decrease, and those of metal hydroxide and oxide increase with increasing number of test cycles (Table A1-11). The atomic concentration ratios of $C-O + C=O$ (TMO) / Fe (substrate) obtained from inside wear scars were calculated from Table A1-11, and those after 130 and 180 cycles are 0.49 and 0.05. The decrease of $C-O + C=O$ (TMO) / Fe (substrate) ratio indicates that the TMO molecules are removed, and iron substrate is revealed by friction.

The curve fitting results of $Fe_{2p3/2}$ spectra outside and inside the wear tracks are presented in Figure A1-14. There is no clear peak of $Fe_{2p3/2}$ outside the wear tracks, however, inside the wear track and

after 130 cycles two peaks assigned to iron (II) and iron (III) are detected [18]. An additional peak from iron (0) is found at 180 cycles.

Table A1-11. Binding energies and atomic concentrations of chemical species identified by curve fitting analyses of XPS spectra on C_{1s}, O_{1s} and Fe_{2p3/2} obtained from tribofilm after ECAT tribotest with TMO.

| | | Peak position, eV | | Concentration, atomic% | |
|------------|-------------|-------------------------------------|---------------------------------------|-------------------------------------|---------------------------------------|
| | | Outside wear track (no friction) | Inside wear track (after friction) | Outside wear track (no friction) | Inside wear track (after friction) |
| 130 cycles | Carbide | - | 282.9 | - | 38.7 |
| | C-C/C-H | 285.0 | 285.0 | 80.8 | 29.9 |
| | C-O | 286.5 | 286.5 | 6.7 | 4.1 |
| | C=O | 289.3 | 289.3 | 2.9 | 1.0 |
| | total | - | - | 90.4 | 73.7 |
| 180 cycles | Carbide | - | 283.3 | - | 23.8 |
| | C-C/C-H | 285.0 | 285.0 | 79.4 | 39.0 |
| | C-O | 286.5 | 286.5 | 7.3 | 1.3 |
| | C=O | 289.3 | 288.4 | 3.5 | 4.6 |
| | total | - | - | 90.2 | 68.7 |
| 130 cycles | Oxide | - | 529.9 | - | 11.4 |
| | Fe-O-H, etc | - | 531.6 | - | 8.2 |
| | C=O | 532.3 | 532.3 | 4.7 | 1.1 |
| | C-O | 533.7 | 533.7 | 4.9 | 1.1 |
| | total | - | - | 9.6 | 21.8 |
| 180 cycles | Oxide | - | 530.0 | - | 7.7 |
| | Fe-O-H, etc | - | 531.5 | - | 13.1 |
| | C=O | 532.4 | 532.4 | 5.0 | 0.3 |
| | C-O | 533.8 | 533.8 | 4.8 | 0.2 |
| | total | - | - | 9.8 | 21.3 |
| 130 cycles | Fe(0) | - | 707.0 | - | 0.2 |
| | Fe(II) | - | 709.8 | - | 2.7 |
| | Fe(III) | - | 710.7 | - | 1.6 |
| | total | - | - | - | 4.5 |
| 180 cycles | Fe(0) | - | 706.8 | - | 6.2 |
| | Fe(II) | - | 709.6 | - | 1.5 |
| | Fe(III) | - | 710.5 | - | 2.3 |
| | total | - | - | - | 10.0 |

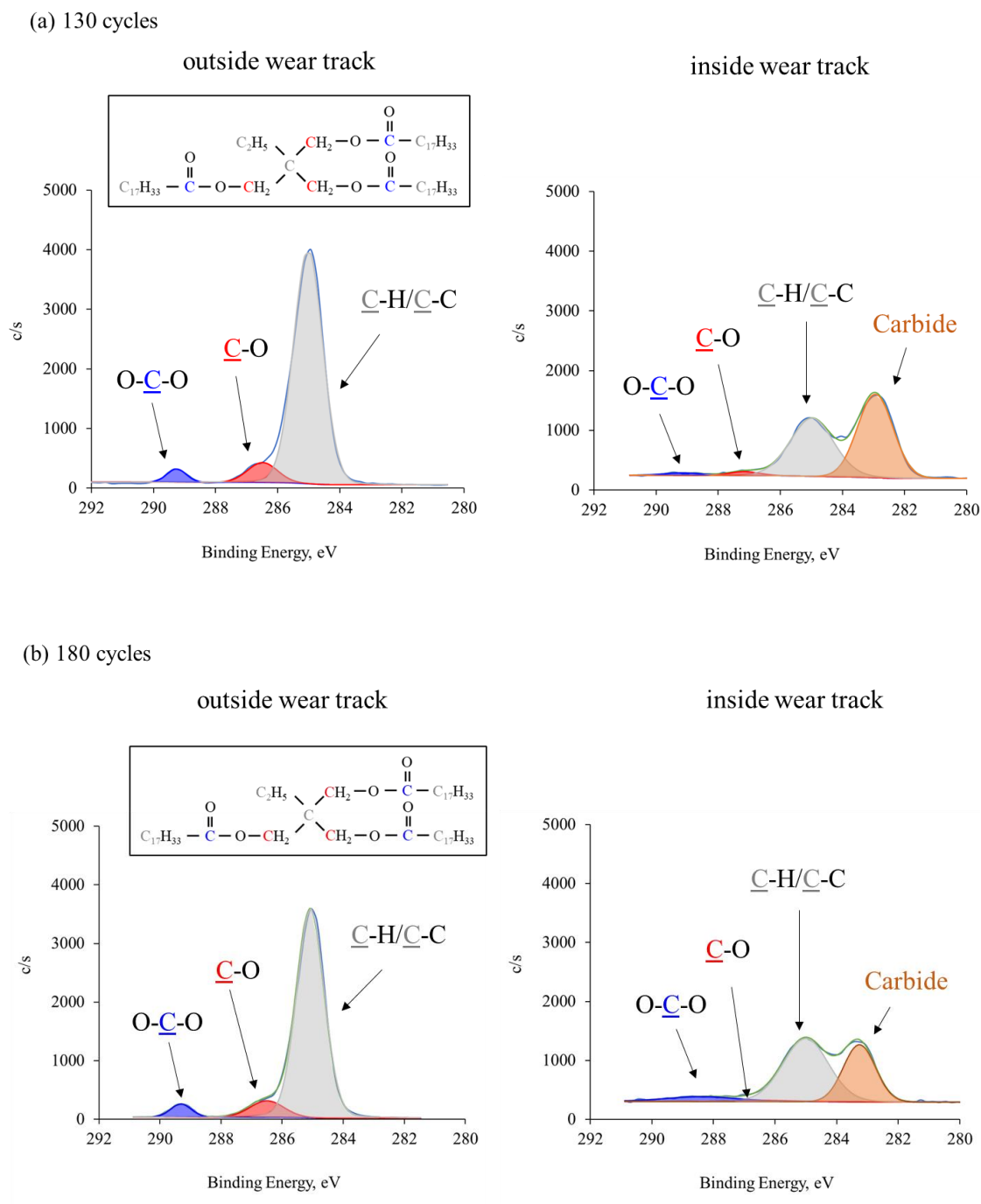
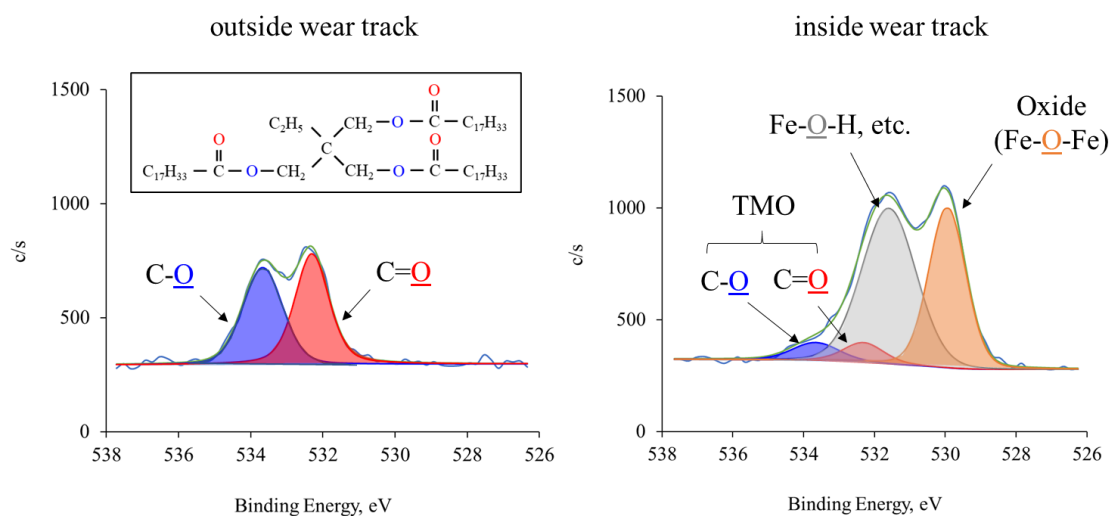


Figure A1-12. XPS curve fitting analyses results on C_{1s} spectra outside and inside the wear tracks obtained from tribofilm after ECAT tribotest with TMO
(a) after 130 cycles and (b) after 180 cycles.

(a) 130 cycles



(b) 180 cycles

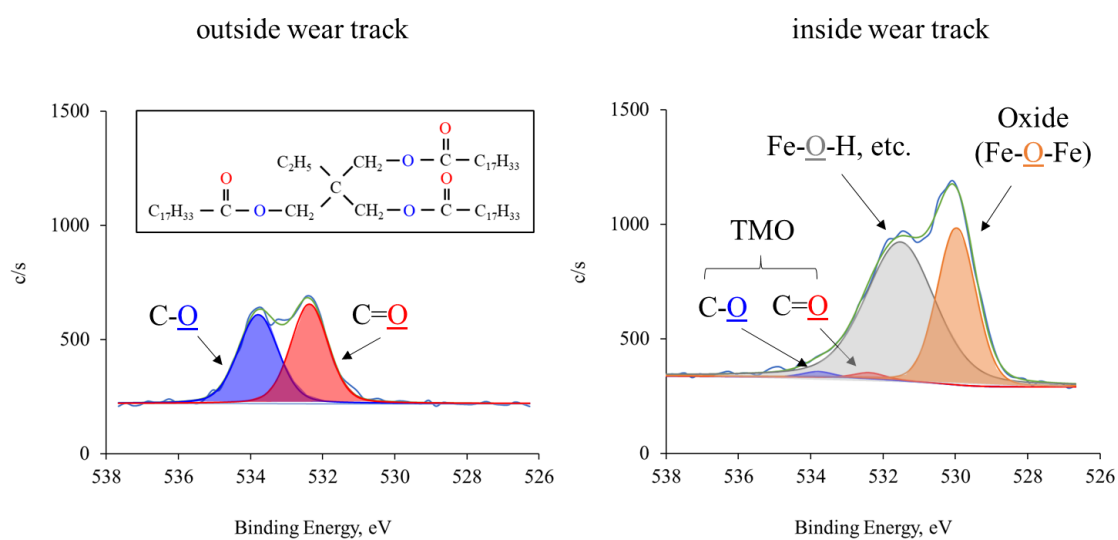
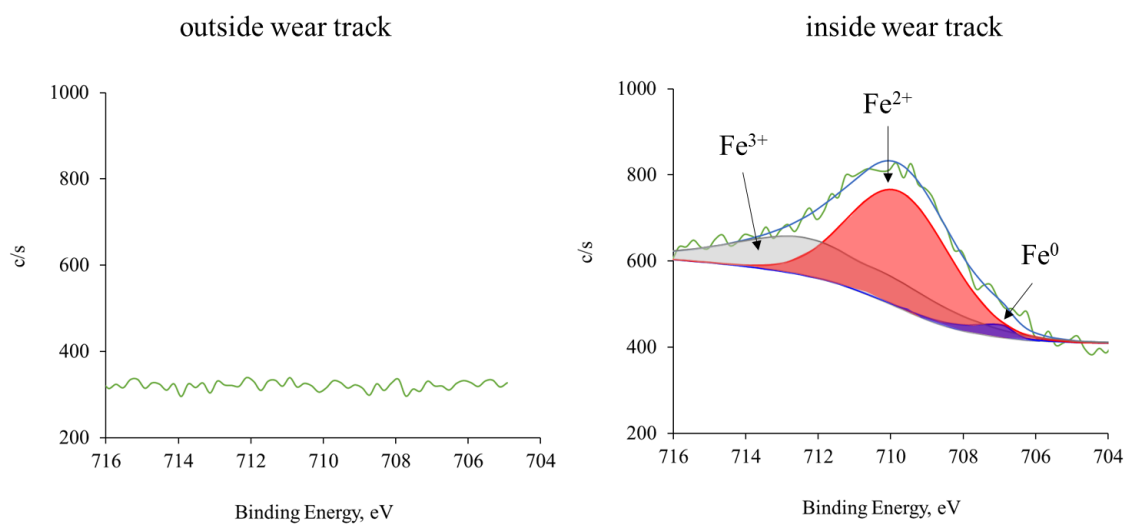


Figure A1-13. XPS curve fitting analyses results on O_{1s} spectra outside and inside the wear tracks obtained from tribofilm after ECAT tribotest with TMO
(a) after 130 cycles and (b) after 180 cycles.

(a) 130 cycles



(b) 180 cycles

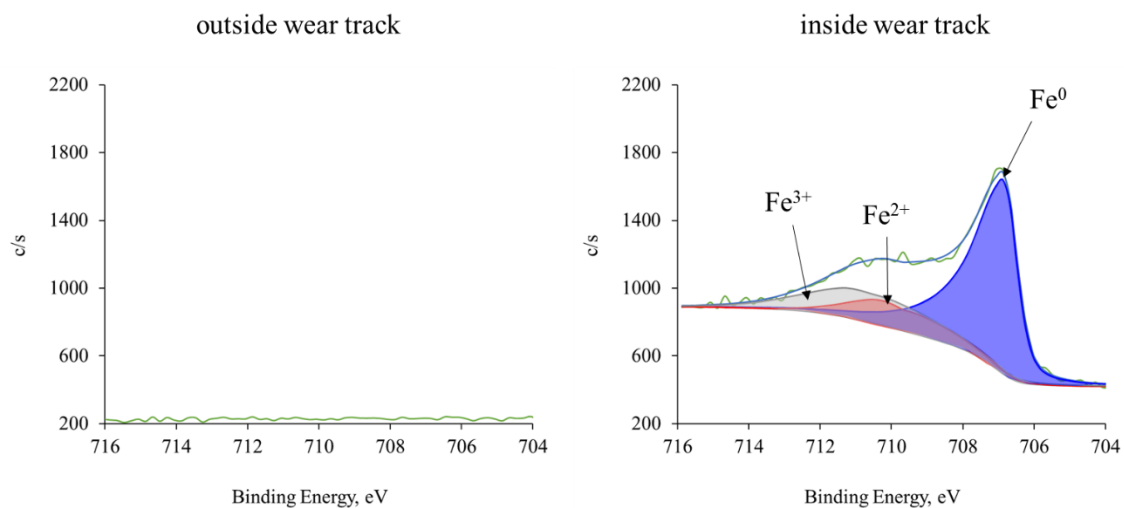


Figure A1-14. XPS curve fitting analyses results on $\text{Fe}_{2p_{3/2}}$ spectra outside and inside the wear tracks obtained from tribofilm after ECAT tribotest with TMO (a) after 130 cycles and (b) after 180 cycles.

4. Discussion of tribochemical reaction with TMO

It is well known that ester base oils often show superior tribological performance compared to mineral base oils [25-26]. However, few research regarding their tribochemical reaction has been carried out up to now. In addition to the study on the tribochemical reaction of DAPA with steel surfaces, we also investigated using the ECAT system how ester base oils react with steel surfaces to reduce wear.

The atomic compositions of carbon and oxygen found outside the wear tracks had almost the same values than those of the TMO molecules. Moreover, the binding energies of $\underline{\text{C}}\text{-OO}$ and $\underline{\text{C}}\text{-O}$ were consistent with those of ester structures. The atomic concentration of iron before the friction test was 0.0-0.1 %, thus proving that the surfaces were covered with the TMO molecules.

The XPS spectra recorded inside the wear tracks after 130 and 180 cycles were different to those obtained outside. After friction tests for 130 and 180 cycles, in addition to peaks of TMO, another peak can be observed at 289.2 and 283.3 eV, respectively, corresponding to a carbide ($\underline{\text{C}}\text{-Metal}$) contribution [22, 24]. In the four-ball test results shown in Table 4-3, DAPA in TMO generates carbides at 196 -392 N. However, no considerable peak of carbide was detected when DAPA in PAO was used as a lubricant. This result suggests that TMO and steel surfaces generate carbide under friction.

The binding energy of $\underline{\text{C}}\text{-OO}$ after 130 cycles does not present significant change, but that of 180 cycles shifts to the lower end. Carboxylates may form on the worn surfaces after 180 cycles, but these carboxylates seem to have no effective AW performance, because the friction coefficient was over 1.0. Considering both O_{1s} and Fe_{2p3} peaks, it can be concluded that iron oxides are detected inside wear tracks after both 130 and 180 cycles. The oxygen contributions on O_{1s} peak characteristic of TMO (C=O and C-O) are less detected inside both wear tracks compared to outside but the signal is more important at 130 cycles than at 180 cycles suggesting that the reduction of friction is due to few TMO remaining molecules.

Annex 2:

Pyrolysis reaction of DAPA

In considering how the DAPA molecules decompose and form tribofilm, it is essential to understand what reactions are thermodynamically favorable under given conditions. Thus, this section investigated the pyrolysis reaction mechanism of DAPA by analyzing generated compounds when DAPA was thermally decomposed. Although this experiment does not directly analyze tribochemical reactions on metal surfaces, it can provide useful information for understanding the way DAPA molecules thermally decompose and so could form tribofilm in presence of mechanical stress.

1 Analysis techniques for decomposition mechanisms of AW additives

1.1 Thermal gravimetric analysis (TGA)

TGA is an analytical technique to evaluate thermal stabilities of materials by measuring the mass of a sample over the time with temperature increase. In this study, TGA was used to investigate the thermal stabilities of phosphorus AW additives under an air atmosphere minute using a SIMADZU DTG-60 thermal analyzer. Each measurement was carried out at a heating rate of 10 °C per minute over a temperature range from 25 to 500 °C.

1.2 Headspace Gas Chromatography-Mass Spectrometry (Headspace GC-MS)

Headspace GC-MS is an analytical technique used to characterize volatile compounds. Figure A2-1 illustrates the experimental procedures of Headspace GC-MS. A phosphorus AW additive (sample) was placed in a closed vessel at an arbitrary temperature, then a vapor phase was installed into GC-MS system to identify volatile components. The present study corrected volatile compounds generated from an AW additive at 250 °C. The sampler, GC and MS systems were Agilent 7697A, Agilent 7890B, and JMS-Y200GCx-Plus (JEOL), respectively.

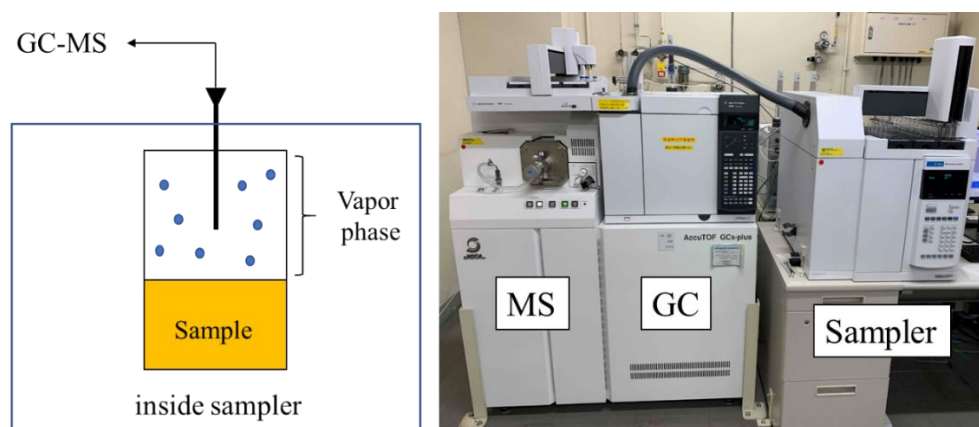


Figure A2-1. The experimental procedures of a headspace-GC-MS analysis

2. Results of Headspace GC

First, decomposition temperature of DAPA was measured using thermogravimetric analysis (SHIMADZU DTG-60) at a heating rate of 10 °C/min, operating from room temperature to 500 °C under air atmosphere at a flow rate of 50 ml min⁻¹. Figure A2-1 illustrates the TGA curve of DAPA. DAPA starts to decompose rapidly at around 200 °C and more than 95 % weight loss of DAPA decomposes before 300 °C.

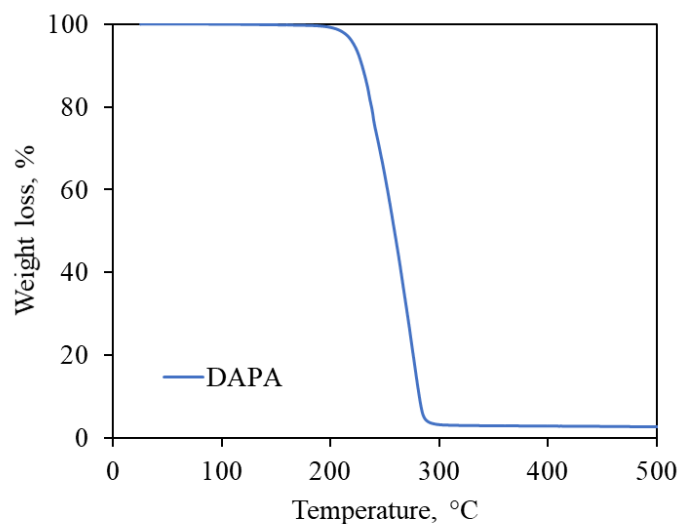


Figure A2-2. TGA curve of DAPA at a heating rate of 10 °C/min, operating from room temperature to 500 °C.

Next, Headspace GC-MS was carried out to investigate the decomposition products of DAPA. This analytical technique can characterize detailed chemical structures of vapor components generated from a sample using GC-MS, whose feature is presented in Figure 2-12 (chapter 2). The TGA result shows that DAPA decomposes between 200-300°C, as shown in Figure A2-2. Therefore, in this experiment, the decomposition products of DAPA generated at 250 °C were investigated.

Figure A2-3 shows the GC spectra of the vapor phase at 250 °C obtained from DAPA. The peaks derived from octanol and methylphosphonate are mainly detected, and the gases including N₂, O₂ and CO₂ were also identified. These results suggest that the P-O and CH₂-COOH bonds of DAPA are dissociated by thermal decomposition. For CO₂, it was not possible to distinguish whether it originates from air or DAPA.

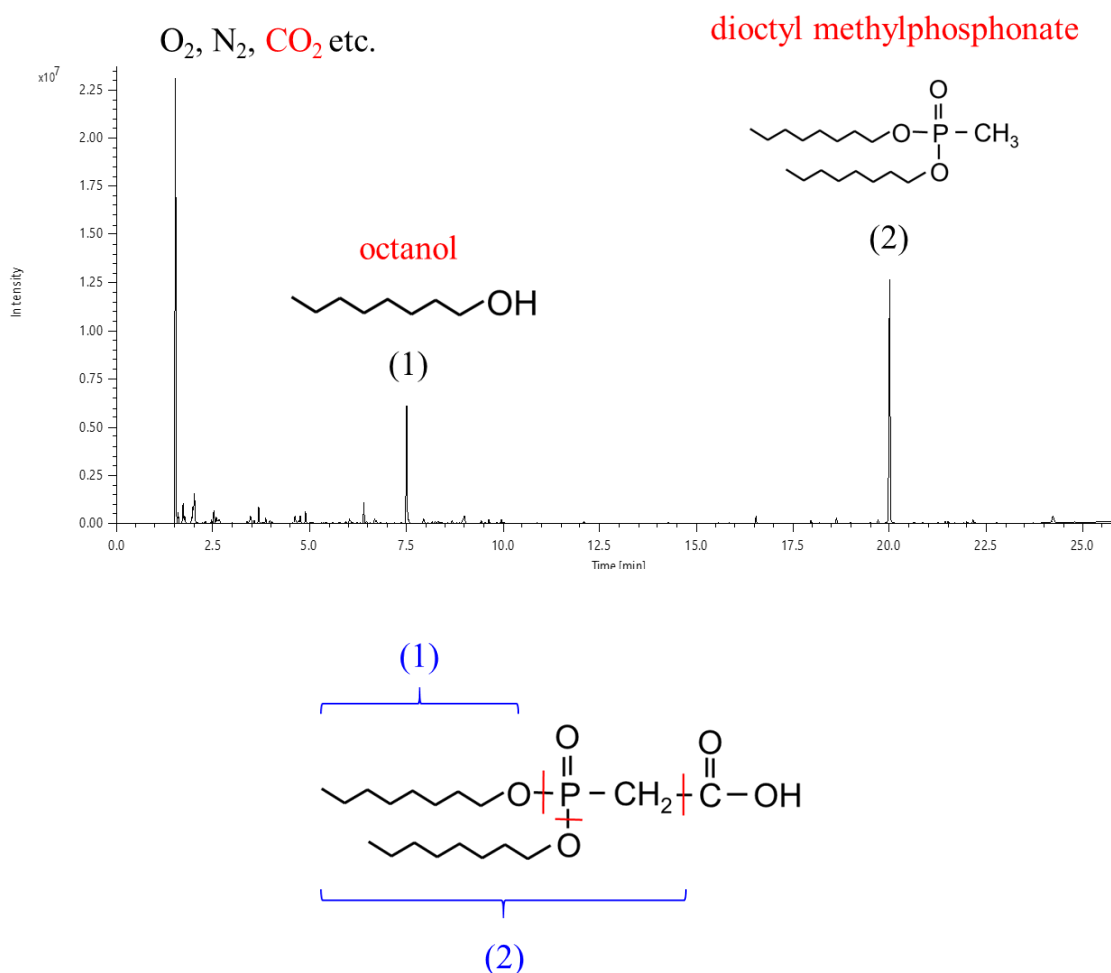


Figure A2-3. GC spectra of volatile components generated from DAPA at 250 °C under air atmosphere.

2. Discussion of pyrolysis mechanisms of DAPA

The TGA demonstrated that DAPA thermally decomposes between 200-300 °C (Figure A2-1). This temperature range may be high enough to induce the pyrolysis of DAPA on friction surfaces. Headspace GC-MS detected octanol and dioctyl methylphosphonate as the main pyrolysis products of DAPA. It was not possible to distinguish whether the detected CO₂ originated from air or DAPA in this technique, but the formation of dioctyl methylphosphonate indicates that the bond cleavage is between P-CH₂ and COOH in the DAPA molecule. From the detected components in the Headspace GC-MS spectra, a proposed pyrolysis reaction mechanisms of DAPA can be drawn in Figure A2-4.

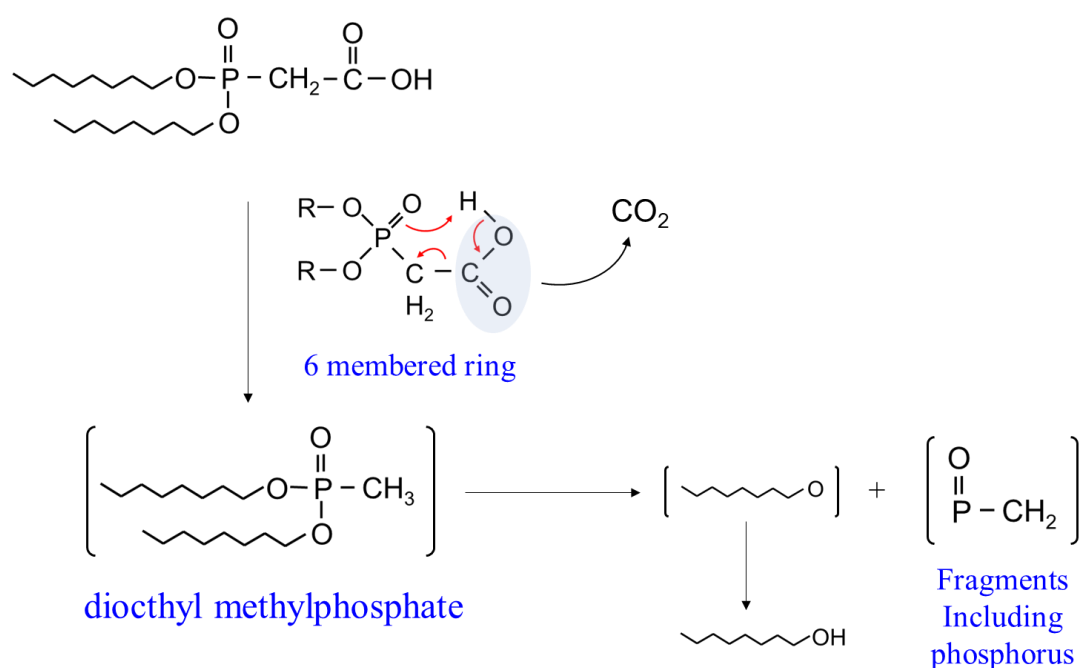


Figure A2-4. Proposed pyrolysis reaction mechanisms of DAPA

It is well known that some AW additives form six-membered rings during their pyrolysis. For example, the pyrolysis of sec-ZDDP occurs with forming a six-membered ring, when the alkyl chain moieties are eliminated [27]. DAPA probably form the six-membered ring to form CO₂ and dioctyl methylphosphonate, as shown in Figure A2-4. The fragments including the P- C bond are probably generated after the removal of the alkyl chain moiety (octanol) from dioctyl methylphosphonate. Those fragments containing phosphorus atom could contribute to the tribofilm formation.

Annex 3:

Dissolving states of DAPA in base oils

In the four-ball experiments, DAPA in TMO have shown better AW performance than DAPA in PAO as reported in Chapter 3. DAPA tribofilms generated from DAPA in TMO and DAPA in PAO were analyzed using various surface analysis techniques in chapter 4, but no significant difference of their compositions was found.

From the fact that DAPA in TMO forms thicker tribofilm at high loads than DAPA in PAO (Figure 4-4), the difference of reactivities to form tribofilm should be considered. As described in section 1.3.2, polar base oils such as TMO are possible to interact with AW additives, on the contrary, non-polar base oils such as PAO has no strong interaction with AW additives as illustrated in Figure A3-1.

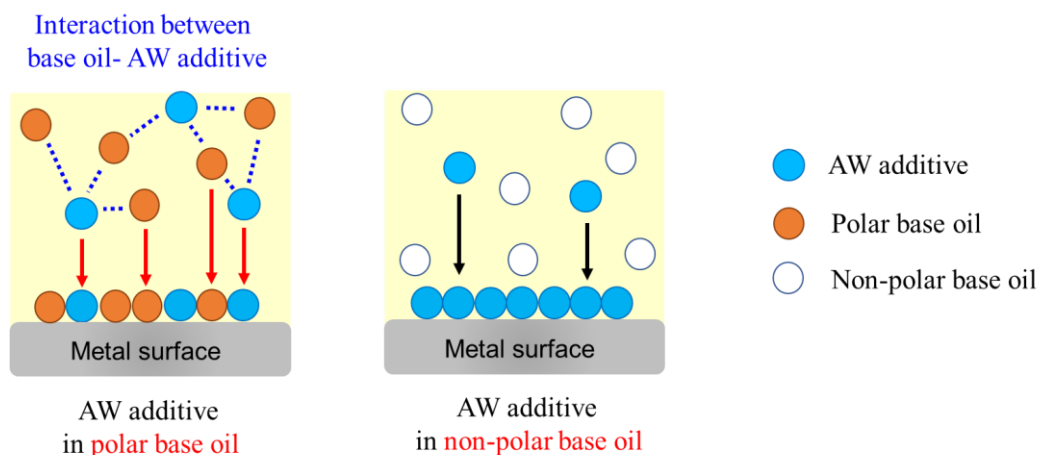


Figure A3-1. Dissolving states of AW additives in polar and non-polar base oils.

[Adapted from Figures 1-33 and 1-34].

Carboxylic acids are known to form intermolecular hydrogen bonds in solvents [28]. Therefore, in this annex, the states of hydrogen bonds of DAPA in the base oils were focused on to discuss the relationship between the hydrogen bond states of DAPA (in TMO and PAO) and their AW performance. The hydrogen bond states of DAPA were investigated experimentally using FT-IR and ^{31}P NMR. Furthermore, simulations using density functional theory (DFT) were also carried out to discuss in detail the chemical states of DAPA in each base oil.

1 Analysis techniques for dissolving states and decomposition mechanisms of AW additives

1.1 Phosphorus Nuclear Magnetic Resonance (^{31}P NMR)

^{31}P NMR spectroscopy is an analytical technique used to investigate chemical states of phosphorus compounds with observing their chemical shifts. This technique was used to follow the dissolving states of phosphorus AW additives in base oils. Table A3-1 specifies the instrument parameters of ^{31}P NMR spectroscopy employed in this study. The chemical shift of 85 % H_3PO_4 was used as standard.

Table A3-1. ^{31}P NMR instrument parameters

| | | |
|-------------------------------------|-------|--------------------------|
| NMR spectrometer | | JNM-ECZ500R/M3 |
| ^{31}P resonance frequency | [MHz] | 202.46831 |
| Temperature | [°C] | 25, 50, 100 |
| Pulse retention time | [s] | 5 |
| Number of scans | | 2000 |
| measurement | | double tube |
| Samle tube diameter | [mm] | 5 (solvent), 10 (Sample) |

2 Results for dissolving states and decomposition mechanisms of AW additives

2.1 FT-IR using isotope labelling method results

Each FT-IR spectrum was obtained at 25 °C and the resolution of 4 cm⁻¹ using FT-IR 5100 (JASCO) apparatus as described in section 2.4.1. Carboxylic acids generally exist as dimers due to the presence of strong intermolecular hydrogen bonds, however, they sometimes exist as monomers in polar solvents [29]. DAPA has a carboxylic acid structure, thus it is expected that DAPA would have different dissolving states in TMO and PAO as TMO has polar structures and PAO has non-polar structures. FT-IR is a useful technique to analyze whether carboxylic acids have dimer or monomer structures: carboxylic acids with monomers generally have the C=O stretching vibration at about 1760 cm⁻¹, whereas those of dimers have at 1740-1715 cm⁻¹ [28-30]. In this experiment, the C=O stretching vibrations of DAPA in base oils were analyzed using FT-IR to discuss the difference of DAPA's dissolving states in PAO and TMO.

First, the C=O stretching vibrations of neat DAPA and TMO were observed. Neat DAPA has the C=O stretching vibrations at 1730 cm⁻¹ and TMO has a peak assigned to TMO group (-COO-) at 1743 cm⁻¹. Their peaks show close values, therefore it is difficult to identify the C=O stretching vibration of DAPA dissolved in TMO. In order to prevent the overlap of the C=O stretching vibrations between TMO and DAPA, isotope labelled DAPA with ¹³C in the carboxylic acid structure was used. A frequency of C-O can be calculated using equations A.1 and A.2.

$$\tilde{\nu} = \frac{1}{2\pi c} \sqrt{\frac{k}{\mu}} \quad (\text{A.1})$$

where $\tilde{\nu}$ is the frequency for C=O, c is the speed of light, k is the spring constant for C=O, and μ is the reduced mass of C=O:

$$\mu = \frac{m_C m_O}{m_C + m_O} \quad (\text{A.2})$$

(m_C, m_O : the mass of C or O atom)

The frequency ratio between ¹²C=O and ¹³C=O ($\tilde{\nu}_{12\text{C=O}}/\tilde{\nu}_{13\text{C=O}}$) can be expressed as below:

$$\frac{\tilde{\nu}_{12\text{C=O}}}{\tilde{\nu}_{13\text{C=O}}} = \frac{\frac{1}{2\pi c} \sqrt{\frac{k}{\mu_{12\text{C=O}}}}}{\frac{1}{2\pi c} \sqrt{\frac{k}{\mu_{13\text{C=O}}}}} = \sqrt{\frac{\mu_{13\text{C=O}}}{\mu_{12\text{C=O}}}} \quad (\text{A.3})$$

The reduced masses (μ) for ¹³C=O and ¹²C=O are 6.24 and 6.00, respectively, and the root of $\tilde{\nu}_{12\text{C=O}}/\tilde{\nu}_{13\text{C=O}}$ becomes 1.02. From this calculation, the ¹³C=O stretching vibration of isotope labelled DAPA is expected to be observed around 1697 cm⁻¹.

Figure A3-2 shows the C=O stretching vibration spectra of PAO, TMO, DAPA and isotope labelled DAPA. PAO has no significant peak at 1600-1800 cm^{-1} . The spectra of isotope labelled DAPA is observed at 1688 cm^{-1} that is 42 cm^{-1} lower than DAPA. The peak shift by the isotope labelling method is observed using the calculation above, although the observed peak has slightly lower wavenumber than the calculation result. Consequently, the isotope labelled method enable us to identify the C=O stretching vibration of DAPA dissolving in TMO.

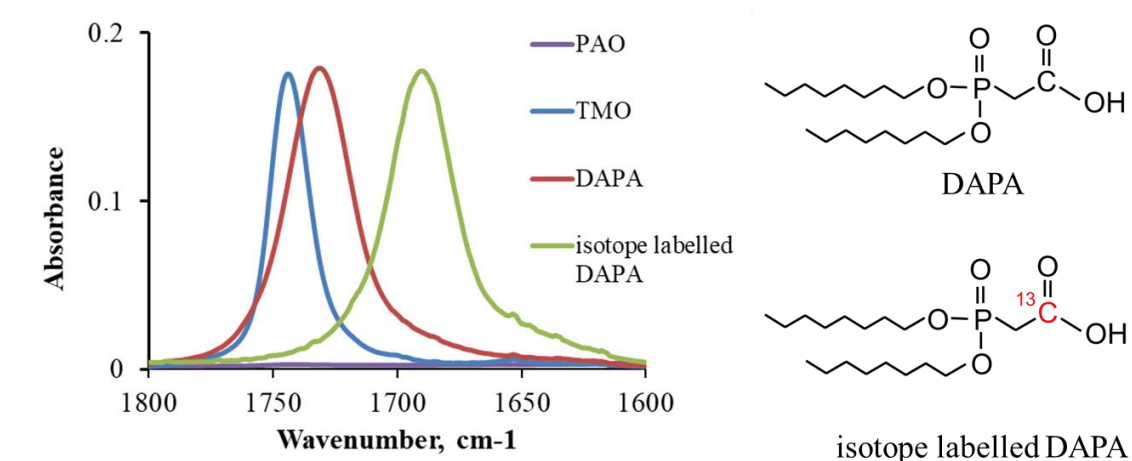


Figure A3-2. C=O stretching vibrations of TMO, DAPA and isotope labelled DAPA.

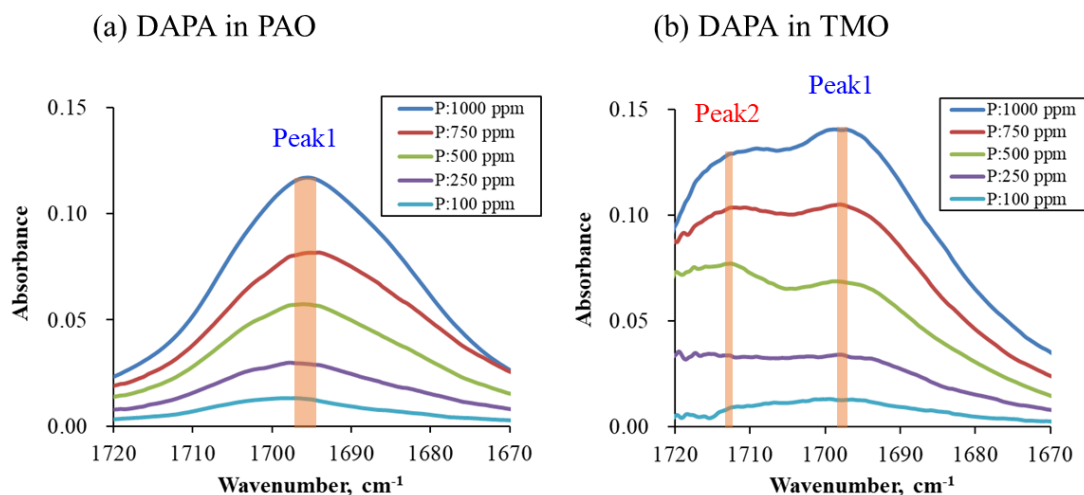


Figure A3-3. C=O stretching vibrations of DAPA in PAO and DAPA in TMO. Phosphorus contents are 100 – 1000 ppm (3.1 -31.0 mmol/kg).

The $^{13}\text{C=O}$ stretching vibration spectra of DAPA in the base oils are shown in Figure A3-3. The phosphorus concentration varies from 100 ppm to 1000 ppm (3.1 - 31.0 mmol /kg). In this

measurement, the spectra of base oils were used as background, and the differential spectra between DAPA in base oils and the base oils (PAO or TMO) were obtained as the data shown in Figure A3-3. DAPA in PAO has peaks at around 1696 cm^{-1} , and the peaks shift to the lower wavenumber end when increasing the phosphorus concentration. DAPA in TMO shows two peaks: Peak 1 is observed at 1695 cm^{-1} (where DAPA in PAO also has a peak), and peak 2 is observed at around 1711 cm^{-1} . The intensity ratio between Peak 1 and Peak 2 becomes higher with the increasing phosphorus concentration. The spectra of DAPA in TMO with phosphorus concentrations of 100 and 250 ppm have no clear peak compared to those at 500, 750, 1000 ppm. TMO has weak peaks at around 1700 cm^{-1} , as shown in Figure A3-3. This may affect the data and make it difficult to obtain clear peaks at low additive concentrations.

Thus, the FT-IR measurements with isotope labelling method revealed that the dissolving states of DAPA in PAO and TMO are different. In order to clarify the states of DAPA at Peak 1 and Peak 2 in detail, computer simulations using Density Function Theory (DFT) were performed.

2.2 DFT calculation

In order to identify Peak 1 and Peak 2, the Gaussian 09 program [31] was used for Density Function Theory (DFT) molecular wave function calculations. In the DFT calculations, the Becke's three parameter hybrid method [32-33] using the basic set B3LYP/6-31G+ (d,p) was used. In this calculation, isotope labelled dimethyl phosphonoacetic acid (DMPA), for which the C=O of DMPA was labelled by ^{13}C , was applied as a model of isotope labeled DAPA. Trimethylolpropane trimethyl TMO was used as a model of TMO in this calculation. In the end, three models of DAPA (monomer DAPA, DAPA interacting with TMO and dimer DAPA) were considered for optimization of vibration frequencies of C=O.

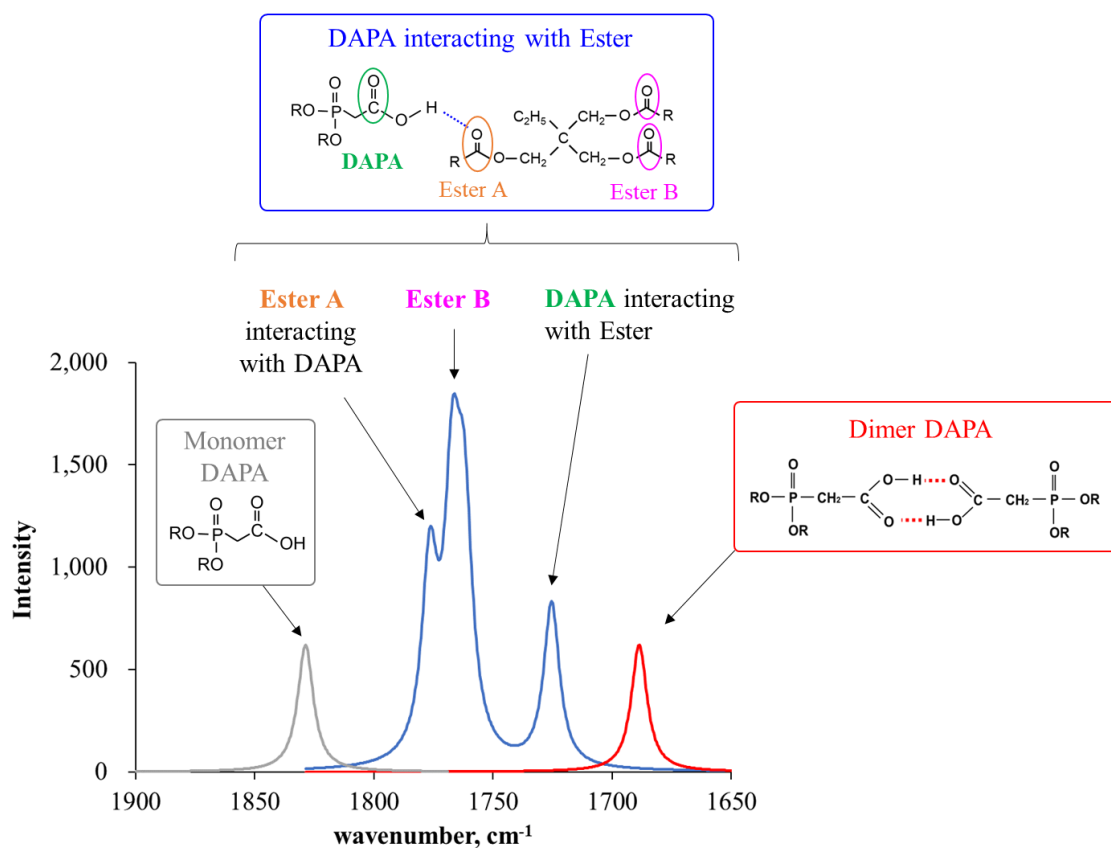


Figure A3-4. Calculated IR spectra with three models: monomer DAPA, DAPA interacting with Ester and dimer DAPA.

Figure A3-4 shows the calculated IR spectra of C=O with monomer DAPA, DAPA interacting with TMO and dimer DAPA. It is well accepted that neat carboxylic acid has dimer structures [28], therefore, the calculated peak position of Dimer DAPA can be considered the same as that of neat DAPA (Figure A3-2). Each calculated peak position was collected based on the position of Dimer DAPA.

DAPA peak. Among the three models of DAPA, the monomer has the highest wavenumber and the peak is found at 1836 cm^{-1} . The C=O stretching vibration of DAPA interacting with Ester has a peak at 1733 cm^{-1} . This peak position is located between monomer DAPA and dimer DAPA. The C=O stretching vibrations of TMO are divided into two peaks. The higher peak (Ester A) is derived from the C=O interacting with DAPA, and the lower (Ester B) is from the C=O without interaction with DAPA.

Regarding interpretation of FT-IR experiments (Figure A3-3), Peak 2 is observed at 1711 cm^{-1} , and the peak position is located between monomer DAPA and dimer DAPA. This wavenumber was closed to the calculated $^{13}\text{C=O}$ stretching vibration of DAPA interacting with TMO even if slightly lower. Peak 2 is so assigned to DAPA that has weak interactions with TMO and not from the dimer structures of DAPA. Peak 1 has a value close to neat DAPA, therefore this should be derived from the dimer structure of DAPA.

There is no significant peak derived from monomer DAPA in this study. The C=O stretching vibrations of monomer carboxylic acids are observed in very dilute solution in non-polar solvents or vapor phase [28]. DAPA in base oils have intermolecular hydrogen bonds or interactions with base oils due to the presence of strong hydrogen bond, thus the peak assigned to monomer DAPA may be not observed.

The computer simulation using DFT revealed that the C=O stretching vibration of DAPA interacting with Ester appears between that of monomer DAPA and dimer DAPA. This suggests that Peak 1 and Peak 2 shown in Figure A3-3 can be assigned to dimer DAPA and DAPA interacting with TMO, respectively, and DAPA exist as dimer structures in PAO.

In order to react with metal surfaces, it may be essential for DAPA to form the monomer state after the cleavage of the hydrogen bonds forming in base oils. Therefore, the strength of hydrogen bonds should be considered to discuss the reactivity of DAPA in base oils. Figure A3-5 illustrates the energies of three models related to DAPA. The energy of monomer DAPA is the highest among three models, and that of DAPA interacting with TMO are between monomer DAPA and dimer DAPA. DAPA interacting with TMO has 48 kJ/mol lower energy than monomer DAPA, and dimer DAPA has 65 kJ/mol lower energy. This suggests that DAPA interacting with TMO has weaker hydrogen bonds than dimer DAPA, and that the cleavage of the former hydrogen bonds is easier than the later ones. Therefore, it can be inferred that DAPA interacting with TMO is more reactive than dimer DAPA.

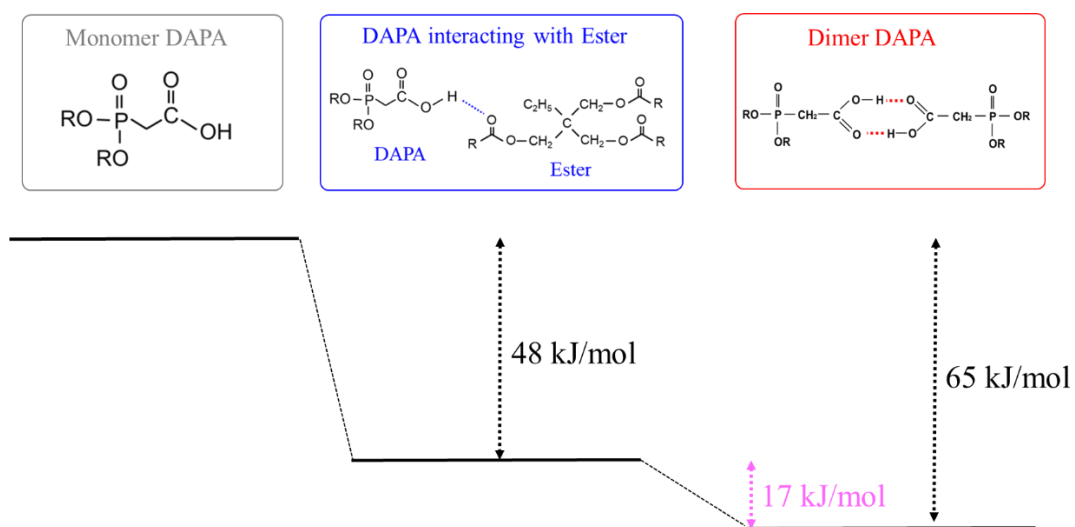


Figure A3-5. Energy comparison of DAPA interacting with TMO and dimer DAPA with monomer DAPA. The energy of monomer DAPA was set as standard. The investigations using FT-IR and DFT indicate that the dissolving states of DAPA in PAO and DAPA in TMO are different. The former has only dimer states, but the later has two dissolving states. One is dimer DAPA that is also observed in PAO and another is DAPA interacting with TMO, which may be more reactive than dimer DAPA.

2.3 ^{31}P NMR

^{31}P NMR is also a useful analysis technique to investigate chemical states of phosphorus compounds such as their binding and valences. In this experiment, chemical states of DAPA in base oils were studied at different concentrations and temperatures using ^{31}P NMR.

Table A3-2 summarizes the observed chemical shifts of DAPA in PAO and TMO with 100, 500, 1000 ppm of the phosphorus concentrations at 25, 50 and 100 °C. The obtained chemical shifts at each concentration are plotted against temperature (Figure A3-6).

Table A3-2. Chemical shifts of DAPA in base oils with 100-1000 ppm at 25-100 °C.

| Peak position of DAPA | | 25 °C | 50 °C | 100 °C |
|-----------------------|----------|-------|-------|--------|
| DAPA in PAO | 1000 ppm | 22.75 | 22.49 | 21.78 |
| | 500 ppm | 21.49 | 21.35 | 21.12 |
| | 100 ppm | 21.53 | 21.06 | 21.17 |
| DAPA in TMO | 1000 ppm | 21.65 | 21.25 | 20.59 |
| | 500 ppm | 21.14 | 20.86 | 20.38 |
| | 100 ppm | 21.12 | 20.81 | 20.30 |

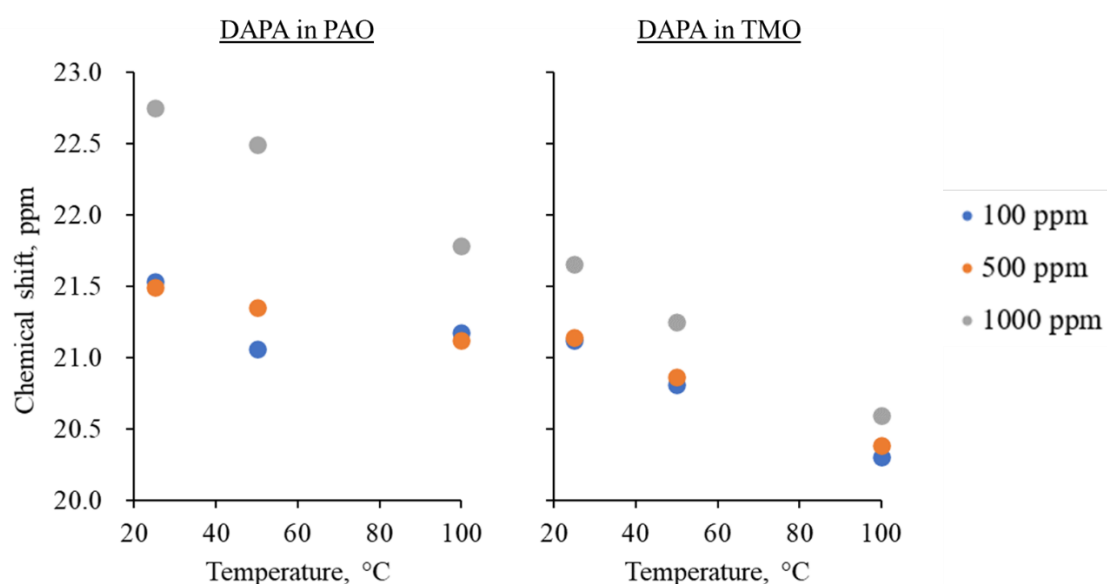


Figure A3-6. Influence of the temperature on chemical shifts of DAPA in PAO and TMO at 100-1000 ppm.

From Table A3-2 and Figure A3-6, two trends can be found. First trend is that the chemical shifts have higher values with the increasing phosphorus concentrations and decreasing temperature. In general, hydrogen bonds of carboxylic acids become stronger at higher concentration and lower temperature [34]. Therefore, this trend would mean that the higher values of chemical shift in ^{31}P NMR are derived from the stronger hydrogen bond between DAPA molecules in the base oils, whereas the lower ones are from weakest hydrogen bonds.

Another trend is that DAPA in TMO has lower values of chemical shifts than DAPA in PAO.-The research using FT-IR with DFT calculations (Figures A3-4 and A3-5) indicates that DAPA in TMO has two dissolving states. One is DAPA which has weak interactions with TMO, and another is the dimer structure of DAPA. The former has weaker hydrogen bond than the later, as calculated in Figure A3-4. From this result, it is likely that the presence of DAPA interacting with TMO makes lower chemical shifts compared to DAPA in PAO that has only the dimer structure.

5. Discussion of dissolving states

As the polar carboxylic acid function is supposed to improve adsorption capabilities of the additive on metallic surfaces for better tribofilm formation, the structure of the additive molecule in the different base oils is an important factor to take into account. The present research using isotope labelled DAPA investigated the difference of the hydrogen bond states of DAPA in PAO and TMO by FT-IR. It was observed that DAPA in PAO exists only as dimer structures while DAPA in TMO has two states: dimer structures and DAPA interacting with TMO. The DFT calculations showed that DAPA interacting with TMO is 17 kJ/mol less stable than the dimer structures of DAPA, suggesting that the former is more reactive than the latter. Therefore, it is likely that DAPA interacting with TMO has the weaker hydrogen bond than the dimer structures of DAPA, suggesting more reactivity of DAPA in TMO rather than in PAO. But Figure 3-6 (chapter 3) suggests a faster tribofilm formation in case of DAPA in PAO compared to TMO. Therefore, this difference of dissolving state does not seem to be enough significant to explain the difference of reactivity between DAPA in PAO and DAPA in TMO.

Reference of Annexes

- [1] D. Philippon, M. I. De Barros Bouchet, Th. Le Mogne, O. Lerasle, A. Bouffet, J. M. Martin, Role of nascent metallic surfaces on the tribochemistry of phosphite lubricant additives., *Tribology International*, **44**, 2011, 684-961.
- [2] D. Philippon, M. I. De Barros Bouchet, Th. Le Mogne, O. Lerasle, E. Gresser, J. M. Martin, Experimental simulation of phosphites additives tribochemical reactions by gas phase lubrication., *Tribology - Materials, Surfaces & Interfaces*, **1**, 2007, 113-123.
- [3] M. Guibert, J. Fontaine, T. Durand, T. Le Mogne, High-precision device for measuring forces, WO2016198766A1, 2016 (Patent)
- [4] M. Guibert, C. Oliver, T. Durand, T. Le Mogne, A. Le Bot, D. Dalmas, J. Scheibert, J. Fontaine, A versatile flexure-based six-axis force/torque sensor and its application to tribology, *Review of Scientific Instruments*, **92**, 2021, 085002
- [5] E. Kontturi, P. C. Thüne, J. W. H. Niemantsverdriet, Cellulose Model Surfaces Simplified Preparation by Spin Coating and Characterization by X-ray Photoelectron Spectroscopy, Infrared Spectroscopy, and Atomic Force Microscopy., *Langmuir*, **19**, 2003, 5735-5741.
- [6] J. M. Martin, Th. Le Mogne, C. Grossiord, Th. Palermo, Adsorption and friction in the UHV tribometer., *Tribology Letters*, **3**, 1997, 87-94.
- [7] J. C. Vickerman, I. S. Gilmore, Surface Analysis – The principal Techniques 2nd Edition, A John Wiley and Sons, Ltd., Publication, 2009.
- [8] M. Olla, G. Navarra, B. Elsener, A. Rossi, Nondestructive in-depth composition profile of oxy-hydroxide nanolayers on iron surfaces from ARXPS measurement., *Surface and Interface Analysis*, **38**, 2006, 964-974.
- [9] C. R. Brundle, T. J. Chuang, K. Wandelt, Core and valence level photoemission studies of iron oxide surfaces and the oxidation of iron., *Surface Science*, **68**, 1977, 459-468.
- [10] F. Mangolini, A. Rossi, N. D. Spencer, Influence of metallic and oxidized iron/steel on the reactivity of triphenyl phosphorothionate in oil solution., *Tribology International*, **44**, 2011, 670-683.
- [11] A. Rossi, F. M. Piras, D. Kim, A. J. Gellman, N.D. Spencer, Surface reactivity of tributyl thiophosphate: effects of temperature and mechanical stress., *Tribology Letters*, **23**, 2006, 197-208.
- [12] F. Bournel, C. Laffon, Ph. Parent, G. Tourillon, Adsorption of some substituted ethylene molecules on Pt(111) at 95 K Part 1: NEXAFS, XPS and UPS studies., *Surface Science*, **350**, 1996, 60-78.
- [13] M. R. Alexander, S. Payan, T. M. Duc, Interfacial interactions of plasma-polymerized acrylic acid and an oxidized aluminium surface investigated using XPS, FTIR and poly(acrylic acid)

- as a model compound., *Surface and Interface Analysis*, **26**, 1998, 967-973.
- [14] M. R. Alexander, G. Beamson, C. J. Blomfield, G. Leggett, T.M. Duce, Interaction of carboxylic acids with the oxyhydroxide surface of aluminium: poly(acrylic acid), acetic acid and propionic acid on pseudoboehmite., *Journal of Electron Spectroscopy and Related Phenomena*, **121**, 2001, 19-32.
- [15] D. R. Wheeler, O. D. Faut, The adsorption and thermal decomposition of tricresylphosphate (TCP) on iron and gold., *Applications of Surface Science*, **18**, 1984, 106-122.
- [16] E.C. Onyiriuka, Zinc phosphate glass surfaces studied by XPS. *J Non-Cryst Solids*, **163**, 1993, 268-273.
- [17] R. Brückner, H. U. Chun, H. Goretzki, M. Sammet, XPS measurements and structural aspects of silicate and phosphate glasses. *J Non-Cryst Solids*, **42**, 1980, 49-60.
- [18] A. P. Grosvenor, B. A. Kobe, M. C. Biesinger, N. S. McIntyre, Investigation of multiplet splitting of Fe 2p XPS spectra and bonding in iron compounds., *SURFACE AND INTERFACE ANALYSIS*, **36**, 2004, 1564-1574.
- [19] D. Wheeler, O. Faut, The Adsorption and Thermal Decomposition of Tricresylphosphate (TCP) on Iron and Gold., *Applied Surface Science* **18**, 1984, 106-122.
- [20] A. Rossi, F. M. Piras, D. Kim, A. J. Gellman, N. D. Spencer, Surface reactivity of tributyl thiophosphate: effects of temperature and mechanical stress., *Tribology Letters*, **23**, 2006, 197-208.
- [21] S. Hoste, D. F. Van De Vondel, G. P. Van Der Kelen, XPS Spectra of organometallic phenyl compounds of P, As, Sb and Bi., *Journal of Electron Spectroscopy and Related Phenomena*, **17**, 1979, 191-195.
- [22] C. S. Kuivila, J. B. Butt, P. C. Stair, Characterization of surface species on iron synthesis catalysts by X-ray photoelectron spectroscopy., *Applied Surface Science*, **32**, 1988, 99-121.
- [23] S. Groudeva-Zotova, R. G. Vitchev, B. Blanpain, Phase composition of Cr-C thin films deposited by a double magnetron sputtering system., *Surface and Interface Analysis*, **30**, 2000, 544-548.
- [24] Gabriel P. López, David G. Castner, Buddy D. Ratner, XPS O 1s binding energies for polymers containing hydroxyl, ether, ketone and ester groups., *SURFACE AND INTERFACE ANALYSIS*, **17**, 1991, 267-272.
- [25] A. Z. Syahir, N. W. M. Zulkifli, H. H. Masjuki, M. A. Kalam, A. Alabdulkarem, M. Gulzar, L. S. Khuong, M. H. Harith, A review on bio-based lubricants and their applications., *Journal of Cleaner Production*, **168**, 2017, 997-1016.
- [26] N. A. Zainal, N. W. M. Zulkifli, M. Gulzar, H. H. Masjuki, A review on the chemistry, production, and technological potential of bio-based lubricants., *Renewable and Sustainable Energy Reviews*, **82**, 2018, 80-102.

- [27] J. J. Dickert Jr, C. N. Rowe, Thermal decomposition of metal O,O-dialkyl phosphorodithioates., *J. Org. Chem*, **32**, 1967, 647-653.
- [28] G. Socrates, Infrared and Raman Characteristic Group Frequencies: Tables and Charts, Third Edition, Wiley, Chichester, 2004.
- [29] J. Bellantano and J.R. Baroello, The infra-red intensities of the carbonyl band in halogenated derivatives of acetic acid., *Spectrochimica Acta*, **16**, 1960, 1333-1343.
- [30] J.R.Barceló and C.Otero, Infra-red spectra of the fluorinated acetic acids in condensed and vapour phase, *Spectrochimica Acta*, **18**, 1962, 1231-1247.
- [31] M.J. Frisch,G.W. Trucks, H.B. Schlegel, G.E. Scuseria, M.A. Robb, J.R. Cheeseman, et al. Gaussian 09, Revision D.01. Wallingford(CT); Gaussian Inc.,; 2009.
- [32] A.D. Becke, Density functional thermochemistry. III. The role of exact exchange, *J. Chem. Phys*, **98**, 1993, 5648-5652.
- [33] C. Lee, W.Yang, R.G. Parr, Development of the Colle-Salvetti correlation-energy formula into a functional of the electron density., *Phys. Rev*, **37**, 1988, 785-789.
- [34] J.Dong, Y.Ozaki, K. Nakashima, Infrared, Raman, and Near-Infrared Spectroscopic Evidence for the Coexistence of Various Hydrogen-Bond Forms in Poly(acrylic acid)., *Macromolecules*, **30**, 1997, 1111-1117.

LIST OF PRESENTATION

T. Oshio*, C. Minfray, F. Dassenoy, J. Galipaud, T. Le Mogne, K. Yagishita, Tribofilm composition of dialkyl phosphonoacetic acid in Ester base oil and PAO, 7th World Tribology Congress, September 5-10, 2021, Lyon, France

T. Oshio*, C. Minfray, F. Dassenoy, J. Galipaud, T. Le Mogne, K. Yagishita, Tribochemical Properties of Dialkyl phosphonoacetic Acid in Synthetic Ester Base Fluid, 22nd International Colloquium Tribology, January 28-30, 2020-Stuttgart, Germany

T. Oshio*, C. Minfray, F. Dassenoy, J. Galipaud, T. Le Mogne, K. Yagishita, TRIBOCHEMICAL PROPERTIES OF DIALKYL PHOSPHONOACETIC ACID IN ENVIRONMENTALLY ADAPTED BASE FLUID, 46th Leeds-Lyon Symposium on Tribology, September 2-4, 2019, Lyon, France

T. Oshio*, C. Minfray, F. Dassenoy, J. Galipaud, T. Le Mogne, K. Yagishita, Study of Antiwear Mechanism of Dialkylphosphonoacetic acid in Biodegradable Synthetic Ester Oils by X-ray Photoelectron Spectroscopy, 7th European Conference on Tribology, June 12-14, 2019, Wien, Austria

LIST OF Publication

“Dialkyl phosphonate with carboxylic acid as antiwear additives for ester-base lubricants”

T.Oshio, C. Minfray, F. Dassenoy, J. Galipaud, K. Yagishita, *Wear*, 530-531, 15 October 2023, 205042, <https://doi.org/10.1016/j.wear.2023.205042>

ACKNOWLEDGEMENTS

First of all, I would like to express my sincere gratitude to my supervisors, Clotilde Minfray and Fabrice Dassenoy, for their warm support to carry out my Ph.D thesis in their laboratory. The constructive and productive discussion with them always encouraged me to continue this work. Without their help, I could not complete this thesis. My gratitude to them is too great for words to express.

I also gratefully acknowledge the help provided by Thierry Le Mogne and Jules Garipard for the XPS experiments. Through discussions with them, I learned the principles of XPS and how to analyze the data, which finally led to obtaining useful data for this thesis. The XPS knowledge I gained from them is highly valuable to me in my research and development of lubricants.

My special thanks to ENEOS Corporation for giving me a great opportunity to do my Ph.D in Ecole Centrale de Lyon. Especially, I would like to thank Kazuhiro Yagishita, Kenichi Komiya, Osamu Kurosawa, Toshiyuki Hasebe, Toru Konishi and Toshiaki Wakabayashi, who gave me the opportunity to start and publish this research using DAPA. In addition, I also appreciate all my colleagues in the lubricants R&D department in ENEOS Corporation, who kindly supported me by sending materials from Japan to France and sometimes obtained essential data for this thesis.

I also thank all the members of the LTDS. Special thanks to my friends, Valentin Salinas, Mayssa Al Kharboutly, Falachadé Nasrya Kossoko, Pushkar Deshpande and Antoine Normant. The memories of sharing the office with them, our wonderful discussions and many coffees, are irreplaceable in my life.

Finally, I would like to thank all my family for their motivating words and warm support. I hope that this research will lead to my son's interest in science.